

QUALITATIVE ANALYSES OF ECOLOGICAL MODELS
—AN AUTOMATED DYNAMICAL SYSTEMS APPROACH

By

Lynn van Coller

B. Sc. University of Natal (UNP), South Africa, 1990

B. Sc. Hons. University of Natal (UNP), South Africa, 1991

M. Sc. University of Natal (UNP), South Africa, 1992

A THESIS SUBMITTED IN PARTIAL FULFILLMENT OF
THE REQUIREMENTS FOR THE DEGREE OF
DOCTOR OF PHILOSOPHY

in

THE FACULTY OF GRADUATE STUDIES
INSTITUTE OF APPLIED MATHEMATICS
DEPARTMENT OF MATHEMATICS

We accept this thesis as conforming
to the required standard

THE UNIVERSITY OF BRITISH COLUMBIA

December 1995

© Lynn van Coller, 1995

In presenting this thesis in partial fulfilment of the requirements for an advanced degree at the University of British Columbia, I agree that the Library shall make it freely available for reference and study. I further agree that permission for extensive copying of this thesis for scholarly purposes may be granted by the head of my department or by his or her representatives. It is understood that copying or publication of this thesis for financial gain shall not be allowed without my written permission.

Department of MATHEMATICS

The University of British Columbia
Vancouver, Canada

Date 10 DECEMBER 1995

Abstract

Ecological models and qualitative analyses of these models can give insight into the most important mechanisms at work in an ecological system. However, the mathematics required for a detailed analysis of the behaviour of a model can be formidable. In this thesis I demonstrate how various computer packages can aid qualitative analyses by implementing techniques from dynamical systems theory. I analyse a number of continuous and discrete models to demonstrate the kinds of results and information that can be obtained.

I begin with three fairly simple predator-prey models in order to introduce the terminology and techniques and to demonstrate the reliability of the computer software. I then look at a more practical system dynamics model of a sheep-pasture-hyrax-lynx system and compare the techniques with a traditional sensitivity analysis. A ratio-dependent model is the focus of the next chapter. The analysis highlights some of the biological implausibilities and mathematical difficulties associated with these models. Two discrete population genetics models are considered in the following chapters. The techniques are able to deal with the complex nonlinearities and lead to insights into the conditions under which stable homomorphisms and polymorphisms occur. The final example is a complicated discrete model of the spruce budworm-forest defoliating system. The mechanisms responsible for insect outbreaks and the relative effects of dispersal and predation are studied.

In all the cases the techniques lead to a better understanding of the interactions between various processes in the system than was possible using traditional techniques. In two cases the results suggest improvements in the formulations of the models. The

techniques also identify parameters or processes which are crucial for determining model behaviour. All these results are obtained fairly easily with the use of the computer packages and do not require an extensive mathematical knowledge of dynamical systems theory or intensive mathematical manipulations.

Table of Contents

Abstract	ii
Table of Contents	iv
List of Tables	x
List of Figures	xi
Acknowledgements	xxi
1 Introduction	1
1.1 General overview	1
1.2 Research objectives	1
1.3 Thesis outline	2
1.4 Motivation	6
1.5 The bigger picture	8
2 Preliminary Example	10
2.1 Introduction	10
2.2 Basic model	11
2.3 Adding intraspecific competition among prey	13
2.4 Adding intraspecific competition among predators	22
2.5 Conclusion	27

3	Sheep-Hyrax-Lynx Model	30
3.1	Introduction	30
3.2	Dynamic models and systems analysis—some background	31
3.3	Model equations	33
3.4	Technical details	38
3.5	Model analysis	39
3.5.1	Reference parameter values	39
3.5.2	Understanding model relationships	41
3.5.3	Adding density-dependence to pasture growth	47
3.5.4	A summary of the effects of culling both hyrax and lynx	51
3.5.5	Biological interpretation of results	54
3.6	Conclusion	57
4	Ratio-Dependent Model	58
4.1	Introduction	58
4.2	Background	60
4.3	Model equations	62
4.4	Nondimensionalisation	64
4.5	Model analysis	70
4.5.1	One-parameter studies	70
4.5.2	Combining plant and herbivore dynamics	92
4.5.3	The role played by the isocline configurations	102
4.6	Conclusion	107
5	Population Genetics Model I	112
5.1	Introduction	112
5.2	New terminology	114

5.3	Background	115
5.4	Model equations	117
5.5	Model analysis	118
5.5.1	Approach	118
5.5.2	One-parameter bifurcation diagrams	119
5.5.3	Two-parameter bifurcation diagram	124
5.5.4	Orbits of period four (and higher)	128
5.6	Conclusion	136
6	Population Genetics Model II	138
6.1	Introduction	138
6.2	Background	140
6.3	Fitness functions	140
6.4	Model analysis	141
6.4.1	Approach	141
6.4.2	(k_{11}, r_{11}) -parameter space	142
6.4.3	Criteria for polymorphisms	146
6.4.4	Stable period-2 polymorphisms	152
7	Spruce Budworm Model	164
7.1	Introduction	164
7.2	Background	165
7.3	Model equations	167
7.3.1	Foliage	167
7.3.2	Branch surface area	168
7.3.3	Budworm	169
7.4	Model analysis	174

7.4.1	Preliminaries	174
7.4.2	The effects of small larval dispersal	177
7.4.3	The effects of adult dispersal	181
7.4.4	Biological interpretation	186
7.4.5	What causes outbreak cycles?	189
7.4.6	The effects of the other processes	194
7.4.7	The effects of predation	196
7.5	Conclusion	203
8	Conclusion	204
8.1	Main results	204
8.2	Limitations	205
8.3	Future possibilities	206
	Bibliography	207
	Appendices	217
A	Dynamical systems theory	217
A.1	Introduction	217
A.2	Basic concepts	217
A.2.1	Bifurcation diagram	217
A.2.2	Bifurcation point	218
A.2.3	Chaos	219
A.2.4	Continuation branch	219
A.2.5	Domain of attraction	219
A.2.6	Equilibrium point	221
A.2.7	Hard loss of stability	221

A.2.8	Heteroclinic orbit	222
A.2.9	Homoclinic orbit	223
A.2.10	Hopf bifurcation	224
A.2.11	Hysteresis	226
A.2.12	Limit cycle	227
A.2.13	Limit point	228
A.2.14	Local stability	229
A.2.15	Parameter	229
A.2.16	Period-doubling bifurcation	230
A.2.17	Phase portrait	230
A.2.18	Pitchfork bifurcation	230
A.2.19	Qualitative behaviour	232
A.2.20	Saddle point	233
A.2.21	Sink	234
A.2.22	Soft loss of stability	234
A.2.23	Source	235
A.2.24	State variable	235
A.2.25	Transcritical bifurcation	236
A.3	Some mathematical details	237
A.3.1	Introduction	237
A.3.2	Equilibrium points and local stability	238
A.3.3	Global bifurcations	245
A.3.4	Periodic orbits	248
A.3.5	Maps (systems of difference equations)	252
A.3.6	Stability of bifurcations under perturbations	256
A.3.7	Multiple degeneracy	258

A.4	Conclusion	258
B	Numerical details	259
B.1	Introduction	259
B.2	Theory	260
B.2.1	Continuation methods	260
B.2.2	Detection of bifurcations	262
B.2.3	Stability	263
B.3	Available computer packages	264
B.3.1	AUTO86	265
B.3.2	Interactive AUTO	269
B.3.3	XPPAUT	270
B.3.4	AUTO94	273
B.3.5	DSTOOL	274
B.3.6	Other packages	275
B.4	Using the packages	276
B.5	Pointers and warnings	281
C	Mathematical details for the sheep-hyrax-lynx model	285
C.1	Modelling delays in system dynamics models	285
C.2	Rescaling model equations	286
D	Mathematical details for the budworm-forest model	287
D.1	Derivation of new foliage equation in spruce budworm model	287
D.2	Summary of model equations	288
	Listings	290

List of Tables

- 3.1 Table showing the processes affecting each state variable and some of the abbreviations used in the sheep-hyrax-lynx model equations. 37
- 4.1 Table showing the reference parameter values for the ratio-dependent model. 71
- 7.1 Table of standard parameter values for the budworm-forest model. 173

List of Figures

2.1	One-parameter bifurcation diagram obtained by varying α in the basic system of equations with $a = 0.6, b = 0.3, c = 0.4$ and $d = 0.2$	13
2.2	Phase portraits for the basic model.	14
2.3	Two-parameter bifurcation diagram of (ϵ, α) -parameter space. (b) Phase portraits corresponding to regions (i), (ii) and (iii) in part (a).	15
2.4	One-parameter bifurcation diagram obtained by varying ϵ in Bazykin's prey competition model with $a = 0.6, b = 0.3, c = 0.4, d = 0.2$ and $\alpha = 0.3$	17
2.5	Two-parameter continuation of the Hopf bifurcation shown in the previous figure.	18
2.6	Two-parameter bifurcation diagram of (ϵ, α) -parameter space for the prey competition model with $a = 0.6, b = 0.3, c = 0.4$ and $d = 0.2$	19
2.7	Phase portraits corresponding to the points marked with *'s in the previous figure.	20
2.8	Time plots corresponding to the phase portraits in the previous figure.	21
2.9	(a) and (b) Two-parameter bifurcation diagrams of (α, μ) -parameter space. (c) Phase portraits corresponding to regions (i), (ii), (iii) and (iv) in parts (a) and (b).	23
2.10	One-parameter bifurcation diagram obtained by varying α in the predator competition model with $a = 0.6, b = 0.3, c = 0.4, d = 0.2$ and $\mu = 0.06$	24
2.11	Diagram showing the period of the limit cycle oscillations in the previous figure as a function of α	25

2.12	A two-parameter bifurcation diagram of (α, μ) -space for $a = 0.6$, $b = 0.3$, $c = 0.4$ and $d = 0.2$	25
2.13	Phase portraits corresponding to the points marked with *'s in the previous figure.	26
2.14	Time plots corresponding to the phase portraits in the previous figure.	27
2.15	One-parameter bifurcation diagrams for (a) $\mu = 0.1$, (b) $\mu = 0.074$ and (c) $\mu = 0.02$	28
3.1	The lynx predation multiplier, L_{PM} , as a function of prey abundance, A_P	36
3.2	Three one-parameter bifurcation diagrams with revenue plotted as a function of H_{CN}	40
3.3	One-parameter bifurcation diagram of revenue versus L_{CN} for $H_{CN}=0.35$	41
3.4	One-parameter bifurcation diagrams obtained from varying S_{FCN}	42
3.5	One-parameter bifurcation diagrams obtained from varying L_{FN}	43
3.6	The grazing multiplier function (G_M) as a function of pasture availability.	46
3.7	The pasture multiplier (P_M) as a function of pasture availability (P_A).	48
3.8	One-parameter bifurcation diagrams obtained from varying S_{FCN} for the new model which includes a pasture limiting multiplier.	49
3.9	One-parameter bifurcation diagrams obtained from varying L_{FN} for the new model which includes a pasture limiting multiplier.	50
3.10	Time plots obtained using (a) the original model and (b) the modified model with $S_{FCN} = 0.5$	51
3.11	One-parameter bifurcation diagram of revenue as a function of L_{CN} for the modified model.	52
3.12	Two-parameter continuation of the limit point in the previous figure.	53

3.13	Two-parameter bifurcation diagram of the H_{CN} and L_{CN} parameter space for the modified model.	54
3.14	(a) Surface plot and (b) contour plot of revenue as a function of the hyrax and lynx culling normals.	55
4.1	Isoclines in the M_1M_2 and M_2M_3 planes for the original model.	68
4.2	One-parameter bifurcation diagrams obtained by varying γ_3 in (a) the original model ($a_i=0$, $i = 1, 2, 3$) and (b) the modified model ($a_i=0.001$, $i = 1, 2, 3$). The state variable M_1 is plotted on the y-axes.	72
4.3	One-parameter bifurcation diagrams obtained by varying ϕ_3 in the original model.	74
4.4	One-parameter bifurcation diagrams obtained by varying ϕ_3 in the modified model.	75
4.5	Time plots of (a) M_1 , (b) M_2 and (c) M_3 for $\phi_3 = 0.16$. All the other parameter values are as in the reference parameter set.	76
4.6	Isoclines in the M_1M_2 plane with $\phi_3 = 0.06$ in (a) and $\phi_3 = 0.05$ in (b) and (c).	78
4.7	One-parameter bifurcation diagrams obtained by varying Ω_3 in the original model.	80
4.8	One-parameter bifurcation diagrams obtained by varying Ω_3 in the modified model.	81
4.9	One-parameter bifurcation diagrams showing the effects of varying ϕ_2 for the original model.	83
4.10	One-parameter bifurcation diagrams showing the effects of varying ϕ_2 for the modified model.	84

4.11	One-parameter bifurcation diagrams showing the effects of varying γ_1 for (a) the original model and (b) the modified model.	85
4.12	Two-parameter bifurcation diagrams showing the effects of varying both γ_1 and ϕ_2 on the positions of the limit points and Hopf bifurcations in the previous figure.	86
4.13	One-parameter bifurcation diagrams showing the effects of varying γ_2 for (a) the original model and (b) the modified model.	87
4.14	Two-parameter bifurcation diagrams showing the effects of varying both γ_2 and ϕ_3 on the positions of the Hopf bifurcations in the previous figure.	88
4.15	Two-parameter bifurcation diagram of the Hopf bifurcation continuations for the modified model with $a_i=0.002$ ($i = 1, 2, 3$).	89
4.16	Time plots corresponding to the points that are marked with *'s in the two-parameter diagrams for the original model and the modified model with $a_i=0.001$ ($i = 1, 2, 3$) and $a_i=0.002$ ($i = 1, 2, 3$).	90
4.17	One-parameter bifurcation diagrams showing the effects of varying Ω_1 for (a) the original model and (b) the modified model.	91
4.18	One-parameter bifurcation diagrams showing the effects of varying Ω_2 for (a) the original model and (b) the modified model.	92
4.19	Two-parameter bifurcation diagram obtained using the modified model with $a_i=0.001$, ($i = 1, 2, 3$) and $\gamma_1 = 0.4$	94
4.20	Two-parameter bifurcation diagram obtained using the modified model with $a_i=0.001$, ($i = 1, 2, 3$) and $\gamma_1 = 0.6$	95
4.21	Two-parameter bifurcation diagram obtained using the modified model with $a_i=0.001$, ($i = 1, 2, 3$) and $\gamma_1 = 1.2$	96
4.22	Two-parameter bifurcation diagram obtained using the modified model with $a_i=0.001$, ($i = 1, 2, 3$) and $\gamma_1 = 1.8$	97

4.23	Two-parameter bifurcation diagram obtained using the modified model with $a_i=0.001$, ($i = 1, 2, 3$) and $\gamma_1 = 2.4$	98
4.24	One-parameter bifurcation diagrams obtained by varying γ_2 with $\gamma_1 = 0.4$ and (a) $\phi_3 = 0.07$, (b) $\phi_3 = 0.17$ and (c) $\phi_3 = 0.25$	99
4.25	One-parameter bifurcation diagram obtained by varying γ_2 with $\gamma_1 = 1.2$ and $\phi_3 = 0.2$	101
4.26	Examples of isocline configurations showing different possibilities for the position of the tritrophic equilibrium.	104
4.27	Examples of isocline configurations at different points in (γ_1, ϕ_2) -space.	105
4.28	Isocline configurations with (a) $a_i = 0$, (b) $a_i = 0.001$ and (c) $a_i = 0.005$ ($i = 1, 2, 3$) together with the reference parameter set.	106
4.29	One-parameter bifurcation diagrams when $a_i = 0.005$ ($i = 1, 2, 3$).	108
4.30	Plant isoclines for (a) the original and (b) the modified model.	109
5.1	Dynamics in the (p, N) -plane for $a_{11} = 2.1$, $a_{12} = 1.9$, $a_{22} = 1.1$, $b_{11} = 1.0$, $b_{12} = 0.904$ and $b_{22} = 0.54$	119
5.2	One-parameter bifurcation diagram with $a_{11} = 2.1$, $a_{12} = 1.9$, $a_{22} = 1.1$, $b_{11} = 1.0$ and $b_{12} = 0.904$ obtained using AUTO.	121
5.3	One-parameter bifurcation diagram with $a_{11} = 2.1$, $a_{12} = 1.9$, $a_{22} = 1.1$, $b_{11} = 1.0$ and $b_{12} = 0.906$. $K_{11} = 2.1$ and $K_{12} = 2.097$	123
5.4	Diagram of the (p, N) -plane for $a_{11} = 2.1$, $a_{12} = 1.9$, $a_{22} = 1.1$, $b_{11} = 1.0$, $b_{12} = 0.906$ and $b_{22} = 0.52$ showing the domains of attraction for the stable phenomena.	124
5.5	Two-parameter bifurcation diagram with $a_{11} = 2.1$, $a_{12} = 1.9$, $a_{22} = 1.1$ and $b_{11} = 1.0$ obtained using AUTO.	125
5.6	Two-parameter bifurcation diagram including additional curves.	126

5.7	One-parameter bifurcation diagram with $a_{11} = 2.1$, $a_{12} = 1.9$, $a_{22} = 1.1$, $b_{11} = 1.0$ and $b_{12} = 0.908$ obtained using AUTO.	127
5.8	Dynamics in the (p, N) -plane with $a_{11} = 2.1$, $a_{12} = 1.9$, $a_{22} = 1.1$, $b_{11} = 1.0$ and various combinations of b_{12} and b_{22} which correspond to regions A to H in the two-parameter figure.	129
5.9	One-parameter bifurcation diagram with $a_{12} = 1.9$, $a_{22} = 1.1$, $b_{11} = 1.0$, $b_{12} = 0.905$ and $b_{22} = 0.525$ obtained using AUTO.	130
5.10	Dynamics in the (p, N) -plane for $a_{12} = 1.9$, $a_{22} = 1.1$, $b_{11} = 1.0$, $b_{12} = 0.905$, $b_{22} = 0.525$ and (a) $a_{11} = 2.68$, (b) $a_{11} = 2.69$ and (c) $a_{11} = 2.75$. In (a) there is a period-8 attractor at $p = 1$. In (b) this changes to a period-16 attractor and in (c) we have what appears to be a chaotic attractor.	132
5.11	One-parameter bifurcation diagram with $a_{11} = 2.1$, $a_{22} = 2.1$, $b_{11} = 1.0$, $b_{12} = 0.908$ and $b_{22} = 0.53$ obtained using AUTO.	133
5.12	Dynamics in the (p, N) -plane for $a_{11} = 2.1$, $a_{12} = 3.8$, $a_{22} = 2.1$, $b_{11} = 1.0$, $b_{12} = 0.908$ and $b_{22} = 0.53$ showing a stable period-4 polymorphism.	133
5.13	Two-parameter continuation of the period-doubling bifurcation with $a_{11} = 2.1$, $a_{22} = 2.1$, $b_{11} = 1.0$ and $b_{12} = 0.908$	134
5.14	Examples of complex dynamics. (a) An interior period-8 orbit for $a_{11} = 2.3$, $a_{12} = 2.9$, $a_{22} = 2.5$, $b_{11} = 1.0$, $b_{12} = 0.908$ and $b_{22} = 0.95$. (b) An interior chaotic attractor for $a_{11} = 2.6$, $a_{12} = 3.1$, $a_{22} = 2.5$, $b_{11} = 1.0$, $b_{12} = 0.908$ and $b_{22} = 0.95$	135
6.1	w_{22} with $r_{22} = 0.8$ and $k_{22} = 0.6$	142
6.2	A one-parameter bifurcation diagram obtained by varying k_{11} with r_{11} fixed at 0.7 ($r_{22} = 0.8$ and $k_{22} = 0.6$).	143

6.3	Diagrams of the (p, N) -plane for a number of different values of k_{11} with r_{11} fixed at 0.7.	144
6.4	Diagrams of the (k_{11}, r_{11}) -parameter space.	145
6.5	Diagrams of the (p, N) -plane corresponding to the regions A to H in the two-parameter diagram.	147
6.6	Diagrams of the (p, N) -plane corresponding to the regions N to P in the two-parameter diagram.	148
6.7	Examples of the fitness functions for parameter values corresponding to (a) a stable polymorphism ($r_{11} = 0.7, k_{11} = 2.0, r_{22} = 0.8, k_{22} = 0.6$) and (b) an unstable polymorphism ($r_{11} = 0.4, k_{11} = 2.0, r_{22} = 0.8, k_{22} = 0.6$). . .	149
6.8	Curves given by $w_1 = w_2$ and $\bar{w} = 1$ for parameter values corresponding to a stable polymorphism ($r_{11} = 0.7, k_{11} = 2.0, r_{22} = 0.8, k_{22} = 0.6$). . . .	151
6.9	(a) Fitness functions and (b) (p, N) -plane for $r_{11} = 1.3, k_{11} = 0.5, r_{22} = 7.5$ and $k_{22} = 4.57$	153
6.10	A partial one-parameter bifurcation diagram obtained by varying r_{22} . . .	154
6.11	Two-parameter continuations of the period-doubling bifurcation HB* in the previous figure obtained by varying (a) r_{11} , (b) k_{11} and (c) k_{22} in addition to r_{22}	155
6.12	(a) Fitness functions and (b) (p, N) -plane for $r_{11} = 0.2, k_{11} = 5.0, r_{22} = 0.3$ and $k_{22} = 0.4$	156
6.13	One-parameter diagrams obtained by varying k_{11} using (a) the original model and (b) the second iterate of the model.	157
6.14	A bifurcation diagram showing the two-parameter continuation of the period-doubling at $k_{11} = 4.226$ and the subsequent period-doubling at $k_{11} = 5.358$ in the previous figure.	158

6.15	An example of an interior chaotic attractor obtained for $r_{11} = 0.18$, $k_{11} = 5.0, r_{22} = 0.3$ and $k_{22} = 0.4$	159
6.16	An example of a fitness function configuration where w_{11} is always superior to w_{22}	160
6.17	The (k_{11}, r_{11}) -parameter space showing the region of higher order stable polymorphic behaviour and the region corresponding to fitness function configurations of the type shown in the previous figure.	160
6.18	w_{22} with $r_{22} = 0.25$ and $k_{22} = 2.5$	161
6.19	The new two-parameter space showing the same regions as before.	161
7.1	Graph of G versus H.	172
7.2	One-parameter bifurcation diagram of budworm larval density versus d_{SL}	177
7.3	Diagrams of budworm larval density versus foliage for (a) $d_{SL} = 0.2$, (b) $d_{SL} = 0.35$, (c) $d_{SL} = 0.8$ and (d) $d_{SL} = 0.9$	178
7.4	Time plots of (a) budworm larval density, (b) foliage density and (c) branch surface area density versus time for $d_{SL} = 0.35$	179
7.5	One-parameter bifurcation diagram of budworm larval density versus A_{thr} for $d_{SL} = 0.45$	181
7.6	Two-parameter bifurcation diagram of A_{thr} versus d_{SL}	182
7.7	Diagrams of budworm larval density versus foliage for the regions marked A-I in the previous figure.	184
7.8	Simplified two-parameter bifurcation diagram of A_{thr} versus d_{SL}	187
7.9	Two-parameter bifurcation diagram of A_{thr} versus d_{SL} for the simplified model which only includes dispersal.	191
7.10	Isoclines of recruitment versus budworm density.	194

7.11	Two-parameter bifurcation diagram of A_{thr} versus d_{SL} for the predation model which includes dispersal as well as predation.	196
7.12	One-parameter bifurcation diagram for p_{max} with $d_{SL} = 0.4$ and $A_{thr} = 5$	198
7.13	Time plots of budworm larval density for (a) $p_{max} = 0.6 \times 23\ 000$ and (b) $p_{max} = 3.4 \times 23\ 000$	200
7.14	Two-parameter bifurcation diagram of p_{max} versus d_{SL}	201
A.1	Time plots and a phase portrait showing the domain of attraction of an equilibrium point.	219
A.2	Phase portrait showing the domains of attraction of equilibrium points in two dimensions.	220
A.3	Hard loss of stability.	221
A.4	Example of a heteroclinic orbit.	222
A.5	Example of a homoclinic orbit.	223
A.6	A bifurcation diagram of a Hopf bifurcation and phase portraits corresponding to different parameter values.	224
A.7	Bifurcation diagram of a Hopf bifurcation where the periodic orbits are unstable.	225
A.8	Bifurcation diagram of hysteresis.	226
A.9	(a) Time plot and (b) phase portrait of limit cycle behaviour.	227
A.10	(a) Bifurcation diagram showing a limit point and (b) a phase portrait corresponding to $\mu = \mu_1$	228
A.11	(a) Period-doubling bifurcations at λ_1 and λ_2 . (b) Behaviour over time for the state variable x_1	230
A.12	Derivation of a phase plane showing the time-dependent behaviour of two variables, x_1 and x_2	231

A.13 (a) Bifurcation diagram of a pitchfork bifurcation and phase portraits corresponding to different parameter values.	232
A.14 Example of a saddle point.	233
A.15 Phase portraits and time plots of a stable node and a spiral attractor. . .	234
A.16 Phase portraits and time plots of an unstable node and a spiral repeller.	235
A.17 (a) A bifurcation diagram of a transcritical bifurcation and phase portraits corresponding to different parameter values.	236
A.18 A summary of the local stability behaviour near an equilibrium point of the continuous system when $m = 2$	240
A.19 (a) Two-parameter bifurcation diagram showing a cusp point and the positions of the two limit points associated with the hysteresis as both μ and λ are varied. (b) One-parameter bifurcation diagrams corresponding to different, fixed values of λ in part (a) and with μ as the bifurcation parameter.	243
A.20 (a) Phase portrait of a saddle connection or heteroclinic orbit. (b) Phase portrait of a saddle loop or homoclinic orbit.	244
A.21 (a) Phase portraits for parameter values near a saddle connection or heteroclinic orbit. (b) Phase portraits for parameter values near a saddle loop or homoclinic orbit.	245
A.22 Phase portraits near a saddle loop or homoclinic orbit showing possible behaviour near the second equilibrium point.	246
A.23 Schematic representation of a Poincaré section and a limit cycle in three dimensions.	248
A.24 Examples of Hopf bifurcations.	249
A.25 State space diagrams of a spiral sink for (a) a continuous model and (b) a discrete model.	252

A.26 (a)One-parameter bifurcation diagram showing period-doubling bifurcations at $\mu = \mu^*_1$ and $\mu = \mu^*_2$ for a discrete system. (b)State space diagrams showing the dynamics at $\mu = \mu_1$, $\mu = \mu_2$ and $\mu = \mu_3$	253
A.27 Time plot of a period-2 orbit.	254
A.28 (a)State space diagram showing an invariant circle. (b) Time plot of the situation in (a) in terms of x_1	255
A.29 Possible results of perturbing transcritical and pitchfork bifurcations. . .	256

Acknowledgements

I could not have researched and written this thesis without the help of numerous people. Foremost among these I would like to thank my supervisor, Don Ludwig, most sincerely for his invaluable suggestions and guidance. I benefited greatly from his experience in both mathematical and ecological disciplines. I would also like to thank Gene Namkoong for suggesting the population genetics models and for giving me both direction and encouragement while I studied them. I am indebted to Bard Ermentrout for writing the package XPPAUT and making it freely available. His suggestions and interest in the project were also greatly appreciated. I am also grateful to Colin Clark, Wayne Nagata, Gene Namkoong and James Varah for reading a previous version of the manuscript and for their numerous helpful comments and suggestions.

There are many others who responded to questions and email messages or provided general encouragement: Leah Edelstein-Keshet, John Hearne, Johan Swart, and also Peter Abrams, Eugene Allgower, Alan Berryman, Eusebius Doedel, Lev Ginzburg, John Guckenheimer, Andrew Gutierrez, Alexander Khibnik, Lixin Liu, Jesse Logan, Peter Turchin, Graeme Wake and Peter Yodzis. Thank-you for your time and your interest. Thank-you also to my fellow graduate students in the Mathematics department for empathising with me through the frustrations which accompany most graduate studies.

A very special thank-you to my family and non-mathematics friends for your endless encouragement and interest. Your support was a continual source of strength to me.

Finally, I would like to acknowledge the Emma Smith, Oppenheimer and I.W. Killam Trusts for their financial support which made my studies at U.B.C. possible.

Chapter 1

Introduction

1.1 General overview

In this thesis I demonstrate how techniques from dynamical systems theory can be applied to ecological models in order to study their qualitative behaviour. The techniques allow one or two parameters to be varied across ranges of values so that a comprehensive picture of their effects on the behaviour of the model can be determined. Since computer software is used to take care of the mathematical details, both mathematicians and ecologists can make use of these techniques. I hope to reach the latter group in particular, by showing how dynamical systems theory can increase our understanding of the behaviour of a model considerably and thus help us formulate more plausible models. Both continuous and discrete models are considered.

In the next section I outline my objectives more formally. I then describe how I go about fulfilling these aims with specific references to later chapters in the thesis. I conclude this introduction with a discussion of why I chose this topic and its place amongst current areas of research.

1.2 Research objectives

Ecological models and qualitative analyses of these models can give insight into the most important mechanisms at work in an ecological system. However, the mathematics required for a detailed analysis of the behaviour of a model can be formidable. Because

of the uncertainty associated with parameter values in nature, solving a system of model equations for a fixed parameter set is insufficient. A more informative approach is to study the behaviour of a model for *ranges* of parameter values, but this requires complicated mathematical techniques. It would be of considerable interest, particularly to ecologists, if some of these techniques could be applied without the requirement of further formal mathematical training.

With the above in mind the main aims of my thesis are twofold:

- to provide examples of the usefulness of dynamical systems theory in analysing the behaviour of ecological models—in particular those techniques which describe the effects of varying parameters across ranges of values, and
- to demonstrate how certain computer packages can aid the analysis by taking care of the mathematical details.

In applying these aims I uncovered biological implausibilities in two models and improved on previously obtained approximate results in another. The techniques also highlighted some limitations of more traditional methods of analysis.

The computer packages I used are DSTOOL [10], Interactive AUTO [117] and XPPAUT [35]. Descriptions of their capabilities, as well as suggestions regarding their use, are included in appendix B together with references to a few other packages that are available.

1.3 Thesis outline

My approach to achieve the above aims was to analyse ecological models—both continuous and discrete—to demonstrate the kinds of results and information that can be obtained using dynamical systems techniques.

I begin in chapter 2 with the analysis of three fairly simple predator-prey models which have already been studied by Bazykin [14]. This chapter is intended as an introduction to some of the terminology and techniques of dynamical systems theory as well as to the use of the available computer packages. Bazykin [14] studied the models analytically. The computer packages allowed me, a novice, to reproduce and in fact improve upon his results. The chapter also illustrates how the computer packages can encourage an iterative approach to modelling which may aid the development of more plausible models.

Having demonstrated the reliability of some of the computer software in chapter 2, I wanted to apply the techniques to a few more recent models from the literature. Since a number of theoretical models have been studied using dynamical systems techniques (for example, [5, 24, 26, 29, 33, 102]), I wanted to look at a more practical example. In chapter 3 a system dynamics model of a sheep-pasture-hyrax-lynx system is analysed. The model is a large one consisting of 10 ordinary differential equations and numerous parameters. Even the most knowledgeable theoretician would find an analysis of this model using pencil and paper a formidable task. The dynamical systems techniques prove to be a useful alternative to the sensitivity analyses which are traditionally used when studying these models. In particular, an improvement to the formulation of the model is suggested as a result of the analysis.

Chapter 4 returns to a more theoretical model describing a plant, a herbivore and a predator. The model is an example from a controversial area of current research known as ratio-dependent modelling. The analysis in this chapter highlights some of the biological implausibilities and mathematical difficulties associated with ratio-dependent models which may be important for guiding future research. A modification to the model equations is analysed in conjunction with the original model and reveals that the latter is structurally unstable.

Many systems in nature (for example, insects having nonoverlapping generations) are

better represented by discrete models than by continuous ones. However, discrete models tend to exhibit more complex behaviour than continuous ones because of the inherent time delays in the equations [84]. As a result detailed analyses have been restricted mainly to one-dimensional examples (see, for example, [82, 83, 84]) although there are some two-dimensional examples (see [15, 94]). In chapters 5 and 6 I consider two population genetics models which are two-dimensional. Both models have fairly simple mathematical formulations involving only two alleles but they are capable of displaying complicated dynamics. I focus on the dynamics of the heterozygote. The model in chapter 5 has been partially studied using pencil and paper and numerical simulation techniques. However, a more detailed analysis was restricted by the need for more complicated methods to take care of the complex nonlinearities. The dynamical systems techniques demonstrate the theoretical results fairly easily and also show the relative frequency with which different types of qualitative behaviour can be expected to occur. The chapter focusses on periodic dynamics as this behaviour is the most difficult to study by hand. The model in chapter 6 is a modification of that in chapter 5 but it has not been studied in detail before. This is not surprising since it is not even possible to find explicit expressions for the equilibrium points. Computers are particularly useful in such situations. For this model it is found that there is always the possibility of one of the alleles being excluded and that the threat of extinction is high for many parameter sets. Criteria for determining the existence and stability of polymorphic equilibria are given and periodic dynamics are also studied.

To round off the thesis I wanted to see how the dynamical systems techniques would fare in the context of a more practical, and hence more complicated, discrete model. Chapter 7 considers a model of a defoliating insect system, namely the spruce budworm-forest system. Despite the complexity of the dynamics, useful insights are obtained into the mechanisms responsible for insect outbreaks and the relative effects of dispersal and predation. Outbreaks are found to occur for a wide range of parameter values and regions

of multiple stable states are also located.

Specific conclusions relating to the particular examples are included at the end of each chapter. More general conclusions are summarised in chapter 8. Special mention should be made of two of the appendices. Appendix A contains a glossary of the basic dynamical systems concepts which are used in the main body of the thesis, as well as a brief introduction to some of the underlying mathematical theory. Diagrams are used wherever possible so as to keep the mathematical details to a minimum as the appendix is intended for those who may have had little prior exposure to dynamical systems concepts.

Appendix B describes how computers can be used to implement the dynamical systems techniques. Descriptions of the capabilities and relative advantages and disadvantages of the packages that I used, as well as procedures for obtaining time plots, phase portraits and bifurcation diagrams, are given. Some pointers and warnings regarding their use are also included. Examples of computer listings for the various models are placed after the appendices.

I must emphasise that it is not my aim to provide a comprehensive structure whereby every detail of a system of equations can be understood. This would be an impossible task. Instead I want to develop a procedure which can be applied to a wide variety of practical situations. I would like to emphasise the word *practical* since it is very easy for a model analysis to become more of a mathematical exercise than one of biological relevance. Detailed mathematical analyses may require more complicated techniques than I have used in order to study complex phenomena. While these phenomena may be of intellectual interest, they are often of little practical use. My viewpoint is summarised by the following quote from Adler and Morris [2]:

Only by avoiding the unthinking use of familiar and mathematically convenient models and by having the discipline to ignore interesting but dynamically unimportant interactions, can we ever hope to develop predictive ecological theory.

1.4 Motivation

Mathematical models have been used to describe ecological systems for many decades. However, the interdisciplinary nature of the field has led to some conflict in opinions. Many experimental ecologists argue that theoretical models are too simple to adequately describe natural systems, but complicated models are often intractable to mathematical analysis. According to Holling *et al.* [62] “a simple but well-understood model is the best interface between a complex system and a complex range of policies.” However, the complexity of ecological systems and the perceived added realism of larger, more complex models has led many ecologists to favour the latter.

Because of the inevitable uncertainty associated with the parameter values in an ecological model [40, 53, 115, 121], it is not sufficient to merely simulate the model equations over time and observe the behaviour. A different set of parameter values may give rise to very different dynamics. According to Walker *et al.* [121] many parameters of ecological models are really variables. They are chosen to be constants for convenience, simplification or because information regarding the relevant dynamics is lacking. Hence, it is important to know whether altering parameter values will significantly affect the predictions of the model. This is not a trivial task when large numbers of parameters are involved.

As has already been mentioned, we can vary parameters across ranges of values using techniques from dynamical systems theory. In this way we can obtain information

regarding the presence and nature of attractors¹ in the system. Whereas transient dynamics vary with the initial values of the state variables and the time period over which solutions are calculated, the techniques in this thesis are concerned with the behaviour of the system once the initial transients have died away. The attractors determine this long-term behaviour. My viewpoint is that these qualitative analyses of ecological models are indispensable if we hope to use the models to gain insight into real ecological systems.

The application of the dynamical systems techniques to a system of nonlinear equations can be a formidable task for a mathematician, let alone a non-mathematician. It is also time-consuming when a large number of parameters is involved. In such circumstances computer programs can be of great assistance. In fact, Seydel [111] asserts that “the extensive application of numerical methods is indispensable for practical bifurcation and stability analysis”. Although analytical methods can provide remarkable results, they have two strong limitations [111]. First, in many cases numerical methods are needed to evaluate analytical expressions anyway. And secondly, analytical results are generally local and only hold for ‘sufficiently small’ distances where ‘sufficiently small’ is left unclarified. Fortunately a number of computer packages have become available in recent years to aid the analysis. A few of these have already been mentioned.

It is one matter to do the analysis but we also need to convey the results effectively. Edelstein-Keshet [34] comments that pictures derived from qualitative analyses are often more informative than mathematical expressions. In this thesis the traditional time plots and phase portraits are used to display results as well as bifurcation diagrams. The latter diagrams provide a concise way of summarising the effects of different parameter values on the behaviour of the system.

¹See section A.2.5 for a definition of this term.

1.5 The bigger picture

Qualitative analyses are not new and can be traced back at least to Poincaré². In ecological circles names such as Lotka and Volterra [73, 120], Rosenzweig and MacArthur [76, 103], Holling [61], May [79, 80, 82, 83] and Gilpin [44], and many others, are well-known for their qualitative analyses of various models. Most studies have involved predator-prey models [14, 44, 79, 80, 98] but other systems have also been analysed [50, 70, 74, 83, 95]. However, all these models are fairly simple theoretical models because of the mathematical difficulties encountered with more complicated models.

The introduction of various computer packages since the mid-1980's has allowed dynamical systems techniques to be applied with greater ease as well as to more complicated models. However, there are relatively few examples where ecological models have been studied using these packages and most of the papers in this category are very technical and require considerable mathematical knowledge [5, 26, 29, 33, 48, 86, 87, 102]. Few people have heeded the suggestion by Oster and Guckenheimer [97] that less exhaustive analyses but of more meaningful models (from a biological viewpoint) would be more useful and of greater interest to biologists.

The papers by Collings [23], Collings and Wollkind [24], Collings *et al.* [25] and Wollkind *et al.* [127] study a fairly practical biological control model of mite interactions. However the mathematics is still complicated and difficult for the reader with little prior exposure to dynamical systems theory. Of particular relevance to this thesis is that these papers demonstrate the power of the computer package AUTO86 [28] and illustrate how conclusions regarding model sensitivity and resilience can be drawn from bifurcation diagrams. They also derive meaningful ecological implications from their results. All four

²A Hopf bifurcation (see section A.2.10), which is an important concept in dynamical systems theory, is also known as a Poincaré-Andronov-Hopf bifurcation and the Poincaré-Bendixon theorem is fundamental to qualitative analyses. Further details can be found in Arnold [7] and Wiggins [124].

papers note that many of their conclusions would not have been obtained without the use of AUTO86 [28]. In particular, Collings and Wollkind [24] obtained three previously undiscovered possibilities for qualitative behaviour using a predator-prey model of the type studied by Bazykin [14].

In this thesis I hope to take the road less travelled by showing how dynamical systems techniques can lead to biologically useful and meaningful results *without* the requirement that the user have an extensive mathematical background in the field. I begin in the next chapter with a few models that have already been studied using pencil and paper and show what I was able to accomplish with the aid of computer packages.

Chapter 2

Preliminary Example

2.1 Introduction

This chapter is for readers for whom concepts such as bifurcations and bifurcation diagrams are relatively new as well as for those who are sceptical about the accuracy and reliability of computer packages such as DSTOOL [10], Interactive AUTO [117] and XPPAUT [35]. Dynamical systems techniques are applied to three fairly simple predator-prey models to show how certain parameter values affect the qualitative behaviour of the models. Both one- and two-parameter bifurcation diagrams are used to summarise the results. Behaviour in different regions of these diagrams is explained using phase portraits. The three models differ from one another by the addition or subtraction of only one or two terms. This chapter therefore exemplifies an iterative approach to modelling—the relative ease with which qualitative analyses may be done using the abovementioned computer packages allows a fairly quick determination of the effects of model alterations. This can facilitate the formulation of more plausible models.

These predator-prey models have already been studied analytically by Bazykin [14]. I have included his results for comparison with those obtained by the computer software. The latter are in fact more accurate in certain situations and the results can be obtained without a detailed knowledge of the underlying mathematical techniques.

I begin the chapter with a description of the first model which is a basis for the other two. I use XPPAUT to obtain a one-parameter bifurcation diagram and show how

this summarises Bazykin's results. The next two sections discuss two modifications to the basic model. Many of the phenomena that occur in later chapters of the thesis are introduced here. For those who plan to read this chapter, a quick reading of the first part of appendix A (namely, section A.2) may prove useful. This section is non-technical but introduces all the basic terminology as well as the conventions I use in the figures.

2.2 Basic model

One of the first predator-prey models to be proposed and extensively studied was the model developed independently by Lotka and Volterra in the 1920's (see [34] for a description of the model and its analysis). The model equations are

$$\begin{aligned}\dot{x} &= ax - bxy \\ \dot{y} &= -cy + dxy\end{aligned}\tag{2.1}$$

where x represents prey density and y predator density. All the parameters are real and positive. The term ax describes the exponential growth of the prey population in the absence of predators and $-cy$ describes the exponential decline in the predator population in the absence of prey. The terms $-bxy$ and dxy describe the interaction between predator and prey. From a biological viewpoint, this linear dependence of the rate of predation and predator reproduction on the number of prey is considered to be a rather unrealistic approximation [14]. Also, from a mathematical viewpoint, the system is structurally unstable since an arbitrarily small perturbation to the model can change its qualitative dynamics. For example, replacing the exponential growth of the prey with logistic growth changes the dynamics from (neutral) cycles to a stable equilibrium (see [34]).

A number of modifications to this model have been studied since the 1920's. In particular, Bazykin's [14] work is well-known among ecologists because of his comprehensive

qualitative analyses of the models and his accompanying diagrams, which summarise the different possible behavioural regimes. One of Bazykin's modifications to the Lotka-Volterra equations (2.1) is given by the system

$$\begin{aligned}\dot{x} &= ax - \frac{bxy}{1+\alpha x} \\ \dot{y} &= -cy + \frac{dxy}{1+\alpha x}.\end{aligned}\tag{2.2}$$

He justified using Michaelis-Menten interaction terms by analogy with the mechanism of enzyme reactions. The denominators of these terms prevent unlimited predation of prey and unlimited growth of the predator population with the growth of prey density, respectively. The Holling type II functional response term is very similar to these terms and is based on biological mechanisms [59, 60].

Before we can apply the dynamical systems techniques we need to choose parameter values. I chose $a = 0.6, b = 0.3, c = 0.4, d = 0.2$ and $\alpha = 0.1$ but any other reasonable values would do. Using XPPAUT (DSTOOL could also have been used) I found that there is only one non-trivial (that is, non-zero) *equilibrium point* (see section A.2.6 for an explanation of this phenomenon) corresponding to these parameter values and that it is *unstable* (see section A.2.14 for an explanation of this term). Using this equilibrium point as a starting value for AUTO (either Interactive AUTO or XPPAUT can be used—see appendix B) I varied α to obtain the *one-parameter bifurcation diagram* (see section A.2.1) shown in figure 2.1. As can be seen from this figure, there are no *bifurcations* (see section A.2.2) and the equilibrium point remains unstable as α is varied. But the figure does show how the equilibrium value of x changes with α . We can also view this diagram in terms of y and α using XPPAUT. The diagram is exactly the same as figure 2.1 because of the symmetry of the equilibrium point with respect to x and y .

Using DSTOOL or XPPAUT we can generate *phase portraits* (see section A.2.17) for different values of α . These are qualitatively the same as those obtained by Bazykin [14]

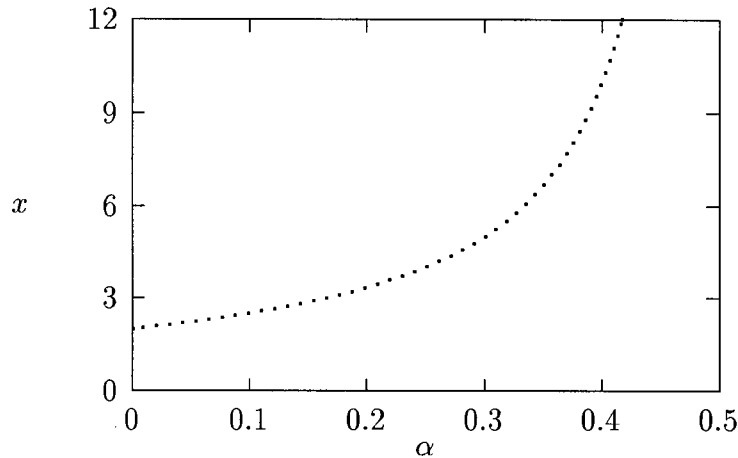


Figure 2.1: One-parameter bifurcation diagram obtained by varying α in system (2.2) with $a = 0.6, b = 0.3, c = 0.4$ and $d = 0.2$. The state variable x is plotted on the y-axis.

(see figure 2.2) and verify that figure 2.1 summarises Bazykin's [14] results. The phase portraits in figure 2.2 show that x increases indefinitely for all values of α . This is an obvious shortcoming of the model and led Bazykin to introduce further modifications.

2.3 Adding intraspecific competition among prey

To improve the model Bazykin added a term to the prey equation to take into account intraspecific competition among prey. Here competition refers to a decrease in reproduction or an increase in death rate with an increase in prey density. The assumption that competition is linearly dependent on prey density results in the system of equations

$$\begin{aligned}\dot{x} &= ax - \frac{bxy}{1+\alpha x} - \epsilon x^2 \\ \dot{y} &= -cy + \frac{dxy}{1+\alpha x}.\end{aligned}\tag{2.3}$$

We can create *one- and two-parameter bifurcation diagrams* (see section A.2.1 for a description of these terms) by varying α and ϵ to see what effects these additional terms have on the behaviour of the model. I chose the same values for a, b, c and d as before.

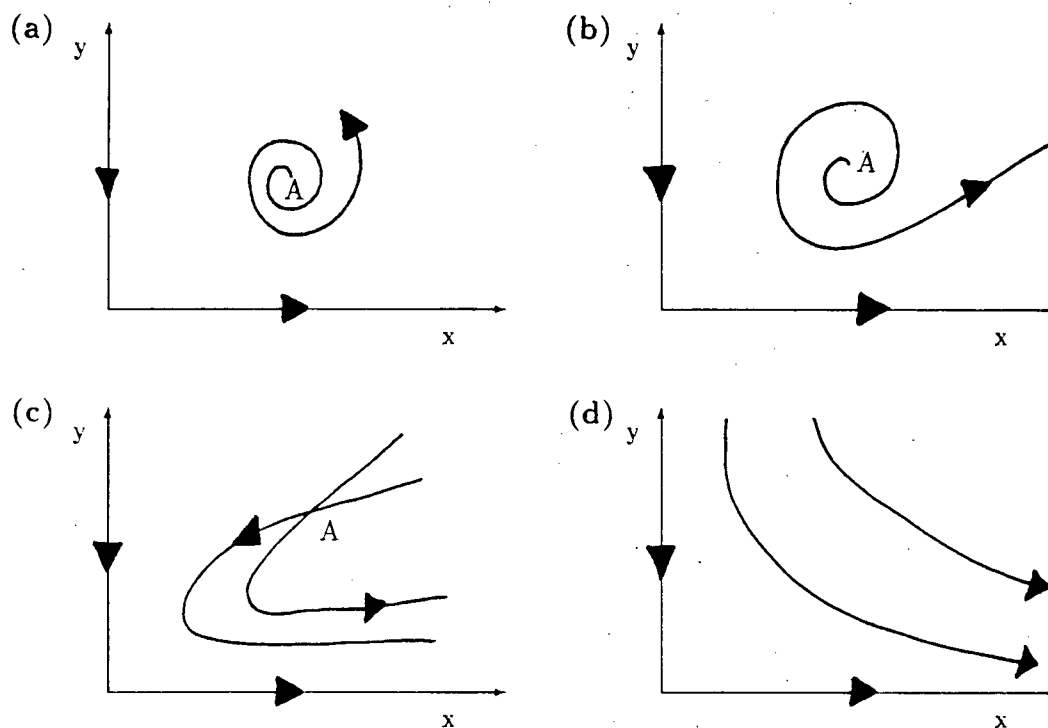


Figure 2.2: Phase portraits obtained by Bazykin for model (2.2). Qualitatively similar diagrams can be obtained by taking $a = 0.6$, $b = 0.3$, $c = 0.4$, $d = 0.2$ and (a) $\alpha = 0.1$, (b) $\alpha = 0.2$, (c) $\alpha = 0.3$ and (d) $\alpha = 0.55$.

Bazykin's [14] results for this system are shown in figure 2.3. There are three regions in (ϵ, α) -parameter space, each corresponding to a different form of qualitative behaviour. The phase portraits indicate the dynamics that occur in these regions. Since there are two equilibrium points of interest, A and B, in regions (i) and (ii) and one equilibrium point of interest, B, in region (iii)¹ we expect a bifurcation to occur as the line with negative slope in figure 2.3(a) is crossed from regions (i) and (ii) into region (iii). In crossing from region (i) to region (ii) point A changes from stable to unstable and a *limit cycle* (see section A.2.12) is initiated. Thus, we expect a curve of *Hopf bifurcations* (see

¹The origin is also an equilibrium point in both cases but only nontrivial equilibrium points having $x \geq 0$ and $y \geq 0$, $(x, y) \neq (0, 0)$ are considered in detail. In region (iii) $y < 0$ at the equilibrium point A and hence this point is not of biological interest.

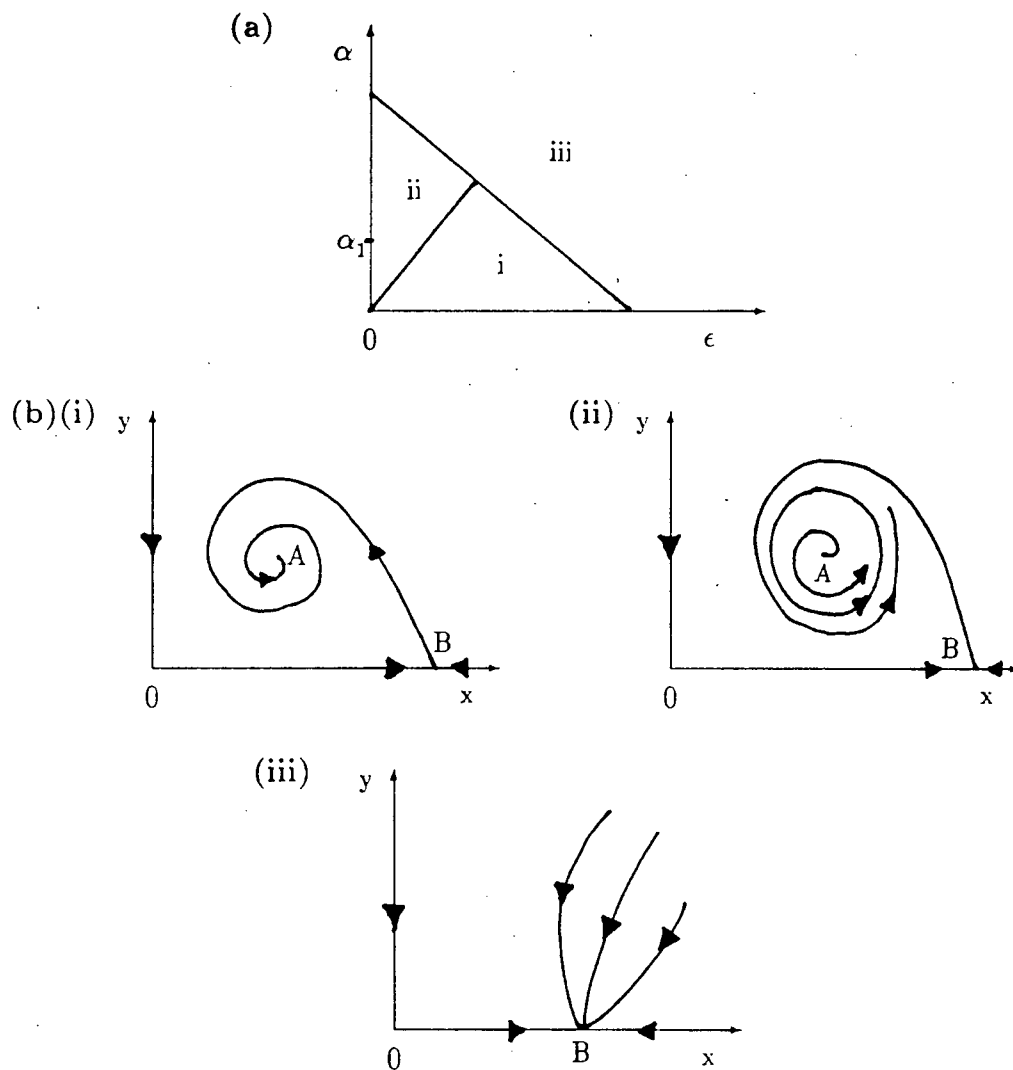


Figure 2.3: The following diagrams are adapted from Bazykin [14]. (a) Two-parameter bifurcation diagram of (ϵ, α) -parameter space. (b) Phase portraits corresponding to regions (i), (ii) and (iii) in part (a).

section A.2.10) to divide these regions.

In order to use AUTO to reproduce Bazykin's results we need a starting point which must be an equilibrium point. By choosing values of 0.3 for α and 0.1 for ϵ , we can either determine such a point analytically (as Bazykin did) or we can use DSTOOL or XPPAUT to perform the task numerically. The latter choice involves integrating the equations forward in time until we are near the equilibrium point. Using XPPAUT this is done by choosing the menu option INTEGRATE followed by GO. Choosing the SINGular POINT option then finds the equilibrium point and indicates whether it is stable or unstable. A separate window appears with this information. The state variable values at the equilibrium point are then entered as the initial point in the initial point window.

Since Bazykin plotted ϵ on the x-axis in figure 2.3(a) I vary this parameter first. In AUTO this is done by choosing ϵ to be the main parameter in the AXES menu. After choosing the RUN-STEADYSTATE commands, AUTO locates a *transcritical bifurcation* (see section A.2.25) at $\epsilon = 0.12$ (see figure 2.4). I then made the value of DS in the NUMERICS window negative so that AUTO would decrease ϵ , chose the point labelled 1 (that is, chose our original starting point) using the GRAB command, and then chose RUN again. AUTO finds a Hopf bifurcation at $\epsilon = 0.045$ in this case. By generating periodic orbits (limit cycles) from this latter point (choose the Hopf bifurcation point using GRAB and then RUN-PERIODIC ORBIT) we can see that there are stable limit cycles surrounding an unstable equilibrium point. Since α is fixed in figure 2.4, this one-parameter diagram describes the dynamics along a horizontal line at, say, $\alpha = \alpha_1$ in figure 2.3(a).

In figure 2.4 I have labelled the *continuation branches* A and B to indicate which equilibrium point corresponds to which branch (see section A.2.4 for a description of a continuation branch). Notice that the x-coordinate of A does not vary with ϵ but the

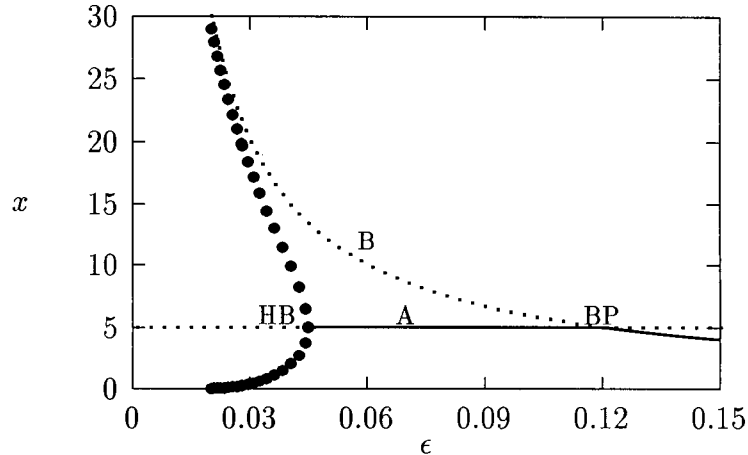


Figure 2.4: One-parameter bifurcation diagram obtained by varying ϵ in system (2.3) with $a = 0.6, b = 0.3, c = 0.4, d = 0.2$ and $\alpha = 0.3$. The labels A and B mark the continuation branches corresponding to the equilibrium points given in equations 2.4, HB stands for Hopf bifurcation and BP for bifurcation point (transcritical in this case). Explanations of the various line types can be found in section A.2.1. In particular, the curves of solid circles mark the maxima and minima of stable limit cycles.

x-coordinate of B does. We can check this observation with the analytical forms of the equilibrium points which are given by

$$\begin{aligned}
 A & \left(x = \frac{c}{d - \alpha c}, y = \frac{d a (d - \alpha c) - \epsilon c}{b (d - \alpha c)^2} \right) \\
 B & \left(x = \frac{a}{\epsilon}, y = 0 \right).
 \end{aligned}
 \tag{2.4}$$

These are obtained by setting the right hand sides in equations (2.3) equal to zero and solving for x and y . As expected, ϵ does not appear in the x-coordinate for A but does appear in that for B.

Figure 2.4 summarises the information given by the phase portraits in figure 2.3. For $0 < \epsilon < 0.045$ point A is unstable (a *source*—see section A.2.23) and B is a *saddle point* (see section A.2.20). There is also a stable limit cycle surrounding A. Hence, these values of ϵ correspond to region (ii) in figure 2.3. For $0.045 < \epsilon < 0.12$ A is a stable equilibrium

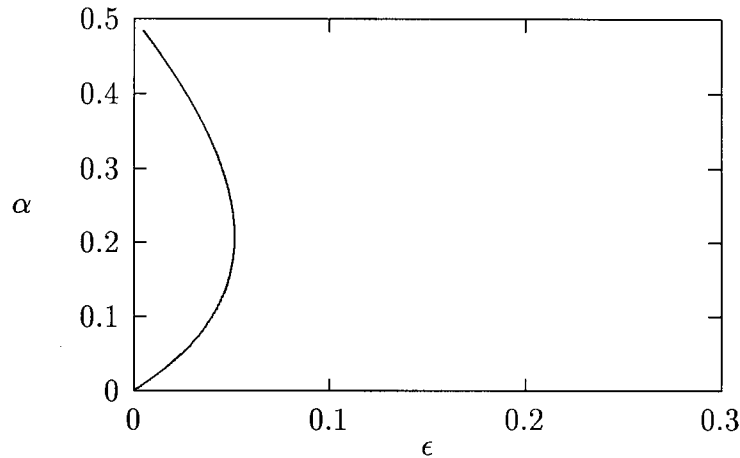


Figure 2.5: Two-parameter continuation of the Hopf bifurcation shown in figure 2.4.

point and B is again a saddle point. This configuration corresponds to region (i) in figure 2.3. For $\epsilon > 0.12$ B is now stable and A is a saddle point, but the numerical output from AUTO shows that the y-coordinate for A is negative for these values of ϵ . Figure 2.3(b)(iii) represents the corresponding dynamics for positive x and y .

We would also like to reproduce Bazykin's two-parameter bifurcation diagram shown in figure 2.3(a). AUTO can be used to continue the Hopf bifurcation at $\epsilon = 0.045$ in α as well as ϵ (see section B.4 for an explanation of how to generate a two-parameter bifurcation diagram). The result is figure 2.5.

The first observation we can make from this diagram is that the curve of Hopf bifurcations is very different from Bazykin's straight line in figure 2.3(a). I will return to this point shortly. A second observation is that, for the given values of a, b, c and d , a Hopf bifurcation (and hence limit cycle behaviour) is only possible if $\epsilon < 0.0515$ and $\alpha < 0.5^2$,

²AUTO slows down considerably as α increases toward 0.5 and ϵ tends to 0 and never actually reaches this point, although the curve does get very close if AUTO is left to run for a sufficiently long time period. It can be verified analytically that the curve does pass through (0,0.5). However, complex behavioural changes occur at this point which is why AUTO has computational difficulties.

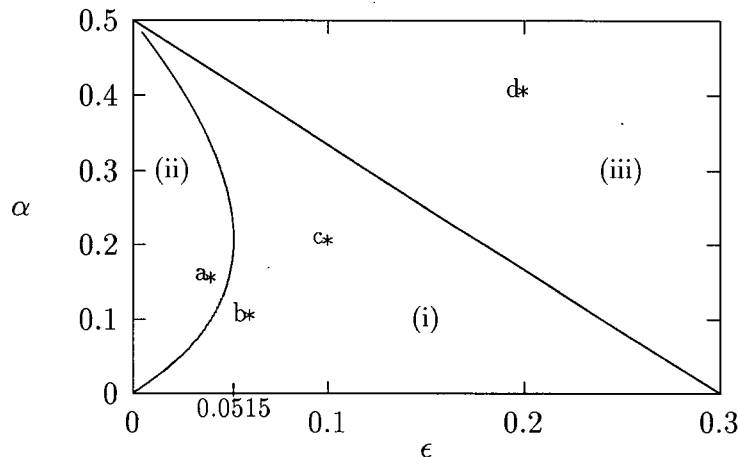


Figure 2.6: Two-parameter bifurcation diagram of (ϵ, α) -parameter space for model (2.3) with $a = 0.6$, $b = 0.3$, $c = 0.4$ and $d = 0.2$. The regions (i), (ii) and (iii) correspond to those in figure 2.3.

which is a fairly small region of parameter space.

It is not possible to continue a transcritical bifurcation in two parameters using AUTO (see page 267 for an explanation). However, if α is fixed at a number of different values and one-parameter bifurcation diagrams similar to figure 2.4 are created by varying ϵ in each case, then the values corresponding to transcritical bifurcations can be recorded. An approximation to the two-parameter curve can then be drawn through these points. Figure 2.6 shows the resulting curve together with the Hopf bifurcation continuation.

Model (2.3) is simple enough for the curves in figure 2.6 to be determined analytically although the algebra is rather messy. It can be shown that transcritical bifurcations occur along the straight line

$$\alpha = -\frac{\epsilon}{a} + \frac{d}{c}$$

and Hopf bifurcations occur along the curve

$$(-ac^2)\alpha^2 + (acd - \epsilon c^2)\alpha - \epsilon dc = 0.$$

(I used MAPLE [122] for some of the algebraic manipulations required to obtain these

results.) These are exactly the curves shown in figure 2.6 as can be verified by substituting points from the curves calculated by AUTO into the above equations. Hence, AUTO's results are more accurate than those given by Bazykin in figure 2.3(a) for the Hopf bifurcation curve. Bazykin did not have a symbolic package such as MAPLE available and made an approximation in calculating this curve. The new regions (i), (ii) and (iii) are shown in figure 2.6. I obtained phase portraits corresponding to the points marked with *'s using DSTOOL (see figure 2.7). XPPAUT could also have been used. These phase portraits are qualitatively the same as Bazykin's diagrams in figure 2.3(b).

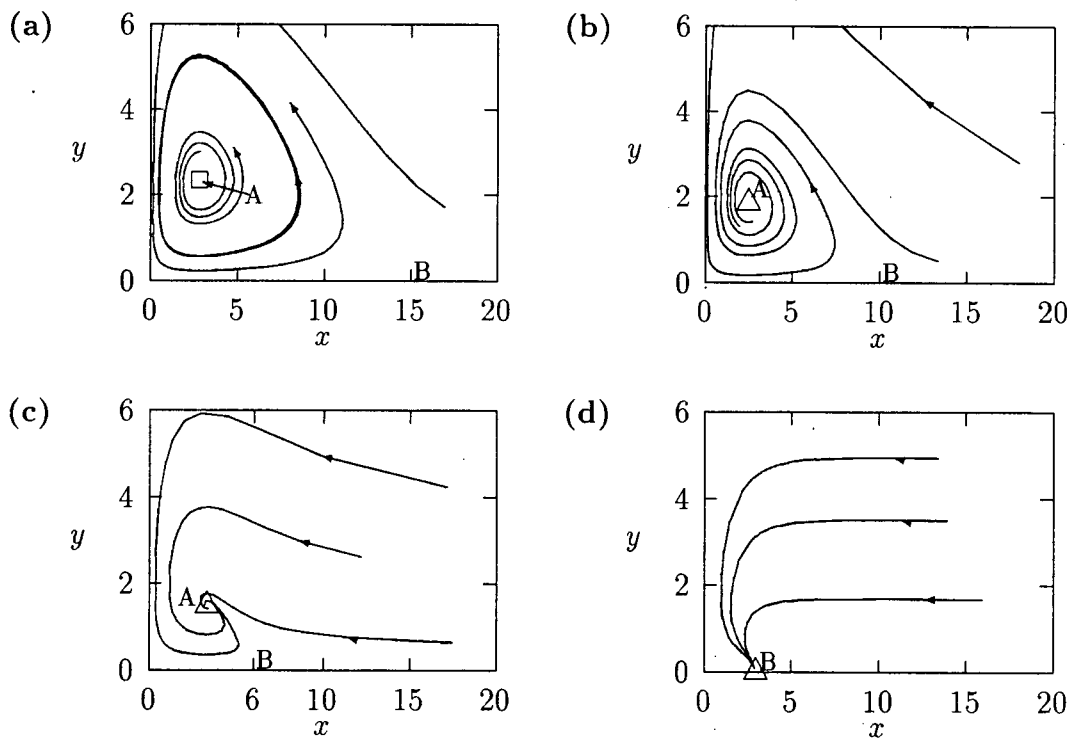


Figure 2.7: Phase portraits corresponding to the points marked with *'s in figure 2.6.

It is also informative to view the temporal dynamics of a model. Time plots corresponding to figure 2.7 for initial values $x = 10$ and $y = 3$ are shown in figure 2.8. These were also obtained using DSTOOL. Time plots are useful for indicating the speed with

which the stable equilibrium or limit cycle is attained and the period of the limit cycle if applicable. If a system takes a long time to approach an *attractor* (see section A.2.14) then the transient dynamics may be of greater practical importance than the long-term behaviour.

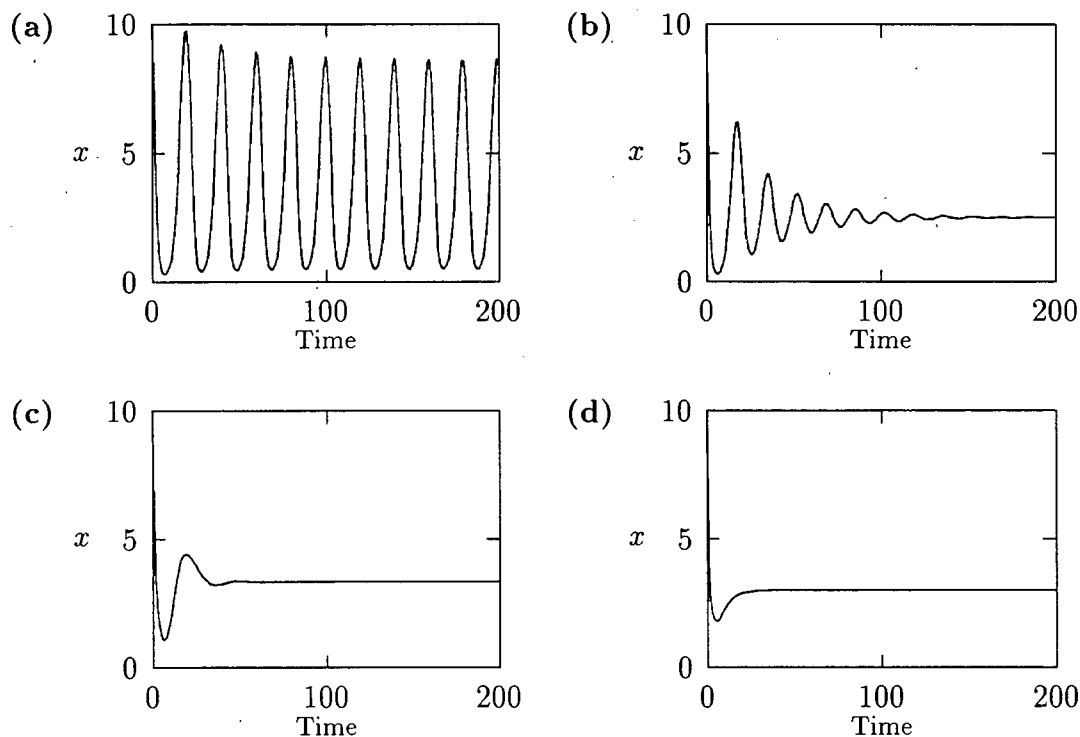


Figure 2.8: Time plots corresponding to the phase portraits in figure 2.7. The initial point $x = 10, y = 3$ was used in each case.

This section has shown how to rederive Bazykin's work [14] on the system of equations (2.3) more accurately and without having to understand the complicated mathematical techniques involved. In the next section I look at another of Bazykin's models in which it is not feasible to do much of the mathematical analysis by hand. Fairly accurate results can be obtained using AUTO.

2.4 Adding intraspecific competition among predators

Suppose that instead of having intraspecific competition among prey we have intraspecific competition among predators. The new system of equations is then

$$\begin{aligned}\dot{x} &= ax - \frac{bxy}{1+\alpha x} \\ \dot{y} &= -cy + \frac{dxy}{1+\alpha x} - \mu y^2.\end{aligned}\tag{2.5}$$

In this model predator population growth is limited even when there is an excess of prey.

Bazykin's results for this system are shown in figure 2.9. Again there are two nontrivial fixed points, A and C, but in this case both have positive coordinates. Whether we have the situation in figure 2.9(a) or (b) depends on the parameter values for a, b, c and d . Using numerical experimentation Bazykin postulated that both variations are possible [14]. He managed to find an analytical approximation to one of the lines OJ , OG but had not found an approximation to the second at the time of writing his paper.

Setting $a = 0.6, b = 0.3, c = 0.4$ and $d = 0.2$ as before and choosing $\mu = 0.06$ and $\alpha = 0.1$, I used DSTOOL to locate equilibrium points and AUTO to generate a one-parameter bifurcation diagram by varying α . The result was figure 2.10. In this case we have a Hopf bifurcation at $\alpha = 0.0977$, a *limit point* (see section A.2.13 for an explanation of this bifurcation point) at $\alpha = 0.176$ and it appears as if the periodic orbit collides with the saddle point C suggesting a *homoclinic bifurcation* (see section A.2.9). All three phenomena can be investigated in two parameters using AUTO. The first two are straightforward two-parameter continuations. Since a homoclinic bifurcation is not actually detected, we need to calculate an approximation to this curve.

As the periodic orbit in figure 2.10 approaches the saddle point it can be seen from AUTO's numerical output that the period of the oscillations increases fairly rapidly. It is possible to plot the period as a function of α if XPPAUT is used (see figure 2.11).

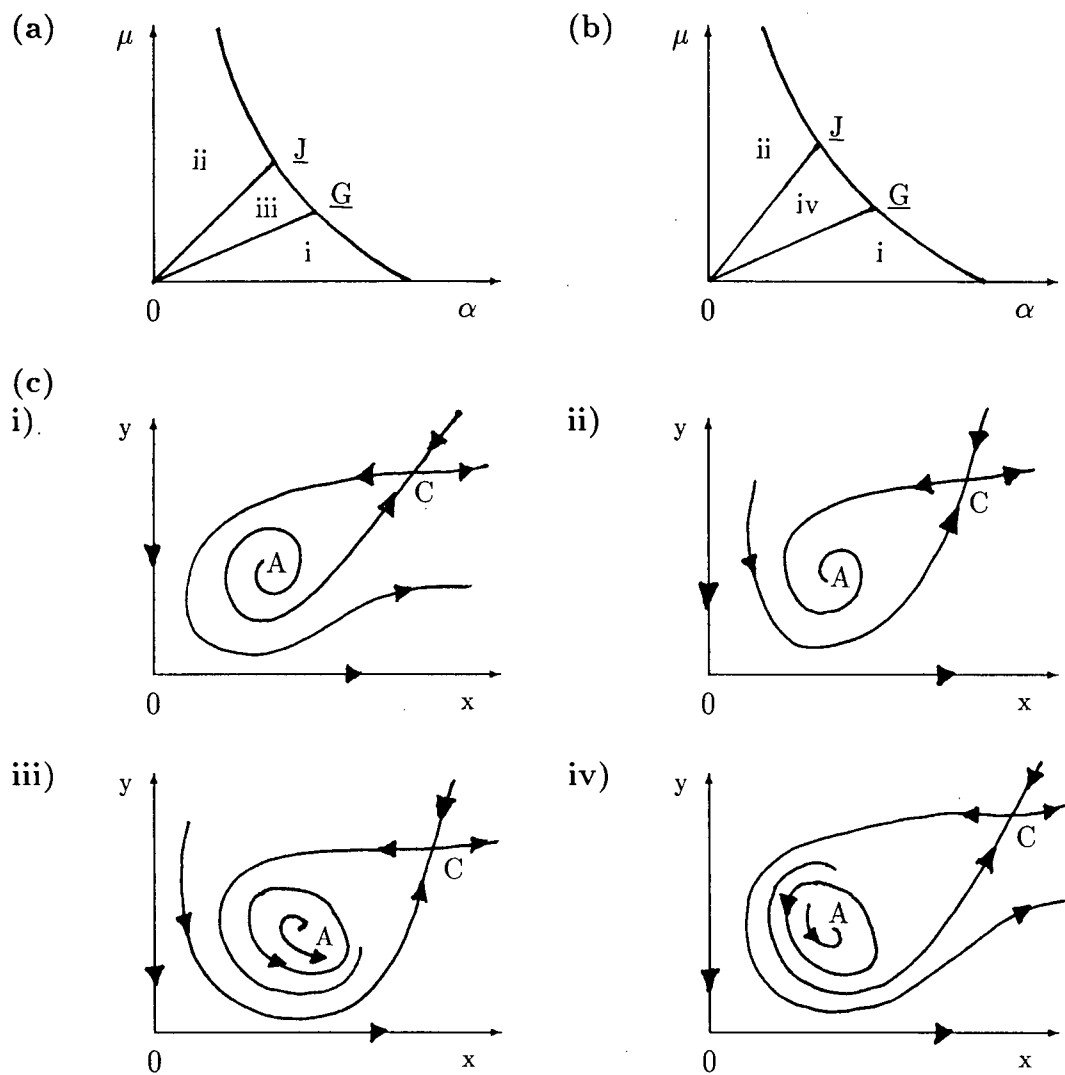


Figure 2.9: These diagrams are adapted from [14]. (a) and (b) Two-parameter bifurcation diagrams of (α, μ) -parameter space. (c) Phase portraits corresponding to regions (i), (ii), (iii) and (iv) in parts (a) and (b).

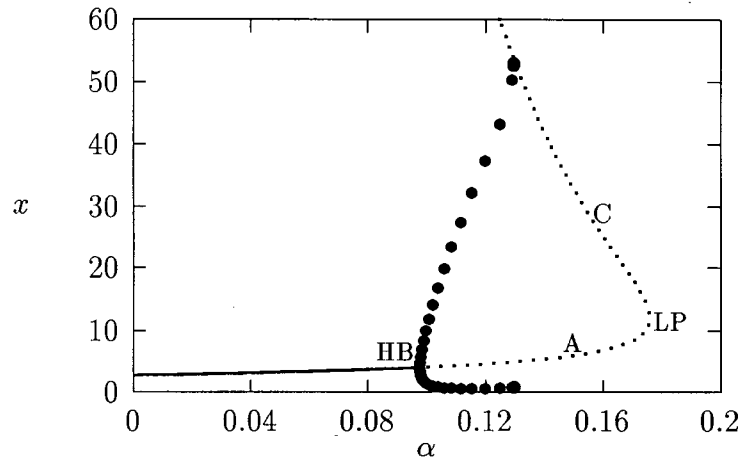


Figure 2.10: One-parameter bifurcation diagram obtained by varying α in system (2.5) with $a = 0.6, b = 0.3, c = 0.4, d = 0.2$ and $\mu = 0.06$. The labels A and C mark the continuation branches for the two nontrivial equilibrium points. HB marks the Hopf bifurcation and LP the limit point.

Such a steep increase in period suggests that a homoclinic orbit is being approached as these orbits have infinite period. To approximate the curve of homoclinic bifurcations we can set a USZR function in AUTO to locate an orbit of high period. The required approximation is obtained by continuing this orbit of fixed period in μ as well as α . The resulting two-parameter diagram in (α, μ) -space is shown in figure 2.12. (I would have liked to have chosen an orbit of period greater than 30 to approximate the curve of homoclinic bifurcations but for this particular model AUTO had difficulty with larger periods. However, one-parameter bifurcation diagrams at different fixed values of μ show that the curve corresponding to a period of 30 provides a fairly good approximation to the required curve.) This figure can be compared with figure 2.9(a). Phase portraits and time plots corresponding to the points marked with *'s in figure 2.12 are shown in figures 2.13 and 2.14 respectively.

These results agree qualitatively with Bazykin's but the approximations to the curves OG and OJ are more accurate. In particular, region (iii) corresponding to stable limit

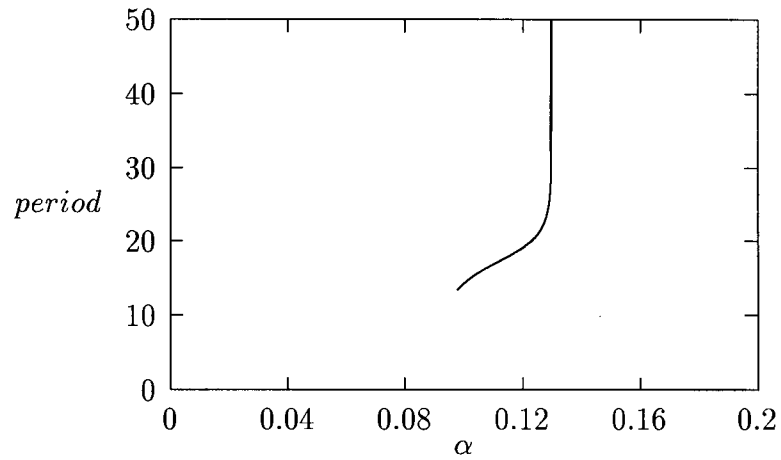


Figure 2.11: Diagram showing the period of the limit cycle oscillations in figure 2.10 as a function of α .

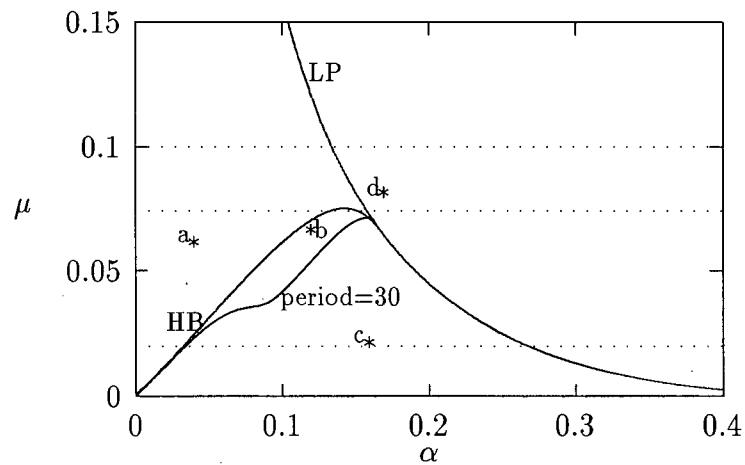


Figure 2.12: Two-parameter bifurcation diagram of (α, μ) -space for $a = 0.6$, $b = 0.3$, $c = 0.4$ and $d = 0.2$. HB marks the Hopf bifurcation continuation, LP marks the limit point continuation and period=30 marks the continuation of the orbit of fixed period.

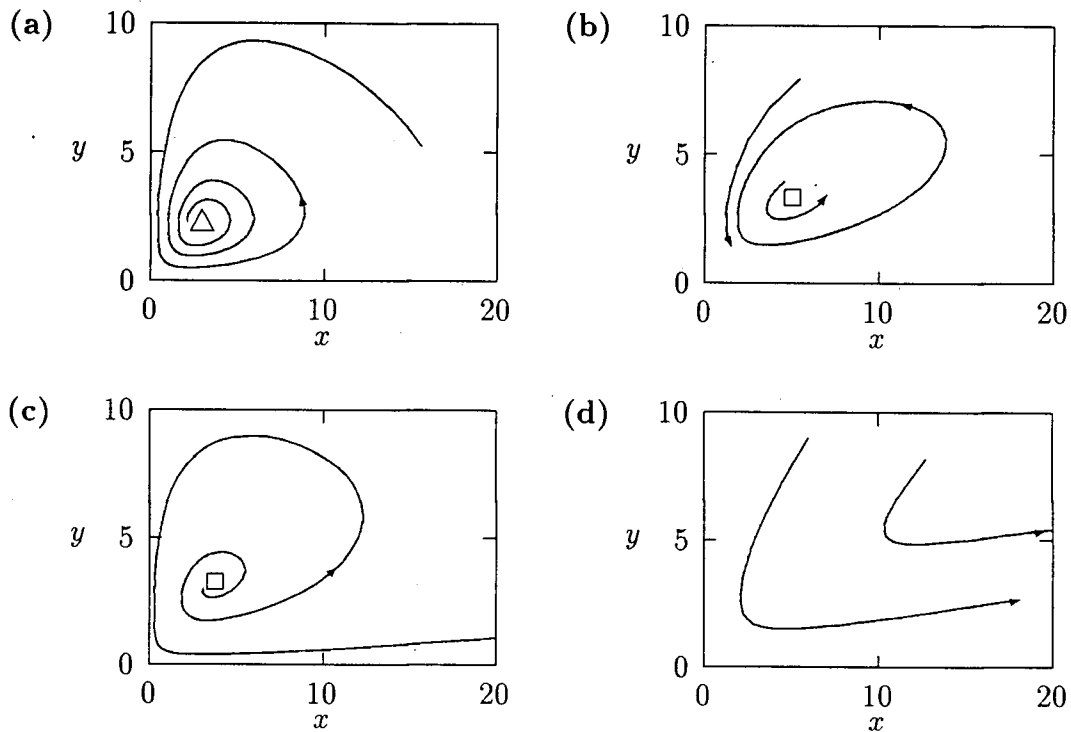


Figure 2.13: Phase portraits corresponding to the points marked with *'s in figure 2.12.

cycle behaviour is very small for these parameter values. As α and μ decrease, the curve of homoclinic bifurcations approaches the Hopf bifurcation curve and almost coincides with it so that for small μ and α the region of limit cycle behaviour is negligible.

We can investigate figure 2.12 further by generating one-parameter bifurcation diagrams for different values of μ . Setting $\mu = 0.1$ gives figure 2.15(a) which corresponds to the horizontal dotted line in figure 2.12 at $\mu = 0.1$. As expected from figure 2.12 there is no Hopf bifurcation or homoclinic bifurcation in this case. For $\mu = 0.074$ we obtain figure 2.15(b) which corresponds to the horizontal dotted line at $\mu = 0.074$. As expected from figure 2.12 there are two Hopf bifurcations in this case but no homoclinic bifurcation. Setting $\mu = 0.02$ results in figure 2.15(c). In this case the curve of periodic orbits is very steep, becomes unstable and then AUTO fails to be able to calculate further and signals

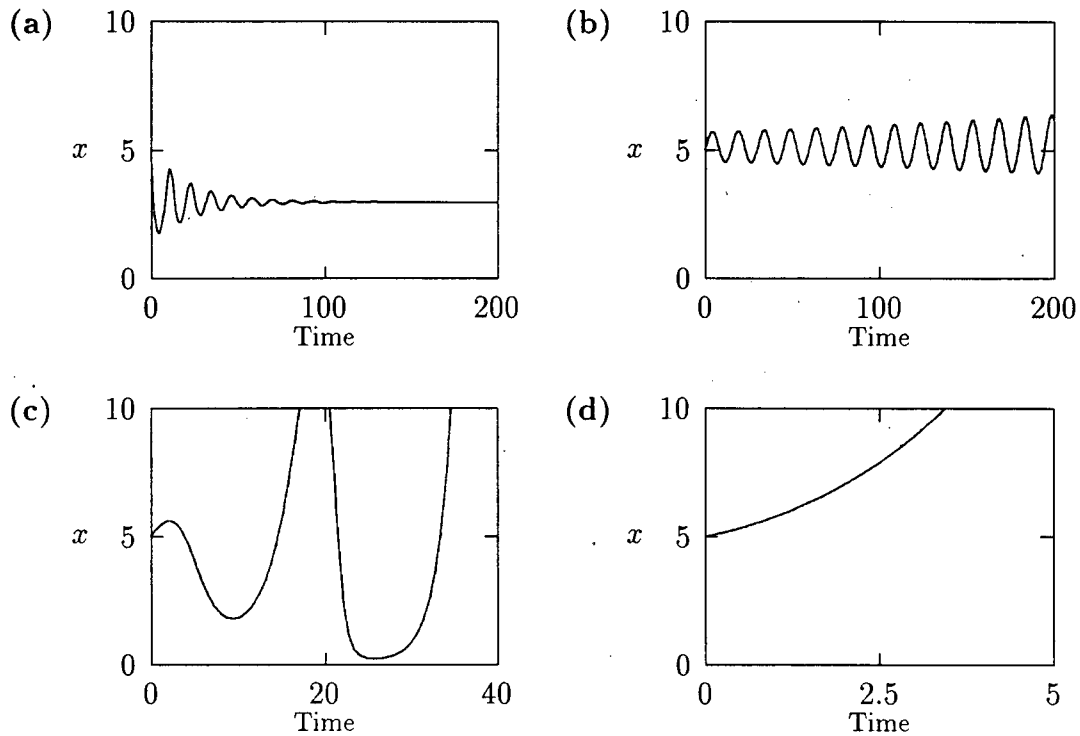


Figure 2.14: Time plots corresponding to the points marked with *'s in figure 2.12. The initial point $x = 5, y = 3$ was used in each case.

non-convergence. This is not unexpected (see the horizontal dotted line in figure 2.12 at $\mu = 0.02$) as the Hopf bifurcation and homoclinic bifurcation curves are very close together for this value of μ .

2.5 Conclusion

This chapter describes how qualitative analyses of three predator-prey models may be done using various computer software. The numerical results are compared with analytical results obtained by Bazykin [14]. For model (2.3) which has intraspecific competition among prey, the numerical results are more accurate than Bazykin's approximate analytic results. This conclusion is possible as I obtained an exact analytical expression for

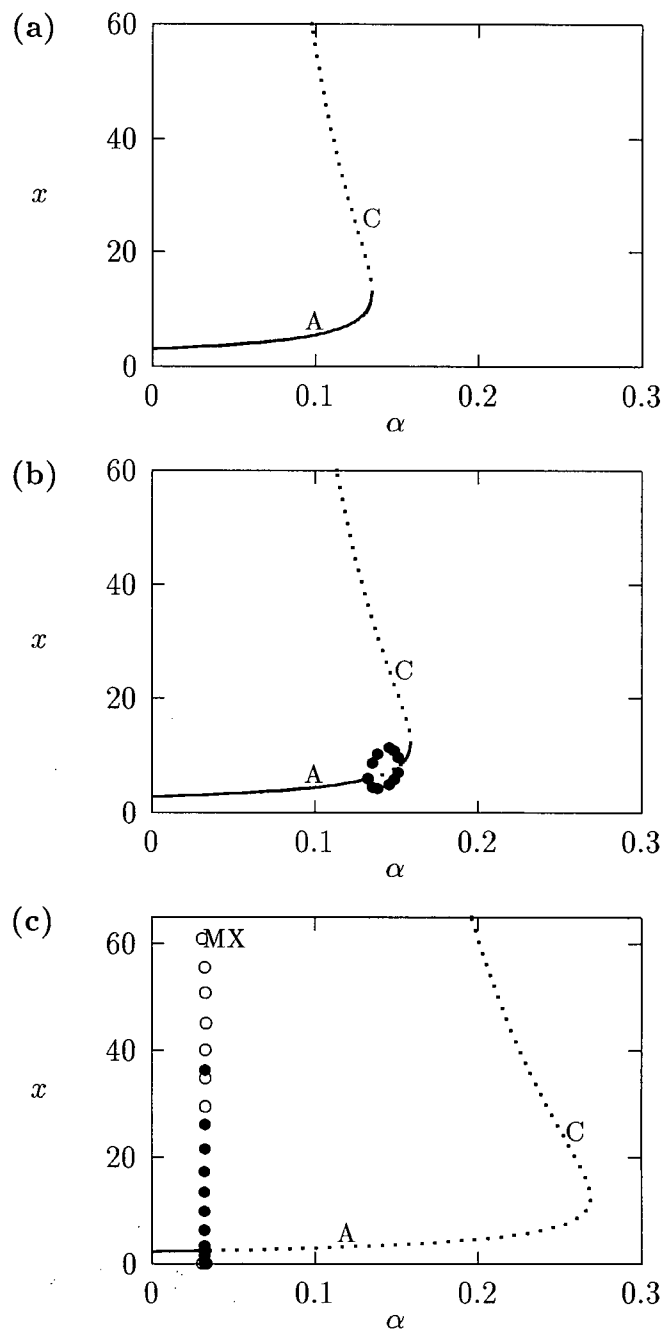


Figure 2.15: One-parameter bifurcation diagrams for (a) $\mu = 0.1$, (b) $\mu = 0.074$ and (c) $\mu = 0.02$. These correspond to the horizontal dotted lines in figure 2.12.

the two-parameter Hopf bifurcation curve for which the discrepancy in results arises. The analysis of model (2.5) results in a numerical approximation to a curve which Bazykin did not describe analytically. The position of this curve results in a very small two-parameter region corresponding to limit cycle behaviour.

A knowledge of the relevant mathematical techniques, such as centre manifold theory and normal form theory (see page 241), is not required to obtain the above results. Computer packages such as AUTO take care of the mathematical details. This is especially useful for models which are too difficult to study by hand, such as model (2.5). It also allows accurate and fairly quick qualitative analyses of models to be done thus facilitating an iterative approach to modelling since modifications of model equations can be investigated fairly easily.

In the next chapter I look at a model which has not been studied before using dynamical systems techniques. In this case the analysis suggests an improvement in the formulation of the model equations.

Chapter 3

Sheep-Hyrax-Lynx Model

3.1 Introduction

This chapter investigates a more complicated model having 10 state variables and a large number of parameters. Analytical work done by hand and isocline analyses are of little use in such situations. Traditionally computers have been used to obtain numerical solutions corresponding to a fixed parameter set and to implement sensitivity analyses¹. I show how dynamical systems techniques can be used to increase our understanding of the relationships between different components in the model. In particular, bifurcation diagrams give more information than sensitivity analyses. These diagrams also highlight an incomplete relationship in the model and lead to an improvement in the formulation of the equations.

The model I have chosen is an example of a system dynamics model and has four main components—sheep, hyrax, lynx and pasture. I begin in section 3.2 with some background to the systems modelling approach for those who may be unfamiliar with it. I also discuss the traditional methods that have been used to solve and analyse such models. In section 3.3 I describe the formulation of the model followed by a few technical details which are required in order to use XPPAUT to analyse the dynamics. Section 3.5 contains the model analysis. I begin by studying the effects of various parameters and density-dependent functions on the behaviour of the model. This analysis shows the limitations of a traditional sensitivity analysis and highlights dynamics which are

¹See section 3.2 for a description of sensitivity analyses.

biologically implausible, namely that pasture growth is unlimited when sheep densities are low. A modification to the pasture growth term is discussed in section 3.5.3. The analysis is completed by a two-parameter study of the effects of culling rates on farmers' revenue. This is followed by section 3.5.5 which interprets the main results of the analysis from a biological viewpoint.

3.2 Dynamic models and systems analysis—some background

The systems approach to modelling was made popular by Forrester [39] in the early 1960's. This approach involves dividing a system into a large number of very simple unit components (Watt [123]) and then using equations to describe the processes affecting each of these components. The methodology was originally applied to industrial, urban, and world population systems but its utility has been extended to ecological applications by a number of researchers (see Jeffers [64] and Watt [123]). Patten [99] summarises the advantages of these *dynamic* or *simulation* models in the ecological context:

The formulation of the models allows for considerable freedom from constraints and assumptions, and allows for the introduction of the non-linearity and feed-back which are apparently characteristic of ecological systems.

This ease of formulation and flexibility are important for modelling ecological systems. A variety of aspects such as age structure, developmental rates and density-dependent relationships can be included explicitly, thus increasing the realism of the model. Kowal [69] notes that an analysis of dynamic models can provide approximations to ecosystem dynamics long before traditional experimental approaches can provide more detailed conclusions. Insights can also be obtained into aspects of the system which may otherwise be obscured by its complexity.

The problem with complex models comes at the time of analysis. Dynamic models usually involve a large number of equations (generally ordinary differential equations) and parameters which makes their behaviour difficult to predict (Patten [99]). We need to find suitable ways of analysing the dynamics of these models.

The traditional approach has been to use numerical routines to obtain solutions over time for a given set of parameter values. Optimisation routines are also often employed (Maynard Smith [85]) to determine the 'best' possible strategy with respect to a cost or revenue function. These routines are implemented using computers. A computer's speed of computation and ability to provide rapid access to large quantities of data makes it particularly suitable for analysing these large models (Jeffers [64]). A description of the basic routines involved can be found in Patten [99] as well as in any introductory textbook on numerical routines for systems of ordinary differential equations (for example, [43, 63]).

While these methods are useful, their results depend on the particular parameter set used. Intuitively a sufficiently small variation in the parameter values should lead to an arbitrarily small change in the solution given by the model if we are to have any faith in the predictions of the model (Hadamard [53]). This corresponds to Hadamard's concept of a well-posed problem with respect to partial differential equations [53] and led to the development of *sensitivity analyses*. For ordinary differential equations this method is based on the ideas of Tomovic [118] and involves changing the values of the input variables and parameter values by a small amount (say 1 percent or 10 percent) and seeing whether these changes produce large or small variations in the predictions of the model (Jeffers [64]). A good description of the basic theory involved, as well as some examples, is given in Brylinsky [18].

Sensitivity analyses are often used when studying system dynamics models and do give some idea of the robustness of model predictions, but the information is limited in that only a single, small perturbation of each parameter is considered. This chapter

shows how additional information can be obtained using dynamical systems techniques to vary parameters across *ranges* of values. The next section describes a particular example of the systems approach to modelling which I will use to illustrate the latter techniques.

3.3 Model equations

Swart and Hearne [116] developed a dynamic model to study the impact of hyrax (a type of rock rabbit) and lynx on sheep farming in a region in South Africa. Two main problems were identified. The first involves competition for pasture between hyrax and sheep; hyrax encroach on farm land when the hyrax population exceeds the carrying capacity of wilderness areas in the region. The second problem is the predation on sheep by lynx. The principal food for lynx is hyrax, but from time to time lynx prey on sheep. It is the latter problem that is of direct concern to farmers—they tend to be more tolerant of the competition with hyrax.

The model in [116] was developed to increase understanding of the problems caused by the spillover of hyrax and lynx from their predator-prey system into the sheep-pasture system, and to determine the effects of different culling strategies for hyrax and lynx. There are 10 state variables in the model. The sheep, hyrax and lynx populations are each divided into three classes—juveniles, female adults and male adults—and there is one variable representing pasture. The quantity of most interest to farmers is revenue. This auxiliary variable is a function of the state variables and is made up of wool sales, mutton sales, the value of sheep stock, and the cost of culling hyrax and lynx.

The differential equation for each state variable is formulated by adding and subtracting quantities representing the processes affecting that variable. For example, the equation for hyrax juveniles is as follows:

$$\left(\begin{array}{l} \text{Rate of change of} \\ \text{hyrax juveniles} \end{array} \right) = \text{births} - \text{maturation} - \text{deaths} - \text{predation} - \text{culling}$$

where

- **births** depend on the number of hyrax female adults and decrease with increasing hyrax density,
- **maturation** represents the number of juveniles that mature to become adults in a given year and is a constant fraction of the number of hyrax juveniles,
- **deaths** are a proportion of the number of hyrax juveniles and increase with increasing hyrax density,
- **predation** (by lynx) varies with the relative number of hyrax and lynx (that is, predation increases as hyrax abundance increases), and
- **culling** is a constant fraction of the number of hyrax juveniles and is determined externally by the farmer or an environmentalist.

In mathematical terms the above equation becomes

$$\frac{dH_J}{dt} = H_{JB} - H_{JM} - H_{JD} - H_{JP} - H_{JC}$$

where H_J is the number of hyrax juveniles, H_{JB} is the number of hyrax births in a given year, H_{JM} is the number of hyrax that mature to become adults during the year, H_{JD} is the number of hyrax juvenile deaths during the year, H_{JP} is the number of hyrax juveniles killed by lynx during the year, and H_{JC} is the number of hyrax juveniles that are culled. A full description of the mathematical formulation of these terms can be found in [116]. By way of example,

$$H_{JM} = H_J \times H_{JMN}$$

where H_{JMN} (hyrax juvenile maturation normal) is the fraction of juveniles that become adults each year and

$$H_{JP} = L_T \times L_{PN} \times L_{PM}(A_P) \times \frac{H_J}{H_J + H_F + H_M} \quad (3.1)$$

where

- $L_T = L_{JR} \times L_J + L_F + L_M$ is the total number of lynx (a lynx juvenile ratio (L_{JR}) converts lynx juveniles into equivalent adult units, for example, 1 juvenile = 0.5 adults),
- L_{PN} is the lynx predation normal which is the average number of sheep killed per lynx per year,
- L_{PM} is the lynx predation multiplier (lynx functional response) which is an increasing function of prey abundance, A_P , and
- $A_P = \frac{H_T}{L_T} / \frac{H_N}{L_N}$ is an index of the availability of hyrax as prey for the lynx population. It is a ratio of the total number of hyrax to the total number of lynx relative to a 'normal' ratio, $\frac{H_N}{L_N}$, representing the usual level of abundance under typical environmental conditions.

The last term in equation (3.1) adjusts the total amount of predation so that only the number of juveniles killed is taken into account in this equation.

A possible choice for the lynx predation multiplier is shown in figure 3.1. An S-shaped functional response is used as the lynx can only eat a limited amount even when prey

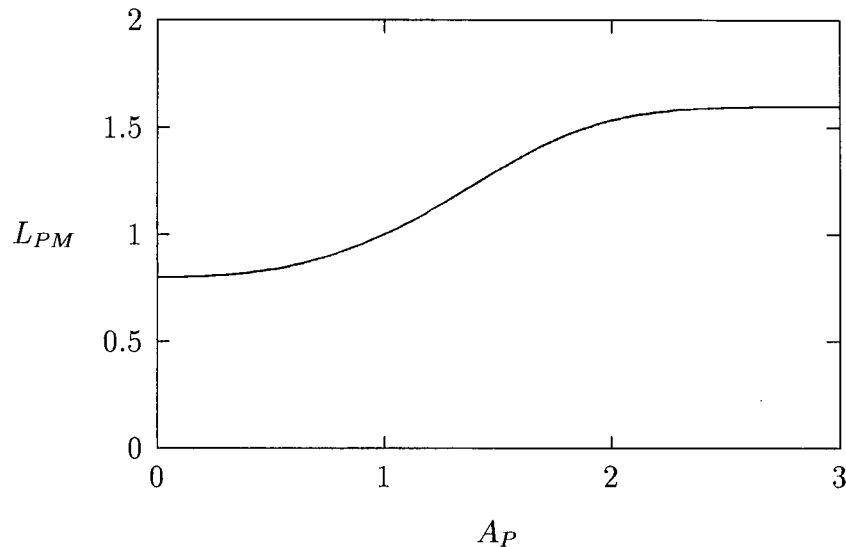


Figure 3.1: The lynx predation multiplier (L_{PM}) as a function of prey abundance (A_P).

abundances are very high, and when abundances are low lynx have difficulty finding hyrax.

The other equations in the model are formulated in a similar manner to the above example for hyrax juveniles. Table 3.1 shows the processes affecting each animal group. Predation is by lynx and culling is done by the farmer (in the case of sheep) or controlled by environmentalists (in the case of hyrax and lynx). Three quantities in the model are averaged using first order delays. A description of how this is included in the model is given in appendix C.

Swart and Hearne [116] used traditional methods to study this model. They used optimisation routines to find the hyrax and lynx culling rates which gave maximum profitability in terms of revenue. They also investigated the sensitivity of the system to parameter perturbations. They found that lynx culling is essential and that substantial increases in both sheep numbers and revenue are possible by simultaneously culling hyrax and lynx. Optimal culling rates in terms of revenue are around 30 percent per annum

State variable	Growth processes	Death processes
Hyrax juveniles (H_J)	births (H_{JB})	deaths (H_{JD}),maturation (H_{JM}), predation (H_{JP}),culling (H_{JC})
Hyrax female adults (H_F)	juvenile maturation (H_{JM})	deaths (H_{FD}),predation (H_{FP}), culling (H_{FC})
Hyrax male adults (H_M)	juvenile maturation (H_{JM})	deaths (H_{MD}),predation (H_{MP}), culling (H_{MC})
Lynx juveniles (L_J)	births (L_{JB})	deaths (L_{JD}),maturation (L_{JM}), culling (L_{JC})
Lynx female adults (L_F)	juvenile maturation (L_{JM})	deaths (L_{FD}),culling (L_{FC})
Lynx male adults (L_M)	juvenile maturation (L_{JM})	deaths (L_{MD}),culling (L_{MC})
Sheep juveniles (S_J)	births (S_{JB})	deaths (S_{JD}),maturation (S_{JM}), predation (S_{JP}),culling (S_{JC})
Sheep female adults (S_F)	juvenile maturation (S_{JM})	deaths (S_{FD}),culling (S_{FC})
Sheep male adults (S_M)	juvenile maturation (S_{JM})	deaths (S_{MD}),culling (S_{MC})
Pasture (P)	production (P_P)	grazing (P_G)

Table 3.1: Table showing the processes affecting each state variable and some of the abbreviations used in the model equations.

for both hyrax and lynx. From a policy point of view the model is robust with respect to small parameter variations.

The purpose of this chapter is not to redo the work done by Swart and Hearne [116]—their model and analysis have accomplished their aims. Instead I want to illustrate the usefulness of the dynamical systems software in this setting.

3.4 Technical details

A few minor modifications to the model are required to facilitate the use of this software. The first involves scaling the state variables so that they all have the same order of magnitude. Combining quantities of very different magnitude may lead to computer round-off errors [43]. I chose values close to the initial values in [116] as scaling constants. In other words, I replaced each state variable v_i by the quantity $s_i v_i$ where s_i is the scaling constant for v_i . Now v_i takes on values between say 0 and 10. In order to calculate the magnitude of the i^{th} population we can multiply this new v_i by s_i . To prevent the scaling from altering the dynamics of the model, the differential equation for v_i is divided through by s_i . The above manipulations are made clearer in appendix C.

Secondly, in order for the computer packages to generate continuous bifurcation diagrams, all functions in the model need to be continuous. The original model represents farmers' sheep culling strategies using two step functions. I replaced these with continuous functions having steep slopes in the region of the step.

In the original model pasture production and fecundity rates vary seasonally. Since this complicates the dynamics considerably when it comes to parameter studies and since the present study is more concerned with long-term equilibrium behaviour than with day to day variations, I did not include the seasonality functions. Solving the system of equations numerically over time is still the best way to study seasonal variation in most cases.

The various versions of AUTO only allow a state variable or the L_2 -norm of the state variables to be displayed on the y-axis of the bifurcation diagrams they generate. The L_2 -norm of a vector $\mathbf{v} = (v_1, \dots, v_m)$ is given by

$$\sqrt{\sum_{i=1}^m v_i^2}.$$

However, the quantity of most interest to farmers is the revenue corresponding to different management strategies. In order to have direct access to revenue values it would be most convenient if revenue were a state variable. The following suggestion by Bard Ermentrout makes this possible.

Let \mathbf{v} be the vector of existing state variables and let $h(\mathbf{v})$ be the revenue function. We can add the equation

$$\frac{dR}{dt} = \frac{-R + h(\mathbf{v})}{\tau},$$

where τ is a small parameter, to the original system. R is the variable that we want to represent revenue. This ordinary differential equation will not affect system equilibria since at these points $R = h(\mathbf{v})$ and hence $\frac{dR}{dt} = 0$ (as required for an equilibrium value). The existence and stability of phenomena such as periodic orbits (limit cycles) are also not affected. Since τ acts as a delay time, we would like it to be small so that R is a close approximation to revenue. However, care must be taken in the choice of τ as very small values can give rise to computer truncation errors. For the current problem I used $\tau = 0.05$. Larger values of τ resulted in R values which were less satisfactory approximations to revenue while smaller values of τ gave hardly any change in the R values.

We are now in a position to begin the analysis.

3.5 Model analysis

3.5.1 Reference parameter values

We need to choose an initial set of parameter values before we can determine the effects of varying parameters across ranges of values. Most of the values are given in [116]. Only values for the hyrax and lynx culling normals (H_{CN} and L_{CN}) need to be chosen. It seems most natural to choose those values which give the maximum revenue at equilibrium. In

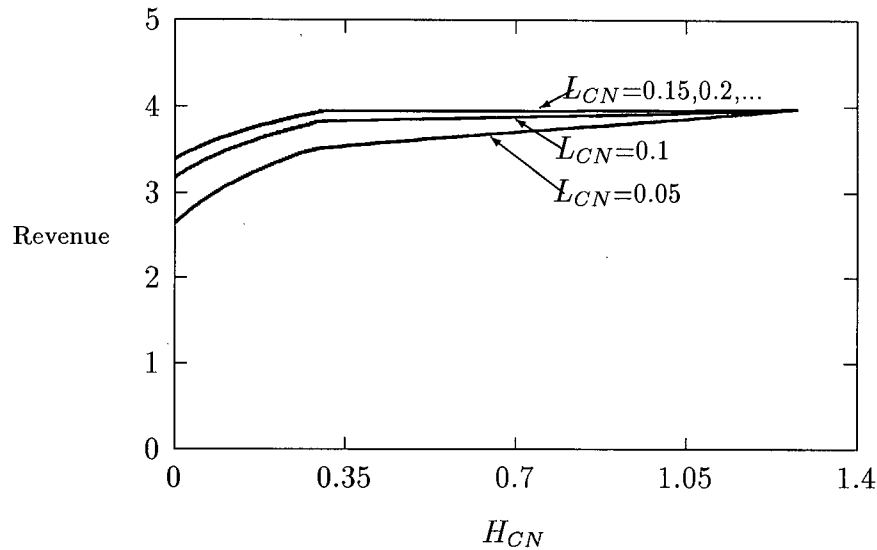


Figure 3.2: Three one-parameter bifurcation diagrams with revenue plotted as a function of H_{CN} . Each curve corresponds to a different (fixed) value of L_{CN} .

order to do this I first fixed L_{CN} at 0.1, chose a value of 0.2 for H_{CN} (any reasonable values would do just as well), and used a numerical solver in XPPAUT to integrate the system of equations until an equilibrium point was reached. Using this equilibrium point as the initial point, I then used the AUTO interface to vary H_{CN} . This is done by choosing H_{CN} to be plotted on the x-axis and one of the state variables (I chose revenue) for the y-axis. Using the RUN and GRAB² commands a parameter diagram can be generated. This diagram shows how the equilibrium revenue changes as H_{CN} varies (see figure 3.2). The above exercise was repeated for a few different values of L_{CN} and the resulting parameter diagrams were plotted on the same pair of axes to give figure 3.2.

It can be seen from this figure that a value of 0.35 for H_{CN} is close to optimal (in terms of revenue) for all values of L_{CN} . I chose this value for H_{CN} and then used XPPAUT to vary L_{CN} in order to find the corresponding optimal value for L_{CN} . This gave figure

²A complete description of the available commands can be found in the XPPAUT documentation as well as in the interactive tutorial that is available—see appendix B.

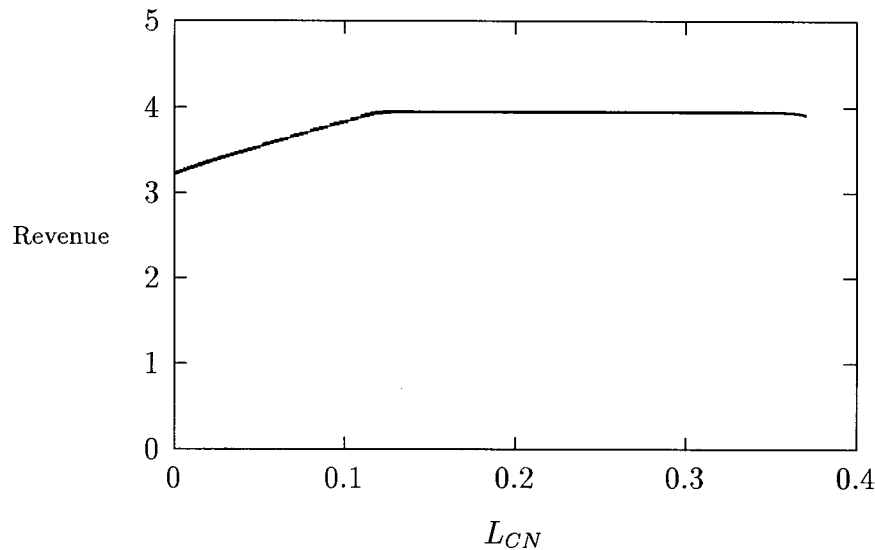


Figure 3.3: One-parameter bifurcation diagram of revenue versus L_{CN} for $H_{CN}=0.35$.

3.3. Lower values for H_{CN} resulted in revenue curves lying below that in figure 3.3 and higher values resulted in curves almost identical to that for $H_{CN}=0.35$.

For the reference parameter set I chose values of 0.35 for H_{CN} and 0.15 for L_{CN} as these values are close to optimal and have the added advantage that small perturbations will not have much effect on revenue, since the revenue surface appears to be fairly flat in a region surrounding these values. At these reference values equilibrium revenue equals 3.94 which is slightly greater than 3.91, the value when $L_{CN} = 0.3$ and $H_{CN} = 0.3$. (Note that the scaling factor for revenue is 10 million Rand so the above values need to be multiplied by this factor to get the true revenue values.)

3.5.2 Understanding model relationships

The effects of culling sheep and of lynx fecundity

There are many parameters in this model which could be used to illustrate the dynamical systems techniques. Those affecting population growth rates are likely to have the

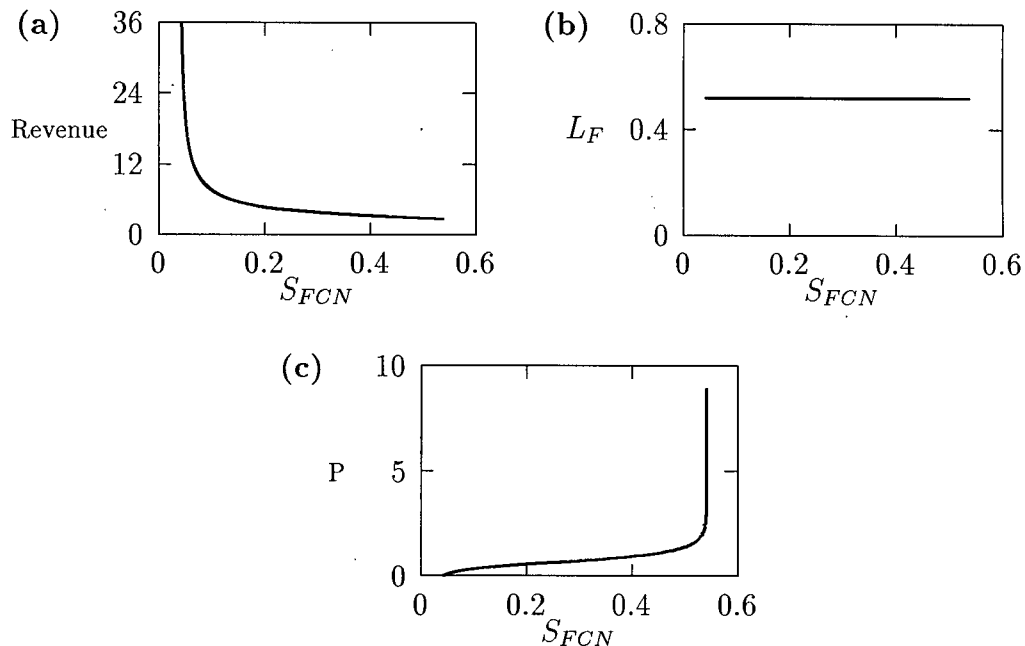


Figure 3.4: One-parameter bifurcation diagrams obtained from varying S_{FCN} (nominal value = 0.28/yr) with $L_{FN}=0.7/\text{yr}$. In (a) revenue is plotted on the y-axis, in (b) the state variable for lynx females is used, and in (c) the state variable for pasture is used.

greatest influence on the dynamics. I have chosen to study two such parameters in this chapter—the sheep female culling normal S_{FCN} , which is the average number of ewes culled by a farmer per year, and the lynx fecundity normal L_{FN} , which is the average number of offspring produced per female lynx per year. As before I used XPPAUT to integrate the system numerically, using the reference parameter values, until an equilibrium was reached. Using these equilibrium values for the state variables as the starting point, I employed XPPAUT's AUTO interface to produce a bifurcation diagram. The results are shown in figures 3.4 and 3.5.

Once a bifurcation diagram has been generated using XPPAUT, it is easy to switch the variable on the y-axis. The effects of varying a parameter with respect to different state variables can then be seen. For each parameter I have chosen three diagrams. One

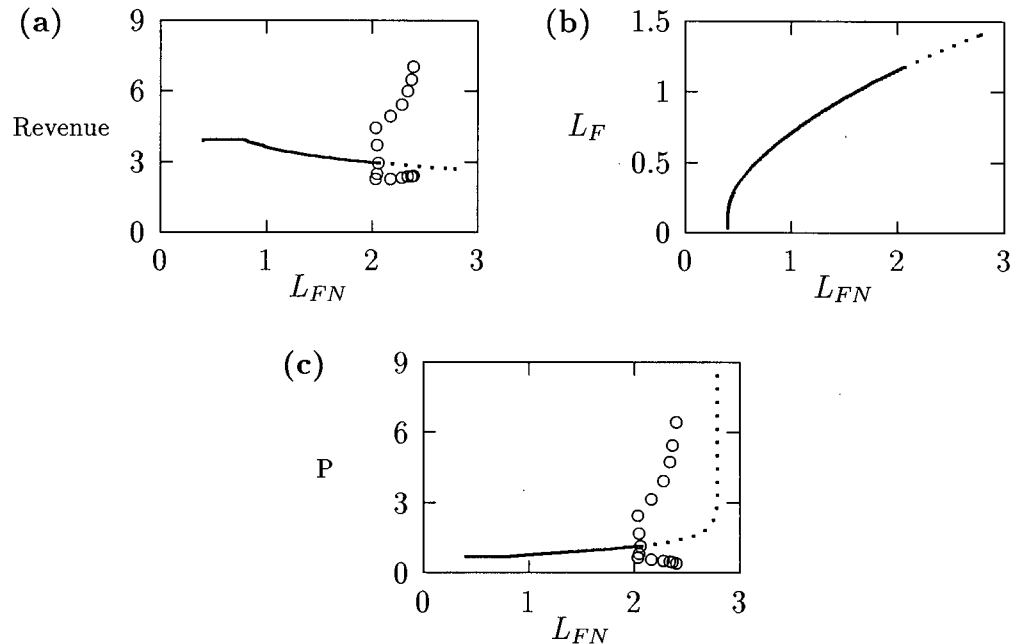


Figure 3.5: One-parameter bifurcation diagrams obtained from varying L_{FN} (nominal value = 0.7/yr) with $S_{FCN}=0.28/\text{yr}$. In (a) revenue is plotted on the y-axis, in (b) the state variable for lynx females is used, and in (c) the state variable for pasture is used.

shows the effect of the parameter on equilibrium revenue, the second the effect on the equilibrium number of lynx females, and the third the effect on the equilibrium amount of pasture.

A number of observations can be made from figures 3.4 and 3.5. The first is that AUTO encounters points beyond which it cannot calculate. In figure 3.4 such a point is $S_{FCN}=0.54$ and in figure 3.5 there are two points, $L_{FN}=0.39$ and $L_{FN}=2.78$. Using XPPAUT to solve the system of equations numerically for parameter values on either side of these limiting points, the causes of these difficulties can be determined. Output from a numerical integration is shown in XPPAUT's data window and from this it was seen that the sheep population dies out for $S_{FCN} > 0.54$ or $L_{FN} > 2.78$, and the lynx population dies out for $L_{FN} < 0.39$. The latter conclusion could also be drawn from figure 3.5(b).

Beyond the limiting values there is no equilibrium at which all three populations are present and, hence, AUTO cannot continue the equilibrium branch any further.

A second observation can be made by looking at the bifurcation diagram for pasture in figure 3.4(c). As the equilibrium number of sheep declines (as S_{FCN} increases and approaches the value corresponding to sheep extinction), the equilibrium value for pasture increases unchecked. Clearly this is unrealistic and suggests that some modification should be made to the model equations to limit pasture growth. I return to this in section 3.5.3.

In figure 3.5 there is a threshold value at $L_{FN}=0.76$ above which revenue declines as L_{FN} increases and below which revenue remains fairly constant as L_{FN} is varied. Again I chose parameter values on either side of this threshold and used XPPAUT to integrate the system of equations numerically until an equilibrium was reached. Viewing the numerical output in the data window lent some insight into the behaviour of the model. I found that as L_{FN} increases through 0.76, prey abundance³ at equilibrium passes through a threshold value above which lynx begin to supplement their diet with lambs. This loss of lambs explains the decrease in revenue.

An important point to note is that if a traditional sensitivity analysis had been done using optimal equilibrium values for the state variables and a nominal value of $L_{FN}=0.6/\text{yr}$, then no change in equilibrium revenue would have been seen for a 10 percent increase in L_{FN} . However, using a nominal value of $0.7/\text{yr}$, a 10 percent increase places L_{FN} at $0.77/\text{yr}$. This is above the threshold point and thus a decrease in equilibrium revenue occurs.

The only stability change in figures 3.4 and 3.5 occurs at $L_{FN}=2.06$. At this point a Hopf bifurcation occurs (see section A.2.10), which means that the stable equilibrium point becomes unstable and a periodic orbit is initiated. However, oscillations are only

³See the explanation under equation (3.1).

associated with the sheep-pasture subsystem. The lynx and hyrax populations do not cycle. In this case the limit cycles associated with the Hopf bifurcation are unstable and thus not of practical interest. In such a case it is more enlightening to examine the temporal dynamics of the system for $2.06 < L_{FN} < 2.78$. Using XPPAUT for this purpose it was found that the sheep population declines to zero in this range of parameter values while the hyrax and lynx populations reach steady states. This trend continues for $L_{FN} > 2.778$ but the sheep population dies out much faster and AUTO fails to converge.

Before modifying the equations to limit pasture growth as suggested earlier, it would be informative to study the roles of the existing density-dependent functions. This can be viewed as another form of sensitivity analysis in which we investigate the system's response to whole functions instead of single parameters.

The effects of density-dependence

There are a number of functions in the model which modify growth and death rates as conditions change. All these functions are normalised to take the value 1 when the quantities on which they depend are at their reference values. For example, the equation governing pasture (P) dynamics is given by

$$\begin{aligned} \frac{dP}{dt} &= \text{pasture production} - \text{pasture grazing} \\ &= A.P_{PN} - T_{SSU}.G_N.G_M(P_A) \end{aligned} \quad (3.2)$$

where A is the area of the farming region under study, P_{PN} is the pasture production normal (average pasture growth rate), T_{SSU} is total small stock units (a representative value for the number of sheep), G_N is the grazing normal (average amount of pasture grazed per unit stock) and G_M is the grazing multiplier which is a function of P_A , the pasture availability index. P_A is given by P/\bar{P} where \bar{P} is an average pasture density. The grazing multiplier has the form shown in figure 3.6.

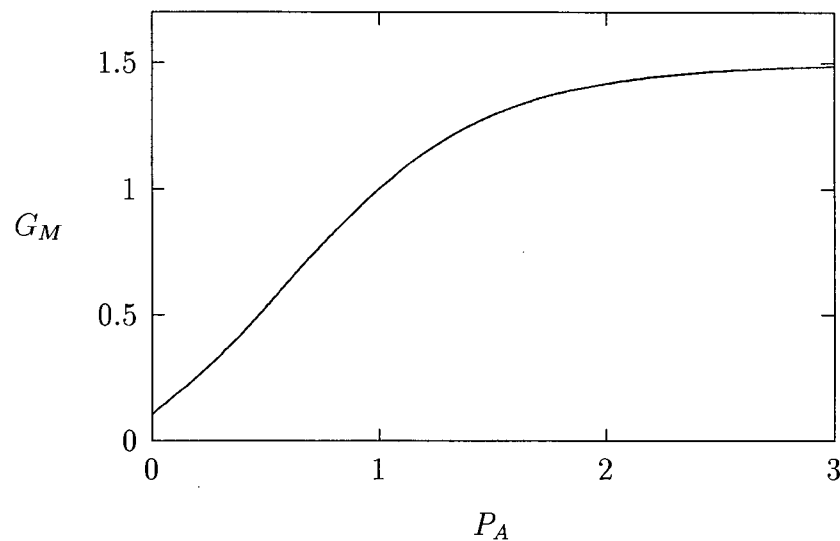


Figure 3.6: The grazing multiplier function (G_M) as a function of pasture availability.

In order to remove a density-dependent function from the model, the simplest approach is to replace it by a constant function. For example, we can set $G_M \equiv 1$. This was done for each multiplier function in turn and bifurcation diagrams obtained from the altered model were compared with those from the original model in each case.

Removing the grazing multiplier, G_M , had the greatest effect on model dynamics. Even after altering a number of parameter values the system did not reach equilibrium. The sheep population either increased indefinitely or decreased to extinction for each parameter set that was tried. This is not surprising since the grazing multiplier affects pasture grazing and sheep fecundity as well as sheep juvenile deaths. Without G_M the density-dependence of pasture grazing and sheep dynamics on pasture availability (G_M is a function of P_A) is removed. The results show that this density-dependence is critical for regulating the sheep-pasture subsystem.

The effects of the other functions in the model were quantitative rather than qualitative. That is, removing them from the model tended to decrease the range of parameter

values over which sheep, hyrax and lynx coexist at equilibrium, but did not alter the qualitative dynamics. In relative terms however, the effects of the fecundity multiplier functions were more noticeable than those of the death and predation multipliers.

The above comments do not imply that the latter multiplier functions play an insignificant role in the model. They have a regulatory effect and reduce the impact of parameter changes on model behaviour. This resilience to disturbances is very desirable [61] and is expected of many natural systems. Thus, although these functions may not be critical in determining model behaviour, they are important for making the model more realistic.

It was observed earlier that the model lacks a feedback relationship that would limit pasture growth when sheep densities are very low. We also know that pasture availability has a significant influence on pasture grazing and sheep fecundity and hence on the predictions of the model. Thus modifying equation (3.2) to include density-dependent growth may have a considerable effect on the behaviour of the model. This modification is discussed in the next section.

3.5.3 Adding density-dependence to pasture growth

The reader will probably have noticed that equilibrium pasture values only become unrealistic for extreme parameter values. However, it is desirable to have a model which can describe a variety of situations instead of one that is only suitable for a small range of values. Also, improving model realism in extreme regions may affect the dynamics corresponding to more normal values and so play an important part in understanding system behaviour. The formulation of a model also affects statistical parameter fitting routines. If important relationships are left out then these routines may give misleading results or fail to converge.

In the sheep-pasture, hyrax-lynx model pasture growth occurs at a fixed rate and

is independent of existing pasture density (see equation 3.2). In order to limit pasture growth, I included a pasture multiplier (P_M) in equation (3.2) as follows:

$$\begin{aligned} \frac{dP}{dt} &= \text{pasture production} - \text{pasture grazing} \\ &= A.P_{PN}.P_M(P_A) - T_{SSU}.G_N.G_M(P_A) \end{aligned} \quad (3.3)$$

where P_M is a function of pasture availability, P_A . For high values of P_A we expect pasture growth to slow down and saturate. We also expect a decline in growth when P_A is very low following the principle that ‘growth promotes growth’. A function having this general form is the Ricker function. Using this type of relationship I introduced a density-dependent function having the shape shown in figure 3.7.

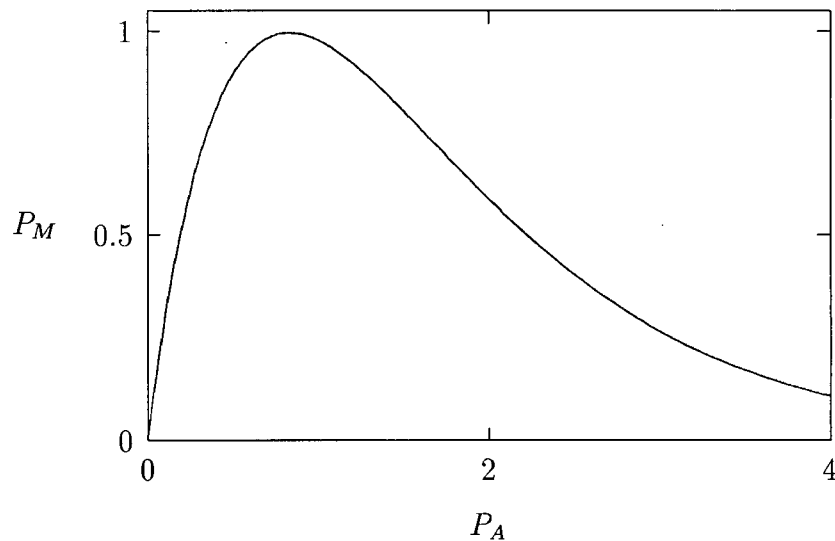


Figure 3.7: The pasture multiplier (P_M) as a function of pasture availability (P_A).

To test the effects of this new function I generated a number of bifurcation diagrams and compared them with those from the original model. Figures 3.8 and 3.9 show those diagrams which correspond to figures 3.4 and 3.5 respectively.

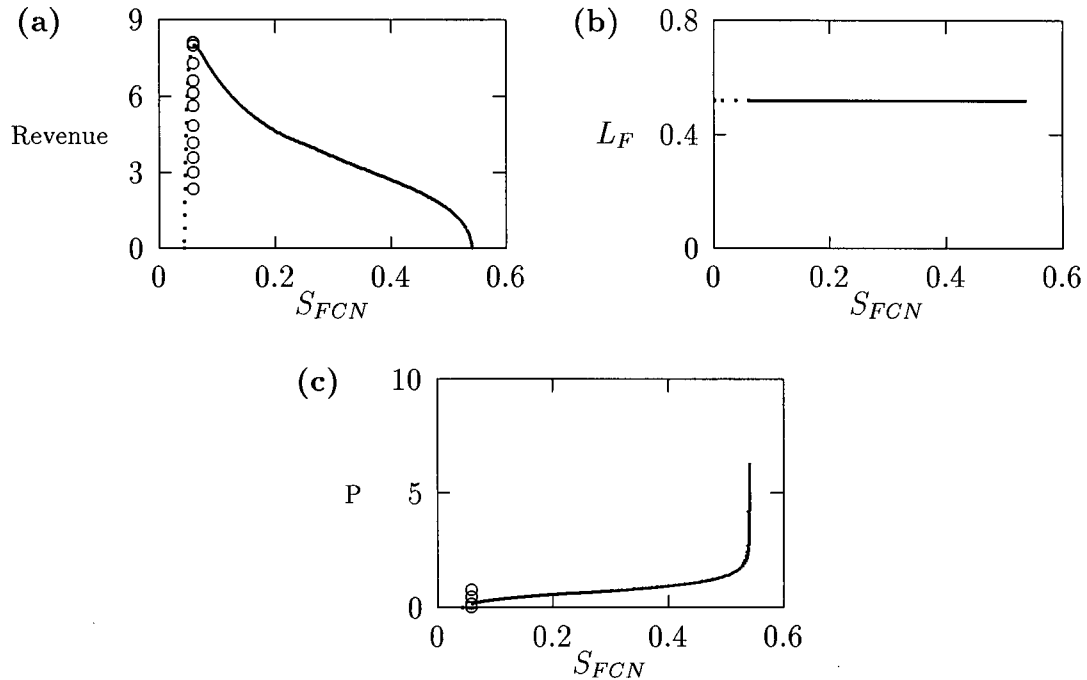


Figure 3.8: One-parameter bifurcation diagrams obtained from varying S_{FCN} (nominal value = 0.28/yr) for the new model which includes a pasture limiting multiplier. In (a) revenue is plotted on the y-axis, in (b) the state variable for lynx females is used, and in (c) the state variable for pasture is used.

In figure 3.8(a) total revenue declines to zero as S_{FCN} increases. This is more mathematically satisfactory than figure 3.4(a), where the curve stops abruptly at a positive revenue value, as it indicates clearly where a positive sheep population is no longer possible. Figure 3.8(c) shows the maximum pasture density which occurs when a positive sheep equilibrium (and hence a positive value for revenue) is impossible. This density is lower than in figure 3.4(c) but depends on the exact nature of the pasture multiplier.

Another observation from figure 3.8 is that instead of AUTO being unable to converge at very low S_{FCN} (sheep female culling normal) values, a Hopf bifurcation occurs and the bifurcation diagrams show that no stable equilibrium at which all three populations

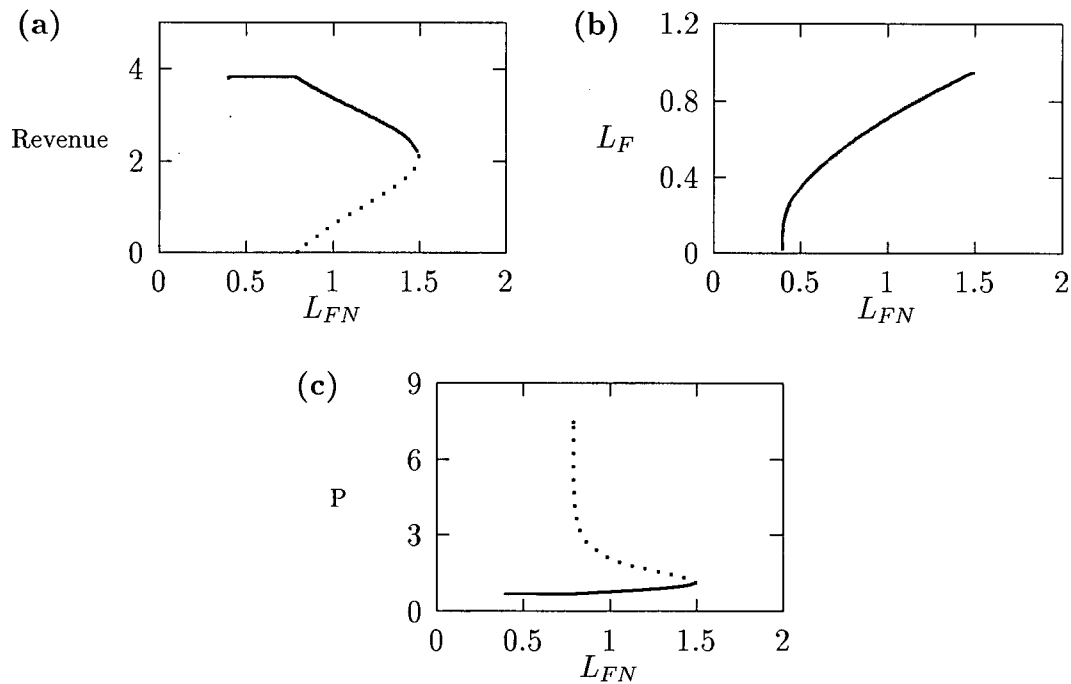


Figure 3.9: One-parameter bifurcation diagrams obtained from varying L_{FN} (nominal value = 0.7/yr) for the new model which includes a pasture limiting multiplier. In (a) revenue is plotted on the y-axis, in (b) the state variable for lynx females is used, and in (c) the state variable for pasture is used.

coexist is possible for $S_{FCN} < 0.059$. For these values there is insufficient pasture to support the high sheep population. Thus, introducing the pasture multiplier has improved the dynamics at low values of S_{FCN} as well as high values and has solved the problem of revenue increasing rapidly as in figure 3.4(a).

In figure 3.9 a limit point (see section A.2.13) has replaced the Hopf bifurcation of figure 3.5. The limit point bifurcation clearly shows that for $L_{FN} > 1.491$ no equilibrium at which all three populations coexist is possible. Again, using XPPAUT to integrate the system numerically gives insight into the dynamics corresponding to the different regions in the bifurcation diagrams. In particular, the temporal dynamics show that the pasture multiplier slows and limits pasture growth as desired. Comparing the dynamics

of the original and modified models at $S_{FCN} = 0.5$ shows that limiting pasture growth has a stabilising influence (see figure 3.10). The oscillatory approach to equilibrium by the original model (figure 3.10(a)) is replaced by a smooth approach in figure 3.10(b).

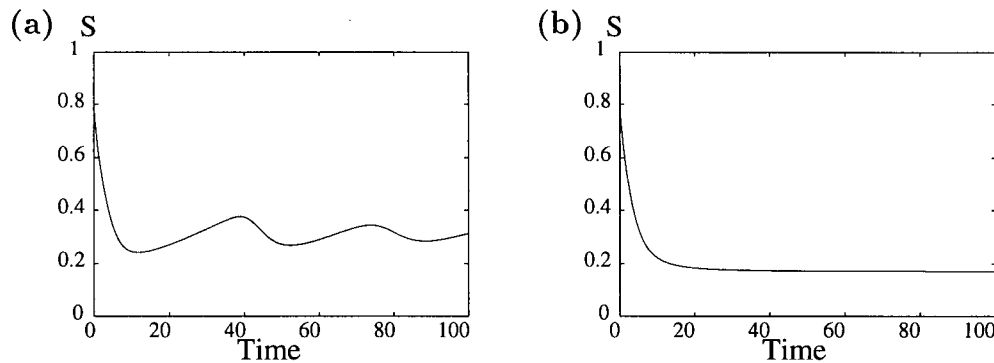


Figure 3.10: Time plots obtained using (a) the original model and (b) the modified model with $S_{FCN} = 0.5$.

The limiting value for pasture in figure 3.8(c) is still rather high but, since I had no experimental data on which to base the form of the pasture multiplier, I did not think it worthwhile to fiddle with the function to obtain a more plausible value. The effects of introducing the multiplier have already been adequately demonstrated.

A closer look at the behaviour exhibited by the model may suggest further modifications to the equations. The above is just one example of how bifurcation diagrams can help in the process of model building. Another example can be found in chapter 4. The next section describes how two-parameter studies can be used to obtain useful summaries of model behaviour.

3.5.4 A summary of the effects of culling both hyrax and lynx

The model in this chapter was originally developed to study the effects of culling hyrax and lynx. As was done in [116] and earlier in this chapter, optimal values (with respect to

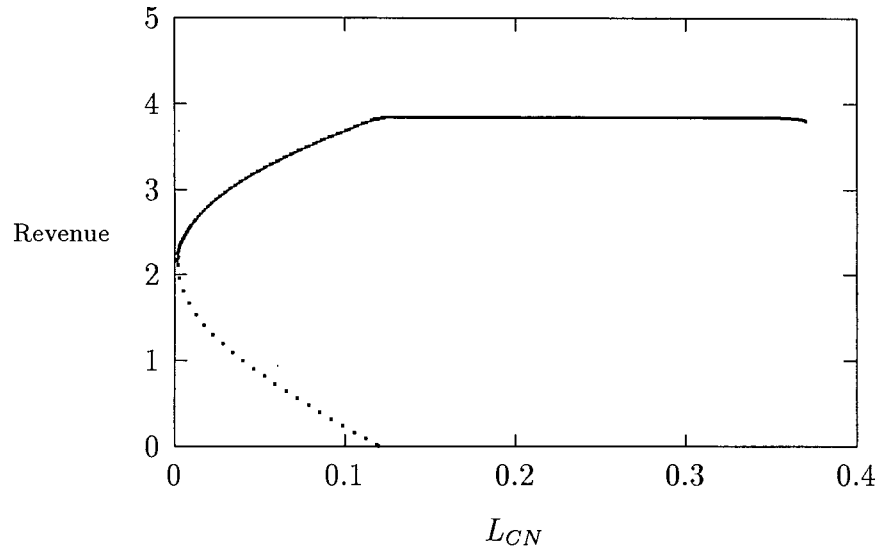


Figure 3.11: One-parameter bifurcation diagram of revenue as a function of L_{CN} for the modified model. The change in stability (denoted by the change from a solid to a dotted line) occurs at a limit point.

revenue) were found for the hyrax and lynx culling normals. However, only one parameter was varied at a time. We can obtain a two-parameter diagram to summarise the effects of varying both parameters simultaneously as follows.

Using the modified model the bifurcation diagrams for the lynx culling normal L_{CN} have the form shown in figure 3.11. For L_{CN} below the limit point the sheep population dies out as there is too much predation by lynx. Using AUTO the limit point can be continued in H_{CN} , the hyrax culling normal, as well as L_{CN} . That is, we can see how the position of this limit point varies as a function of both H_{CN} and L_{CN} . This gives the two-parameter bifurcation diagram in figure 3.12. From this figure it can be seen that sheep become extinct as a result of the combined effect of lynx predation and competition with hyrax for pasture since both L_{CN} and H_{CN} are low in the region where sheep die out. Note that figure 3.12 could not have been produced using the original model as there was no limit point in the corresponding L_{CN} bifurcation diagrams (see figure 3.3)—AUTO

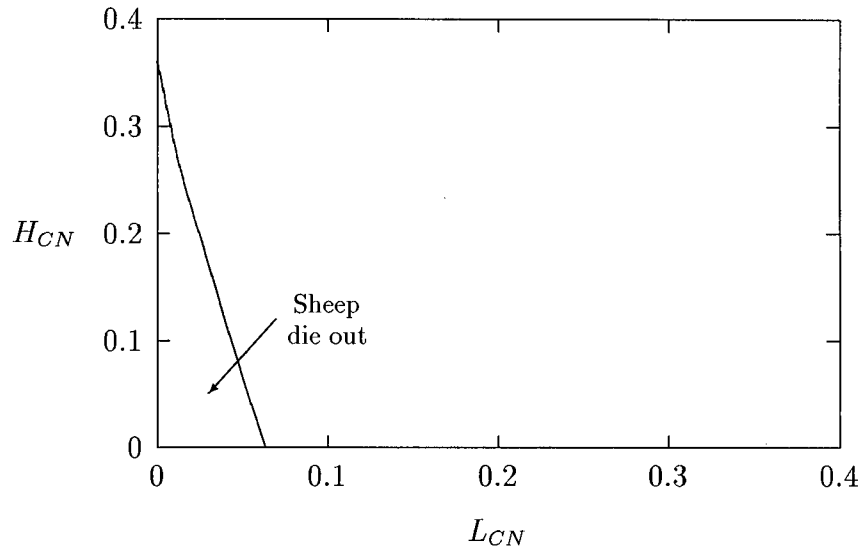


Figure 3.12: Two-parameter continuation of the limit point in figure 3.11. (To determine the behaviour corresponding to a particular region in this two-parameter diagram, choose values for H_{CN} and L_{CN} in this region and then use XPPAUT to integrate the system numerically.)

signalled non-convergence and stopped calculating.

Combining figure 3.12 with the observation that the lynx population dies out for $L_{CN} > 0.37$ for all values of H_{CN} gives figure 3.13. This was determined by generating bifurcation diagrams for L_{CN} for a number of different (fixed) H_{CN} values. Conversely, varying H_{CN} for a variety of fixed L_{CN} values does not produce any parameter ranges where the hyrax population dies out.

Figure 3.13 shows that all three populations coexist at equilibrium for a large set of culling rates. The diagram would be of even greater use if we knew the revenue value corresponding to each point in this two parameter space. This can be done by recording information given by XPPAUT and using some other graphics package to plot a three-dimensional surface.

Using the modified model developed in the previous section I fixed the value of H_{CN} , chose $L_{CN} = 0.15$ (say) and used XPPAUT to find the equilibrium point numerically. I

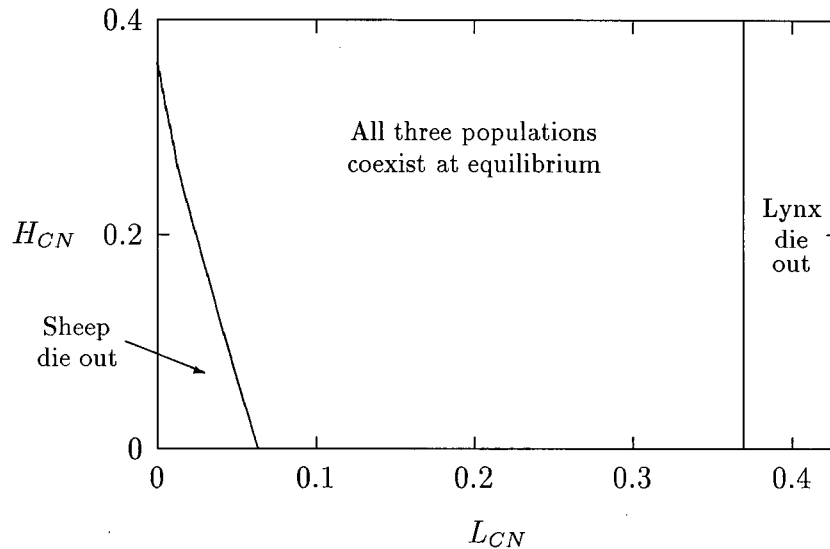


Figure 3.13: Two-parameter bifurcation diagram of the H_{CN} and L_{CN} parameter space for the modified model.

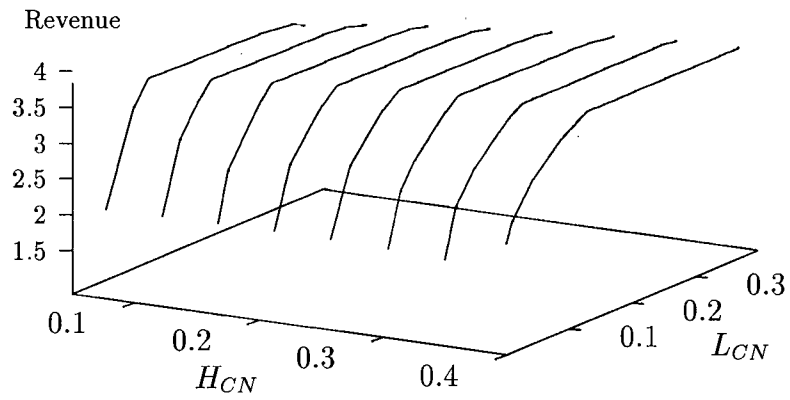
then used the AUTO interface to vary L_{CN} in both directions. Using the GRAB feature of XPPAUT to move along the branch of equilibrium points, I recorded the revenue values at regular intervals along the curve. I did this for a number of H_{CN} values and plotted the results using the public domain graphics package GNUPLOT [125]. A surface plot and corresponding contour plot are shown in figure 3.14.

As can be seen from the figure there is a large region of parameter space over which revenue does not vary much indicating that the model is very robust to changes in the culling rates in this region. This is a desirable property when it comes to developing management strategies.

3.5.5 Biological interpretation of results

The analysis of the previous sections has led to a number of insights into the sheep-pasture, hyrax-lynx system. Figure 3.8 shows that altering the number of ewes that are

(a)



(b)

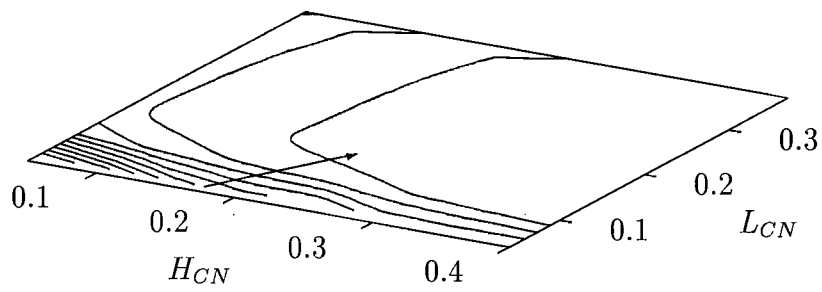


Figure 3.14: (a) Surface plot and (b) contour plot of revenue as a function of the hyrax and lynx culling normals. The arrow in (b) indicates the direction of increasing revenue.

culled only affects the sheep-pasture subsystem. However, the effects on this subsystem are considerable. Culling too many ewes will obviously cause sheep numbers to decline. More important is the effect on revenue. Significant increases in revenue are possible if the farmer culls fewer ewes as there is a greater return if these sheep are allowed to reproduce than if they are taken to market. (This is provided that the sheep stock is not too large for the pasture to support it, that is, provided $S_{FCN} > 0.059$.) However, there is a trade-off as culling fewer ewes results in a lower cash flow. Another trade-off results from the decrease in pasture availability which accompanies a larger sheep stock. This is already reflected in the model by the dependence of sheep fecundity on pasture availability. However, an additional quantity representing the *quality* of sheep may be useful as this will affect the returns from wool and mutton sales and hence revenue. This presents another opportunity for improving the model.

Figure 3.9 summarises the effects of lynx fecundity on the system. If lynx fecundity is very high ($L_{FN} > 1.5$) then the sheep population will not be able to survive. However, if lynx fecundity is sufficiently low ($L_{FN} < 0.78$) then the lynx population does not need to prey on sheep as it can be supported by the hyrax population. Further decreases in lynx fecundity at these values have no effect on revenue. For intermediate values ($0.78 < L_{FN} < 1.5$) considerable increases in revenue are possible if lynx fecundity is decreased. This favours the culling of lynx females in particular.

In section 3.5.2 we found that density-dependence of sheep and pasture dynamics on pasture availability is critical for regulating the sheep-pasture subsystem. In fact this encouraged the modification of pasture growth to include density-dependence. This modification restricts both pasture and revenue values from increasing indefinitely (compare figures 3.4 and 3.8) and also stabilises the temporal dynamics (see figure 3.10).

Finally, the effects of culling both hyrax and lynx were summarised using two-parameter diagrams. In particular, figure 3.14 shows that the model is robust to changes

in culling rates provided these rates are sufficiently high.

3.6 Conclusion

This chapter has illustrated a number of potential uses of bifurcation analyses using packages such as XPPAUT. First, models having a large number of state variables and parameters can be analysed in greater depth than was previously practical. For system dynamics models bifurcation diagrams give more information than traditional sensitivity analyses as they summarise the behaviour of the model across a range of parameter values instead of being restricted to a single, fixed perturbation. As a result these diagrams can indicate where model relationships are incomplete and can thus aid in model formulation. Another example of this can be found in chapter 4.

The analysis also showed that the model is quite robust in a qualitative sense—the stability of the system is not greatly affected by parameter variations. However, revenue magnitudes are sensitive to certain parameters. This is an important observation for farmers as they seek to maximise their revenue. Trade-offs between higher long-term revenue and lower cash flows as well as higher revenue and lower sheep quality were also noted.

The dynamics of the model turned out to be fairly simple from a bifurcation viewpoint. Other similar models may not be quite so robust. An analysis similar to the one in this chapter can be useful for uncovering regions of more complex behaviour in such cases.

Chapter 4

Ratio-Dependent Model

4.1 Introduction

Despite having a large number of state variables and parameters, the system dynamics model in the previous chapter turned out to have fairly simple dynamics. This chapter focusses on a more theoretical model having only three state variables but whose dynamics are more complex. In addition to describing how an analysis of such a model may be approached using dynamical systems techniques, a dual aim of the chapter is to highlight some of the difficulties associated with ratio-dependent models. These models are currently a topic of considerable controversy in ecological circles.

The example that I have chosen is a tritrophic model of a plant, herbivore and predator system developed by Gutierrez *et al.* [52]. It is a general model and is physiologically based—a property which the authors claim makes estimation of parameter values from experimental data fairly straightforward. However, there are a number of correction factors in the model whose function is to scale potential rates to realised rates. These factors complicate parameter estimation considerably. Nevertheless, having appeared in a leading journal, this model is sure to receive attention and further analysis of its dynamics may be of interest.

In the next section I summarise the arguments for and against ratio-dependent models. Following this I describe the model equations and the technique of nondimensionalisation that I used to scale the equations and reduce the number of parameters in the model. I

also introduce a small modification to the ratio-dependent terms. In the analysis that follows I consider both the original and this modified model in order to highlight some of the difficulties associated with ratio-dependent models.

After choosing a set of parameter values which give rise to a stable tritrophic equilibrium (that is, a stable equilibrium at which the plant, herbivore and predator populations are all nonzero) I begin the analysis by varying each parameter value in turn to see what effect it has on the dynamics and to determine the range of behaviour that the model can exhibit. Two-parameter bifurcation diagrams summarising the effects on system behaviour of the plant and herbivore respectively complete the preliminary analysis.

Having identified those parameters which have the greatest influence on the dynamics, I obtain a series of two-parameter diagrams using the modified model. These diagrams illustrate the combined effects of the lower two trophic levels on the behaviour of the model. Of particular interest are parameter combinations which give rise to multiple stable states. In some cases a stable tritrophic equilibrium coexists with a stable limit cycle suggesting the possibility of an abrupt change in the behaviour of the system if it is sufficiently perturbed (see section A.2.7).

To complete the study the limits of isocline analysis¹ in a three-dimensional setting are demonstrated. Gutierrez *et al.* [52] used this technique in their analysis of the model. Although isocline analyses have been employed in many settings and with considerable success [36, 38, 44, 56, 74, 92, 103], in more complicated higher dimensional models for which the categorisation of variables as *slow* versus *fast*² is not possible, their application is limited. An isocline analysis allows at most two variables to vary simultaneously. This means that for the current model one variable is held fixed which results in a partly static

¹A description of this technique together with examples can be found in [34].

²If the state variables in a model vary on different time scales it is often possible to approximate the system by a two-dimensional model representing either the slow or the fast dynamics. An isocline analysis can then be done using the reduced system.

representation of the dynamics. The dynamical systems techniques allow all three state variables to vary simultaneously thus permitting a more accurate analysis.

4.2 Background

Ratio-dependent models assume that the functional response terms depend on ratios of the state variables rather than on absolute values or products of variables as is the case for classical models. Although not a new idea, the concept of ratio-dependence in predator-prey interactions has been approached with fresh interest in ecological theory in recent years (Berryman [17]).

Among the advantages of these types of models are that they prevent the paradoxes of enrichment³ and biological control⁴ predicted by classical models [17]. Experimental observations of Arditi and Saïah [6] suggest that prey-dependent models are appropriate in homogeneous situations and ratio-dependent models in heterogeneous situations. In support of this Ginzburg and Akçakaya [45] and McCarthy *et al.* [88] conclude from their work that natural systems are closer to ratio-dependence than to prey-dependence and Gutierrez [51] develops a physiological basis for the theory.

Gleeson [46], however, questions the assumptions of ratio-dependent models and notes that direct density-dependence, or self-regulation, in the top consumer is sufficient to preclude the paradox of enrichment from classical models. From his work on whether patterns among trophic levels are a reliable way of distinguishing between prey- and ratio-dependence, Sarnelle [107] concludes that the ratio-dependent approach should only be applied when the predator and prey are the top two trophic levels in an ecosystem. Abrams [1] argues that patterns and experimental results that have been used in support

³Classical models predict that enriching a system will cause an increase in the equilibrium density of the predator but not the prey and will destabilise the community equilibrium (see Berryman [17]).

⁴Classical models predict that it is not possible to have both a very low and a stable pest (prey) equilibrium density (Berryman [17]).

of ratio-dependent predation are consistent with numerous other explanations and that these other explanations do not suffer from pathological behaviours and a lack of plausible mechanism as do ratio-dependent models. Lundberg and Fryxell [75] note that it may be difficult to distinguish between competing hypotheses without a proper mechanistic understanding of the processes involved.

In a recent paper Akçakaya *et al.* [3] respond to some of the above criticisms. The argument relevant to the current chapter concerns their refutation of the pathological behaviour of ratio-dependent models. Freedman and Mathsen [41] note that ratio-dependent models are invalid near the axes (that is, where the state variables are close to zero) as the ratios tend to infinity in these regions. As a result even when prey (resource) densities are very low, ratio-dependent models predict a positive rate of predator (consumer) increase provided that predator densities are low enough, since the number of prey available per predator increases to infinity as predator density declines to zero [1, 46]. In terms of isoclines, the problem stems from the fact that the predator isocline passes through the origin in ratio-dependent models which means that, even at low prey densities, a sufficiently small predator population can increase. According to Hanski [55] this is against intuition and many field observations. It also means that ratio-dependent models cannot be used to study extinction of species.

However, Akçakaya *et al.* [3] state that the above problems near the axes are only pathological in a mathematical sense and that in biological terms the result would be that both species increase initially and then predators consume all the prey and both species become extinct. Since prey-dependent models cannot predict this outcome they are pathological in a biological sense. However, I show below that ratio-dependent models do not necessarily predict this outcome either. The ratio-dependent model that I will describe in the next section predicts oscillations of large amplitude in these 'pathological' regions (see figure 4.3). While these large amplitude oscillations may be interpreted as

signalling extinction from a practical viewpoint, this is not the prediction of the ratio-dependent model.

Akçakaya *et al.* [3] state that:

A realistic model of prey-predator interactions should be able to predict the whole range of dynamics observed in such systems in nature. A ratio-dependent model can have stable equilibria, limit cycles, and the extinction of both species as a result of overexploitation.

However, a few sentences later they agree that ratio-dependent models are not valid at very low densities (which are a precursor of extinction) and earlier in the paper they state that:

...we do agree that it is at the extremes of low and high densities that strict ratio dependence may not be valid.

In an attempt to clarify some of the arguments in this debate, I introduce a small modification to the ratio-dependent model of Gutierrez *et al.* [52] and study this modified model in conjunction with the original one. The analysis given below shows that the original model is structurally unstable as a small perturbation to the ratio-dependent terms substantially alters the dynamics.

4.3 Model equations

The model equations are functionally homogeneous (that is, all three equations contain the same basic terms) as the authors argue that the same generalised functional and numerical responses must describe the search, acquisition and conversion of all organisms as they seek to satisfy their metabolic requirements. Details of the formulation of the model can be found in Gutierrez *et al.* [52]. The final equations are:

$$\begin{aligned}
\frac{dM_1}{dt} &= \left(\theta_1 \phi_{\eta,1} \phi_{\omega,1} \left(1 - \exp \left[-\frac{\alpha_1 M_0}{D_1 M_1} \right] \right) D_1 - r_1 M_1^{b_1} \right) M_1 \\
&\quad - \left(1 - \exp \left[-\frac{\alpha_2 M_1}{D_2 M_2} \right] \right) D_2 M_2 \\
\frac{dM_2}{dt} &= \left(\theta_2 \left(1 - \exp \left[-\frac{\alpha_2 M_1}{D_2 M_2} \right] \right) D_2 - r_2 M_2^{b_2} \right) M_2 \\
&\quad - \left(1 - \exp \left[-\frac{\alpha_3 M_2}{D_3 M_3} \right] \right) D_3 M_3 \\
\frac{dM_3}{dt} &= \left(\theta_3 \left(1 - \exp \left[-\frac{\alpha_3 M_2}{D_3 M_3} \right] \right) D_3 - r_3 M_3^{b_3} \right) M_3
\end{aligned} \tag{4.1}$$

where M_1 is the biomass of plants, M_2 is the biomass of herbivores, and M_3 is the biomass of predators. The parameters θ_i represent assimilation rates corrected for the efficiency of biomass conversion; α_i represents the proportion of the resource that is available to its consumers (that is, its apparency); D_i is the per unit demand of the consumer for resources; r_i is the base respiration rate corrected for the efficiency of biomass conversion; and b_i is the degree of self-limitation. M_0 represents a biomass equivalent of the light energy incident in the growing space of the plants, and $\phi_{\eta,1}$ and $\phi_{\omega,1}$ (which both lie between 0 and 1) scale the potential photosynthesis rate to the realised rate.

The respiration term, $r_i M_i^{1+b_i}$, requires further explanation. Respiration usually increases with population density [52] and thus should be an increasing function of M_i . However, introducing such a functional dependence increases the complexity of the model and, since the effect is usually small, the authors chose the simpler formulation $r_i M_i^{1+b_i}$ where b_i has a value between 0.02 and 0.05. The disadvantage of this choice is that r_i must have rather unusual units⁵ which depend on b_i so that the term $r_i M_i^{1+b_i}$ has the same units as $\frac{dM_i}{dt}$ (namely, $g \cdot \text{day}^{-1}$ where g are the units of M_i). This dependence of the units on b_i is not satisfactory from a mathematical viewpoint but since b_i is small I chose to ignore this initially. In the next section I discuss a small alteration to the model

⁵The units of r_i are $g^{-b_i} \text{day}^{-1}$ where g are the units of M_i .

which takes care of the difficulty.

Gutierrez *et al.* [52] use parameter values corresponding to a cassava⁶-mealybug⁷-parasitoid⁸ system in Africa and claim that their analysis demonstrates that the parasitoid *Epidinocarsis lopezi* (De Santis) can control the mealybug (except on poor soils) whereas *Epidinocarsis diversicornis* (Howard) and native natural enemies cannot.

My first aim was to reproduce the results in the paper [52]. However, the parameter values for the cassava-mealybug-parasitoid system given to me by the authors (only values for θ_i, α_i, D_i are reported in the paper) did not yield the isocline configurations or the behaviour that they described. Only after changing some of the parameter values by several orders of magnitude did I succeed in producing qualitatively similar diagrams.

This haphazard approach of fiddling with parameter values is not satisfactory. Scaling the equations would give a better idea of the relative magnitudes of the parameters. The procedure involved is discussed in the next section.

4.4 Nondimensionalisation

The technique of nondimensionalising or scaling is commonly used to simplify a system of equations as it has a number of other advantages. It illuminates which parameters are most important in determining the dynamics of the model (Edelstein-Keshet [34]) and gives insight into the relative magnitudes of the parameters required to produce biologically reasonable behaviour. Also, the state variables are scaled so that they all have the same order of magnitude, say between 0 and 1. This is important when solving the equations numerically as very different magnitudes can lead to computer round-off errors (Gerald and Wheatley [43]). In the cassava-mealybug-parasitoid system the

⁶*Manihot esculenta* Crantz

⁷*Phenacoccus manihoti* Mat.-Ferr.

⁸The larvae of a parasitoid feed on living host tissue such that the host is not killed until larval development is finished.

biomass of cassava is much larger than that of the mealybug and the parasitoid (an average cassava plant has a mass of about 2kg whereas the mealybug and parasitoids have average masses around 2mg). Scaling M_1 , at least, is thus vital.

Natural scalings⁹ for the state variables are given by their carrying capacities when resources are abundant. Gutierrez *et al.* [52] calculate these to be

$$K_i = \left[\frac{\theta_i D_i}{r_i} \right]^{\frac{1}{b_i}} \quad i = 1, 2, 3.$$

Replacing M_i by $K_i \bar{M}_i$ ($i=1,2,3$) and t by τt^* (here K_i has the dimensions of M_i and τ the dimensions of t and hence \bar{M}_i ($i=1,2,3$) and t^* are dimensionless variables) transforms equations (4.1) into system (4.2)¹⁰.

$$\begin{aligned} \frac{d\bar{M}_1}{dt^*} &= \frac{d\bar{M}_1}{dM_1} \frac{dM_1}{dt} \frac{dt}{dt^*} \\ &= \tau \left(\theta_1 D_1 \left(1 - \exp \left[-\frac{\alpha_1 M_0}{D_1 K_1 \bar{M}_1} \right] \right) - r_1 (K_1 \bar{M}_1)^{b_1} \right) \bar{M}_1 \\ &\quad - \tau \left(1 - \exp \left[-\frac{\alpha_2 K_1 \bar{M}_1}{D_2 K_2 \bar{M}_2} \right] \right) \frac{D_2 K_2}{K_1} \bar{M}_2 \\ \frac{d\bar{M}_2}{dt^*} &= \tau \left(\theta_2 D_2 \left(1 - \exp \left[-\frac{\alpha_2 K_1 \bar{M}_1}{D_2 K_2 \bar{M}_2} \right] \right) - r_2 (K_2 \bar{M}_2)^{b_2} \right) \bar{M}_2 \\ &\quad - \tau \left(1 - \exp \left[-\frac{\alpha_3 K_2 \bar{M}_2}{D_3 K_3 \bar{M}_3} \right] \right) \frac{D_3 K_3}{K_2} \bar{M}_3 \\ \frac{d\bar{M}_3}{dt^*} &= \tau \left(\theta_3 D_3 \left(1 - \exp \left[-\frac{\alpha_3 K_2 \bar{M}_2}{D_3 K_3 \bar{M}_3} \right] \right) - r_3 (K_3 \bar{M}_3)^{b_3} \right) \bar{M}_3. \end{aligned} \quad (4.2)$$

Note that $r_i K_i^{b_i} = \theta_i D_i$. Choosing the dimensionless combinations of parameters

$$\begin{aligned} \gamma_i &= \tau \theta_i D_i \quad i = 1, 2, 3 \\ \phi_i &= \tau \alpha_i \quad i = 2, 3 \\ \Omega_i &= \frac{\alpha_i K_i^{i-1}}{D_i K_i} \quad i = 1, 2, 3 \end{aligned}$$

⁹For an introduction to nondimensionalising systems of ordinary differential equations see [34].

¹⁰I replaced the product $\theta_1 \phi_{\eta,1} \phi_{\omega,1}$ by θ_1 since all three parameters have the same effect on the dynamics and, thus, do not need to be considered separately.

where $K_o = M_o$, gives the nondimensionalised equations (4.3) where I have replaced \bar{M}_i by M_i and t^* by t for convenience.

$$\begin{aligned}\frac{dM_1}{dt} &= \gamma_1 \left(\left(1 - \exp \left[-\frac{\Omega_1}{M_1} \right] \right) - M_1^{b_1} \right) M_1 - \frac{\phi_2}{\Omega_2} \left(1 - \exp \left[-\frac{\Omega_2 M_1}{M_2} \right] \right) M_2 \\ \frac{dM_2}{dt} &= \gamma_2 \left(\left(1 - \exp \left[-\frac{\Omega_2 M_1}{M_2} \right] \right) - M_2^{b_2} \right) M_2 - \frac{\phi_3}{\Omega_3} \left(1 - \exp \left[-\frac{\Omega_3 M_2}{M_3} \right] \right) M_3 \\ \frac{dM_3}{dt} &= \gamma_3 \left(\left(1 - \exp \left[-\frac{\Omega_3 M_2}{M_3} \right] \right) - M_3^{b_3} \right) M_3.\end{aligned}\quad (4.3)$$

The choice of dimensionless parameters is not unique. Other combinations would have led to slightly different final equations, however the above choices lend themselves to biological interpretation. For example, γ_i can be thought of as the potential per unit biomass growth rate [52] or as the conversion efficiency of the consumer in converting the resource into biomass. ϕ_i can be thought of as the availability of the resource to the consumer or perhaps the nutritional value of the resource. Ω_i is made up of a ratio of quantities. The numerator can be thought of as the maximum amount of resource available to the consumer and the denominator as the maximum demand of consumers for resource. More simply, Ω_i gives a measure of the ratio of supply to demand. The results in [52] are based on the relationship between ϕ_i and γ_i since τ is just a scaling factor, and hence results using equations (4.3) are comparable with those in [52].

I mentioned earlier that the parameters r_i in the original model have units which depend on b_i . This can be prevented by replacing the terms $r_i M_i^{1+b_i}$ with terms of the form $r_i M_i \left(\frac{M_i}{T_i} \right)^{b_i}$ where T_i has the same units as M_i . T_i can be thought of as a threshold value above which self-limitation becomes noticeable. With this modification the units of r_i are day^{-1} and r_i can be interpreted as a respiration rate as was originally intended. The new carrying capacities are given by

$$\left[\frac{\theta_i D_i}{r_i} \right]^{\frac{1}{b_i}} T_i ; i = 1, 2, 3.$$

It can be shown that setting the K_i 's equal to these new values and scaling the equations as above results in system (4.3) once again. Thus the problems with the respiration term can be ignored in the rest of the analysis.

Having scaled the equations we need to choose values for the parameters. An advantage of scaling is that there are now 11 parameters instead of the original 18. For comparison with the results of Gutierrez *et al.* [52] I wanted to find values which resulted in isocline configurations similar to those in their paper. XPPAUT calculates and displays isoclines in two dimensions and parameter values can be altered interactively. This proved useful for studying the effects of the different parameters on the isoclines. Since the competition effect is very small but difficult to quantify, I followed Gutierrez (personal communication) and chose $b_i = 0.02$ ($i=1,2,3$). Values of $\gamma_1 = 2.0$, $\gamma_2 = 0.4$, $\gamma_3 = 0.1$, $\Omega_1 = 9.0$, $\Omega_2 = 8.0$, $\Omega_3 = 10.0$, $\phi_2 = 0.4$, $\phi_3 = 0.05$ gave the isocline configurations shown in figure 4.1. These isoclines have similar shapes to those in [52]. A noticeable difference is that the M_3 isocline intersects the M_2 isocline to the left of the M_2 -peak. In fact, using the techniques in [52] it would not have been possible to conclude that the tritrophic equilibrium is stable for the isocline configuration shown in figure 4.1 because of the position of the intersection point in the M_2M_3 plane. For the above parameter set (which I shall call the reference set) there is also a stable limit cycle. The initial values of M_1 , M_2 and M_3 determine whether the system approaches the stable equilibrium or the limit cycle.

Biological considerations suggest that the above values for the Ω_i are rather high and that the value for ϕ_3 is rather low. However, in the absence of better information and since this parameter set has a nontrivial, stable equilibrium point, it is a convenient starting point.

Before beginning an analysis of the model I would like to introduce a small modification to the equations. Since the problems associated with ratio-dependent models

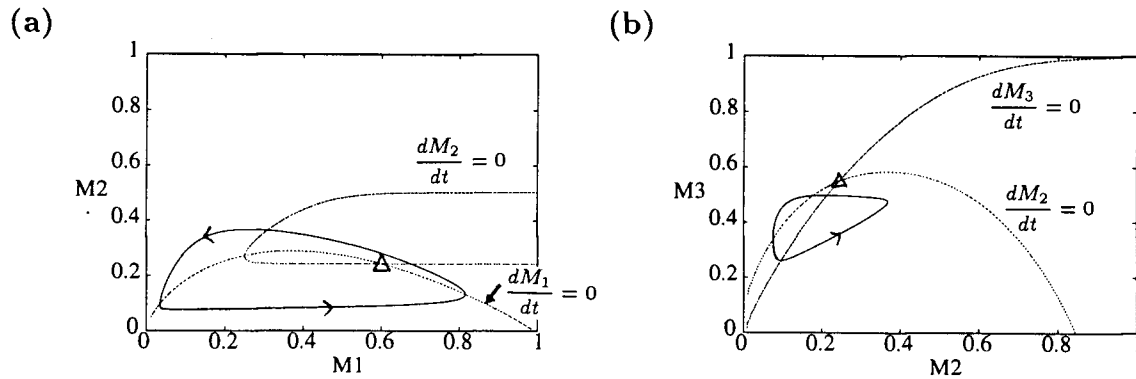


Figure 4.1: Isoclines in the (a) M_1M_2 and (b) M_2M_3 planes for $\gamma_1 = 2.0$, $\gamma_2 = 0.4$, $\gamma_3 = 0.1$, $\Omega_1 = 9.0$, $\Omega_2 = 8.0$, $\Omega_3 = 10.0$, $\phi_2 = 0.4$, $\phi_3 = 0.05$, and $b_i = 0.02$ ($i=1,2,3$). Both the stable equilibrium point and the limit cycle are shown. M_3 is fixed at 0.550 in (a) and M_1 is fixed at 0.602 in (b). These values correspond to the equilibrium point.

mentioned in section 4.2 involve low population densities, it would be interesting to know what effects a small modification to the model, which prevents the denominators of the ratios from getting too close to zero, would have on the dynamics. Abrams [1] states that modifications to ratio-dependent models cannot be made biologically realistic because the original models have no clear mechanistic derivation. However, some form of modification which prevents the ratios from tending to infinity may be useful for revealing any spurious behaviour near the axes which may result from the ratio-dependence.

The ratios in model (4.3) have the form

$$\frac{\Omega_i M_{i-1}}{M_i}.$$

The difficulties are experienced when M_i approaches zero. Adding a constant in the denominator, that is replacing the ratio by

$$\frac{\Omega_i M_{i-1}}{a_i + M_i}, \quad (4.4)$$

would alleviate the problem. Although this addition may appear difficult to justify

biologically, Gutierrez [51] used an exponent of this form in his functional response term. That model is physiologically based as is the present one.

In model (4.3) the ratio-dependent terms have the form

$$k \left(1 - \exp \left[-\frac{\Omega_i M_{i-1}}{M_i} \right] \right) M_i \quad (4.5)$$

where k is a parameter or combination of parameters. When the exponent is small we have

$$\begin{aligned} k \left(1 - \exp \left[-\frac{\Omega_i M_{i-1}}{M_i} \right] \right) M_i &\approx k \left(1 - \left(1 - \frac{\Omega_i M_{i-1}}{M_i} \right) \right) M_i \\ &= k \Omega_i M_{i-1}. \end{aligned}$$

In order to preserve this property when using the modified term (4.4), I replaced (4.5) by

$$k \left(1 - \exp \left[-\frac{\Omega_i M_{i-1}}{a_i + M_i} \right] \right) (a_i + M_i)$$

where a_i is a small constant, say 0.001. The resulting equations are:

$$\begin{aligned} \frac{dM_1}{dt} &= \gamma_1 \left(1 - \exp \left[-\frac{\Omega_1}{a_1 + M_1} \right] \right) (a_1 + M_1) - \gamma_1 M_1^{1+b_1} \\ &\quad - \frac{\phi_2}{\Omega_2} \left(1 - \exp \left[-\frac{\Omega_2 M_1}{a_2 + M_2} \right] \right) (a_2 + M_2) \\ \frac{dM_2}{dt} &= \gamma_2 \left(1 - \exp \left[-\frac{\Omega_2 M_1}{a_2 + M_2} \right] \right) (a_2 + M_2) - \gamma_2 M_2^{1+b_2} \\ &\quad - \frac{\phi_3}{\Omega_3} \left(1 - \exp \left[-\frac{\Omega_3 M_2}{a_3 + M_3} \right] \right) (a_3 + M_3) \\ \frac{dM_3}{dt} &= \gamma_3 \left(1 - \exp \left[-\frac{\Omega_3 M_2}{a_3 + M_3} \right] \right) (a_3 + M_3) - \gamma_3 M_3^{1+b_3}. \end{aligned} \quad (4.6)$$

If $a_i=0$ ($i = 1, 2, 3$) then the above model is equivalent to system (4.3). We are now in a position to begin the analysis.

4.5 Model analysis

4.5.1 One-parameter studies

Since a partial qualitative analysis of the original model was done by Gutierrez *et al.* [52] but using different techniques (namely, isocline analysis), it will be informative to compare some of the results. The choice of dimensionless parameters was done with this in mind. I begin the analysis by varying each parameter in turn using AUTO (through XPPAUT) to see how it affects the dynamics. This will be done for all the parameters except the b_i 's due to the observation that intraspecific competition at the i^{th} trophic level now increases as b_i decreases since M_i now lies between 0 and 1 as a result of the scaling. This was overlooked in the original model and can only be rectified by changing the formulation of the respiration term. Rather than modifying the model at this stage I chose instead to keep the b_i 's fixed. (For a given value of b_i respiration still increases with biomass as required.)

Since one of the main conclusions in Gutierrez *et al.* [52] concerns the relative efficacy of two parasitoids in controlling the cassava mealybug population, I begin by studying those parameters affecting the third trophic level, namely γ_3 , ϕ_3 and Ω_3 . I then discuss the remaining parameters. Both the original model corresponding to $a_i=0$ ($i = 1, 2, 3$) in system (4.6) and the modified model with $a_i=0.001$ ($i = 1, 2, 3$) are investigated. I chose this particular value for the a_i 's as it only affects the isocline configurations in figure 4.1 at low values of the state variables which is where the difficulties are encountered. I also investigate a few other values. The reference values for the other parameters are summarised in table 4.1. The results, together with possible biological interpretations, are described in the next section. For generality I will refer to the plant, herbivore (or prey) and predator biomasses rather than the cassava, mealybug and parasitoid since the reference parameter set was not chosen from experimental data.

Parameter	Description	Value
γ_1	potential growth rate per unit plant	2.0
γ_2	potential growth rate per unit herbivore	0.4
γ_3	potential growth rate per unit predator	0.1
ϕ_2	availability of plant to herbivore	0.4
ϕ_3	availability of herbivore to predator	0.05
Ω_1	supply of resources/demand by plants	9.0
Ω_2	supply of plants/demand by herbivores	8.0
Ω_3	supply of herbivores/demand by predators	10.0
b_1	degree of self-limitation for plants	0.02
b_2	degree of self-limitation for herbivores	0.02
b_3	degree of self-limitation for predators	0.02

Table 4.1: Reference parameter set. In the subsequent figures in this chapter, only those parameters which are explicitly mentioned have been altered. The values for all the other parameters correspond to the ones in this table.

Analysis of the predator parameters

The parameter γ_3 can be thought of as the potential predator biomass growth rate when prey are abundant, or as the predator's conversion efficiency in the presence of abundant prey. An important observation is that the value of γ_3 does not affect the isoclines. The M_3 zero isocline is given by $\frac{dM_3}{dt} = 0$ and the solution of this equation is independent of γ_3 (see equations (4.6)). Hence, an isocline analysis similar to that done in [52] would not give any insight into how this parameter influences the behaviour of the system.

Bifurcation diagrams showing the effects of varying γ_3 for both the original model and the modified model are shown in figure 4.2. M_1 is plotted on the y-axis. These diagrams were obtained using AUTO through XPPAUT. The system was first integrated numerically until it was close to an equilibrium and then XPPAUT was used to find the exact location of the equilibrium point (singular point). This point was used as a starting point for AUTO.

In both the diagrams in figure 4.2 the position of the equilibrium point does not vary

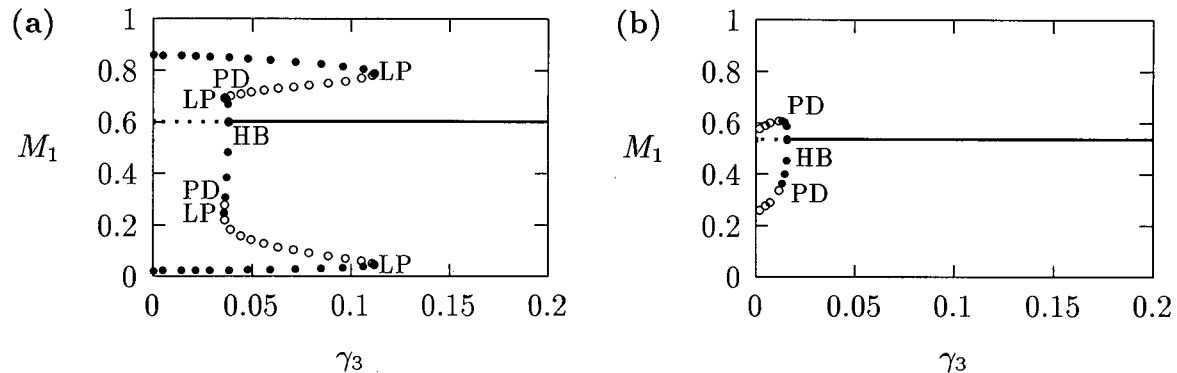


Figure 4.2: One-parameter bifurcation diagrams obtained by varying γ_3 in (a) the original model ($a_i=0$, $i = 1, 2, 3$) and (b) the modified model ($a_i=0.001$, $i = 1, 2, 3$). The state variable M_1 is plotted on the y-axes. HB denotes a Hopf bifurcation, LP a limit point and PD a period-doubling bifurcation.

with γ_3 , which agrees with the previous observation that γ_3 does not affect the isocline configuration. However, γ_3 does affect the stability of the system. In both cases the equilibrium point is unstable for very low values of γ_3 (low predator growth rate) and the stable attractor is a limit cycle for these values. For the original model we have an example of *hard loss of stability* (see section A.2.7) so that for certain values of γ_3 there are two stable attractors—a sink and a stable limit cycle (such as in figure 4.1). The initial values of the state variables determine which final state is reached. Also, perturbations to the system may cause a jump from one stable attractor to the other if the disturbance is sufficiently large. For a very small range of γ_3 values there are two stable limit cycles in figure 4.2(a). The range of values is so small, however, that it is not of much biological significance.

Observing the temporal dynamics of the system (using XPPAUT) for different values of γ_3 I found that larger values of γ_3 decrease the time taken to reach equilibrium. Thus, increasing γ_3 , the potential growth rate of the predator, has a stabilising influence on the system. This seems biologically plausible as higher values of γ_3 suggest that the predator is better adapted to controlling its prey. It is interesting, however, that this trait does

not affect any of the equilibrium biomasses.

The modified model has a much smaller range of parameter values over which cycles occur and the amplitudes of these cycles are smaller than for the original model (see figure 4.2). Thus, even though the a_i 's have small values, they appear to have a stabilising influence on the dynamics.

Another parameter which directly affects the predator is ϕ_3 , the availability (or nutritional value) of the herbivore to the predator. Bifurcation diagrams for the original and modified models respectively and for all three state variables are shown in figures 4.3 and 4.4.

From these figures we can see that as ϕ_3 increases there is a general increase in the M_1 equilibrium value or limit cycle maximum. The larger ϕ_3 the greater the availability of the herbivore to the predator and the easier it is for the predator to control the herbivore. Obviously, the lower the herbivore population the higher the plant equilibrium. As the M_1 equilibrium value approaches the M_1 carrying capacity in the original model, a Hopf bifurcation (see section A.2.10) occurs at $\phi_3 = 0.09$ (see figure 4.3). The periodic orbit associated with this Hopf bifurcation undergoes a number of period-doubling bifurcations (see section A.2.16) which leads to more complicated cycling behaviour. An example of the temporal dynamics when $\phi_3 = 0.16$ is shown in figure 4.5. There are two complete cycles in these diagrams. It is interesting that the predator dynamics are less variable than those of the plant and the herbivore. This cycling behaviour also contrasts with that described by Akçakaya *et al.* [3] as being biologically plausible for low herbivore and predator values (see section 4.2).

As ϕ_3 increases above the upper Hopf bifurcation the minima of the M_2 and M_3 cycles in particular get very small (of the order of 10^{-15} and lower according to XPPAUT's data window). From a practical viewpoint these populations would be considered extinct due to statistical variation in which case the plant population would increase to its carrying

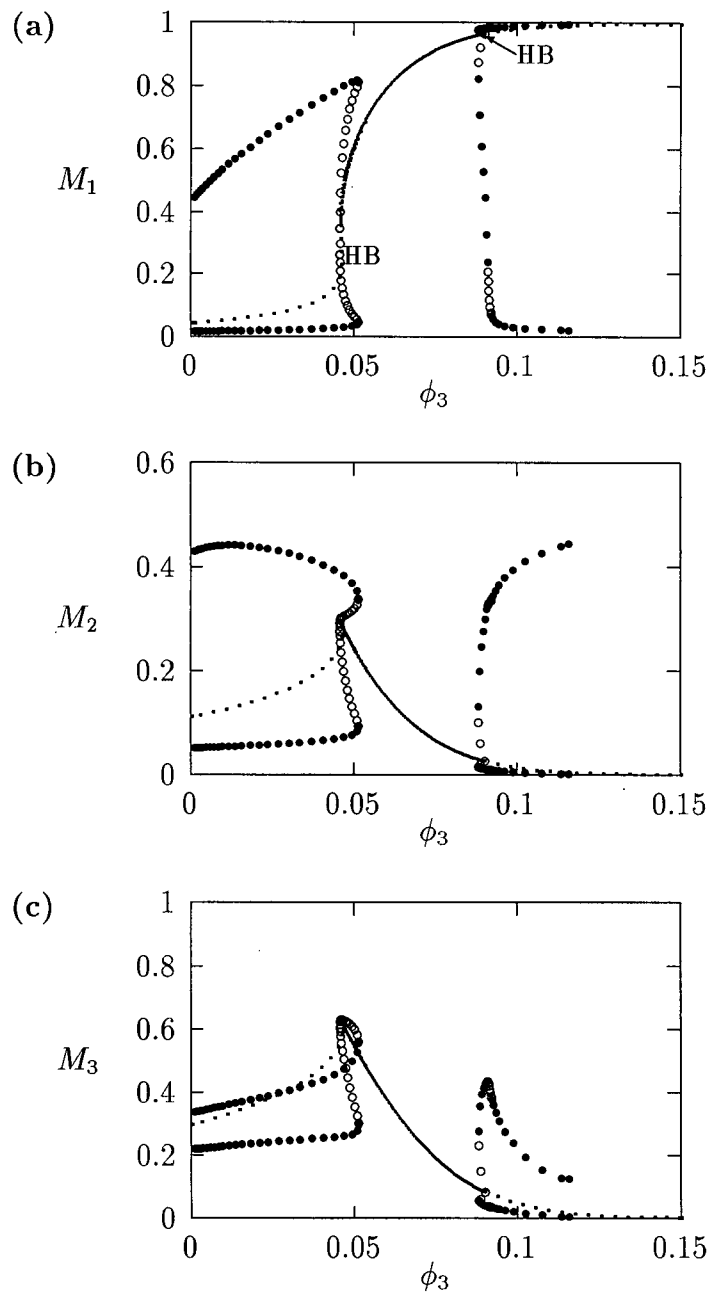


Figure 4.3: One-parameter bifurcation diagrams obtained by varying ϕ_3 in the original model. The state variables M_1 , M_2 and M_3 are plotted on the y-axes in (a), (b) and (c) respectively. Only the positions of the Hopf bifurcations have been indicated. The changes in stability of the limit cycles occur at limit points or period-doubling bifurcations but these have not been marked in the diagrams.

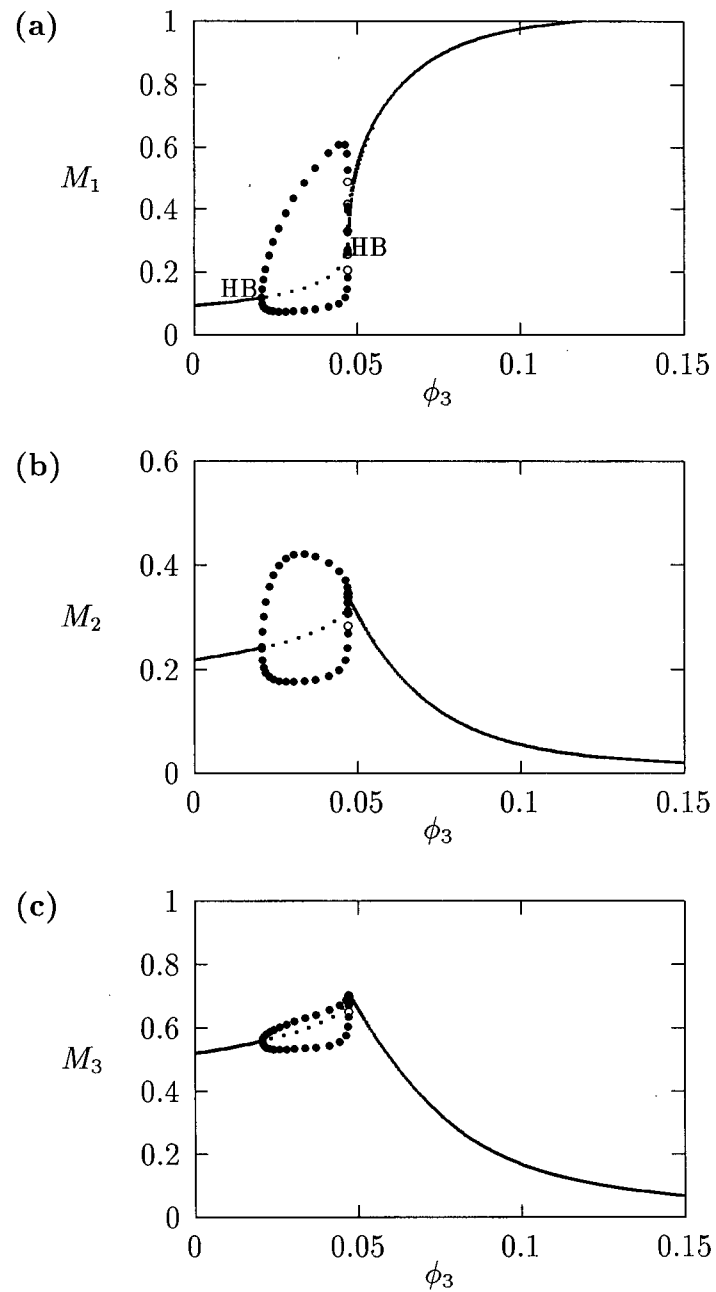


Figure 4.4: One-parameter bifurcation diagrams obtained by varying ϕ_3 in the modified model. The state variables M_1 , M_2 and M_3 are plotted on the y-axes in (a), (b) and (c) respectively.

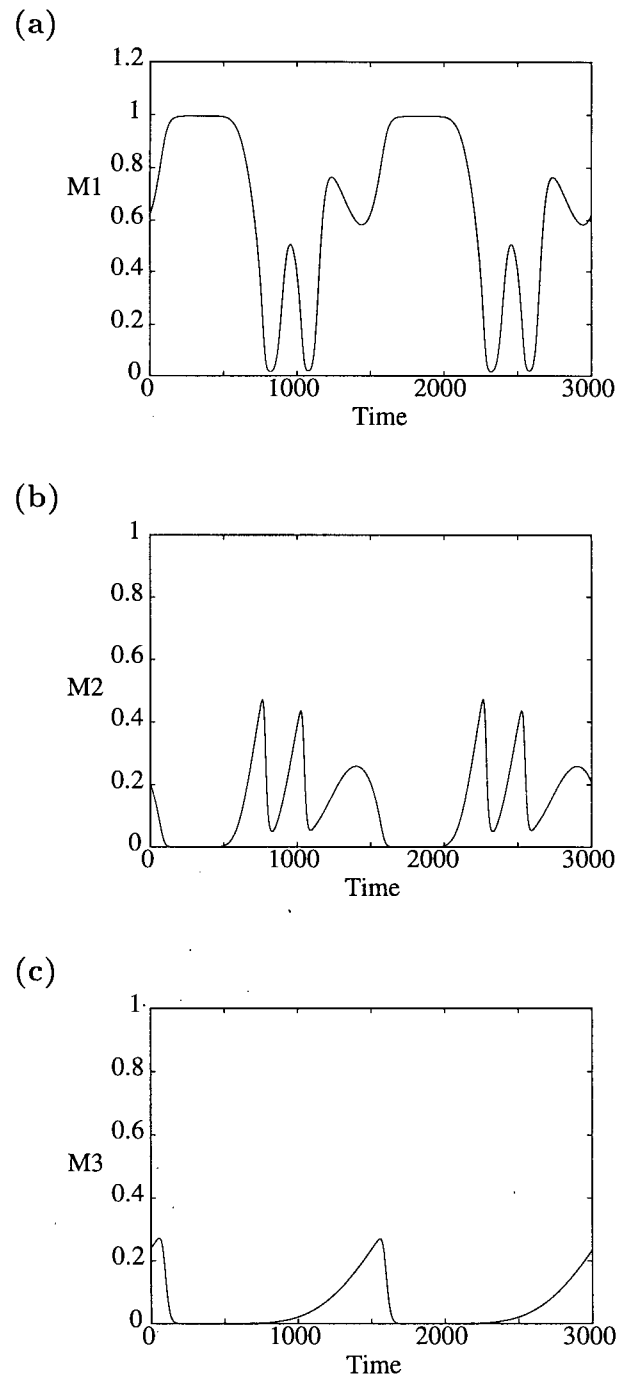


Figure 4.5: Time plots of (a) M_1 , (b) M_2 and (c) M_3 for $\phi_3 = 0.16$. All the other parameter values are as in the reference parameter set.

capacity for these values of ϕ_3 . This is exactly the case for the modified model (see figure 4.4). Thus the upper Hopf bifurcation may be an artifact of ratio-dependent models. This will be discussed in more detail later.

Another problem with these low minima is that they lead to numerical difficulties. This occurs as a result of the way in which the model is formulated—the dependence of many of the terms on the ratio $\frac{M_{i-1}}{M_i}$ in particular. These ratios become difficult to evaluate numerically as M_i approaches zero causing the ratio to tend to infinity. XPPAUT cannot calculate zero isoclines and crashes while AUTO often enters an infinite loop if such a situation arises and may crash. Setting the total number of steps for a continuation fairly low sometimes allows AUTO to break out of the loop and signal non-convergence. Manually stopping a continuation when one of the state variables gets very close to zero also prevents the package from crashing. This explains why the limit cycles in figure 4.3 are only calculated up to $\phi_3 = 0.12$. The above problems do not occur when using the modified model.

It may have been noticed that ϕ_3 has a significant effect on the equilibrium values of all three state variables. This is in agreement with Gutierrez *et al.* [52]. However, the way in which they arrive at this conclusion is not entirely correct. In Gutierrez *et al.* [52] it is stated that a less efficient parasitoid has a wider C-shaped M_2 -isocline. It is true that if ϕ_3 is decreased the M_2 -isocline widens (see figures 4.6(a) and (b)). But this is *provided that M_3 is constant*. If the system is integrated and M_3 is allowed to vary until a new equilibrium is reached and the isoclines are plotted with this new equilibrium M_3 value, then the final M_2 -isocline may in fact have a narrower C-shape than before (see figure 4.6(c)).

The third parameter which directly affects the predator is Ω_3 . It is more difficult to interpret this parameter biologically but it can be thought of as the ratio of the ‘supply’ of herbivore to the ‘demand’ of the predator when both populations are at their carrying

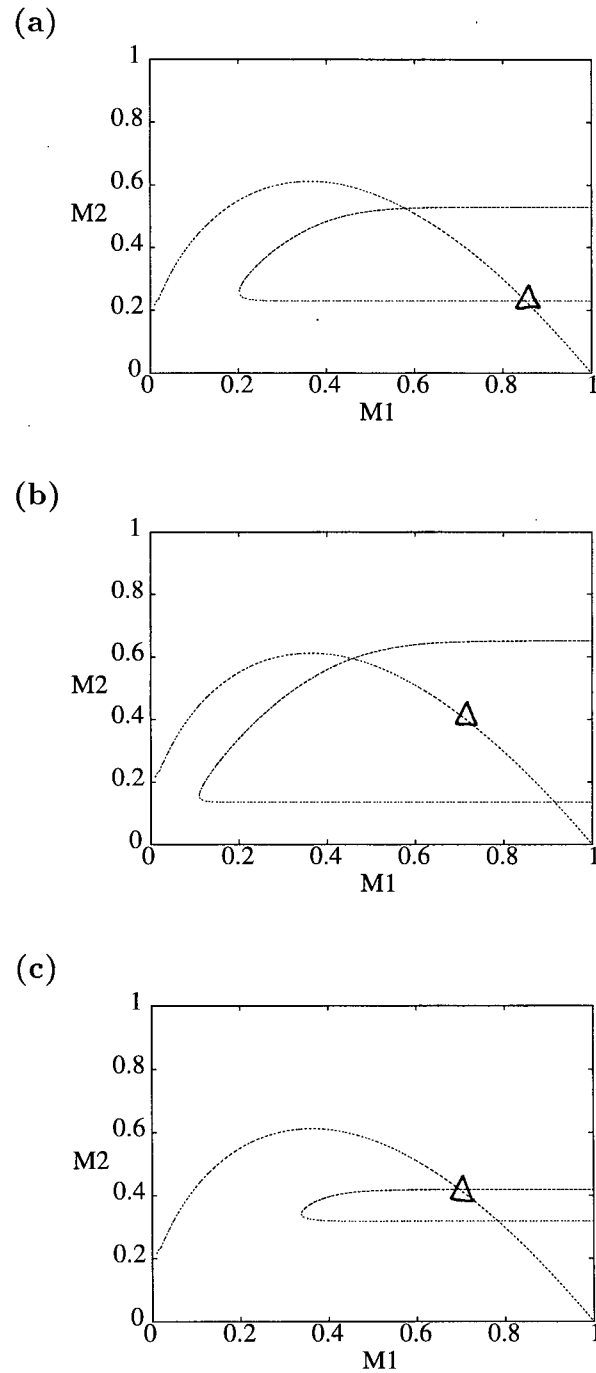


Figure 4.6: Isoclines in the M_1M_2 plane. In (a) $\phi_3 = 0.06$ and in (b) and (c) $\phi_3 = 0.05$. All the other parameter values are fixed. In (a) and (b) M_3 has the same value—the value corresponding to the stable tritrophic equilibrium point in (a) when $\phi_3 = 0.06$. In (c) M_3 has the value corresponding to the equilibrium point when $\phi_3 = 0.05$.

capacities. Hence it reflects how limiting resources are to the predator. Figure 4.7 shows the bifurcation diagrams corresponding to the original model for all three state variables.

For most values of Ω_3 there is no change in the qualitative behaviour which in this case is given by stable limit cycles. Even the amplitudes of these cycles do not alter much although those for M_3 decline slowly as Ω_3 is increased. It is only at low values of Ω_3 that a change in dynamics occurs. It is also at these low values that Ω_3 has the greatest effect on equilibrium magnitudes. Low values of Ω_3 suggest a restricted supply in relation to demand and are reflected in both low M_2 and low M_3 equilibrium values. Since there are *relatively* fewer herbivores available (in relation to predators) the predators are able to control them better but the lower herbivore equilibrium also restricts the number of predators that can survive. As expected, lower equilibrium values for M_2 correspond to higher equilibrium values for M_1 .

The corresponding bifurcation diagrams for the modified model are shown in figure 4.8. These diagrams are very similar to those in figure 4.7 except that there is a second Hopf bifurcation resulting in first a decline in the amplitudes of the cycles followed by a stable tritrophic equilibrium as Ω_3 is increased. Again the introduction of the a_i 's has had a stabilising influence on the dynamics. From figure 4.8 we can clearly see that high values of Ω_3 are, however, undesirable as the M_1 equilibrium value is low while that for M_2 is relatively high.

The above analysis has shown that the properties of the predator affect the stability of the system as well as the equilibrium magnitudes of the herbivore (directly) and the plant (indirectly). The extent of these effects depends on the properties of both the plant and the herbivore. In the next section the parameters affecting these lower two trophic levels are examined in more detail.

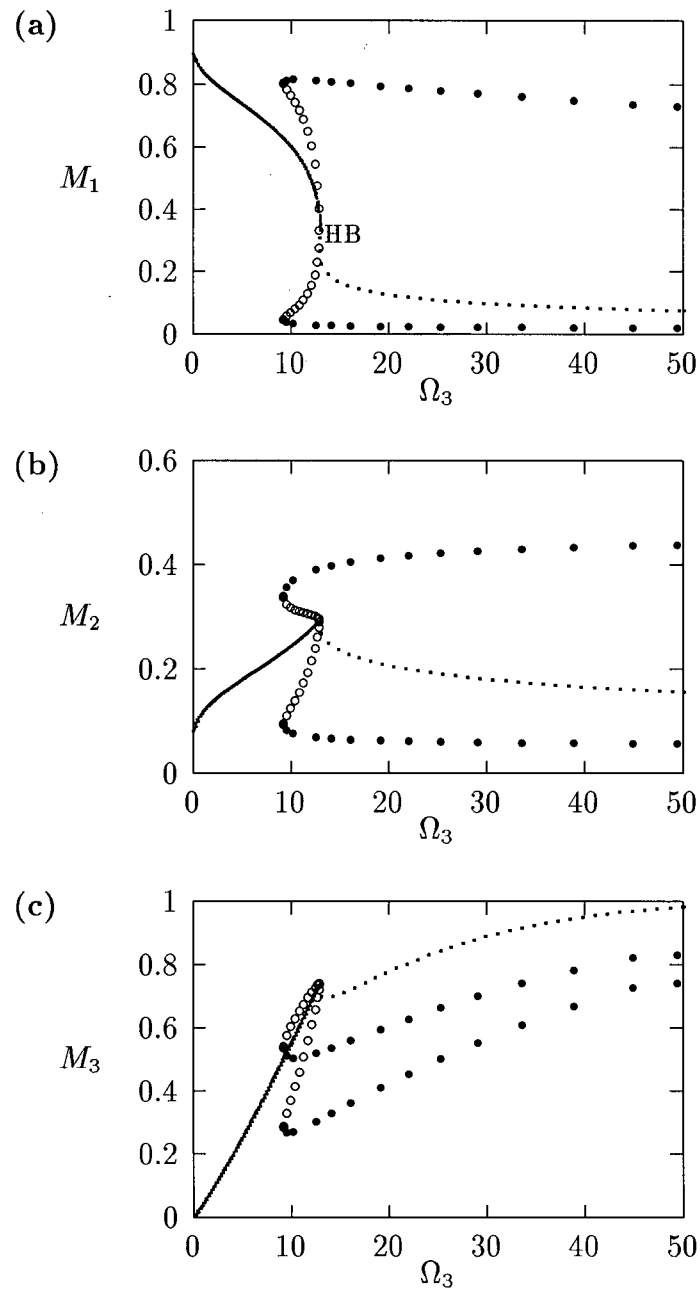


Figure 4.7: One-parameter bifurcation diagrams obtained by varying Ω_3 in the original model. The state variables M_1 , M_2 and M_3 are plotted on the y-axes in (a), (b) and (c) respectively.

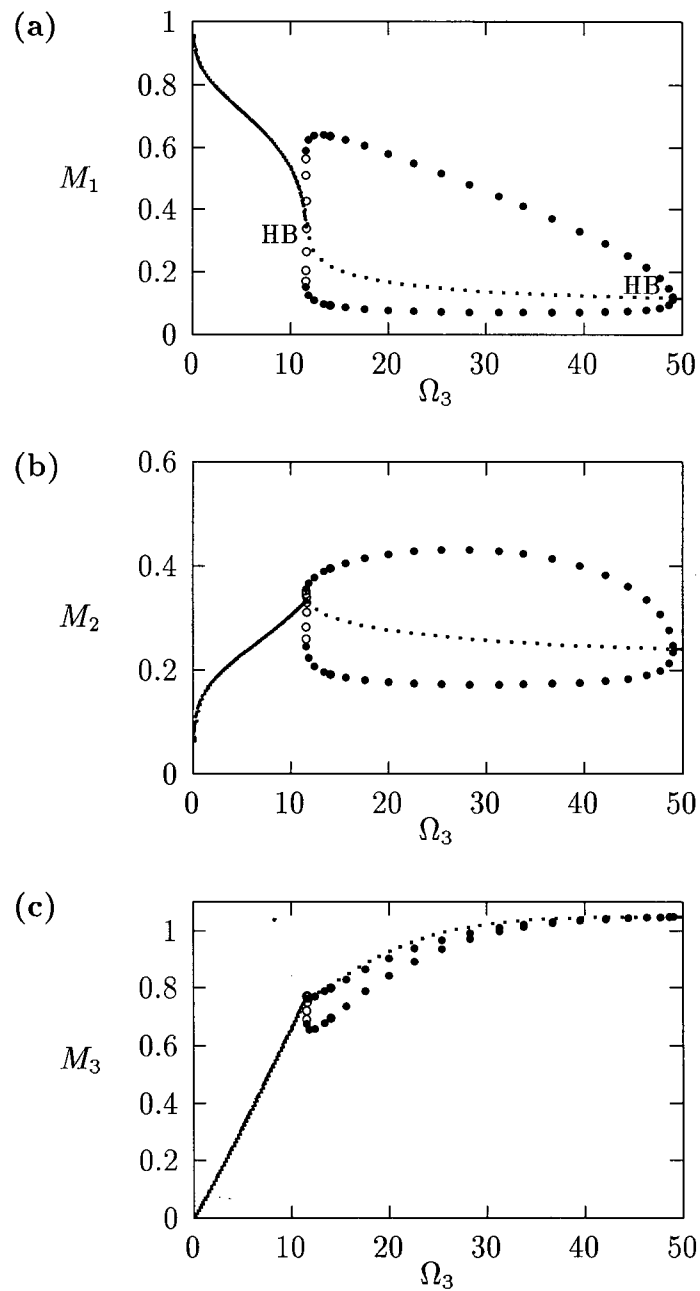


Figure 4.8: One-parameter bifurcation diagrams obtained by varying Ω_3 in the modified model. The state variables M_1 , M_2 and M_3 are plotted on the y-axes in (a), (b) and (c) respectively.

Analysis of the plant and herbivore parameters

The parameter ϕ_2 can be thought of as the availability or the nutritional value of the plant to the herbivore. The bifurcation diagrams for the original and modified models respectively and for M_1 , M_2 and M_3 are shown in figures 4.9 and 4.10.

For both models the values of M_2 and M_3 at equilibrium remain constant for the most part as ϕ_2 is varied (up to a limiting point) while the M_1 equilibrium value declines. A possible explanation is that, due to the greater availability of the plant to the herbivore, a lower plant biomass can support the same biomass of herbivore at a higher ϕ_2 value. This enables the herbivore to have an even greater impact on the plant. If ϕ_2 is sufficiently high then the herbivore can send the plant population to extinction. This is suggested by the very low cycle minima for the original model and is even clearer for the modified model where the M_1 equilibrium value is very low for $\phi_2 > 1.061$ (the location of the Hopf bifurcation). Of course, once the plant is extinct both the herbivore and the predator are forced into extinction as well. This can be checked by observing the temporal dynamics of the system using XPPAUT for ϕ_2 to the right of the upper Hopf bifurcation ($\phi_2 > 1.061$) using the modified model.

For the original model we again have the problem of very low cycle minima for the state variables. These are biologically unrealistic and cause numerical difficulties. The modified model does not have this problem.

Suppose we vary γ_1 , the assimilation or conversion efficiency of the plant when resources are abundant. The bifurcation diagrams are shown in figure 4.11. Comparing these diagrams with figures 4.9 and 4.10 we see that they are almost mirror images. That is, decreasing γ_1 has a very similar effect to increasing ϕ_2 . Both parameters can be thought of as affecting the resistance of the plant to the herbivore. Decreasing γ_1 lowers the quality of the plant as it cannot convert resources as effectively. As a result the

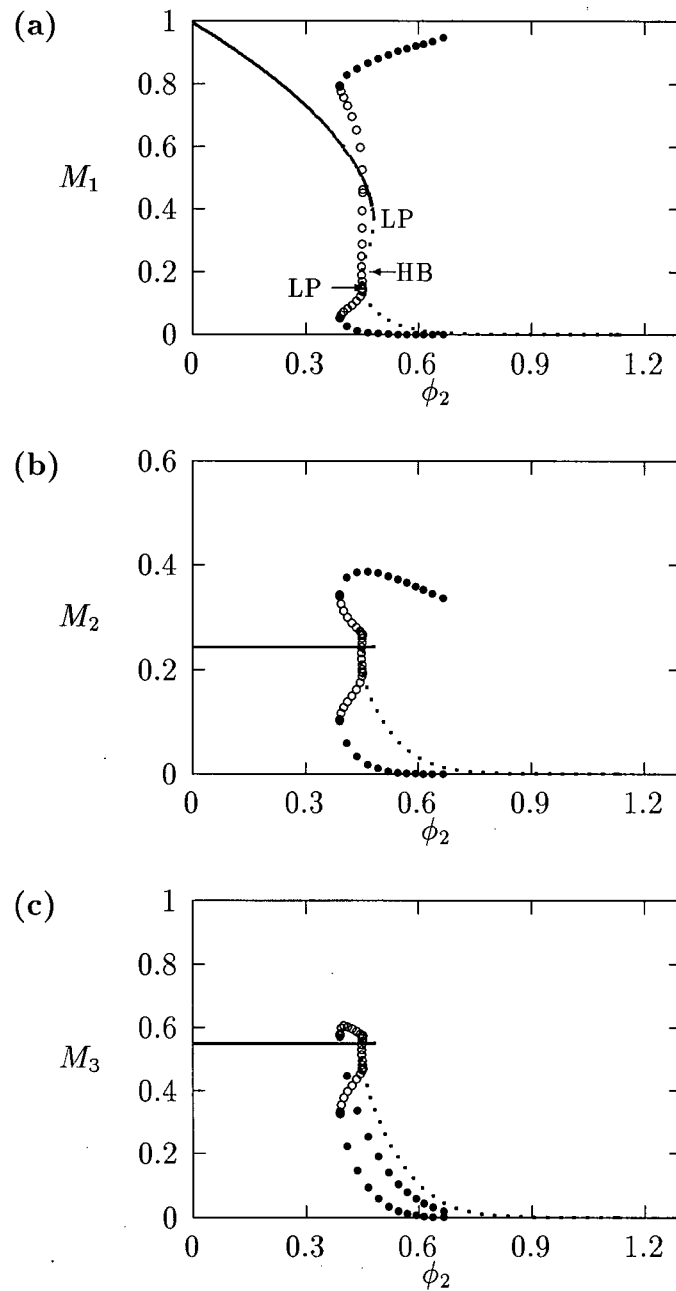


Figure 4.9: One-parameter bifurcation diagrams showing the effects of varying ϕ_2 for the original model. The state variables M_1 , M_2 and M_3 are plotted on the y-axes in (a), (b) and (c) respectively.

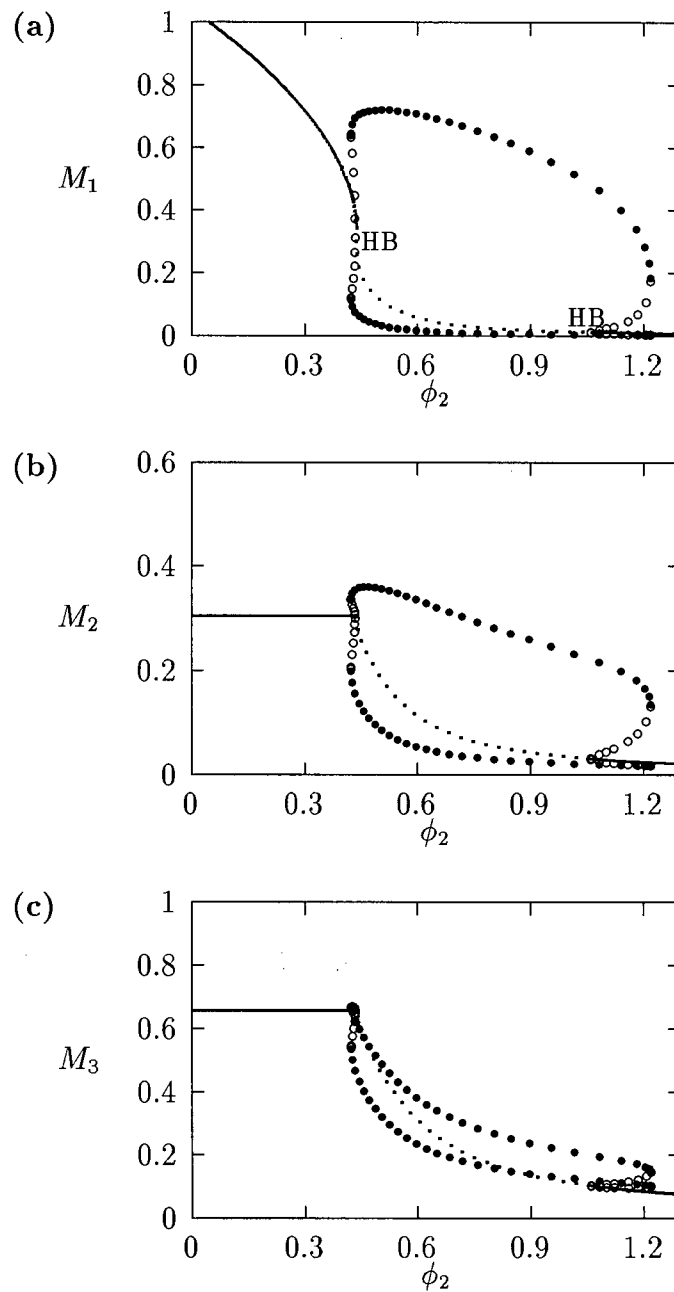


Figure 4.10: One-parameter bifurcation diagrams showing the effects of varying ϕ_2 for the modified model. The state variables M_1 , M_2 and M_3 are plotted on the y-axes in (a), (b) and (c) respectively.

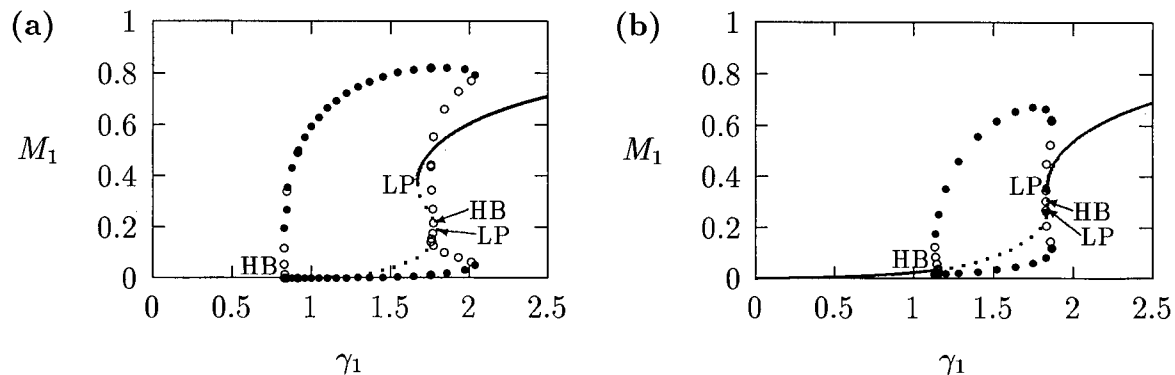


Figure 4.11: One-parameter bifurcation diagrams showing the effects of varying γ_1 for (a) the original model and (b) the modified model. The state variable M_1 is plotted on the y-axes. The limit points (LP) mark the endpoints of the region of hysteresis (see section A.2.11).

detrimental effect of the herbivore on the plant is greater. Increasing ϕ_2 , the availability (nutritional value) of the plant to the herbivore, achieves the same result but more directly.

We can generate two-parameter diagrams in (γ_1, ϕ_2) -space by continuing the limit points and the Hopf bifurcations in two parameters (see sections A.2.1 and B.4). The results are shown in figure 4.12—solid lines indicate Hopf bifurcation continuations and dotted lines indicate limit point continuations. These diagrams show clearly that decreasing ϕ_2 or increasing γ_1 has a similar effect and that there is a transition between different types of qualitative behaviour as the region enclosed by the limit point continuations is crossed.

Part of this result could have been predicted from [52] since they note that it is the *ratio* of γ_1 and ϕ_2 that determines the nature of the plant isocline. We thus expect this inverse relationship. However, the one-parameter bifurcation diagrams have given us the additional information that for certain parameter ranges limit cycles and/or multiple stable states are possible. Both these phenomena are important biologically.

We can make a number of observations by comparing figures 4.12(a) and (b). First,

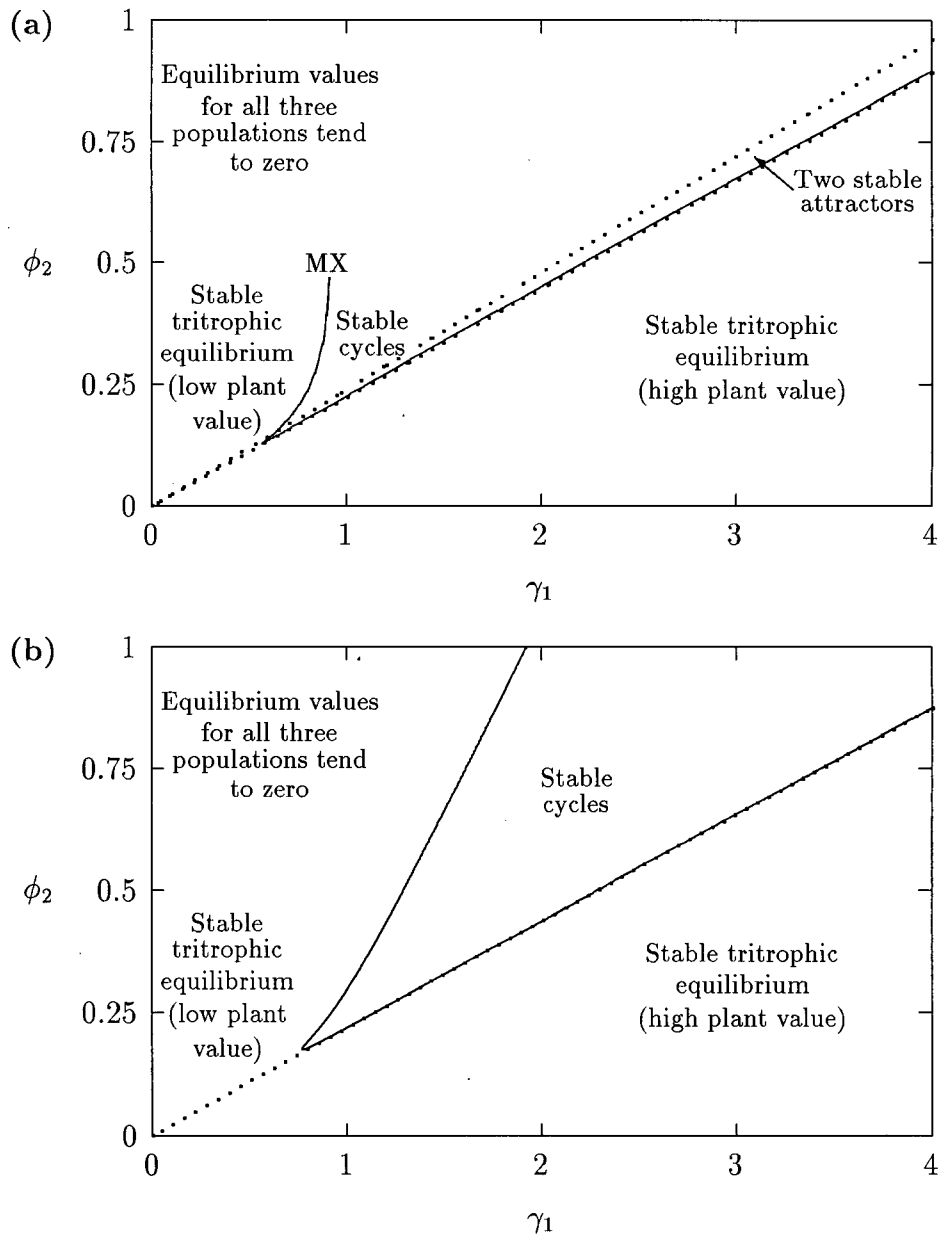


Figure 4.12: Two-parameter bifurcation diagrams showing the effects of varying both γ_1 and ϕ_2 on the positions of the limit points and Hopf bifurcations in figure 4.11. The diagram in (a) corresponds to the original model and that in (b) to the modified model. Solid lines indicate Hopf bifurcation continuations and dotted lines indicate limit point continuations.

whereas in (a) AUTO could not calculate beyond the point denoted by MX, this problem does not occur in (b). A closer investigation reveals that the equilibrium values for the state variables are close to zero in the upper left triangle of the two-parameter space and this results in numerical problems when using the original model. XPPAUT also has difficulty calculating zero isoclines in this region and often crashes. However, figure 4.12(b) gives a more complete picture of the dynamics. There are three distinct regions in this diagram two of which correspond to stable tritrophic equilibria while stable cycles occur in the other. One of the regions of stable equilibria has high equilibrium values of M_1 but the other has low equilibrium values—an important distinction ecologically.

The parameters γ_2 and ϕ_3 also appear to have inverse effects if we compare the average of the cycle maxima and minima when γ_2 and ϕ_3 are varied independently (compare figures 4.3, 4.4 and 4.13). We can investigate this relationship in more detail by continuing the Hopf bifurcations in figure 4.13 in ϕ_3 as well as γ_2 . The results are shown in figure 4.14.

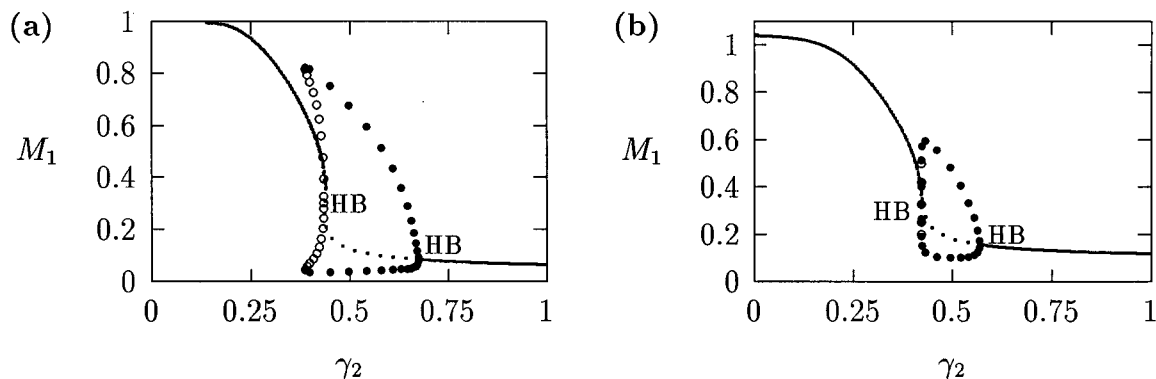


Figure 4.13: One-parameter bifurcation diagrams showing the effects of varying γ_2 for (a) the original model and (b) the modified model.

Again, in general decreasing ϕ_3 has a similar effect to increasing γ_2 . However there are a few more Hopf bifurcations associated with these parameters. AUTO stops at the

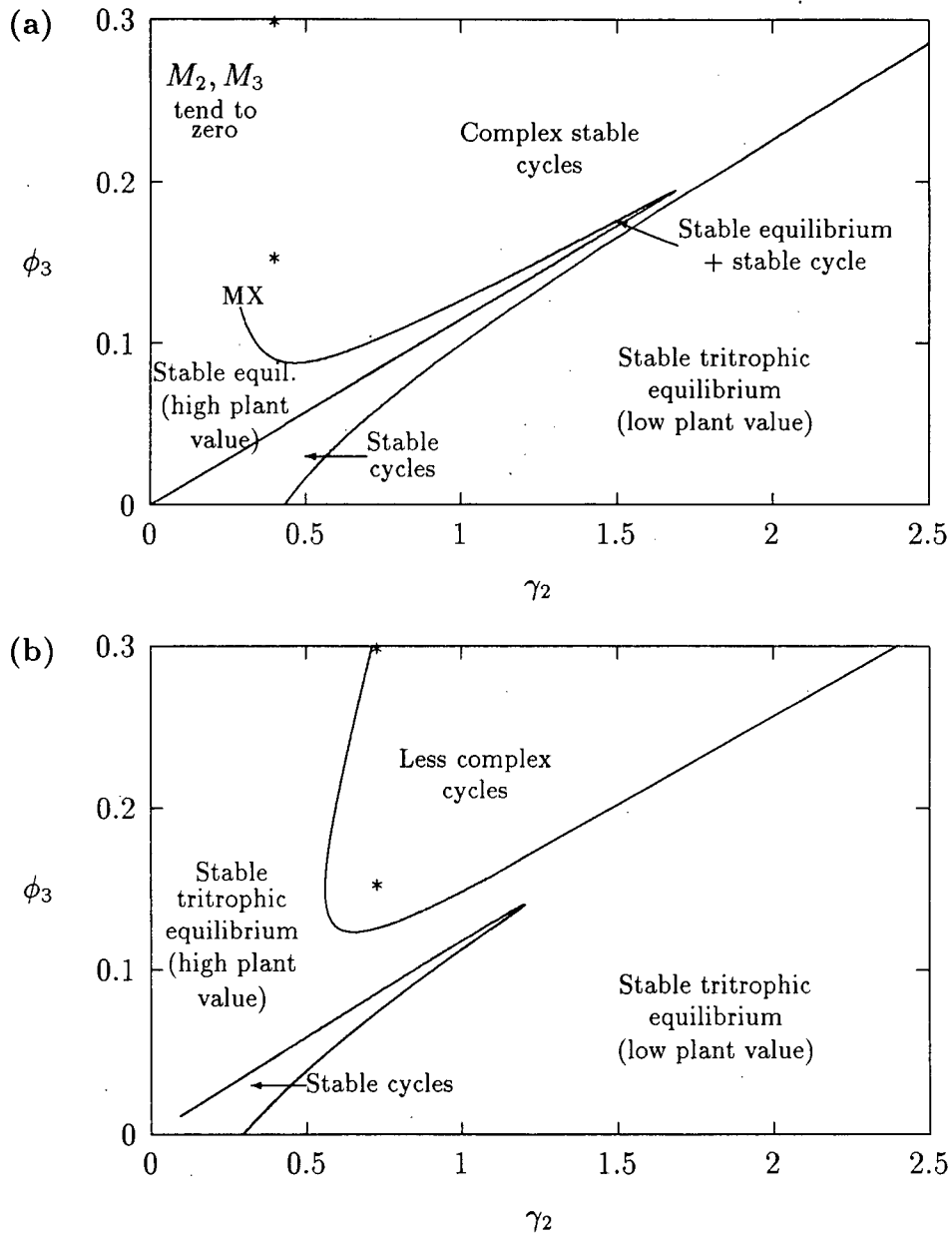


Figure 4.14: Two-parameter bifurcation diagrams showing the effects of varying both γ_2 and ϕ_3 on the positions of the Hopf bifurcations in figure 4.13.

point marked MX when using the original model since the equilibrium values for M_2 and M_3 are very small here. The complete continuation is shown in figure 4.14(b) using the modified model. By comparing the two diagrams in figure 4.14 it can be seen that the dynamics for the modified model, while very similar to those for the original model, are more stable in general. The regions corresponding to tritrophic equilibria are larger and the cycles in the upper half of the two-parameter space are less complex. These claims are made clearer in figures 4.15 and 4.16.

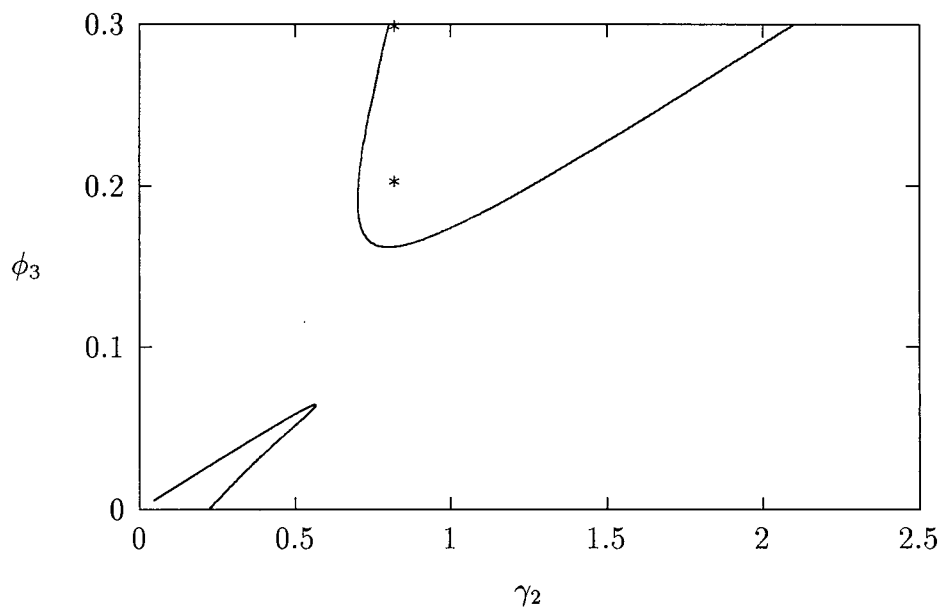


Figure 4.15: Two-parameter bifurcation diagram of the Hopf bifurcation continuations in (γ_2, ϕ_3) -space for the modified model with $a_i=0.002$ ($i = 1, 2, 3$).

Figure 4.15 shows the (γ_2, ϕ_3) -space for the modified model with $a_i=0.002$ ($i = 1, 2, 3$). The regions of stable equilibria are even larger than in figure 4.14(b) resulting in smaller regions of cycles. The presence of the a_i 's seems to have a stabilising effect on the dynamics of the system.

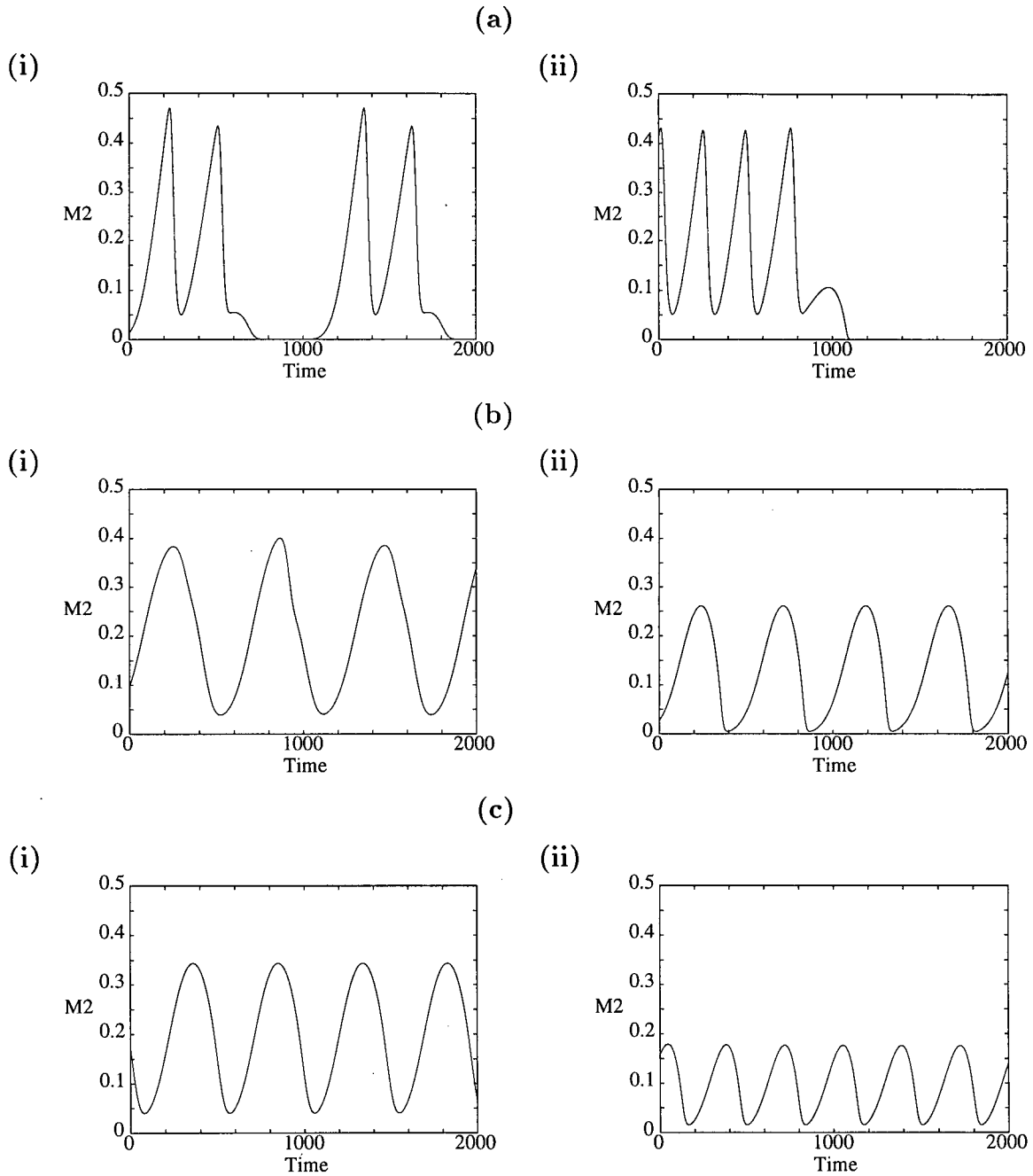


Figure 4.16: Time plots corresponding to the points marked with *'s in figures 4.14(a), 4.14(b) and 4.15. (a) These plots were obtained using the original model with (i) $\gamma_2=0.4$, $\phi_3=0.15$ and (ii) $\gamma_2=0.4$, $\phi_3=0.3$. (b) These plots were obtained using the modified model with $a_i=0.001$ ($i = 1, 2, 3$) and (i) $\gamma_2=0.7$, $\phi_3=0.15$ and (ii) $\gamma_2=0.7$, $\phi_3=0.3$. (c) These plots were obtained using the modified model with $a_i=0.002$ ($i = 1, 2, 3$) and (i) $\gamma_2=0.8$, $\phi_3=0.2$ and (ii) $\gamma_2=0.8$, $\phi_3=0.3$.

Figure 4.16 shows the time plots corresponding to points marked with *'s in the left-hand section of the upper region of cycles in figures 4.14(a),(b) and 4.15. The left-hand portion of this region is where the values of M_2 and M_3 are low and, hence, where the nonzero a_i 's have most effect. Clearly nonzero a_i 's reduce the complexity of the cycles (even for very small values) and increasing their value also reduces the cycle amplitude. An additional point to note is that the cycles for the original model ($a_i=0$, $i = 1, 2, 3$) undergo long periods of extremely low values which is unrealistic from an ecological viewpoint.

The only parameters that have not been discussed so far are Ω_1 and Ω_2 . Bifurcation diagrams corresponding to Ω_1 are shown in figure 4.17. Only the diagrams for M_1

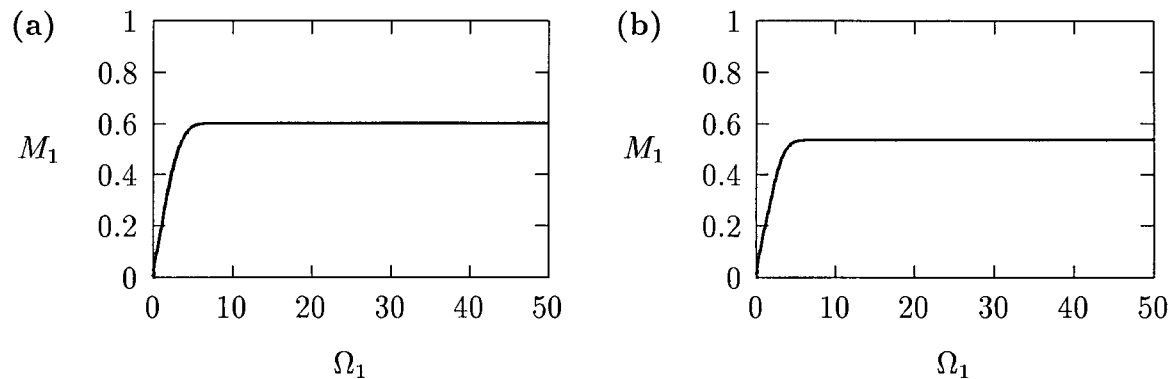


Figure 4.17: One-parameter bifurcation diagrams showing the effects of varying Ω_1 for (a) the original model and (b) the modified model. The state variable M_1 is plotted on the y-axes.

have been shown but those for M_2 and M_3 have the same shape—the carrying capacity equilibria are however different. As can be seen from figure 4.17, in both cases Ω_1 does not affect the stability of the equilibrium point and only affects equilibrium magnitudes when it drops to low values.

Similar conclusions can be made regarding Ω_2 (see figure 4.18) except that at low Ω_2 values there is a change in dynamics to stable limit cycles for both models although the

range of parameter values giving rise to cycles is slightly smaller for the modified model.

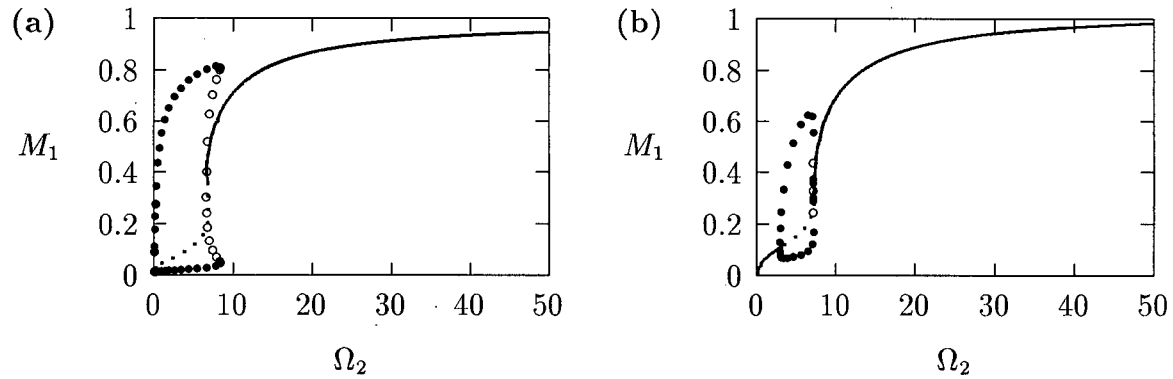


Figure 4.18: One-parameter bifurcation diagrams showing the effects of varying Ω_2 for (a) the original model and (b) the modified model. The state variable M_1 is plotted on the y-axes.

4.5.2 Combining plant and herbivore dynamics

In the previous section it was seen that γ_1 , ϕ_2 , γ_2 and ϕ_3 all have significant effects on the dynamics of the model. The former two parameters determine the properties of the plant and the latter two the properties of the herbivore. The two-parameter diagrams in figures 4.12 and 4.14 thus summarise the effects of the plant and herbivore trophic levels respectively provided that the dynamics of the other trophic levels are constant. It would be interesting to know how the behaviour of the model changes as *both* the plant and the herbivore dynamics are altered. This is the focus of the present section. The modified model with $a_i=0.001$, ($i = 1, 2, 3$) is used to investigate the interaction of the two trophic levels as this model allows a more complete picture of the dynamics to be obtained than the original model.

Figure 4.12 shows that increasing γ_1 or decreasing ϕ_2 has a similar effect. Generating two-parameter diagrams of the (γ_2, ϕ_3) -space for different (fixed) values of one of these

plant parameters, say γ_1 , will thus give an idea of the combined effects of the plant and herbivore. Figures 4.19, 4.20, 4.21, 4.22 and 4.23 show the Hopf bifurcation and limit point continuations for five values of γ_1 , namely $\gamma_1 = 0.4, 0.6, 1.2, 1.8$ and 2.4 . Figure 4.14(b) corresponds to $\gamma_1 = 2.0$ and can be viewed in conjunction with these diagrams.

As can be seen from these diagrams, altering γ_1 affects the shape and/or the position of the Hopf bifurcation continuations (solid lines) and the limit point continuations (dotted lines). Let us consider the limit point continuations first. Figures 4.24(a), (b) and (c) show one-parameter bifurcation diagrams obtained by varying γ_2 with $\gamma_1 = 0.4$ and $\phi_3 = 0.07, 0.17$ and 0.25 respectively. These diagrams correspond to the horizontal dotted lines in figure 4.19. The limit points in these diagrams demarcate the region of hysteresis, that is, the range of parameter values giving rise to multiple equilibria. We can see that this range of values increases as ϕ_3 increases.

The existence of a hysteresis phenomenon does not imply the existence of two *stable* equilibria. This depends on other factors such as the occurrence of Hopf bifurcations. In figure 4.24(a) there are two stable equilibria for γ_2 between the two limit points ($0.18 < \gamma_2 < 0.30$). One of these stable equilibria corresponds to a low equilibrium M_1 value and the other to a high equilibrium M_1 value. The unstable equilibrium intermediate to these stable equilibria demarcates their domains of attraction and indicates the extent of the perturbation (in terms of M_1) required to move the system from one stable attractor to the other (refer to section A.2.11). In figures 4.24(b) and (c) the region of two stable equilibria occurs between the lower limit point and the Hopf bifurcation on the upper branch of equilibria ($0.41 < \gamma_2 < 0.57$ in (b) and $0.60 < \gamma_2 < 0.65$ in (c)).

Collating the information obtained from figure 4.24 allows us to classify the different regions in figure 4.19 according to the qualitative behaviour that is found there. That is, the region enclosed by the limit point continuations (region of hysteresis) can be divided into a region of two stable equilibria and a region of only one stable equilibrium having a

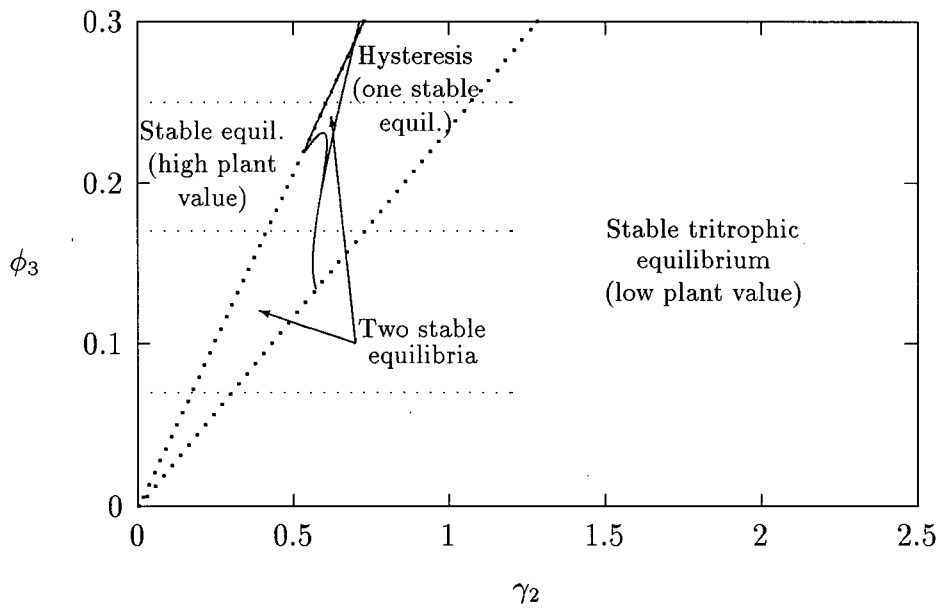


Figure 4.19: Two-parameter bifurcation diagram obtained using the modified model with $a_i=0.001$, ($i = 1, 2, 3$) and $\gamma_1 = 0.4$. The Hopf bifurcation continuations are indicated by solid lines and the limit point continuations by dotted lines.

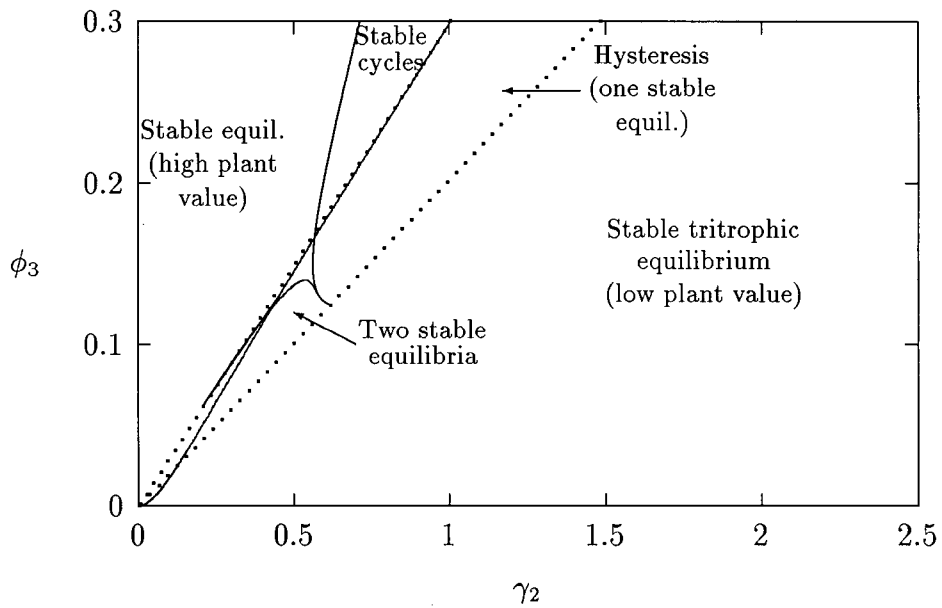


Figure 4.20: Two-parameter bifurcation diagram obtained using the modified model with $a_i=0.001$, ($i = 1, 2, 3$) and $\gamma_1 = 0.6$. The Hopf bifurcation continuations are indicated by solid lines and the limit point continuations by dotted lines.

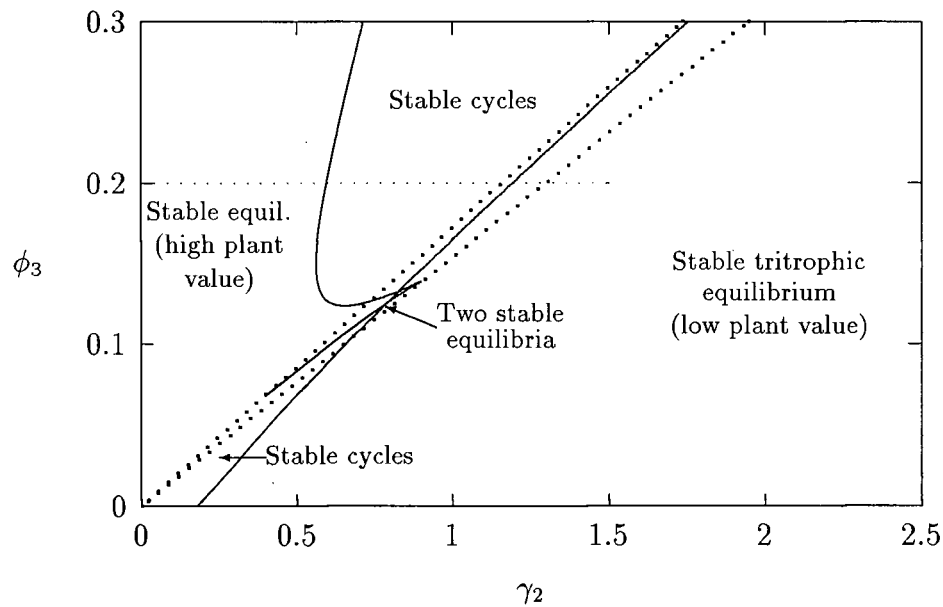


Figure 4.21: Two-parameter bifurcation diagram obtained using the modified model with $a_i=0.001$, ($i = 1, 2, 3$) and $\gamma_1 = 1.2$. The Hopf bifurcation continuations are indicated by solid lines and the limit point continuations by dotted lines.

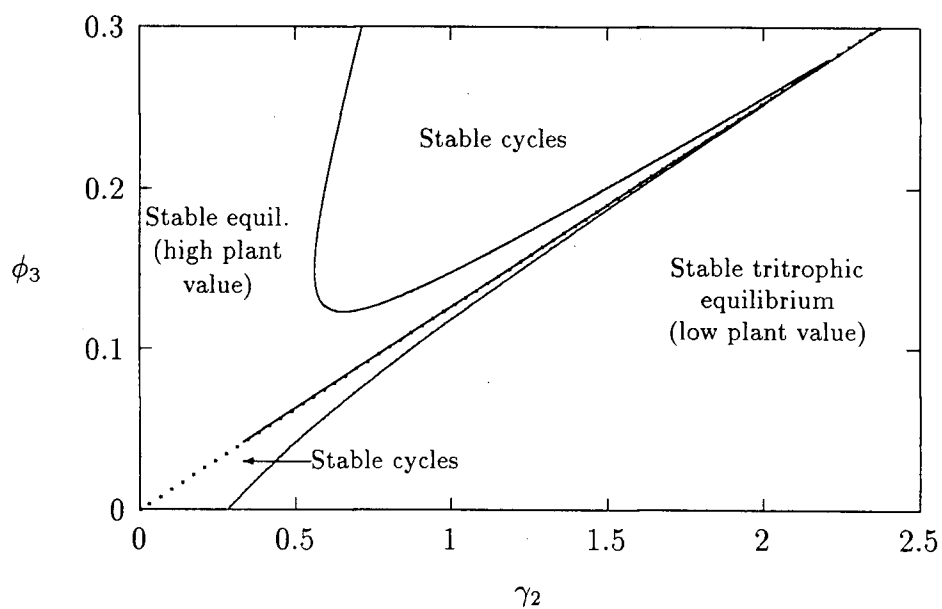


Figure 4.22: Two-parameter bifurcation diagram obtained using the modified model with $a_i=0.001$, ($i = 1, 2, 3$) and $\gamma_1 = 1.8$. The Hopf bifurcation continuations are indicated by solid lines and the limit point continuations by dotted lines.

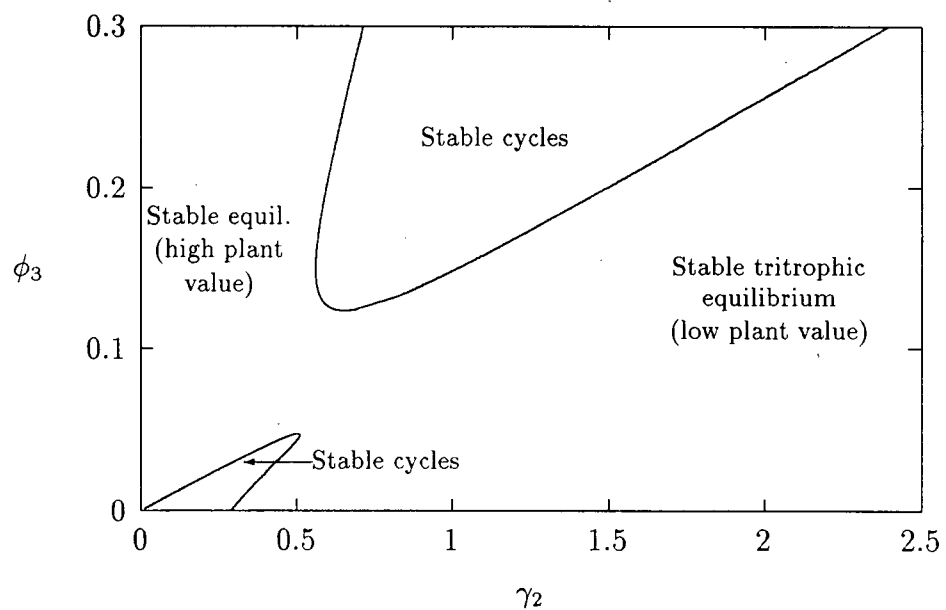


Figure 4.23: Two-parameter bifurcation diagram obtained using the modified model with $a_i=0.001$, ($i = 1, 2, 3$) and $\gamma_1 = 2.4$. The Hopf bifurcation continuations are indicated by solid lines and the limit point continuations by dotted lines.

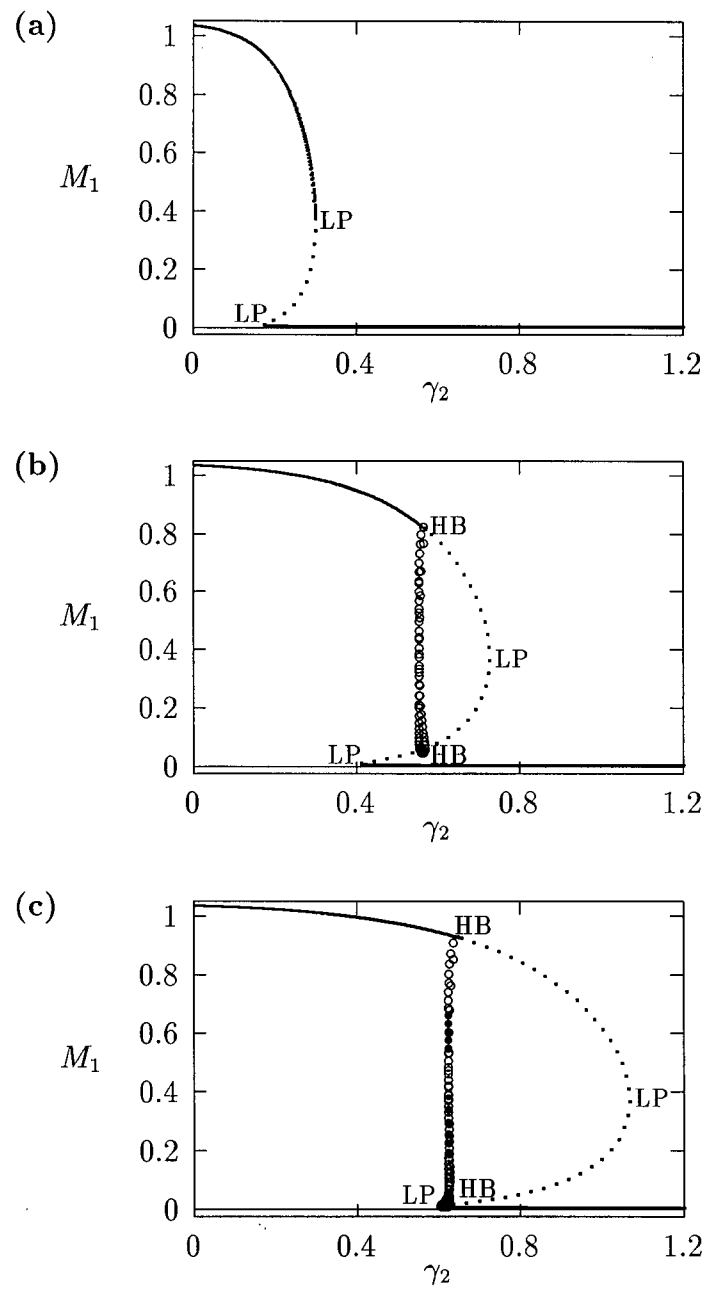


Figure 4.24: One-parameter bifurcation diagrams obtained by varying γ_2 with $\gamma_1 = 0.4$ and (a) $\phi_3 = 0.07$, (b) $\phi_3 = 0.17$ and (c) $\phi_3 = 0.25$. (These correspond to the horizontal dotted lines in figure 4.19.)

low value for M_1 . The regions outside the limit point continuations have one equilibrium point and it is stable. Those to the left of the hysteresis region have high equilibrium M_1 values and those to the right have low equilibrium M_1 values.

The diagrams in figures 4.20–4.23 can also be divided into different qualitative regions using information from one-parameter studies. In these two-parameter diagrams the Hopf bifurcation continuations are not contained within the limit point continuations. The one-parameter bifurcation diagram in figure 4.25 corresponds to the horizontal dotted line in figure 4.21 (that is, $\gamma_1 = 1.2$ and $\phi_3 = 0.2$). In this case there are no parameter combinations which give rise to two stable *equilibria* but there is a region of stable limit cycles. Starting at $\gamma_2 = 1.5$, as γ_2 is decreased we have a single stable equilibrium with a low M_1 value. At the (lower) Hopf bifurcation this stable equilibrium is replaced by stable limit cycles which increase in amplitude as γ_2 is decreased. As the upper Hopf bifurcation is approached the cycles undergo some period-doubling bifurcations and then rapidly decrease in amplitude. Due to a hard loss of stability associated with this upper Hopf bifurcation, the region of stable cycles extends just beyond the Hopf bifurcation point creating a very small parameter range where both a stable equilibrium and stable cycles are present. This occurs near the upper Hopf bifurcation for the other two-parameter diagrams too but the regions are very small and have not been marked.

Figure 4.25 shows which values of γ_2 give rise to stable limit cycles when $\phi_3 = 0.2$. Using this information together with results obtained from one-parameter diagrams at different fixed values of ϕ_3 allows us to determine the regions in figure 4.21 which give rise to stable cycles. Such regions also occur in figures 4.20, 4.22 and 4.23. Although figure 4.19 contains Hopf bifurcations, the cycles associated with them are unstable (see, for example, figure 4.24) and occur over such a small parameter range that they are not of much biological interest.

Having classified the qualitative dynamics in the various regions of the two-parameter

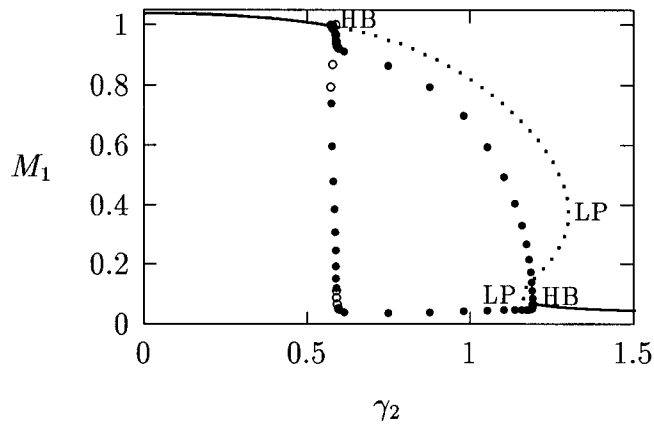


Figure 4.25: One-parameter bifurcation diagram obtained by varying γ_2 with $\gamma_1 = 1.2$ and $\phi_3 = 0.2$. (This corresponds to the horizontal dotted line in figure 4.21.)

diagrams in figures 4.19–4.23 we can make a number of general observations. First, as γ_1 increases the limit point continuation curves move closer together until in figure 4.23 there are no limit points at all. Hence, increasing γ_1 reduces the amount of hysteresis and the possibility of multiple stable states. Also, the positions of the limit point continuations in two-parameter space change as γ_1 is increased resulting in relatively smaller regions of low M_1 equilibrium values. Since higher γ_1 values correspond to faster plant growth rates this is not surprising.

We have seen that stable cycles occur for higher values of γ_1 (figures 4.20–4.23). Comparing these diagrams we can see that increasing γ_1 increases the area of the upper region of stable cycles thereby increasing the probability of finding cycles for a random choice of γ_2 and ϕ_3 within the given two-parameter space. This occurs until $\gamma_1 = 1.8$. For larger values of γ_1 this upper region of cycles does not change position or shape (compare figures 4.14(b) and 4.23). There is also a second, smaller region of cycles which can be seen in figures 4.21–4.23. The size of this region first increases and then decreases until, for sufficiently high γ_1 values, it ceases to exist.

We know that higher γ_1 values correspond to a faster plant growth rate and also that the herbivore population, and hence the predator population, depend on the availability of plants for survival. From the above observations we can deduce that when plant resources are limited (at low values of γ_1) the potential for having two stable equilibria is greater and the region corresponding to low M_1 equilibrium values is larger. When plant resources are not as restricted (at higher values of γ_1) there is a greater chance of stable population cycles but less chance of metastability (multiple stable states). For $\gamma_1 \geq 2$ two-parameter diagrams of (γ_2, ϕ_3) -space are very similar for all values of γ_1 (only the lower region of cycles decreases in area) suggesting that the system is no longer limited by plant availability. Herbivore properties (as determined by γ_2 and ϕ_3) have a greater influence on the behaviour of the system at these values of γ_1 .

In particular the properties of the herbivore determine whether stable cycling behaviour or a stable equilibrium occurs as well as the magnitude of the plant biomass at the equilibrium. Low values of ϕ_3 (the availability or nutritional value of the herbivore to the predator) together with high values of γ_2 (the potential growth rate of herbivore biomass) are particularly detrimental to the plant while the reverse situation allows the plant to maintain fairly high biomasses. At intermediate values of these parameters population cycles may occur provided the value of ϕ_3 is sufficiently high.

The preceding analysis has made use of various dynamical systems techniques to help us gain insight into the behaviour of the model. In the next section I discuss the results that can be obtained using a zero isocline analysis—the method used by Gutierrez *et al.* [52].

4.5.3 The role played by the isocline configurations

From their isocline analysis of model (4.1) Gutierrez *et al.* [52] conclude that the parasitoid *E. lopezi* could control the cassava mealybug while *E. diversicornis* could not.

However, with three state variables all having similar time scales, these deductions are not as straightforward as they may seem.

First, the equilibrium isocline configuration in the M_1M_2 (M_2M_3) phase plane depends on the value of M_3 (M_1) as well as on the parameter values. This was shown in figure 4.6. Thus, noting how an isocline changes as a parameter is varied does not give a complete picture. Secondly, it is not possible to tell from the qualitative structure of the isoclines which intersection point in the M_1M_2 plane corresponds to a tritrophic equilibrium. Figure 4.26 shows three possibilities. Two of these (namely, (b) and (c)) appear in [52] but it was assumed that the equilibrium point in (b) was unstable.

Even if the exact position of the equilibrium point is known, it is not possible to tell from the qualitative structure of the isoclines whether this point is stable or unstable and whether or not limit cycles occur. For example, although altering the parameter γ_3 has no effect on the isoclines, low values of γ_3 give rise to unstable fixed points and stable limit cycles and high values to a stable equilibrium (see figure 4.2). Thus, numerical computation is needed to determine the exact location as well as the local stability of an equilibrium point for the current model.

The isocline configuration obviously has some effect on the behaviour of the system. Figure 4.27 shows the basic configurations for different points in figure 4.12(b). The qualitative structure of the isoclines changes as the diagonal lines (corresponding to a Hopf bifurcation and two limit point continuations) are crossed. In general, it is the proximity of the tritrophic equilibrium point to the peaks of the M_1 and M_2 isoclines in the M_1M_2 and M_2M_3 planes respectively that is important for determining the robustness of model behaviour with respect to parameter perturbations. If the equilibrium point is close to one of these peaks (as is the case near the diagonal lines in figure 4.27) then a small parameter perturbation may change the qualitative structure of the isoclines and hence the dynamics. However, to obtain this information the exact equilibrium isocline

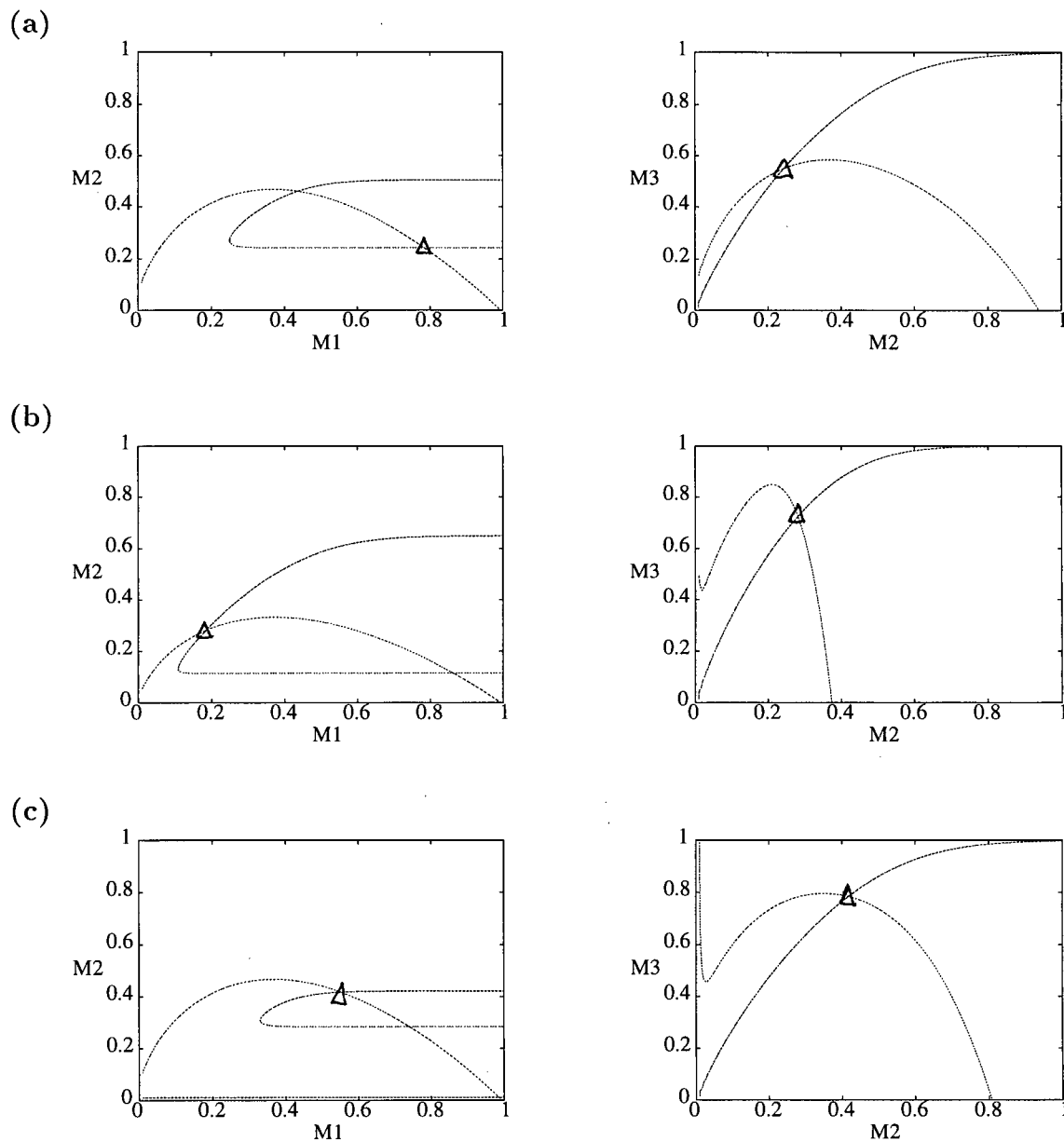


Figure 4.26: Examples of isocline configurations showing different possibilities for the position of the tritrophic equilibrium.

configuration for a given set of parameter values needs to be known.

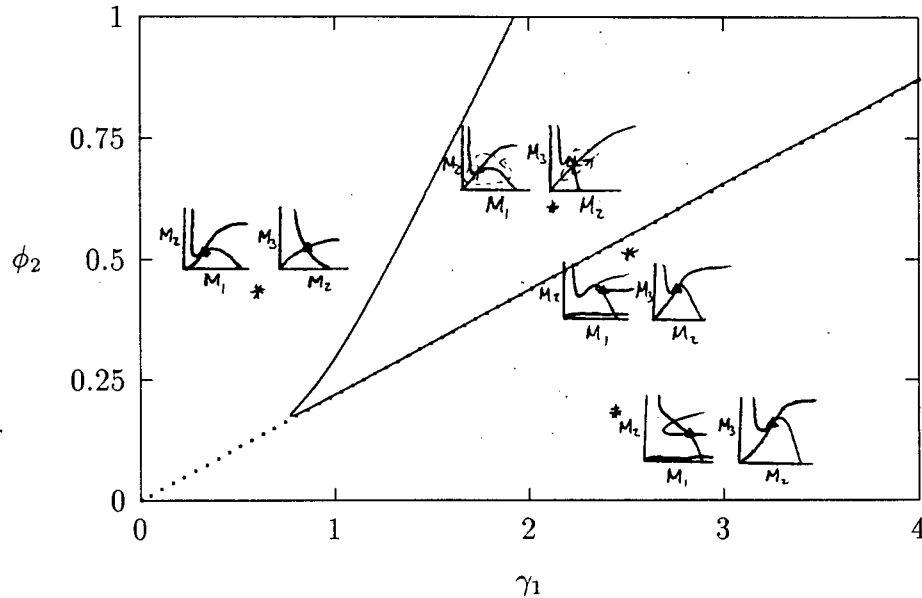


Figure 4.27: Examples of isocline configurations at different points in (γ_1, ϕ_2) -space.

By inference the above criticisms have all noted that if the exact positions of the isoclines and the tritrophic equilibrium were known in both phase planes, then we could obtain a fair amount of information from them. Using XPPAUT this is possible. In particular we can study the effects of introducing nonzero values for the a_i 's. Figure 4.28 shows the results obtained using the reference parameter set for model (4.6) with $a_i = 0$, $a_i = 0.001$ and $a_i = 0.005$ ($i = 1, 2, 3$).

Comparing figures 4.28(a) and (b) we can see that introducing the a_i 's prevents the M_1 and M_2 isoclines from passing through the origin. Hence the equilibrium values for the state variables do not approach zero as rapidly as for the original model and the modified model is more robust to parameter variations in this region of low biomasses. Increasing the a_i 's from 0.001 to 0.005 reduces the humped shape of the M_1 and M_2 isoclines.

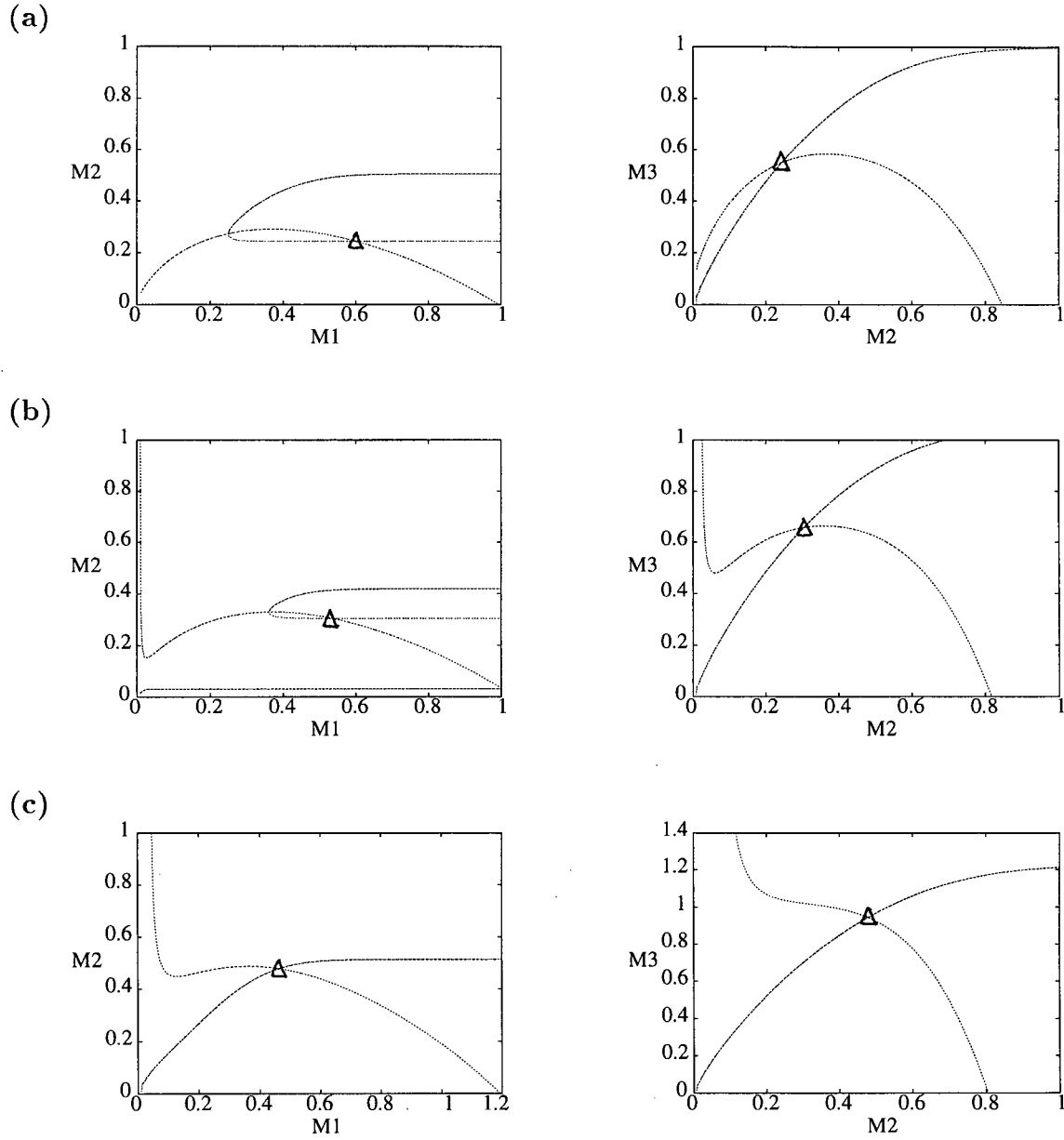


Figure 4.28: Isocline configurations for model (4.6) with (a) $a_i = 0$, (b) $a_i = 0.001$ and (c) $a_i = 0.005$ ($i = 1, 2, 3$) together with the reference parameter set.

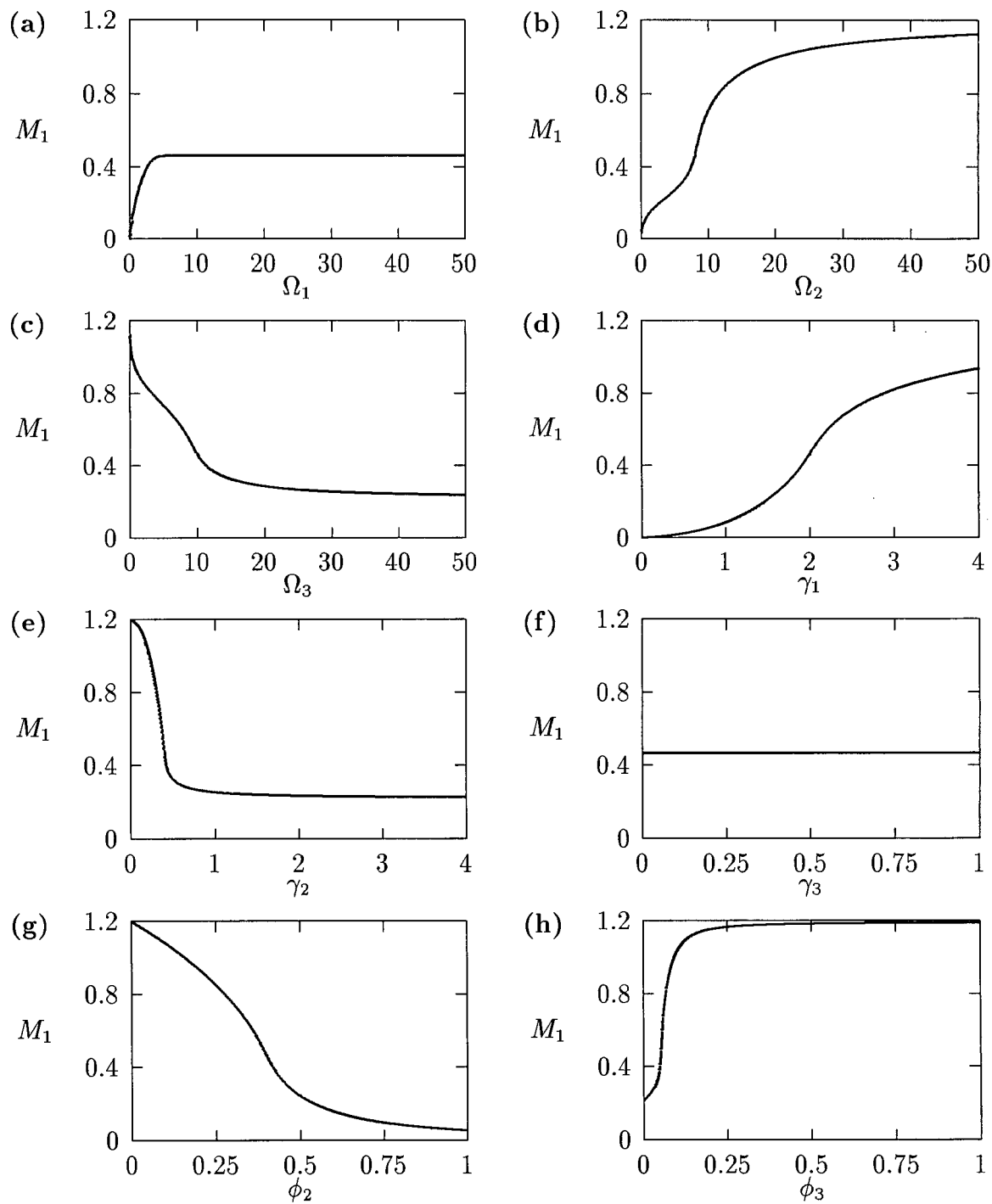
The result is an even more robust model. The stabilising influence of increasing the values of the a_i 's is illustrated by the bifurcation diagrams in figure 4.29 corresponding to $a_i = 0.005$ ($i = 1, 2, 3$). No regions of cycling behaviour are encountered. Since values of 0.005 are still small, this suggests that the model is structurally unstable and hence predictions from ratio-dependent models should be treated with caution.

Another consequence of introducing nonzero a_i 's is that we no longer get abrupt changes in the qualitative shapes of the isoclines. Consider the plant isocline. For $\gamma_1 < \phi_2$ the plant isocline has the hump shape shown in figure 4.30(a)(i). If one or both of these parameter values is altered so that the inequality is reversed, we get the asymptotic isocline in figure 4.30(a)(ii). Using the modified model this abrupt change does not occur. Instead there is a gradual change from the cubic curve in figure 4.30(b)(i) to the asymptotic curve in figure 4.30(b)(ii). The same applies to the herbivore isocline in the M_2M_3 plane.

4.6 Conclusion

In this chapter a partial analysis of a tritrophic ratio-dependent model has been done. Large differences in the magnitudes of the state variables and uncertainty regarding the relative magnitudes of parameter values necessitated a scaling of the equations. This also reduced the number of parameters in the model.

The bifurcation analysis revealed a number of cases of multiple stable states. Many of these phenomena occur over very small parameter ranges and are therefore not of much biological interest. However, those occurring over larger ranges are important as they indicate the potential for sudden behavioural changes if the system is perturbed sufficiently. Many of the instances of multiple stable states arise from a hard loss of stability associated with a Hopf bifurcation. This means that a stable equilibrium and

Figure 4.29: One-parameter bifurcation diagrams when $a_i = 0.005$ ($i = 1, 2, 3$).

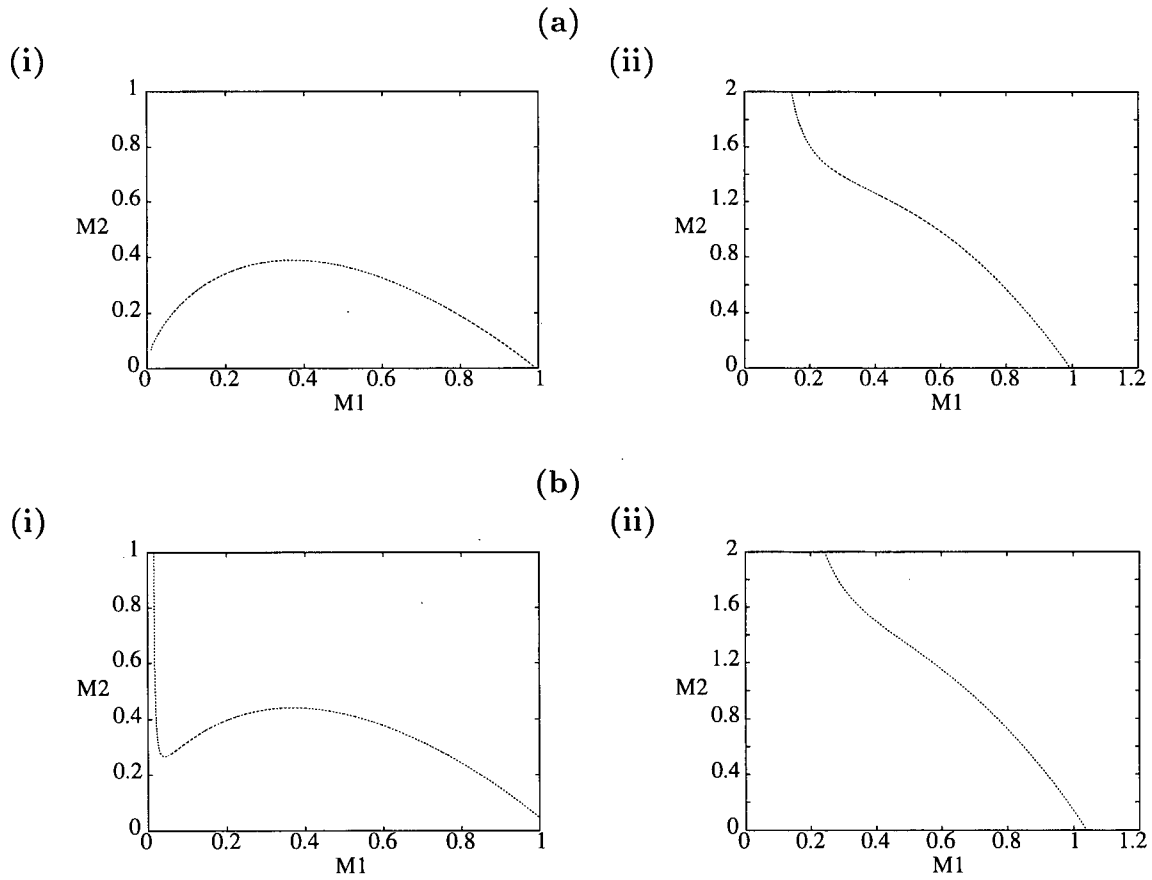


Figure 4.30: Plant isoclines for (a) the original and (b) the modified model. The $M_1 M_2$ plane is shown in (a)(i) and (b)(i) and the $M_2 M_3$ plane is shown in (a)(ii) and (b)(ii).

a stable limit cycle can coexist for a given set of parameter values. If a parameter is varied (as conditions alter), there may be an abrupt change between limit cycles of large amplitude and a stable equilibrium. A point worth noting is that if the Hopf bifurcation associated with the limit cycles had been studied analytically, the algebra required to identify the hard loss of stability would have been very time-consuming and possibly too difficult to do by hand. Only the initial unstable cycles would have been located. Computers are invaluable in such circumstances.

All the parameters were found to affect the dynamics of the model to some extent although the parameter ratios $\frac{\gamma_1}{\phi_2}$ and $\frac{\gamma_2}{\phi_3}$ had the most significant effect. This is in general agreement with Gutierrez *et al.* [52] (in terms of their model the ratios $\frac{\theta_1 D_1}{\alpha_2}$ and $\frac{\theta_2 D_2}{\alpha_3}$ were found to be important) although they did not explicitly describe these effects as was done in this study using bifurcation diagrams. In particular the two-parameter diagrams summarise the effects of the plant and the herbivore properties on the behaviour of the system. Both trophic levels affect the magnitude of M_1 at equilibrium, whether or not cycles occur, and the period and amplitude of these cycles. The consequences of a slowly growing plant were also shown, namely smaller regions of cycling behaviour, lower equilibrium M_1 values and larger regions of multiple stable states.

It may seem that predator dynamics are not as important as those for the lower two trophic levels. However, it should be noted that increasing γ_3 , the efficiency of the predator, can stabilise an oscillating system. The parameters affecting predator dynamics also affect the equilibrium biomasses.

In the course of the analysis some previously noted criticisms of ratio-dependent models were highlighted as they caused numerical difficulties and biological implausibilities. In particular, such models are not valid when a state variable which occurs in the denominator of a ratio approaches zero (that is, as a population approaches extinction) since a small perturbation to the model alters the dynamics in this region. This was

shown using a modification to the ratio-dependent terms. While this modification had very little effect on the dynamics for parameter values corresponding to reasonable equilibrium values of the state variables (provided the a_i 's were sufficiently small), it did remove the numerical problems which occurred when one or more of the state variables approached zero (causing one or more ratios to tend to infinity). It also revealed that the ratio-dependence causes complex dynamics in regions where the state variables are small. Even the addition of very small terms ($a_i = 0.001$) reduced the complexity of the cycles. The above results support the argument that ratio-dependent models exhibit pathological behaviour and that they are not valid near the axes. Thus they cannot be used to study extinction or situations where one of the state variables attains low values. However, the model by Gutierrez et al. (1994) that has been analysed in this chapter is a biological control model whose aim is to suggest what kind of predator can keep herbivore numbers low.

Finally, the zero isocline configurations in the M_1M_2 and M_2M_3 planes were investigated and some limitations of the three-dimensional setting were discussed. In order to obtain useful information from the isoclines their exact equilibrium positions need to be determined so that the position and nature of the tritrophic equilibrium and its proximity to the isocline peaks can be found.

Uncertainty regarding the parameter values for this model for a particular ecological system makes it difficult to interpret the results biologically except in a very general sense. However, it is informative to see the kind of behaviour that the model can exhibit and the effects of ratio-dependence. It would be easy to apply the results and perform the same type of analysis if more accurate parameter values were obtained.

Chapter 5

Population Genetics Model I

5.1 Introduction

So far only continuous-time models have been considered. In the remaining chapters we will look at discrete-time models. The model in this chapter is a population genetics one in which both population size and gene frequency are state variables. It is a single locus, two allele model with density-dependent fitness functions and it has already been studied in Asmussen [8] and Namkoong *et al.* [93]. Although the model equations are fairly simple, interesting dynamics arise as a result of the discreteness. No new theoretical results are obtained in this study but the dynamical systems techniques prove useful in a number of ways: first, the theoretical results are demonstrated fairly easily and without having to struggle with the mathematical details. The dynamical systems techniques also provide a more systematic way of locating different kinds of behaviour when theoretical predictions are not possible or too difficult to obtain. Previous studies have tested various parameter combinations numerically using trial and error to try and locate the desired dynamics. In addition, while the theoretical results note the *existence* of various types of qualitative behaviour, they do not give information regarding the *extents* of the regions in parameter space corresponding to these dynamics. In other words, they indicate the possibility of a certain type of behaviour occurring but not the relative frequency of occurrence. The latter information is important from an ecological perspective as it influences the amount of attention that is given to various possibilities. It will be shown

that bifurcation diagrams (two-parameter ones in particular) can be useful for indicating the sizes of regions in parameter space corresponding to various types of behaviour.

Another useful result is the location of stable polymorphic period-2 cycles. It is very difficult to predict the existence of these cycles intuitively or analytically as the bifurcation point at which they are initiated does not coincide with changes in the relative carrying capacities of the genotypes. Also, the period-2 cycle is initially unstable and a further bifurcation is required before it becomes stable. Numerical techniques are indispensable in such situations.

I begin in the next section with a list of new terminology that is used in this chapter as well as in chapter 6. I then summarise some background information on population genetics models and the main theoretical results relating to the particular model that is studied in the rest of the chapter. Section 5.4 describes the model equations and is followed by the model analysis. The focus in the latter section is on cycling or periodic behaviour as this behaviour is the most difficult to study by hand. The analysis begins with one-parameter studies which investigate the effects of altering relative carrying capacities. A two-parameter bifurcation diagram is then obtained. This diagram divides the two-parameter space into regions corresponding to different qualitative behaviour. The region of stable period-2 polymorphisms is larger than that for stable polymorphic equilibria for the particular case studied and intersects regions of heterozygote inferiority, superiority as well as regions of partial dominance. Finally, section 5.5.4 studies higher period cycles. Polymorphic period-4 cycles are found but only for high genotypic growth rates. Of greater interest is the observation that the relative carrying capacities of the genotypes determine the location of attractors (boundary or interior) while the growth rates of the genotypes are responsible for the type of attractor (equilibrium or periodic cycle). Questions for further study are included in the conclusion.

5.2 New terminology

Some new terminology is required in this chapter as well as in chapter 6 to explain both the discrete dynamics and the biological significance of the results.

- **period-k cycle or orbit:** For discrete models we do not get limit cycles as in the continuous case. However, the values of the state variables may oscillate in a repetitive manner. If there are k points which are repeated then we refer to a period- k cycle or orbit. A period-1 point is the same as an equilibrium point (see section A.2.6). For further details on discrete models refer to section A.3.5.
- **period-k sink:** This is a period- k cycle which is locally stable (see sections A.2.14 and A.2.21). **Period-k saddles** and **sources** are period- k cycles which are locally unstable (see sections A.2.20 and A.2.23).
- **gene frequency:** This is the number of gametes or individuals carrying a particular allele divided by the total number of gametes.
- **genotype:** Suppose we have two alleles, A_1 and A_2 . Then there are three possible genotypes: A_1A_1 , A_1A_2 and A_2A_2 .
- **fitness:** The fitness of a genotype is the contribution that it makes to the next generation's gene pool, that is, it is a measure of the successful survival and reproduction of that genotype [110].
- **homozygote:** The genotypes A_1A_1 and A_2A_2 are homozygotes.
- **heterozygote:** The genotype A_1A_2 is a heterozygote.
- **fixed or homomorphic equilibrium:** This is an equilibrium point at which only one allele is present, that is, at which only a homozygote is present.

- **polymorphic equilibrium:** This is an equilibrium point where more than one allele is present, that is, where a heterozygote is present.
- **carrying capacity:** This refers to the equilibrium population density corresponding to a particular genotype when only that genotype is present. It is denoted by K_{ij} for the genotype A_iA_j in this thesis.
- **heterozygote superiority:** Heterozygote superiority or **overdominance** occurs when the heterozygote's carrying capacity is greater than those for the homozygotes, that is $K_{12} > K_{11}, K_{22}$ for the case of two alleles. **Heterozygote inferiority** or **underdominance** refers to the situation when the inequality is reversed.
- **partial dominance:** This refers to the situation where the heterozygote is neither superior nor inferior, that is, $K_{11} < K_{12} < K_{22}$ or $K_{22} < K_{12} < K_{11}$ for the case of two alleles.

5.3 Background

In the past the theories of population dynamics and population genetics were considered to be separate pursuits since it was thought that evolution by natural selection proceeded on a much longer time scale than changes in population size (Roughgarden [104]). However, once it was realised that gene substitution could occur in the same length of time as that needed by a population to reach an equilibrium, the dangers of this separation were acknowledged. Since the late 1960's a number of models in which *both* population size and gene frequency are variables have been studied. The classical one locus, two allele selection models in this category used constant viabilities for the genes and predicted monotonic population convergence to a unique stable equilibrium (Asmussen [8]). However, incorporating density-dependent selection can have a dramatic effect on the

dynamics—both regular and chaotic cycles can arise.

Studies of the effects of density-dependence for discrete generation organisms can be found in [8, 9, 93, 104]. In particular, Asmussen and Feldman [9] and Asmussen [8] show that in such situations local stability analyses may be inadequate to explain the global behaviour related to changes in gene frequency and population size. In addition to fixed and polymorphic stable equilibria, Asmussen [8] found regular and chaotic cycles when using monotone decreasing density-dependent fitness functions. In certain situations equilibria and cycles exist simultaneously. Asmussen [8] also shows that stable periodic polymorphisms may occur in the absence of heterozygote superiority—the latter condition being necessary for polymorphic equilibria when strictly decreasing fitness functions are used. In fact, using the same model Namkoong *et al.* [93] demonstrate the existence of an attracting polymorphic period-2 cycle for a case of heterozygote inferiority. Thus, overdominance in heterozygote carrying capacity is not necessary for the maintenance of genetic variation. Another important conclusion by Asmussen [8] is that an inherently stable genetic system can exert a stabilising influence on a model, allowing stable equilibria and stable limit cycles to persist for higher growth rates than would be possible with the model's purely ecological counterpart.

The above conclusions were arrived at analytically for linear (logistic) monotone decreasing fitness functions. However, when the density-dependence is modelled using exponential fitness functions, Asmussen [8] comments that the mathematics becomes very difficult. Numerical solutions then become necessary. In [8, 93] it is also noted that when more complex, higher order behaviour (such as a cycle) is present, intuition and local stability analyses break down. Again numerical techniques are required.

5.4 Model equations

Suppose we have a single population and two alleles, A_1 and A_2 . At time t the population size is denoted by N_t and the frequency of allele A_1 is denoted by p_t . The fitness of genotype $A_i A_j$ ($i, j = 1, 2$) at time t is denoted by w_{ij}^t . The marginal fitness of A_i is thus

$$w_i^t = p_t w_{i1}^t + (1 - p_t) w_{i2}^t \quad (i = 1, 2)$$

and the mean population fitness is

$$\bar{w}^t = p_t w_1^t + (1 - p_t) w_2^t.$$

Differences in fitness among genotypes may be interpreted as the result of different responses to ecological pressures. Following Asmussen [8] and Namkoong *et al.* [93] exponential density-dependent fitness functions of the form

$$w_{ij}^t = \exp(a_{ij} - b_{ij} N_t) \quad a_{ij}, b_{ij} > 0, \quad i, j = 1, 2 \quad (5.1)$$

are used in this chapter. Such monotone decreasing functions of population density are often used to model the detrimental effects of population crowding [110].

If Hardy-Weinberg frequencies are assumed at each time t , then the recursion equations for p and N are:

$$\begin{aligned} p_{t+1} &= p_t \frac{w_1^t}{\bar{w}^t} \\ N_{t+1} &= \bar{w}^t N_t \end{aligned} \quad (5.2)$$

where the region of practical significance is $0 \leq p \leq 1, N \geq 0$. With the above equations the carrying capacity K_{ij} for genotype $A_i A_j$ acting alone is given by

$$K_{ij} = \frac{a_{ij}}{b_{ij}}.$$

For a more detailed description of the model see Namkoong *et al.* [93].

In studying this model I will be looking for attracting boundaries at $p = 0$ or $p = 1$, interior (polymorphic) equilibria having $0 < p < 1$, period-2 and also higher period stable orbits. Attracting boundaries correspond to situations where one allele survives at the expense of the other, while at interior attractors both alleles persist thus maintaining genetic diversity. Other phenomena of importance are the extents of the domains of attraction corresponding to the stable phenomena (see section A.2.5) and the associated relative carrying capacities of the homozygotes and heterozygote. The methods of analysis and the results are discussed in the next section.

5.5 Model analysis

5.5.1 Approach

Equilibria and their associated stability properties have been studied analytically for models such as the one described above. These theoretical results help predict the conditions under which stable equilibria can be expected (see, for example, [8, 104]). However, periodic dynamics (particularly polymorphic cycles) are more difficult to study [8, 93]. I chose to concentrate on these more difficult phenomena to demonstrate the utility of the available software. I used DSTOOL to solve the system over time and to generate starting points for AUTO. The bifurcation diagrams were obtained using Interactive AUTO. The AUTO interface in XPPAUT is not yet set up to deal with discrete systems of equations. I used fairly small stepsizes when generating bifurcation diagrams for this model ($ds=0.0001$ and $dsmax$ between 0.001 and 0.01) as the changes in behaviour occur over small parameter ranges.

Namkoong *et al.* [93] state that alleles that affect seedling survival can increase carrying capacity and simultaneously destabilise population growth dynamics. This can be simulated by choosing $a_{11} > 2.0$ so as to force the A_1A_1 genotypes to exhibit unstable

growth if they grow as a purely homozygous population. In order to investigate the effects of altering relative carrying capacities, I begin by setting $a_{11} = 2.1$, $a_{12} = 1.9$, $a_{22} = 1.1$, $b_{11} = 1.0$, $b_{12} = 0.904$ and varying b_{22} . The results agree with those in [93]. I then go on to determine the effects of simultaneously varying the heterozygote parameter, b_{12} , by generating a two-parameter bifurcation diagram in (b_{22}, b_{12}) -parameter space. I conclude the analysis by investigating higher period orbits.

5.5.2 One-parameter bifurcation diagrams

Namkoong *et al.* [93] found that an interior period-2 attractor exists for $b_{22} > 0.526$. An example is shown in figure 5.1 for the value $b_{22} = 0.54$. In this figure there is a

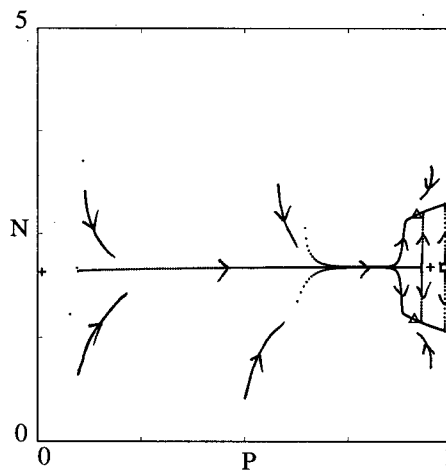


Figure 5.1: Dynamics in the (p, N) -plane for model (5.2) with $a_{11} = 2.1$, $a_{12} = 1.9$, $a_{22} = 1.1$, $b_{11} = 1.0$, $b_{12} = 0.904$ and $b_{22} = 0.54$. This diagram was obtained using DSTOOL.

period-1 source at $(p, N) = (1.000, 2.100)$ and period-1 saddles at $(0.956, 2.10007)$ and $(0.000, 2.037)$. The points $(1.000, 2.878)$ and $(1.000, 1.322)$ correspond to a period-2 saddle and the points $(0.917, 1.466)$ and $(0.923, 2.734)$ to a period-2 sink. Thus, in this case both boundaries are repelling and there is an interior attracting period-2 orbit as expected.

Comparing the carrying capacities $K_{11} = 2.100$, $K_{12} = 2.102$ and $K_{22} = 2.037$ we see that we are just within the region of heterozygote superiority.

We can now use AUTO to vary b_{22} . It is noted in appendix B that for discrete systems AUTO can detect period-doubling bifurcations but cannot continue the resulting period-2 orbits, and hence cannot detect higher period orbits. This is clearly a disadvantage in the present situation where we are specifically interested in the period-2 orbits. A way of overcoming this problem is to study the second iterate of the model since period-2 orbits will become equilibria in this new model (see section A.3.5). In terms of the original model AUTO will then be able to detect period-1 equilibria (since these are also period-2 equilibria), period-2 orbits and bifurcations to period-4 orbits.

For a model as simple as the one under discussion, the second iterate is easy to determine. From equations (5.2) we obtain

$$\begin{aligned} p_{t+2} &= p_{t+1} \frac{w_1^{t+1}}{\bar{w}^{t+1}} = p_t \frac{w_1^t w_1^{t+1}}{\bar{w}^t \bar{w}^{t+1}} \\ N_{t+2} &= \bar{w}^{t+1} N_{t+1} = \bar{w}^{t+1} \bar{w}^t N_t \end{aligned} \quad (5.3)$$

where

$$\begin{aligned} w_i^{t+1} &= p_{t+1} w_{i1}^{t+1} + (1 - p_{t+1}) w_{i2}^{t+1} \\ &= p_t \frac{w_1^t}{\bar{w}^t} \exp(a_{i1} - b_{i1} \bar{w}^t N_t) + (1 - p_t \frac{w_1^t}{\bar{w}^t}) \exp(a_{i2} - b_{i2} \bar{w}^t N_t) \end{aligned}$$

and

$$\begin{aligned} \bar{w}^{t+1} &= p_{t+1} w_1^{t+1} + (1 - p_{t+1}) w_2^{t+1} \\ &= p_t \frac{w_1^t}{\bar{w}^t} w_1^{t+1} + (1 - p_t \frac{w_1^t}{\bar{w}^t}) w_2^{t+1}. \end{aligned}$$

Figure 5.2 shows the results obtained from varying b_{22} using the second iterate of the

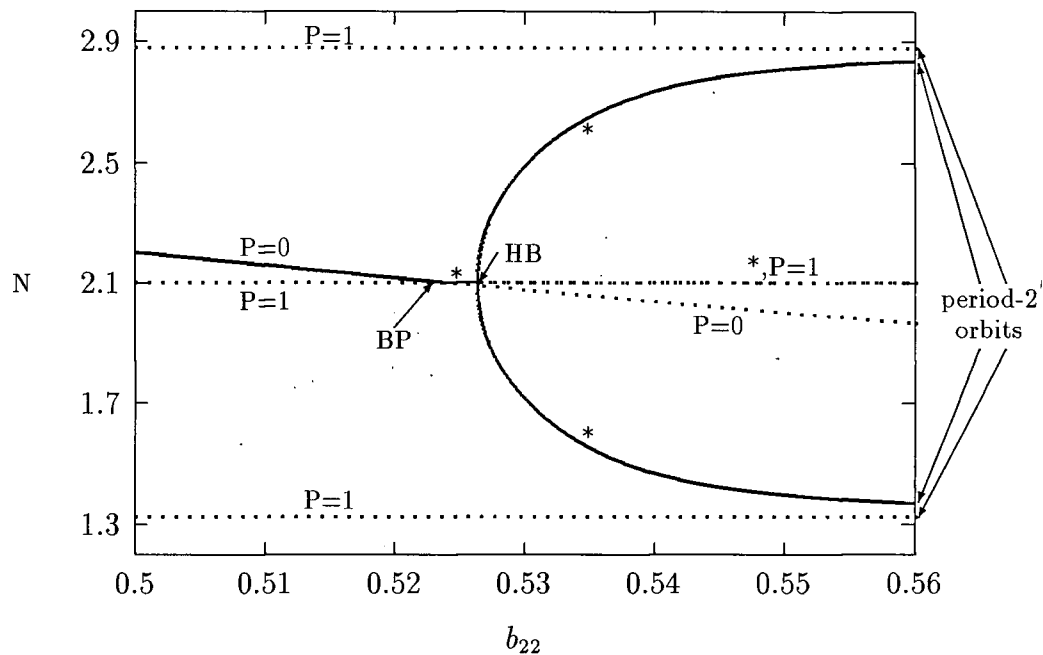


Figure 5.2: One-parameter bifurcation diagram of model (5.3) with $a_{11} = 2.1$, $a_{12} = 1.9$, $a_{22} = 1.1$, $b_{11} = 1.0$ and $b_{12} = 0.904$ obtained using AUTO. (Behaviour for smaller and larger values of b_{22} than indicated in the figure can be found by extrapolating the curves and lines at the boundaries of the figure. The period-2 orbits are indicated in the figure. The phenomena corresponding to boundary values of p , namely $p = 0$ or $p = 1$, are labelled. Branches marked with a * correspond to interior values of p , namely $0 < p < 1$. HB stands for Hopf bifurcation. This is really a period-doubling bifurcation but AUTO marks it with the HB symbol.)

model¹. I plotted N versus b_{22} instead of p versus b_{22} as the period-2 orbits can be seen with greater clarity this way. The p -values for the two points on these period-2 orbits are very similar and thus the continuation curves are difficult to distinguish. Also, a large number of bifurcations occur at $p = 1$. Plotting p versus b_{22} would result in many branches lying on top of one another.

For $b_{22} < 0.523$ we can see that the boundary at $p = 0$ is attracting with a single

¹Some very complicated bifurcation diagrams can be generated when studying this model, however not all continuation branches are of interest. Those branches which have $p < 0$, $p > 1$ or $N < 0$ are not practically significant but it is good practice to continue such branches within the parameter range under study in case a bifurcation occurs and they re-enter the ranges of interest.

equilibrium point. At $b_{22} = 0.523$ the genotype A_2A_2 loses superiority in carrying capacity and we move into the region ($b_{22} > 0.523$) of heterozygote superiority. While the difference in carrying capacities is not too large we still have a unique equilibrium (an interior equilibrium this time) but as b_{22} increases, causing the carrying capacity of A_2A_2 to decline and the instability of A_1A_1 to have a greater influence on the dynamics, this equilibrium bifurcates to become an attracting interior period-2 orbit. As b_{22} increases further this period-2 polymorphism moves closer and closer to the $p = 1$ boundary where there is a repelling period-2 orbit as well as an unstable period-1 saddle. These results match those in [93] and are in agreement with previous findings that heterozygote superiority in equilibrium carrying capacity is a necessary condition for a stable polymorphic equilibrium when fitness is a decreasing function of population size. In addition, figure 5.2 shows clearly that heterozygote superiority is not a *sufficient* condition for a stable polymorphic equilibrium since no such phenomena occur for $b_{22} > 0.526$. Stable period-2 polymorphisms exist in this region.

In [93] it was found that stable period-2 polymorphisms, unlike polymorphic equilibria, can exist in the absence of overdominance. Suppose we set $b_{12} = 0.906$, then $K_{12} = 2.097$ which means that we no longer have any regions of heterozygote superiority. The one-parameter bifurcation diagram shown in figure 5.3 was obtained by using DSTOOL to calculate starting points and Interactive AUTO to vary b_{22} once again.

In this case the dynamics are a little more complicated. We still have an equilibrium at $p = 0$ which is attracting for $b_{22} < 0.525$ (the region of heterozygote inferiority) and unstable otherwise. However, at $p = 1$ there is now a stable period-2 orbit for all values of b_{22} . For $0.520 < b_{22} < 0.522$ ($2.116 > K_{22} > 2.109$) there is also a stable interior period-2 orbit. Intuition could not have been used to guess the existence of these orbits since the bifurcation values do not coincide with changes in the relative carrying capacities of the genotypes. It would also have been difficult to predict their existence analytically since

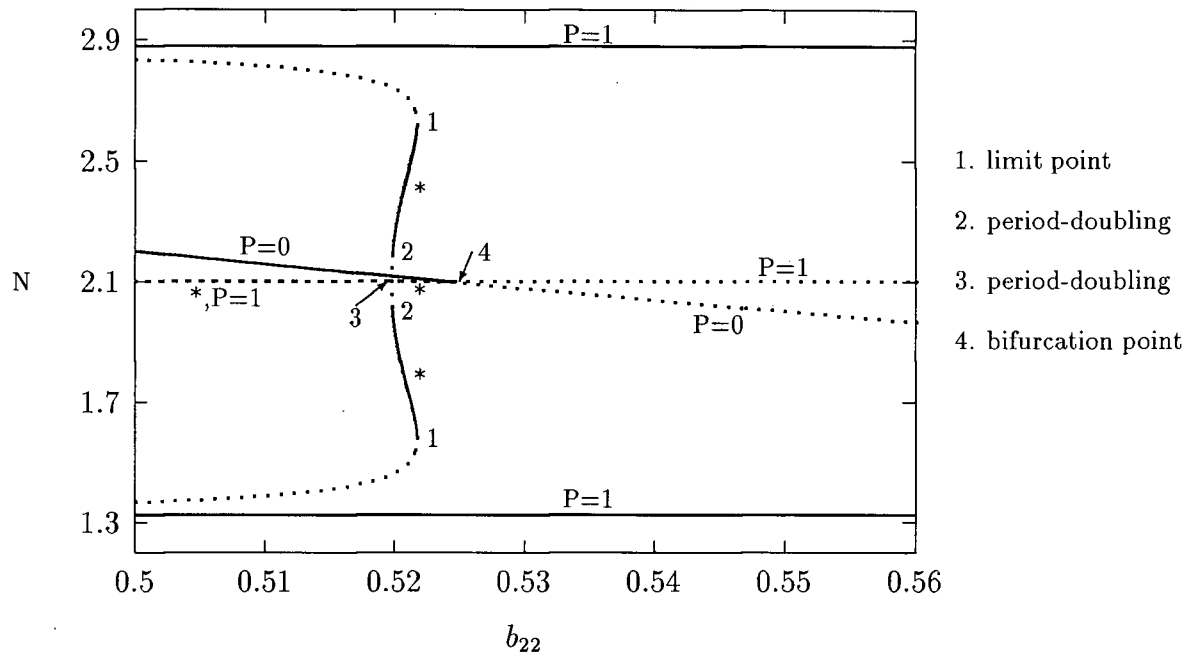


Figure 5.3: One-parameter bifurcation diagram of model (5.3) with $a_{11} = 2.1$, $a_{12} = 1.9$, $a_{22} = 1.1$, $b_{11} = 1.0$ and $b_{12} = 0.906$ obtained using AUTO. $K_{11} = 2.1$ and $K_{12} = 2.097$. Branches marked with a * correspond to interior values of p , namely $0 < p < 1$.

the period-doubling bifurcation which initiates the interior period-2 orbit occurs when $b_{22} = 0.519$ but the orbit is initially unstable and only becomes stable after a further bifurcation. An idea of the extent of the domain of attraction (see section A.2.5) of the period-2 polymorphism in terms of population density can also be seen in figure 5.3 by noting the positions of the unstable period-2 orbit and the unstable equilibria since these phenomena separate the domains of attraction of the stable phenomena. Figure 5.4 shows the (p, N) -plane corresponding to $b_{22} = 0.521$ and indicates the domains of attraction for this particular value of b_{22} . The region denoted by a is the domain of attraction for the sink at $p = 0$, b is the domain of attraction for the period-2 polymorphism, and c is the domain of attraction for the period-2 orbit at $p = 1$.

The above-mentioned figures indicate the ranges of b_{22} values corresponding to stable

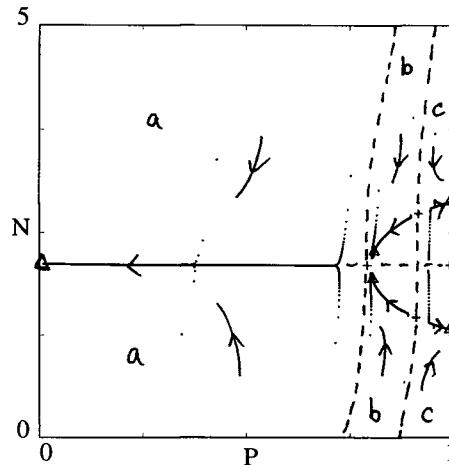


Figure 5.4: The (p, N) -plane using model (5.3) for $a_{11} = 2.1$, $a_{12} = 1.9$, $a_{22} = 1.1$, $b_{11} = 1.0$, $b_{12} = 0.906$ and $b_{22} = 0.52$ showing the domains of attraction for the stable phenomena.

equilibria and period-2 orbits at the boundaries as well as in the interior. Comparing figures 5.2 and 5.3 we can see that the regions of occurrence of these phenomena vary with b_{12} as well as b_{22} . We can find out more about this dependence on b_{12} by generating a two-parameter bifurcation diagram.

5.5.3 Two-parameter bifurcation diagram

Using AUTO we can trace the paths of period-doubling bifurcations² and limit points in two-parameter space. Points 2 in figure 5.3 are period-doubling bifurcations and points 1 are limit points. These points are only located when using the second iterate of the model since they are on the period-2 orbits. Point 3 is also a period-doubling bifurcation but from period-1 to period-2 orbits and thus is only labelled as such by AUTO when using the original model (5.2). Hence, to continue this point in two parameters we need to use the original model. The resulting two-parameter diagram can then be superimposed

²AUTO labels period-doubling bifurcations as Hopf bifurcations for discrete models (see section A.3.5). Thus points marked HB in the figures are really period-doubling bifurcations.

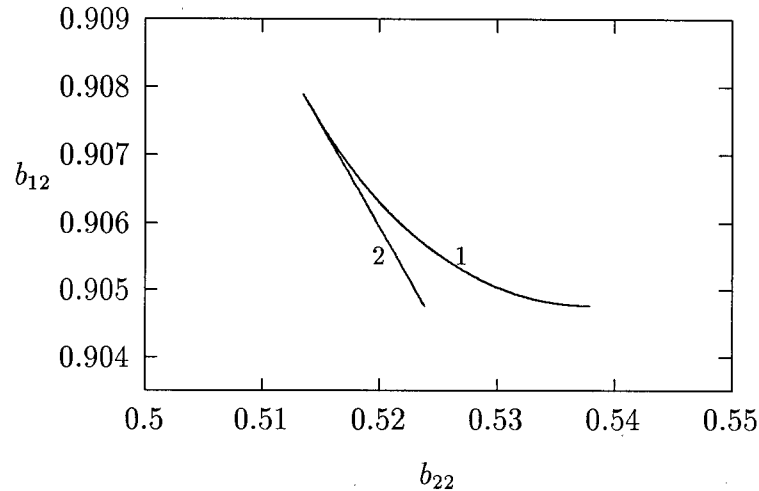


Figure 5.5: Two-parameter bifurcation diagram of model (5.3) with $a_{11} = 2.1$, $a_{12} = 1.9$, $a_{22} = 1.1$ and $b_{11} = 1.0$ obtained using AUTO. Curve 1 is the limit point continuation and curve 2 the period-doubling bifurcation continuation.

on the one obtained for the second iterate of the model by using the READP command in Interactive AUTO. We could choose any one of the parameters a_{11} , a_{12} , a_{22} , b_{11} or b_{12} as the second parameter to vary. Since the parameter b_{22} corresponds to one of the homozygotes, it may be interesting to vary one of the heterozygote parameters. The parameter b_{12} was chosen for this illustration to compliment the results in the previous section.

Figure 5.5 shows the results obtained from continuing points 1 and 2 in figure 5.3 in two-parameter space. The two-parameter continuation of point 3 in figure 5.3 can be obtained from the original model as mentioned earlier. AUTO cannot continue transcritical bifurcation points such as point 4 in figure 5.3. However, we can obtain a good approximation to the relevant line or curve by doing a number of one-parameter continuations as in section 5.5.2 and noting the coordinates at which the bifurcation at $p = 0$ occurs. We already have the points $(b_{22}, b_{12}) = (0.523, 0.904)$ and $(b_{22}, b_{12}) = (0.525, 0.906)$ from figures 5.2 and 5.3 respectively. If the resulting approximate curve is combined with

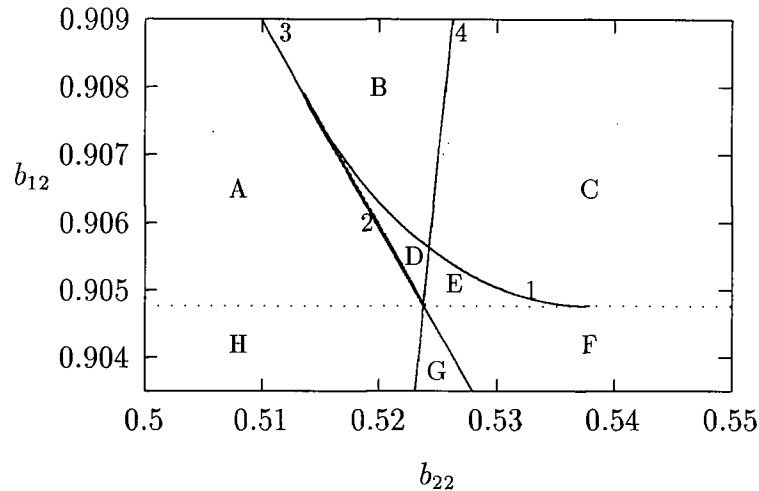


Figure 5.6: Two-parameter bifurcation diagram of model (5.3) with $a_{11} = 2.1$, $a_{12} = 1.9$, $a_{22} = 1.1$ and $b_{11} = 1.0$ obtained using AUTO. Curve 1 is the limit point continuation and curve 2 the period-doubling bifurcation continuation. Curve 3 is the period-doubling continuation obtained using the original model (5.2) and curve 4 is the curve where the bifurcation at $p = 0$ occurs.

figure 5.5 and the two-parameter continuation of point 3, then we obtain figure 5.6.

There are many other bifurcation curves that could have been included in figure 5.6 but only those of interest for the present discussion have been drawn. The dotted line has been included to demarcate, together with line 4, the regions of heterozygote superiority and inferiority³. In regions F and G there is heterozygote superiority and in regions A, B and D there is heterozygote inferiority. C, E and H are regions of partial dominance. These distinctions in relative carrying capacities will be referred to again shortly.

To help us understand figure 5.6 we can refer back to the one-parameter bifurcation diagrams, figures 5.2 and 5.3, which are horizontal slices of figure 5.6 at $b_{12} = 0.904$ and $b_{12} = 0.906$ respectively. Figure 5.6 indicates the types of phenomena corresponding to different parameter combinations and the one-parameter diagrams show the values of

³These lines can be obtained analytically using the definition of heterozygote superiority. The dotted line could also have been obtained from one-parameter bifurcation diagrams where b_{12} is varied instead of b_{22} as it is along this line that the period-2 orbit at $p = 1$ changes its stability properties.

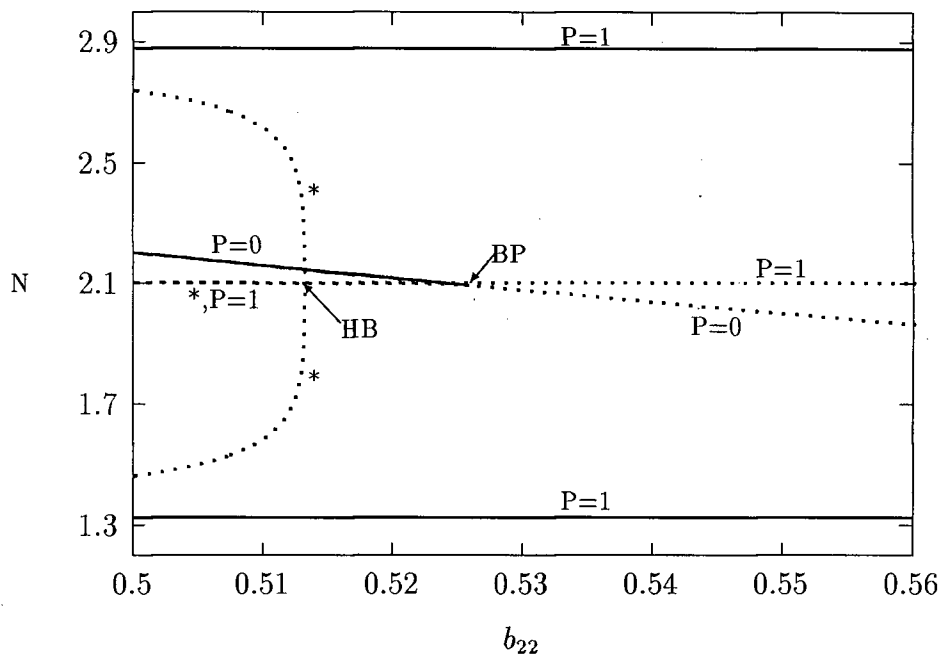


Figure 5.7: One-parameter bifurcation diagram of model (5.3) with $a_{11} = 2.1$, $a_{12} = 1.9$, $a_{22} = 1.1$, $b_{11} = 1.0$ and $b_{12} = 0.908$ obtained using AUTO. Branches marked with a * correspond to interior values of p , namely $0 < p < 1$. HB marks a period-doubling bifurcation.

N at which these phenomena occur and, hence, their relative positions in state space. We can also use figure 5.6 to predict the behaviour corresponding to different parameter combinations. Consider fixing b_{12} at 0.908. From figure 5.6 we expect a period-doubling bifurcation to occur as b_{22} increases through line 3 but we do not expect any region of stable interior period-2 cycles as we are above the region where curve 1, the limit point of such a phenomenon, occurs. Also from figure 5.6, we expect the equilibrium at $p = 0$ to change stability as we pass through line 4. Using AUTO to generate a one-parameter diagram with b_{12} fixed at 0.908 gives figure 5.7 which is just as we predicted. The above exercise can be repeated for other values of b_{12} as well.

A complementary way of obtaining insight into figure 5.6 is to choose points in regions A to H and to display the dynamics in the (p, N) -plane. This is a straightforward exercise

using DSTOOL. The results are shown in figure 5.8. Strictly speaking dots should be used for the trajectories instead of continuous lines since the model is discrete. However, it is easier to denote the direction of flow and the qualitative behaviour when lines are used. These diagrams also give a better idea of the domains of attraction corresponding to the different stable phenomena.

Using figures 5.6 and 5.8 we can make some important observations. In regions D, E, F and G stable polymorphisms occur. D lies in the area of heterozygote inferiority and E in a region of partial dominance, that is, of neither heterozygote inferiority nor superiority. While Asmussen [8] and Namkoong *et al.* [93] documented the occurrence of stable period-2 polymorphisms in such regions, they did not investigate the extent of the regions corresponding to such phenomena. From figure 5.6 we can see that regions D and E occupy a fairly small region in the (b_{22}, b_{12}) parameter space and thus may have limited ecological significance.

Another observation is that the region of stable polymorphic equilibria (region G) is very small. Thus, in the region of heterozygote superiority, stable period-2 polymorphisms are much more likely than stable polymorphic equilibria. It appears that the instability of the A_1A_1 genotype (a result of choosing $a_{11} > 2.0$) has a significant effect on the dynamics of the model.

In the next section it is shown how the preceding analysis can be extended to look for higher period polymorphisms. Asmussen [8] found cases of interior chaotic attractors. Since repeated period-doubling is a well-known path to chaos (see, for example, Seydel (1988) or Wiggins (1990)), we can expect to find higher period stable polymorphisms.

5.5.4 Orbits of period four (and higher)

Consider first orbits of period 4. Since I did not find such orbits by varying b_{12} and b_{22} , I chose b_{12} and b_{22} to lie in region E, a region where more complex behaviour already

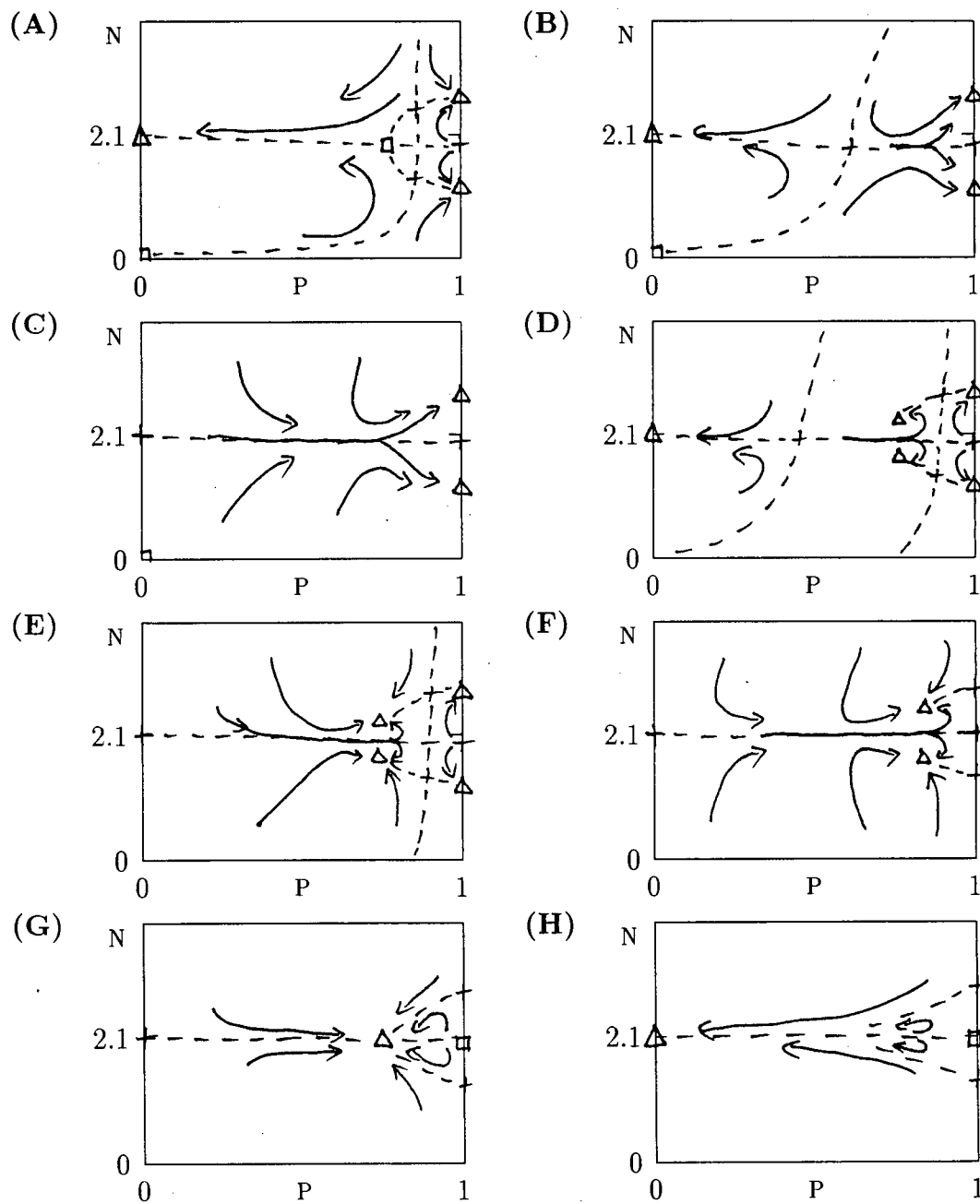


Figure 5.8: Dynamics in the (p, N) -plane with $a_{11} = 2.1$, $a_{12} = 1.9$, $a_{22} = 1.1$, $b_{11} = 1.0$ and various combinations of b_{12} and b_{22} which correspond to regions A to H in figure 5.6.

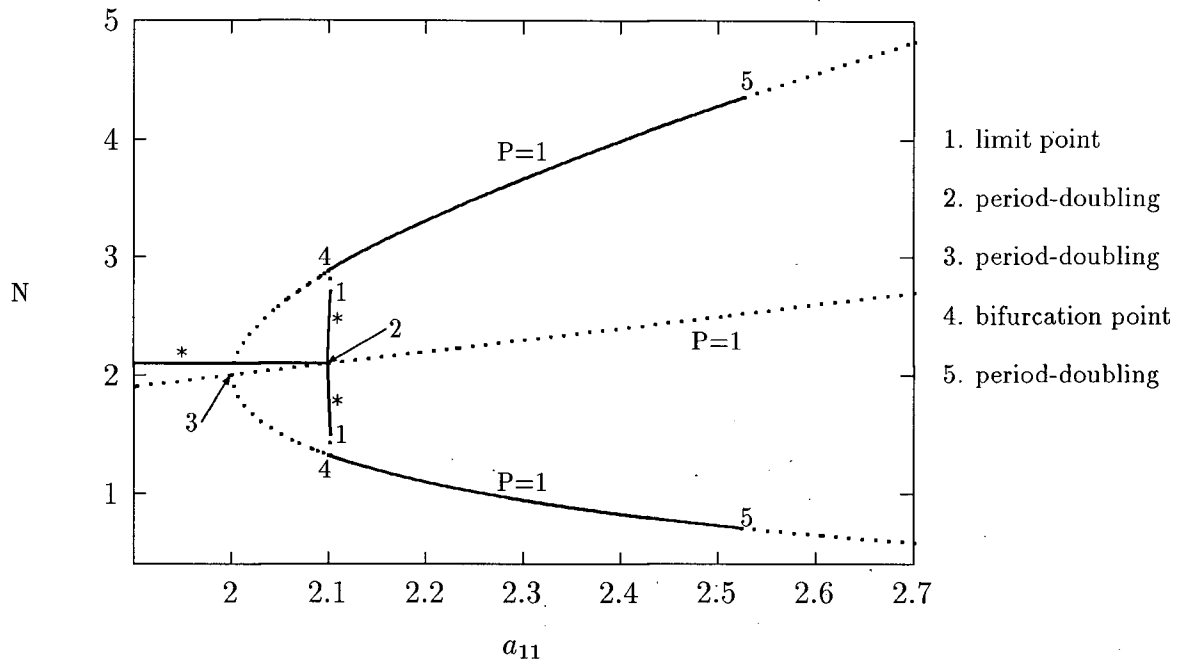


Figure 5.9: One-parameter bifurcation diagram of model (5.3) with $a_{12} = 1.9$, $a_{22} = 1.1$, $b_{11} = 1.0$, $b_{12} = 0.905$ and $b_{22} = 0.525$ obtained using AUTO. Branches marked with a * correspond to interior values of p , namely $0 < p < 1$.

occurs in the form of period-2 cycles, and then varied the other parameter values in turn.

Consider $b_{12} = 0.905$ and $b_{22} = 0.525$ and suppose a_{11} is varied. This yields a period-doubling bifurcation at $a_{11} = 2.526$ (see figure 5.9). Since I used the second iterate of the map, this period-doubling is a bifurcation from period-2 to period-4 orbits at the boundary $p = 1$. This can be checked by using DSTOOL to generate diagrams in the (p, N) -plane for nearby values of a_{11} .

From studies of other discrete systems (for example, [71]) it is likely that there will be period-doublings to higher and higher order orbits as a_{11} is increased. Unfortunately these cannot be detected using AUTO unless higher order iterates of the map (5.2) are determined analytically and then studied. However, using DSTOOL we can determine the dynamics in the (p, N) -plane for fixed values of a_{11} . Some examples are given in

figure 5.10.

Two-parameter continuations of the period-doubling bifurcation in figure 5.9 show that the position of this bifurcation depends only on a_{11} . None of the other parameters affects the value of a_{11} at which it occurs. Thus we can conclude that it is the growth rate of the A_1A_1 genotype that determines the degree of instability of its dynamics. This supports the comment in [93] that alleles that affect seedling survival can increase carrying capacity and simultaneously destabilise population growth dynamics.

Interior period-4 orbits

But what about the dynamics of the heterozygote? It seems likely that complex polymorphic behaviour would exist in regions where *both* homozygotes exhibit unstable dynamics. In order to investigate this question I chose both a_{11} and a_{22} to be greater than 2.0. Using the parameter values $a_{11} = 2.1$, $a_{12} = 1.9$, $a_{22} = 2.1$, $b_{11} = 1.0$, $b_{12} = 0.908$ and $b_{22} = 0.53$, I found a set of starting points using DSTOOL and then varied each parameter in turn using AUTO.

The only interior period-doubling bifurcation was found by increasing a_{12} . Figure 5.11 shows the results. There are period-2 orbits at both $p = 0$ and $p = 1$ for all values of a_{12} . This is expected since both a_{11} and a_{22} are greater than 2.0. The period-2 orbit at $p = 1$ is attracting for $a_{12} < 1.907$ (the region of heterozygote inferiority) and the orbit at $p = 0$ is attracting for $a_{12} < 3.598$. At this latter point the heterozygote becomes dominant, a bifurcation occurs and a stable interior period-2 orbit is initiated. As a_{12} is increased further, a period-doubling bifurcation occurs at $a_{12} = 3.750$. Although the period-4 orbits are not shown by AUTO, we can verify that such orbits exist using DSTOOL. Figure 5.12 shows the dynamics in the (p, N) -plane for $a_{12} = 3.8$.

From the above results it appears that the relative carrying capacities of the genotypes determine whether the boundaries and/or interior are attracting but that the growth

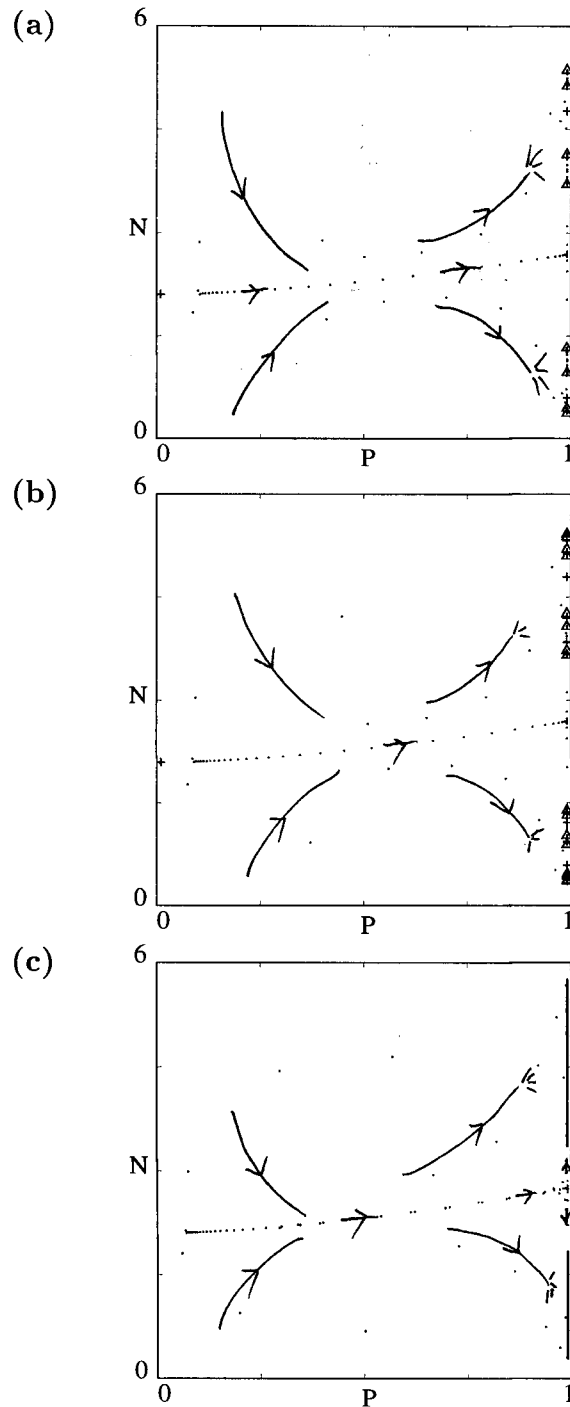


Figure 5.10: Dynamics in the (p, N) -plane for $a_{12} = 1.9$, $a_{22} = 1.1$, $b_{11} = 1.0$, $b_{12} = 0.905$, $b_{22} = 0.525$ and (a) $a_{11} = 2.68$, (b) $a_{11} = 2.69$ and (c) $a_{11} = 2.75$. In (a) there is a period-8 attractor at $p = 1$. In (b) this changes to a period-16 attractor and in (c) we have what appears to be a chaotic attractor.

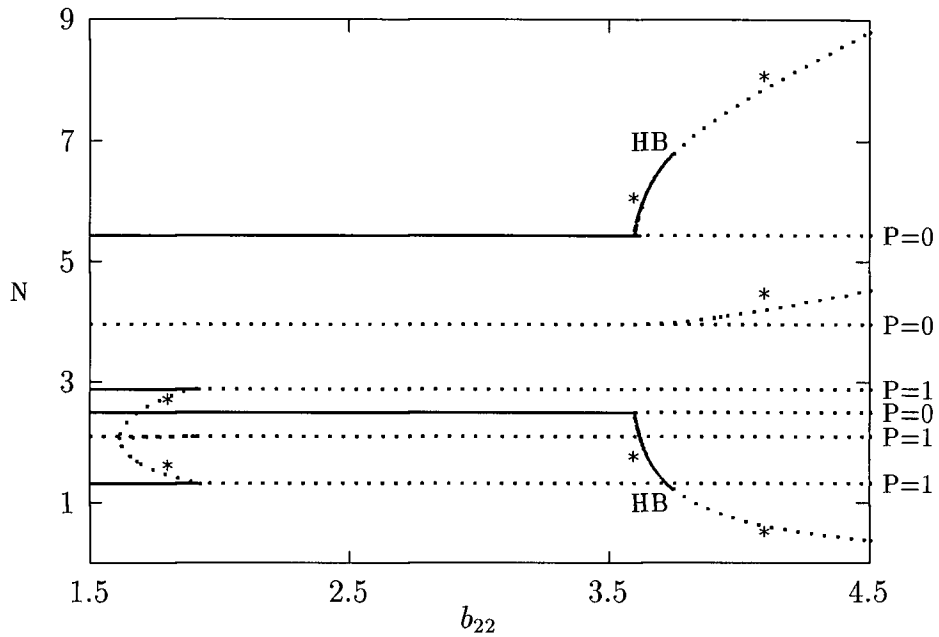


Figure 5.11: One-parameter bifurcation diagram of model (5.3) with $a_{11} = 2.1$, $a_{22} = 2.1$, $b_{11} = 1.0$, $b_{12} = 0.908$ and $b_{22} = 0.53$ obtained using AUTO. Branches marked with a * correspond to interior values of p , namely $0 < p < 1$. HB marks a period-doubling bifurcation from period-2 to period-4 orbits.

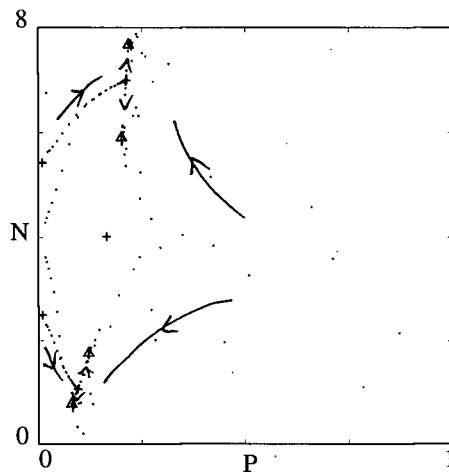


Figure 5.12: Dynamics in the (p, N) -plane for $a_{11} = 2.1$, $a_{12} = 3.8$, $a_{22} = 2.1$, $b_{11} = 1.0$, $b_{12} = 0.908$ and $b_{22} = 0.53$ showing a stable period-4 polymorphism.

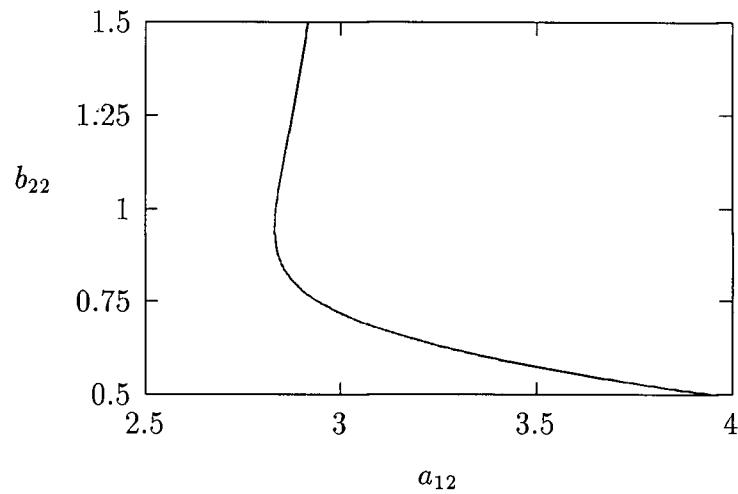


Figure 5.13: Two-parameter continuation of the period-doubling bifurcation (HB) in figure 5.11 with $a_{11} = 2.1$, $a_{22} = 2.1$, $b_{11} = 1.0$ and $b_{12} = 0.908$.

rates, a_{ij} , determine the type of attractor, that is, whether the attractors are equilibria or periodic cycles of various orders. Since the only way to alter the carrying capacity of A_iA_j without affecting its growth rate is to vary b_{ij} , we can conclude that the b_{ij} 's greatest influence is on stability whereas the a_{ij} 's determine the type or order of the behaviour.

Although we have located a stable polymorphic period-4 orbit, the values of a_{12} for which it occurs are very high. We would like to know whether such a phenomenon is possible for lower values of a_{12} but different values of some of the other parameters. It is only in the region of heterozygote superiority that polymorphic attractors exist in figure 5.11 and since $K_{22} = 3.962$ is large, this region is only entered when a_{12} is large. Hence, by decreasing K_{22} we may be able to find stable interior period-4 orbits for lower values of a_{12} . Figure 5.13 shows a two-parameter continuation of the period-doubling bifurcation labelled 5 in figure 5.11. The parameter b_{22} is varied in addition to a_{12} . From figure 5.13 it can be seen that the period-doubling bifurcation point is reduced to $a_{12} = 2.831$ if b_{22}

is increased to 0.945. This is substantially lower than before.

If we wanted to use AUTO to study orbits of period greater than 4, we would have to calculate higher order iterates of the map (5.2). This is rather tedious and is perhaps more of mathematical than of ecological interest. However, using DSTOOL, we can increase the a_{ij} values and observe the results for particular parameter combinations. Some examples of more complex dynamics are shown in figure 5.14.

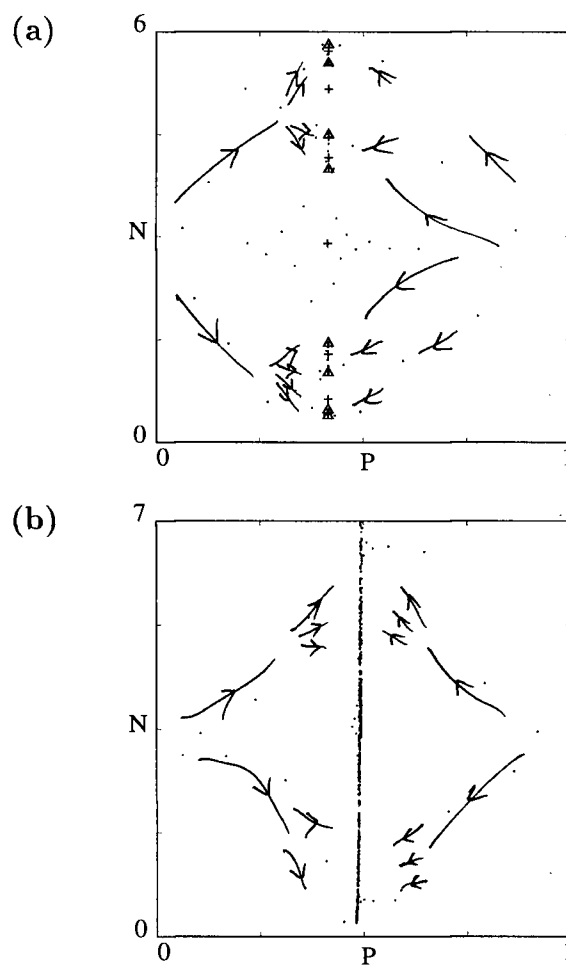


Figure 5.14: Examples of complex dynamics. (a) An interior period-8 orbit for $a_{11} = 2.3$, $a_{12} = 2.9$, $a_{22} = 2.5$, $b_{11} = 1.0$, $b_{12} = 0.908$ and $b_{22} = 0.95$. (b) An interior chaotic attractor for $a_{11} = 2.6$, $a_{12} = 3.1$, $a_{22} = 2.5$, $b_{11} = 1.0$, $b_{12} = 0.908$ and $b_{22} = 0.95$.

5.6 Conclusion

In this chapter a partial analysis of a population genetics model with monotone density-dependent fitness functions has been done. Although most of the theoretical results had been obtained by Asmussen [8] and Namkoong *et al.* [93], this study gave rise to a two-parameter bifurcation diagram which indicates the relative frequency of occurrence of the various types of dynamical behaviour in addition to proving their existence. Using AUTO and DSTOOL, stable polymorphic period-2 and higher period orbits were located. Asmussen [8] found these phenomena particularly difficult to study by hand when using exponential fitness functions but they can be found without too much difficulty using the available software. In addition to locating equilibria and higher period orbits I concluded that the parameters b_{ij} ($i,j=1,2$) have the greatest influence on the stability of these phenomena whereas the a_{ij} 's determine the type or order of the behaviour.

A number of opportunities for further research arise naturally from the results of this chapter. First, could the numerical results be used as a basis for arriving at analytical relationships between the parameters or at biological conditions that would determine the existence of polymorphisms? For the model that I have considered this would be particularly difficult to decide because of the exponential fitnesses, but a start could be made using linear fitness functions. It would also be informative to know the relationship between the behaviour of periodic attractors for the homozygotes and for the full genetic system. Specifically, if both homozygotes have period-2 dynamics when acting alone, is it only possible to obtain period-2 polymorphic behaviour or are polymorphic equilibria and higher period polymorphic attractors also possible? If one homozygote exhibits period- x dynamics and the other period- y dynamics when acting alone ($x < y$), does the full system exhibit dynamics of period- x , period- y , or some combination of x and y ?

In the next chapter the same basic model is analysed but this time non-monotone fitness functions are considered. The model has not been studied in detail before.

Chapter 6

Population Genetics Model II

6.1 Introduction

In the last chapter a single locus, two allele population genetics model with monotone density-dependent fitness functions was analysed. Most studies assume such monotonically decreasing fitness functions because of the detrimental effects of population density on growth [110]. However, this assumption is not biologically realistic for all population densities [110]. At low densities, increases in density may benefit both reproduction and survival. In this chapter I consider the same basic model as in chapter 5 but with non-monotone density-dependent fitness functions which have a single hump. This model is more difficult to study than that in the previous chapter because of the increased complexity in the fitness functions. Instead of a single carrying capacity each fitness function has two fixed points corresponding to the values of N where $w_{ij} = 1$. The terminology described in section 5.2 is used again in this chapter.

As in chapter 5 the study focusses mainly on stable polymorphic behaviour—both equilibria and higher period orbits. Such phenomena correspond to the maintenance of genetic diversity in a population. From an ecological perspective we would like to know how common or rare these phenomena are, that is, how likely they are to occur. In contrast to chapter 5 (see section 5.5.3) it is found that a large number of parameter combinations give rise to stable polymorphic equilibria but that stable periodic polymorphisms are not as common. The latter phenomena are only found to occur in situations

where the dynamics corresponding to one of the homozygotes are fairly unstable and where the fitnesses of the two homozygotes acting alone are very different. Other formulations for hump-shaped fitness functions may, however, lead to different results.

An interesting result is that there is always a possibility of one allele being excluded, even when a polymorphic attractor is present. Diagrams in the (p, N) -plane indicate the domains of attraction for the homomorphic and polymorphic attractors. The possibility of extinction is also high for most parameter sets. Criteria for determining the existence and stability of polymorphic equilibria are also given. These combine theoretical and numerical results.

In the next section I outline some previous results which apply to the model. I then describe the functional forms of the non-monotone fitness functions. The model analysis begins by fixing the fitness function corresponding to one of the homozygotes and varying the two parameters corresponding to the other. A two-parameter bifurcation diagram shows which parameter combinations give rise to homomorphic attractors and which to polymorphic attractors. Section 6.4.3 finds criteria for predicting the existence and stability properties of polymorphic equilibria, and stable period-2 polymorphisms are the focus of section 6.4.4. A small modification to the fitness functions is required before the latter phenomena are located. The results are summarised in a two-parameter bifurcation diagram. Further two-parameter bifurcation diagrams show that period-2 polymorphisms do not correspond to fitness functions where both homozygotes have similar properties but one of the homozygotes has a greater fitness than the other at every population density.

6.2 Background

One of the few studies which considers the more general setting of non-monotone density-dependent fitness functions is by Selgrade and Namkoong [110]. They prove a number of results concerning the existence and stability of polymorphic equilibria for both continuous and discrete two-dimensional models. In particular, a necessary condition for the existence of a polymorphism is that the heterozygote fitness be either superior or inferior to both homozygote fitnesses at the equilibrium. For the case of heterozygote inferiority the equilibrium is unstable. For the discrete model (which is the one considered in this chapter), if the heterozygote is superior and $-2 < N \frac{\partial \bar{w}}{\partial N} < 0$ (N =population density, \bar{w} =mean fitness) at the polymorphic equilibrium then this equilibrium is stable. Higher order attractors are not studied in [110] and it is noted that arguments concerning global dynamics are more difficult for these non-monotone fitness functions because of the complicated nature of the mean fitness curve.

6.3 Fitness functions

The fitness functions used in this chapter are given by

$$w_{ij}^t = k_{ij} N_t \exp[r_{ij}(1 - k_{ij} N_t)] \quad i, j = 1, 2 \quad (6.1)$$

$$\text{and } w_{ij}^t = k_{ij} N_t \exp[r_{ij}(1 - k_{ij} N_t) N_t] \quad i, j = 1, 2. \quad (6.2)$$

Expressions of the form (6.1) can be found in [109] and also in [110] for the analogous continuous model. These functions have a single hump (see figure 6.1) and are known as climax fitness functions in some applications [109].

Apart from the results for polymorphic equilibria obtained by Selgrade and Namkoong [110], not much work has been done on discrete models such as (5.2) in which both genotypes have climax fitnesses. In order to simplify the analysis I look at an additive model

in which the fitness parameters for the heterozygote are averages of the corresponding parameters for the homozygotes. That is,

$$k_{12} = \frac{k_{11} + k_{22}}{2}$$
$$\text{and } r_{12} = \frac{r_{11} + r_{22}}{2}.$$

This reduces the number of parameters for consideration.

6.4 Model analysis

6.4.1 Approach

I begin by studying the existence and relative frequency of occurrence of stable equilibria for the additive model with fitness functions given by (6.1). I then look for stable periodic polymorphisms using fitness functions given first by equations (6.1) and then by equations (6.2).

As in the previous chapter bifurcation diagrams and plots of the (p, N) -plane are the main tools for communicating results. In some situations the fitness functions are plotted so that the relative fitnesses for various population densities can be seen. This is analogous to calculating relative carrying capacities in the previous chapter.

In order to begin we need to choose a starting set of parameter values. There are four parameters in this model— k_{11}, r_{11}, k_{22} and r_{22} (k_{12} and r_{12} are averages of the corresponding homozygote parameters). Since there were no prior results with which to begin, I used MAPLE¹ [122] to plot the three fitness functions and chose parameter values which led to plausible-looking curves. Since there are four parameters and AUTO can vary at most two at a time, I fixed r_{22} and k_{22} (that is, I fixed the fitness function w_{22}) and investigated the (k_{11}, r_{11}) -parameter space. Therefore, the results will indicate

¹Any other mathematical graphics package, such as MATHEMATICA [126] or GNUPLOT [125], could have been used.

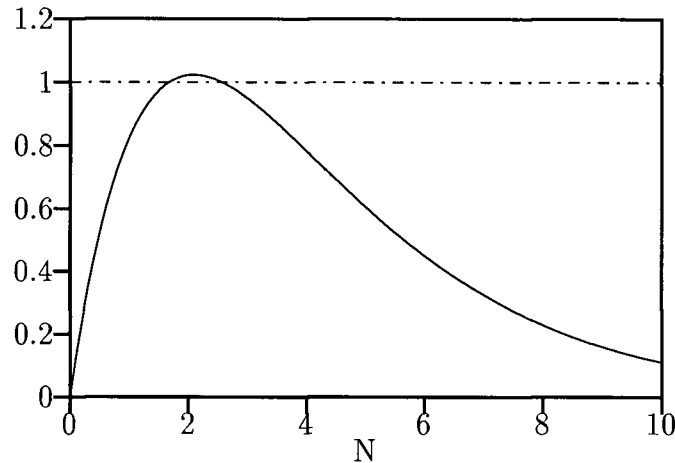


Figure 6.1: w_{22} with $r_{22} = 0.8$ and $k_{22} = 0.6$.

the effects of varying the relative positions and magnitudes of the fitness functions. It should be kept in mind that altering r_{11} and k_{11} will affect both w_{11} and w_{12} .

6.4.2 (k_{11}, r_{11}) -parameter space

After using AUTO to vary the parameters one by one to locate a stable polymorphism, I chose $r_{22} = 0.8$ and $k_{22} = 0.6$ as starting values, which gave the w_{22} fitness function shown in figure 6.1. The aim is to divide the (k_{11}, r_{11}) -parameter space into regions corresponding to stable fixed points at $p = 0, p = 1$ (homomorphic equilibria) or $0 < p < 1$ (polymorphic equilibria).

The first step is to generate a one-parameter bifurcation diagram. Choosing values for r_{11} and k_{11} , I used DSTOOL to find fixed points as starting points for AUTO. Figure 6.2 was obtained by varying k_{11} with $r_{11} = 0.7$. Only branches corresponding to $0 \leq p \leq 1$ have been drawn and no distinction between sources and saddles has been made so as to keep the diagram as clear as possible. (Interactive AUTO uses magenta to represent sources and blue to represent saddles.)

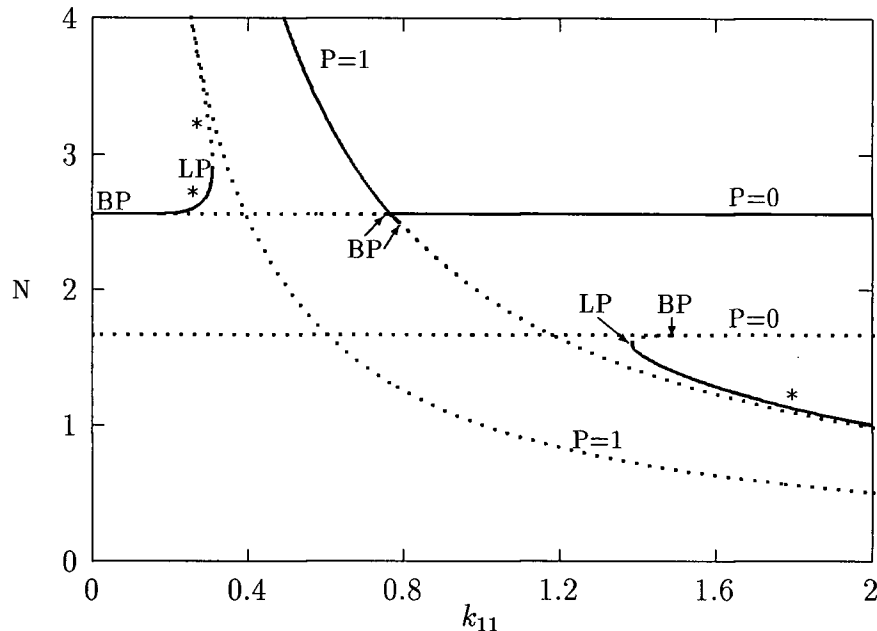


Figure 6.2: A one-parameter bifurcation diagram obtained by varying k_{11} with r_{11} fixed at 0.7 ($r_{22} = 0.8$ and $k_{22} = 0.6$). Branches marked with a * correspond to interior values of p , namely $0 < p < 1$. LP marks the limit points and BP the transcritical bifurcation points.

There are many bifurcations in figure 6.2. Most are transcritical bifurcations (see section A.2.25) but there are also two limit points (see section A.2.13). Diagrams of the (p, N) -plane for a number of different values of k_{11} are shown in figure 6.3 to help clarify the changes in dynamical behaviour that occur as k_{11} increases through these bifurcation points. Note that for this value of r_{11} there are two ranges of k_{11} -values where stable polymorphic equilibria occur. Another important observation from an ecological perspective is that the possibility of extinction is fairly high for all the situations shown in figure 6.3.

AUTO can only continue limit points and period-doubling bifurcations in two parameters. As can be seen from figure 6.2 we will also need to know how the positions of the *transcritical* bifurcations vary with r_{11} if we want to delimit regions of stable behaviour

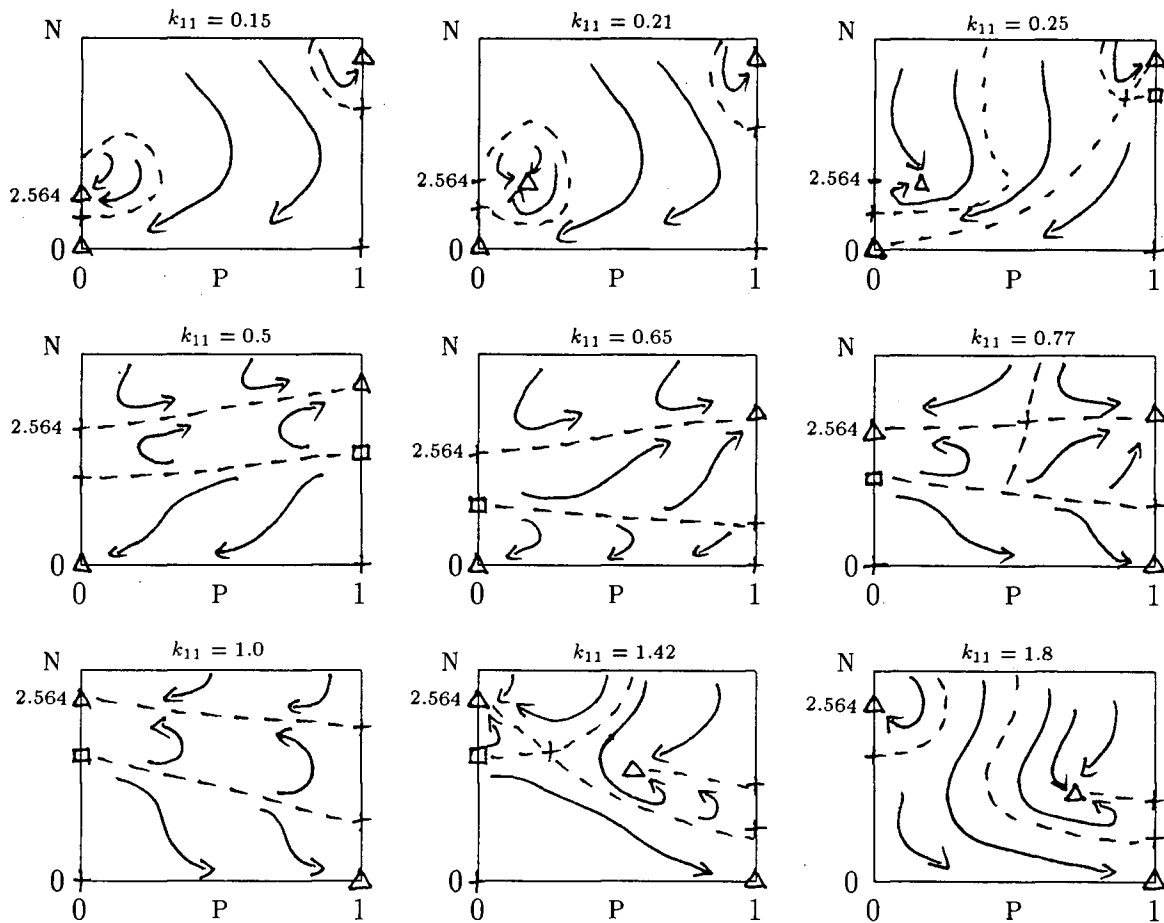


Figure 6.3: Diagrams of the (p, N) -plane (obtained using DSTOOL) for a number of different values of k_{11} with r_{11} fixed at 0.7.

in two-parameter space. In order to do this I chose a number of different r_{11} -values (such as 0.3, 0.5, 0.7, ...). For each value I obtained starting points (that is, equilibrium points) for AUTO using DSTOOL². I then used AUTO to generate a one-parameter bifurcation diagram by varying k_{11} in both directions, and recorded the k_{11} -values corresponding to the various bifurcations—both transcritical and limit point. Using the graphics package GNUPLOT [125] to plot the recorded points, I obtained figure 6.4(a). Figures 6.4(b), (c)

²It is important that a number of different fixed points are located for each parameter set to ensure that unconnected continuation branches are not missed.

and (d) show the same diagram with shaded regions corresponding to stable equilibria at $0 < p < 1$, $p = 0$ and $p = 1$ respectively. Although figure 6.4 only gives approximations to the various bifurcation curves, they are sufficient for a qualitative analysis. I am more interested in the different types of qualitative behaviour that can occur than the actual parameter values at which transitions take place.

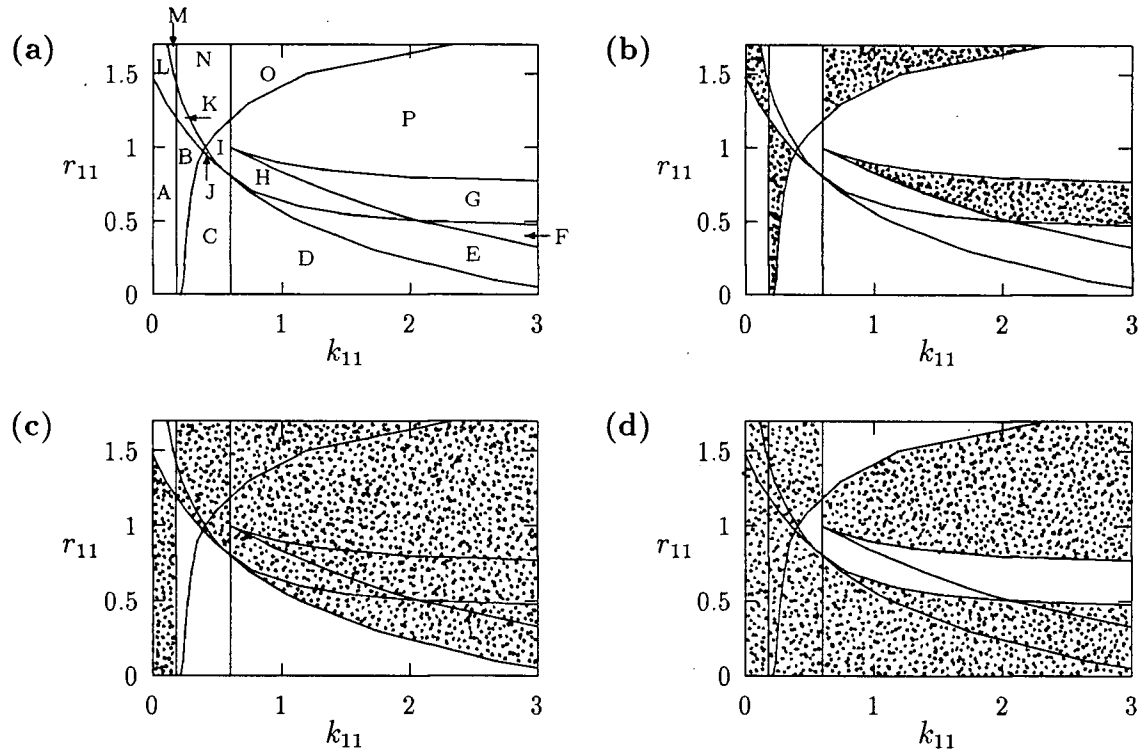


Figure 6.4: Diagrams of the (k_{11}, r_{11}) -parameter space. (a) The basic diagram showing a number of bifurcation curves. (b) The regions corresponding to stable polymorphisms are shaded. (c) The regions corresponding to stable equilibria at $p = 0, N > 0$ are shaded. (d) The regions corresponding to stable equilibria at $p = 1, N > 0$ are shaded.

In order to clarify figure 6.4, diagrams of the (p, N) -plane corresponding to the regions marked A to P are shown in figures 6.5 and 6.6. These figures are schematic representations of diagrams obtained using DSTOOL. The dashed lines in these diagrams approximate the one-dimensional manifolds of the saddle points (see page 241) and indicate the boundaries of the domains of attraction of the sinks.

In addition to revealing the extents of the regions corresponding to homomorphic and polymorphic equilibria, figure 6.4 shows where we can expect simultaneous homomorphic and polymorphic attractors. In fact, there are no regions where the only attractor is in the interior. Thus, there is always the possibility that one of the alleles will be excluded. The relative sizes of the domains of attraction of the homomorphic and polymorphic equilibria are shown in figures 6.5 and 6.6. These diagrams also highlight the ever-present possibility of extinction.

6.4.3 Criteria for polymorphisms

It would be helpful to be able to predict when a stable polymorphic equilibrium is likely to occur. One possibility is to investigate the fitness functions corresponding to the different regions in figure 6.4(a). Computer packages such as GNUPLOT [125], MAPLE [122] and MATHEMATICA [126] are convenient for such investigations as the fitness functions w_{11} , w_{12} and w_{22} can be plotted on the same pair of axes. Fixed points at $p = 0$ and $p = 1$ occur at those values of N where $w_{22} = 1$ and $w_{11} = 1$ respectively. The stability of these points depends on the relative fitnesses of the homozygotes and the heterozygote.

In each of the regions corresponding to a stable polymorphism it was found that the heterozygote is superior at the point where the downward slope of the w_{12} fitness function crosses the line $w_{12} = 1$ (see figure 6.7(a)). Similarly, interior saddle points correspond to heterozygote inferiority at this point (see figure 6.7(b)). However, not

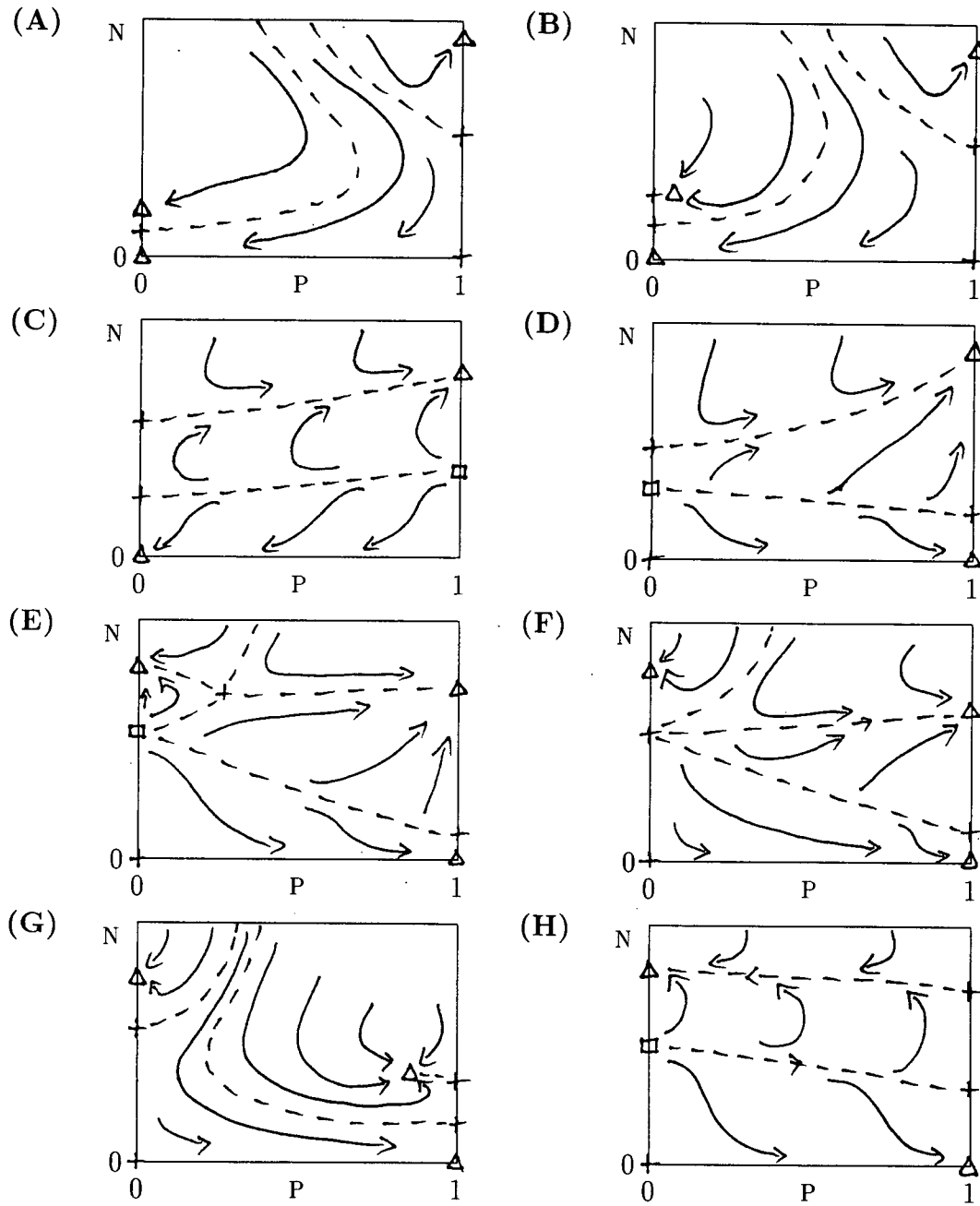


Figure 6.5: Diagrams of the (p, N) -plane corresponding to the regions A to H in figure 6.4(a).

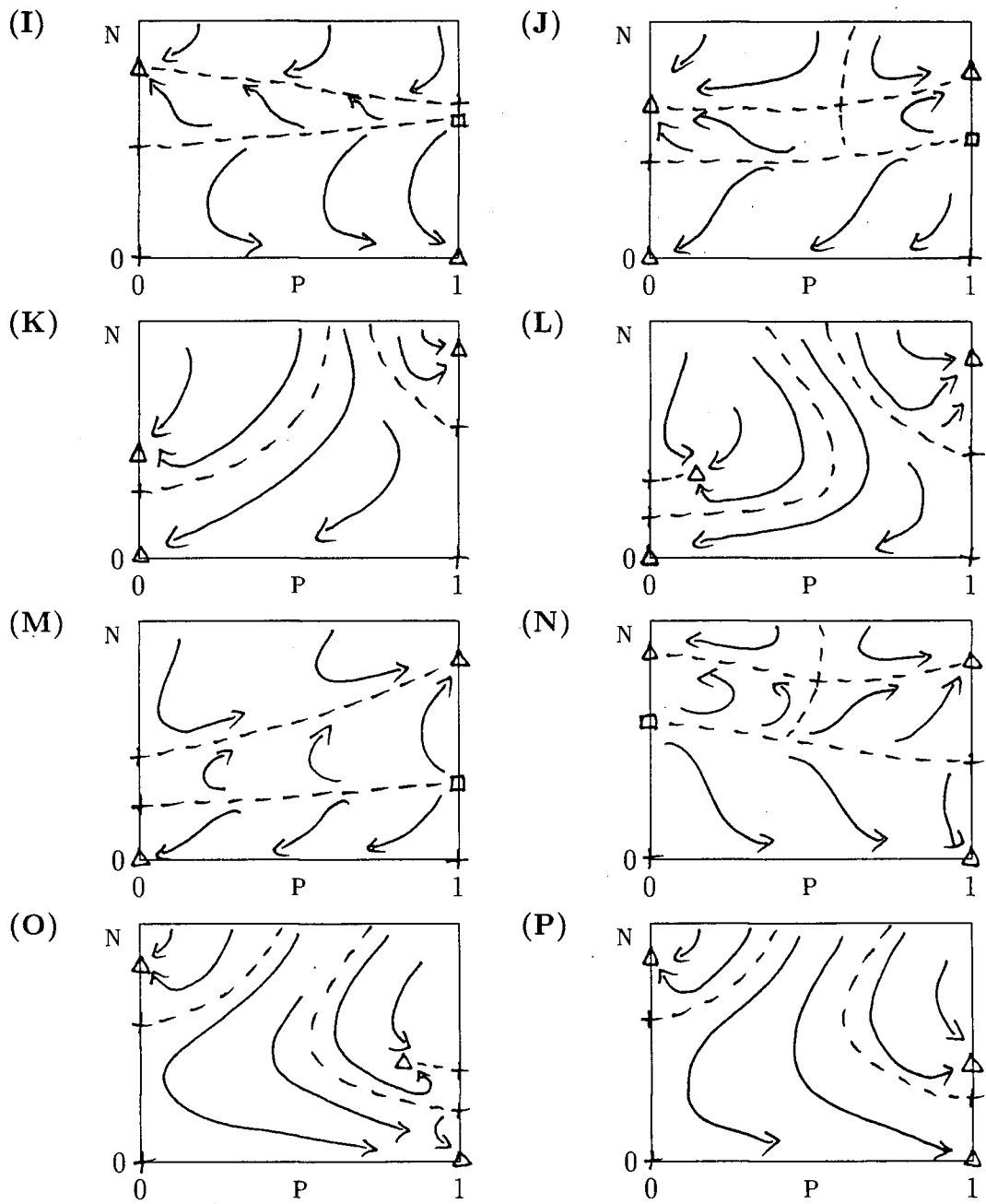


Figure 6.6: Diagrams of the (p, N) -plane corresponding to the regions N to P in figure 6.4(a).

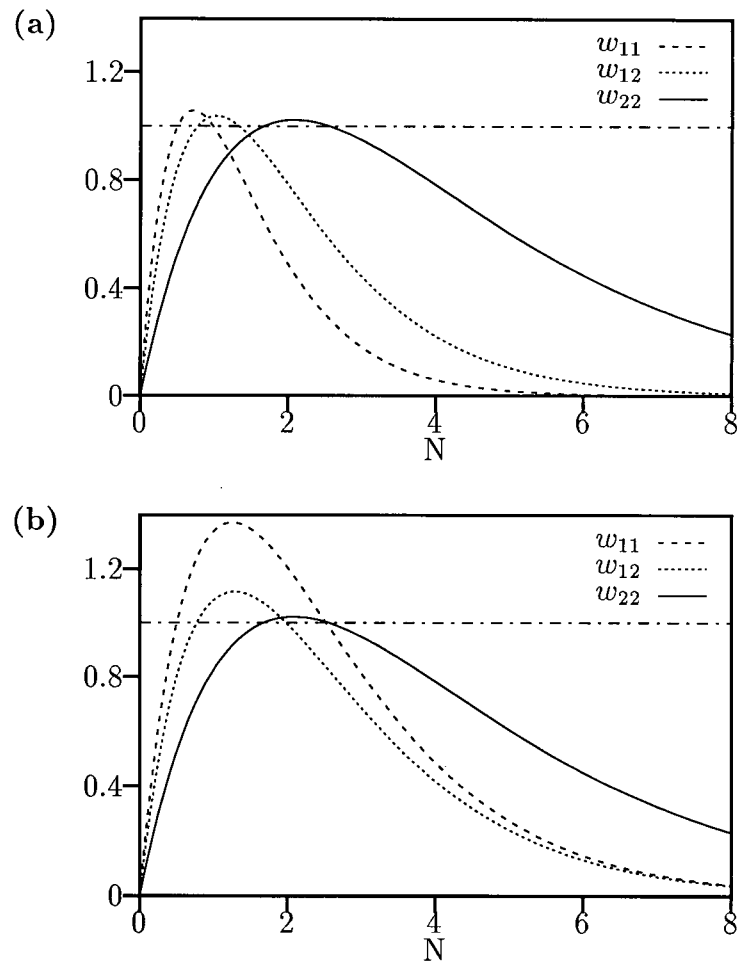


Figure 6.7: Examples of the fitness functions for parameter values corresponding to (a) a stable polymorphism ($r_{11} = 0.7, k_{11} = 2.0, r_{22} = 0.8, k_{22} = 0.6$) and (b) an unstable polymorphism ($r_{11} = 0.4, k_{11} = 2.0, r_{22} = 0.8, k_{22} = 0.6$).

all parameter combinations which gave similar configurations of the fitness functions correspond to the existence of polymorphisms. This supports the conclusion in [110] that heterozygote inferiority or superiority is *necessary* but not *sufficient* for a polymorphism to occur. Hence, it appears that this method of looking at the fitness functions is not too informative when it comes to the question of existence of polymorphisms.

An alternative is to investigate the mean fitness functions:

$$\begin{aligned}w_1^t &= p_t w_{11}^t + (1 - p_t) w_{12}^t, \\w_2^t &= p_t w_{12}^t + (1 - p_t) w_{22}^t, \\ \text{and } \bar{w}^t &= p_t w_1^t + (1 - p_t) w_2^t,\end{aligned}$$

where w_i^t is the marginal fitness of allele A_i and \bar{w}^t is the mean population fitness at time t . An interior equilibrium ($0 < p < 1$, $N > 0$) requires

$$\begin{aligned}p_{t+1} &= p_t \\ \text{and } N_{t+1} &= N_t.\end{aligned}$$

From equations (5.2) in the previous chapter we can see that the above equations will be satisfied if

$$\bar{w}^t = 1 \tag{6.3}$$

$$\text{and } w_1^t = \bar{w}^t. \tag{6.4}$$

For $0 < p < 1$ the latter condition can only be satisfied if

$$w_1^t = w_2^t. \tag{6.5}$$

We need to solve conditions (6.3) and (6.5) simultaneously for p and N but an explicit mathematical solution is not possible because of the exponential terms in the fitness functions. We can use a computer package such as GNU PLOT [125] to plot these equations numerically. An example is shown in figure 6.8.

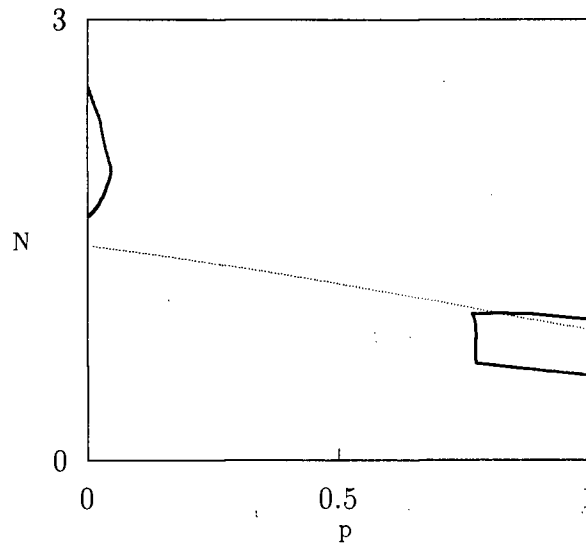


Figure 6.8: Curves given by $w_1 = w_2$ (thin dotted line) and $\bar{w} = 1$ (thick solid line) for parameter values corresponding to a stable polymorphism ($r_{11} = 0.7, k_{11} = 2.0, r_{22} = 0.8, k_{22} = 0.6$).

From the above mathematical analysis we know that the curves corresponding to the two equations (6.3) and (6.5) always intersect when a polymorphism is present and do not intersect in other regions. Each intersection corresponds to a unique polymorphic equilibrium. Thus, we can predict the existence of polymorphic equilibria. However, it is not possible to distinguish between stable polymorphisms and interior saddle points on the basis of these diagrams.

Using *both* plots of the mean fitness function configurations and the results in [110] mentioned in section 6.2 for determining the stability of interior equilibria, we can predict the existence and the stability properties of polymorphic equilibria. The relative positions of the fitness functions, such as in figure 6.7, give most of the required stability information but for a stable polymorphism the quantity $N \frac{\partial \bar{w}}{\partial N}$ also needs to be checked (see [110]). Although it is satisfying to have neat mathematical criteria, for a given situation it is probably easier and quicker to use DSTOOL to find and classify the fixed

points.

In the next section I turn to higher order dynamics. As in the previous chapter we would like to know whether stable period-2 (and higher period) polymorphisms are possible with this additive model since the maintenance of genetic diversity need not be restricted to the existence of polymorphic equilibria.

6.4.4 Stable period-2 polymorphisms

Attempts to find a stable period-2 polymorphism using DSTOOL and AUTO proved to be time-consuming. However, I was finally successful in locating a period-2 sink for $r_{11} = 1.3, k_{11} = 0.5, r_{22} = 7.5$ and $k_{22} = 4.57$. The fitness functions and (p, N) -plane corresponding to these parameter values are shown in figure 6.9. As can be seen from figure 6.9(b), the domain of attraction for this period-2 orbit is very small. Also, figure 6.9(a) shows that the fitness function w_{22} has an unrealistically high maximum. Neither situation is particularly satisfying.

The r_{ij} values determine the heights of the fitness function maxima. We would like to know whether altering one of the other parameter values would allow r_{22} to be lowered while still maintaining the interior period-2 attractor. AUTO can be used to generate two-parameter diagrams for this purpose. The first step is to create a one-parameter bifurcation diagram by varying r_{22} . The relevant curves are shown in figure 6.10. The period-doubling bifurcation HB^* is the point at which stable period-2 orbits are initiated. Using AUTO we can see how the position of this period-doubling bifurcation changes as a second parameter is varied. The diagrams obtained using r_{11}, k_{11} and k_{22} as the second parameter are shown in figures 6.11(a), (b) and (c) respectively. As can be seen from these diagrams, r_{22} needs to be greater than 6.4 for a stable period-2 polymorphism. This is still rather large and not particularly satisfactory.

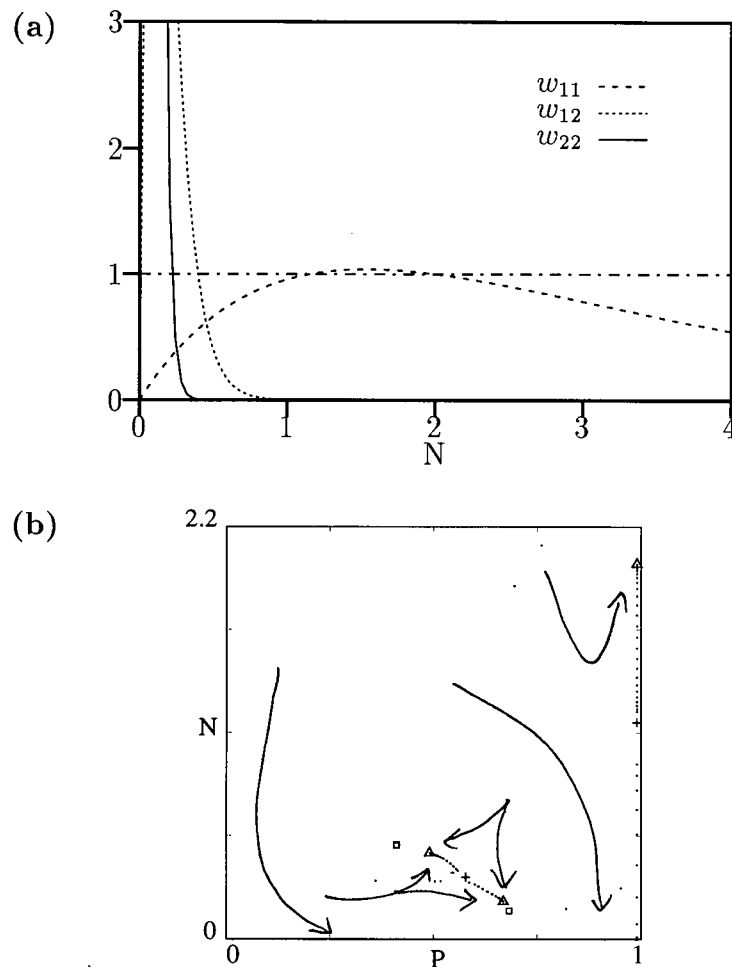


Figure 6.9: (a) Fitness functions and (b) (p, N) -plane for $r_{11} = 1.3$, $k_{11} = 0.5$, $r_{22} = 7.5$ and $k_{22} = 4.57$.

There is no reason why we should be confined to the fitness functions given in equations (6.1). The only requirements for this study were that the fitness functions be density-dependent and have a single hump, and that the model be additive (that is, the heterozygote parameters must be linear combinations of the homozygote parameters). The steeper the slopes of the fitness functions (the right-hand slope in particular), the less stable the dynamics corresponding to that homozygote. This is similar to the previous chapter where higher growth rates, which caused exponential fitnesses with steeper

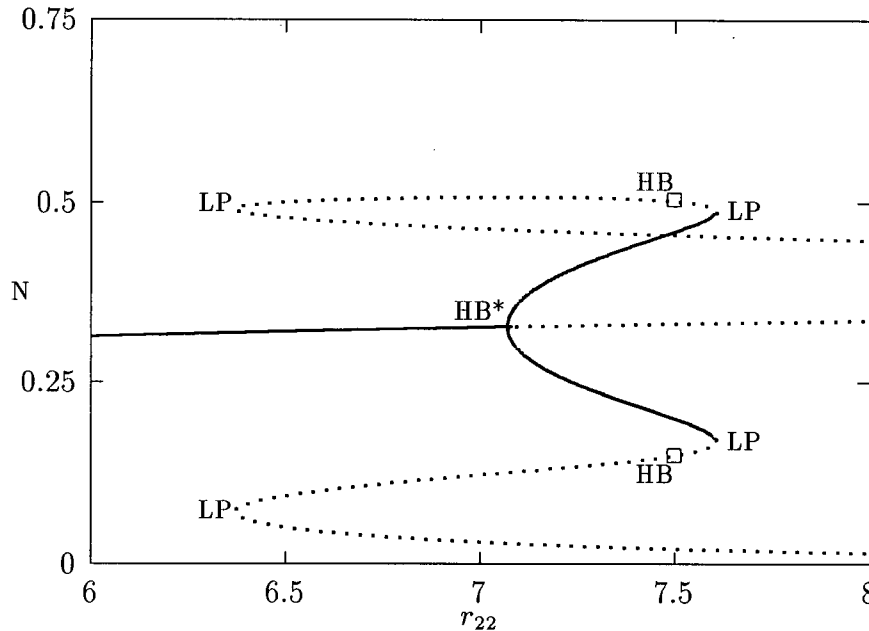


Figure 6.10: A partial one-parameter bifurcation diagram obtained by varying r_{22} using Interactive AUTO. Only branches satisfying $0 < p < 1$ are shown. The second iterate of the model was used so that the period-2 orbits could be continued. However, using this model the period-doubling bifurcation HB^* is labelled as a bifurcation point by AUTO which means that it cannot be continued in two parameters. The original model needs to be used for such a continuation.

slopes, resulted in more complex dynamics. We expect higher period interior orbits to occur in regions of less stable behaviour at the boundaries $p = 0$ or $p = 1$ and, thus, one-humped fitness functions whose slopes are steeper than those given by equations (6.1) may give more reasonable results. Fitness functions of the form (6.2) have the required property. With these fitness functions I found a stable period-2 polymorphism for $r_{11} = 0.2$, $k_{11} = 5.0$, $r_{22} = 0.3$ and $k_{22} = 0.4$. Both DSTOOL and AUTO were used in the search. The fitness functions and (p, N) -plane corresponding to these values can be found in figure 6.12. As can be seen from figure 6.12(a), the fitness functions are much more reasonable than before.

Again we can get some idea of the size of the region in parameter space for which

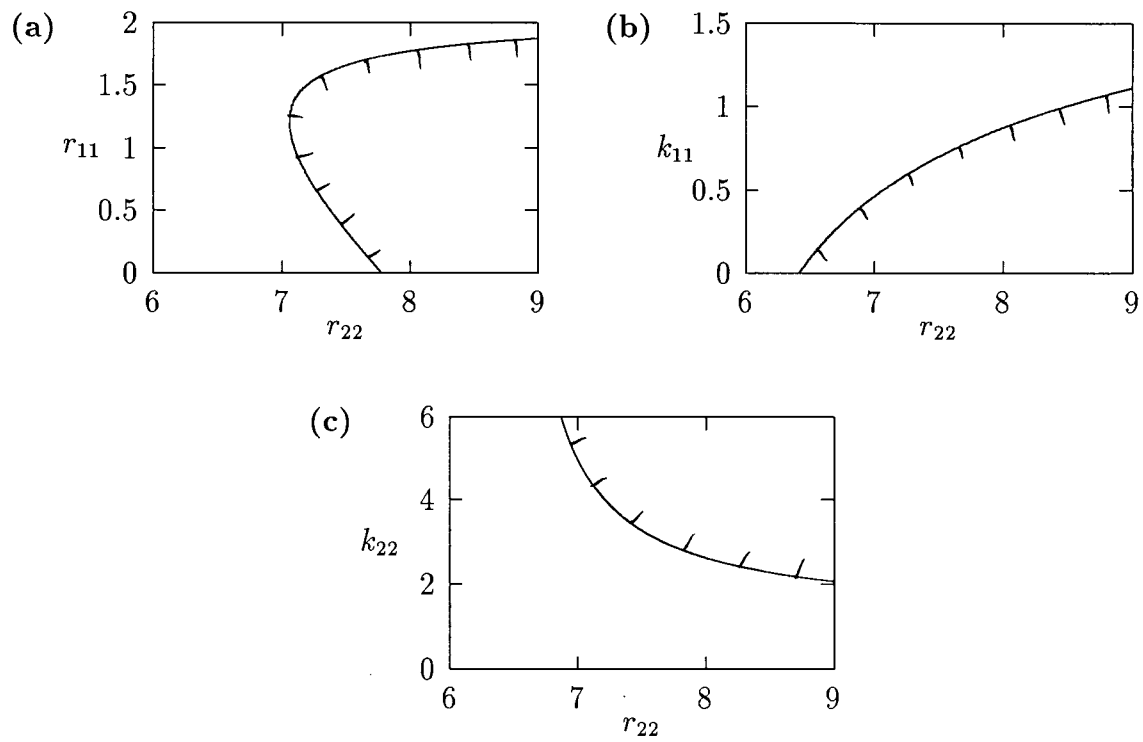


Figure 6.11: Two-parameter continuations of the period-doubling bifurcation HB^* in figure 6.10 obtained by varying (a) r_{11} , (b) k_{11} and (c) k_{22} in addition to r_{22} . The shaded regions indicate which side of the bifurcation continuations corresponds to periodic behaviour.

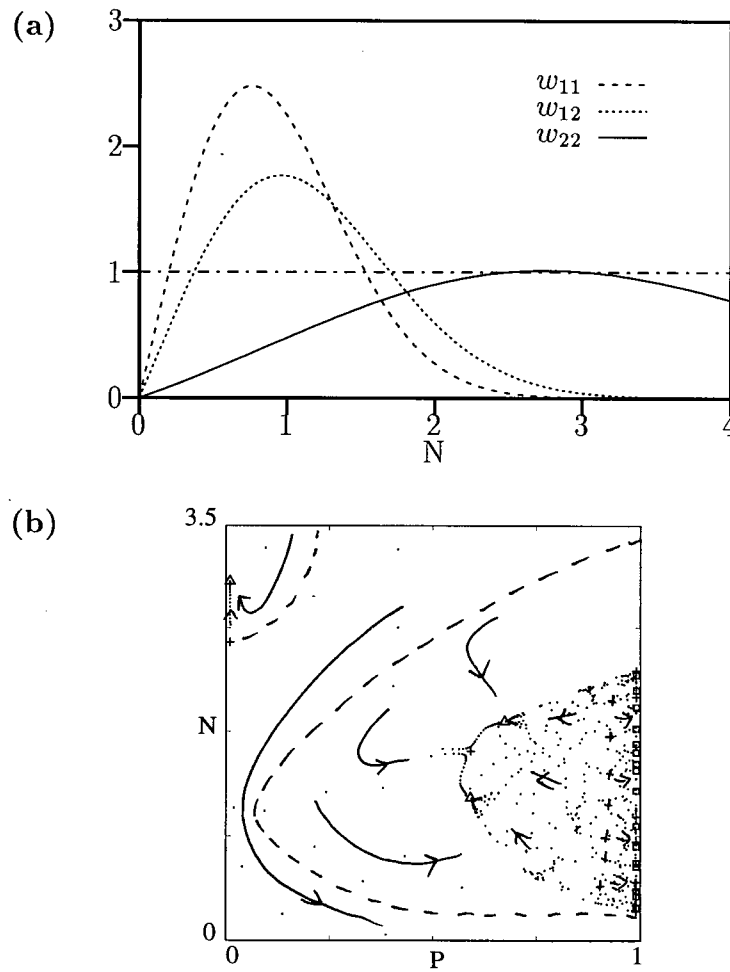


Figure 6.12: (a) Fitness functions and (b) (p, N) -plane for $r_{11} = 0.2$, $k_{11} = 5.0$, $r_{22} = 0.3$ and $k_{22} = 0.4$.

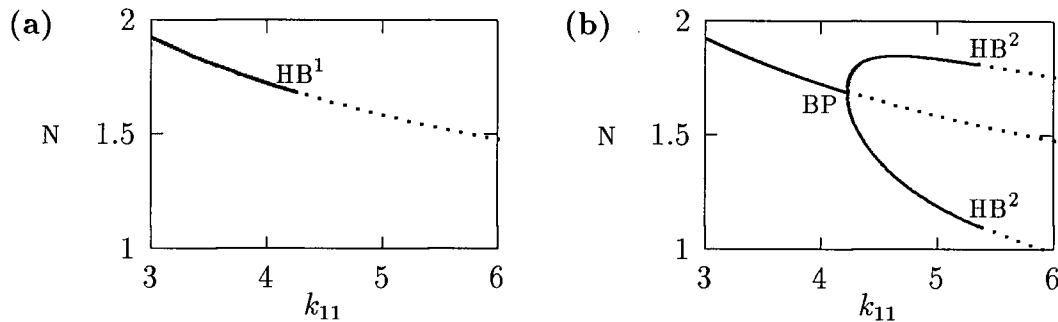


Figure 6.13: One-parameter diagrams obtained by varying k_{11} using (a) the original model and (b) the second iterate of the model. Only branches satisfying $0 < p < 1$ are shown.

these higher order stable polymorphisms occur. I decided to fix w_{22} (that is, fix r_{22} and k_{22}) and examine the (k_{11}, r_{11}) -parameter space as was done earlier. The first step is to use AUTO to create a one-parameter bifurcation diagram by varying k_{11} . DSTOOL was used to generate starting points for AUTO. Using the first iterate of the model equations resulted in figure 6.13(a). Only the period-doubling bifurcation indicating the change from a stable equilibrium to a stable period-2 orbit is shown. In order to plot the period-2 orbits the second iterate of the model needs to be used. This gives figure 6.13(b). Notice that the period-doubling at $k_{11} = 4.226$ is now labelled as a bifurcation point (transcritical) by AUTO instead of as a period-doubling bifurcation. This second bifurcation diagram shows a further period-doubling at $k_{11} = 5.358$ from period-2 to period-4 orbits but the stable period-4 orbits are not continued by AUTO. However, their existence can be verified using DSTOOL.

Using the first iterate of the model we can see how the position of the first period-doubling (at $k_{11} = 4.226$) changes as r_{11} is varied in addition to k_{11} . In order to obtain a rough idea of the extent of the region of interior higher order stable behaviour, we can vary r_{11} using the second iterate of the model and trace out the path of the second period-doubling (at $k_{11} = 5.358$ in figure 6.13(b)). Both curves are plotted on the same

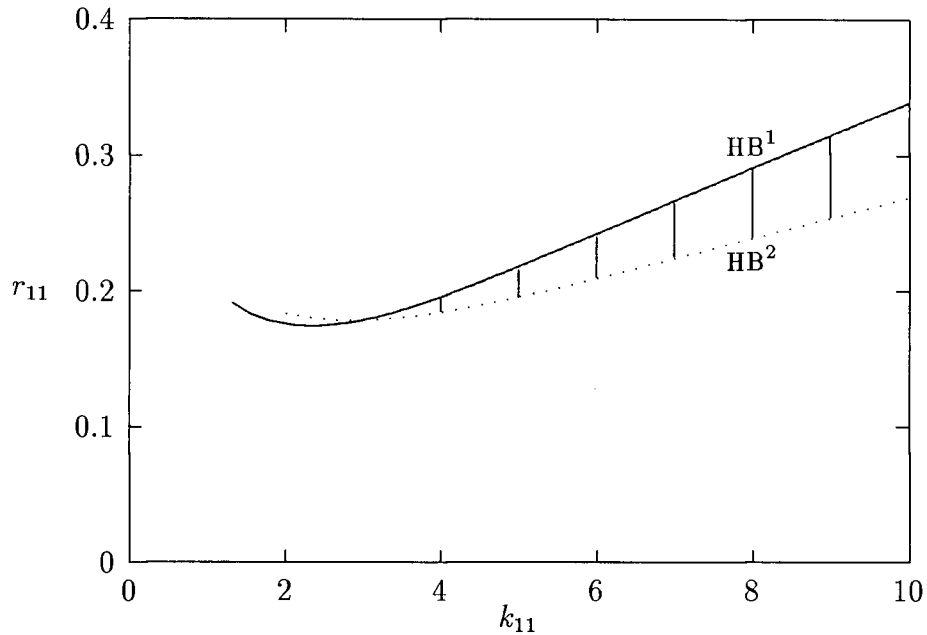


Figure 6.14: A bifurcation diagram showing the two-parameter continuation of the period-doubling at $k_{11} = 4.226$ and the subsequent period-doubling at $k_{11} = 5.358$ in figure 6.13. The shaded region approximates the region of stable polymorphisms of period greater than 1.

set of axes in figure 6.14. The shaded area in this figure approximates the region of parameter space corresponding to higher order stable interior behaviour. In general, the further the parameters are from the solid line (first period-doubling) within this shaded region, the more complex the dynamics. For example, for $r_{11} = 0.18$ and $k_{11} = 5.0$ there is an interior chaotic attractor as shown in figure 6.15.

In figure 6.12 the fitness functions corresponding to the two homozygotes are fairly different in terms of magnitude and the steepness of their slopes. This is true throughout the shaded region in figure 6.14 and can be deduced from the diagrams in the (p, N) -plane by noting the contrast between the complex dynamics near the $p = 1$ boundary and the much simpler behaviour near the $p = 0$ boundary. An important question is whether a fitness function configuration of the form shown in figure 6.16 could result in period-2 (or

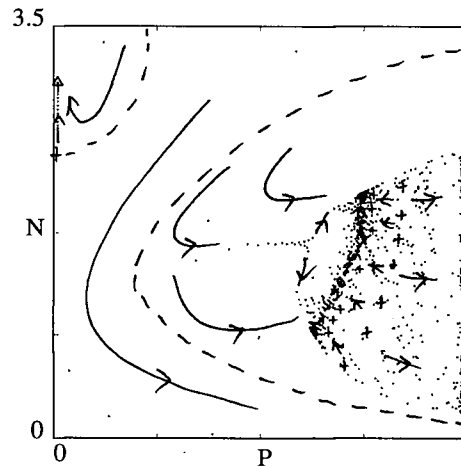


Figure 6.15: An example of an interior chaotic attractor obtained for $r_{11} = 0.18$, $k_{11} = 5.0$, $r_{22} = 0.3$ and $k_{22} = 0.4$.

higher period) stable polymorphisms. In such a situation both homozygotes have similar fitness properties but with one of the homozygotes slightly out-competing the other at each population density. The region in (k_{11}, r_{11}) -parameter space corresponding to such fitness configurations is plotted together with figure 6.14 to produce figure 6.17. Clearly, in this case the two regions do not overlap. Thus in this range it is not possible to have additivity (in the sense just described for the fitness functions) and stable polymorphic behaviour.

So far w_{22} has been fixed to have the shape shown in figure 6.12(a). The slopes of this function are fairly gentle. Suppose we replace w_{22} by the function shown in figure 6.18. We expect such an alteration to reduce the stability of the dynamics near the $p = 0$ boundary and hope that this might reduce the differences between the homozygote fitnesses that were previously required to obtain a stable period-2 polymorphism.

Figure 6.19 was obtained using the same procedure as for figure 6.17. Again the two regions do not overlap but their relative positions have now changed. An obvious question

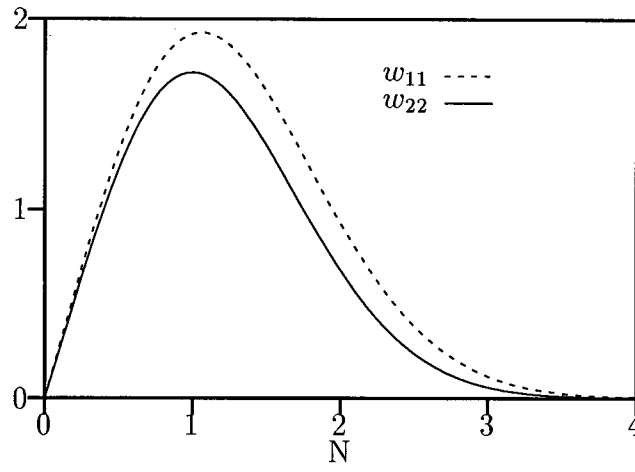


Figure 6.16: An example of a fitness function configuration where w_{11} is always superior to w_{22} .

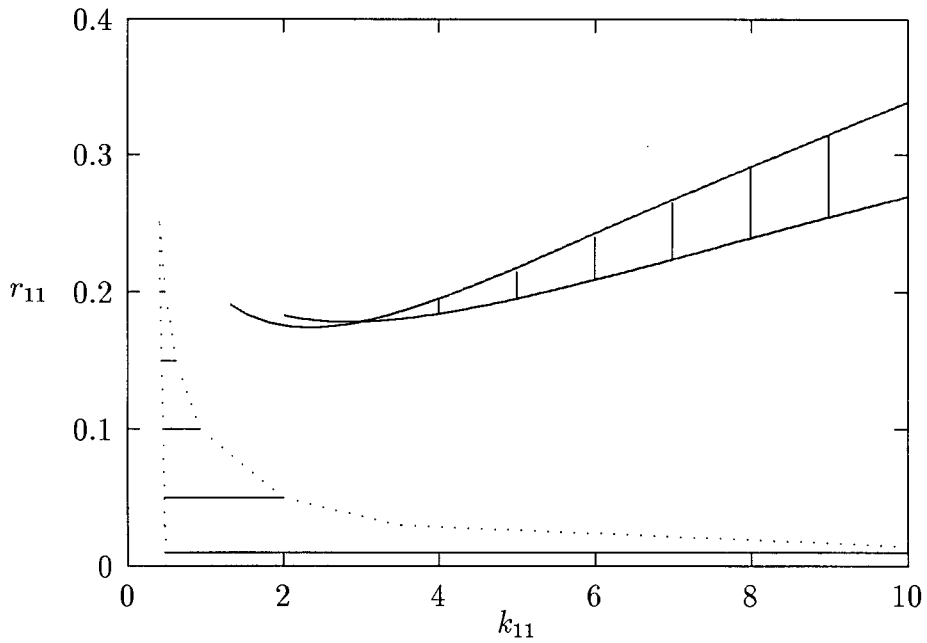


Figure 6.17: The (k_{11}, r_{11}) -parameter space showing the region of higher order stable polymorphic behaviour corresponding to figure 6.14 (vertical lines) and the region corresponding to fitness function configurations of the type shown in figure 6.16 (horizontal lines).

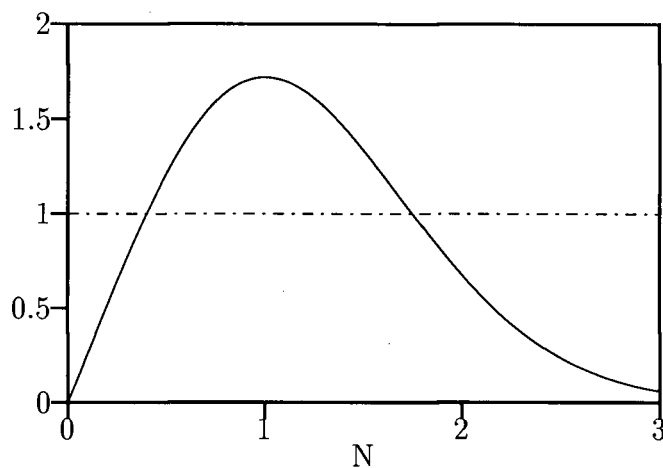


Figure 6.18: w_{22} with $r_{22} = 0.25$ and $k_{22} = 2.5$.

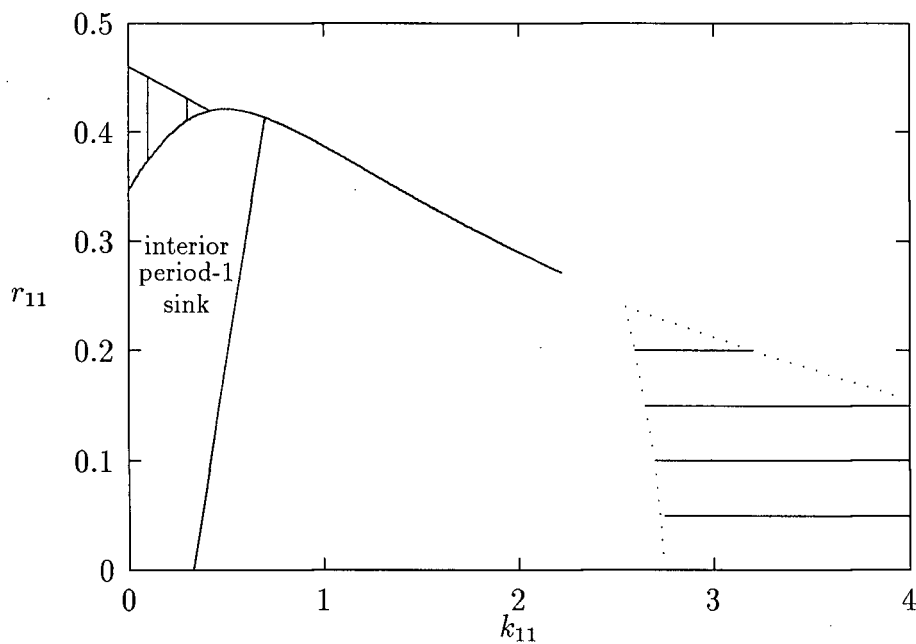


Figure 6.19: The new two-parameter space showing the region of higher order stable polymorphic behaviour (vertical lines) and the region corresponding to fitness function configurations of the type shown in figure 6.18 (horizontal lines).

would be to ask whether there are intermediate parameter values where the two regions do overlap. Numerous investigations using both DSTOOL and AUTO did not reveal any situations of this type. For the additive model with fitness functions given by (6.2) it appears that the fitness properties of the homozygotes need to be fairly different before higher order stable polymorphisms are found. This result is comparable with results in the previous chapter for period-4 orbits.

6.5 Conclusion

The population genetics model studied in this chapter is more complicated than that of the previous chapter due to the form of the fitness functions. As a result any mathematical analysis using pencil and paper is very difficult, if not impossible, since many of the fixed points do not have closed algebraic forms. However, AUTO and DSTOOL proved invaluable for investigating certain aspects of the behaviour of the model and led to some important conclusions.

In particular, it was found that for the additive model with one-humped fitness functions, period-1 stable polymorphisms (interior equilibria) are much more probable than period-2 (and higher period) stable polymorphisms. Homozygote fitnesses need to differ greatly in magnitude and slope properties for the latter to occur. A method for predicting the occurrence of interior equilibria from mean fitnesses was demonstrated and the relationships between interior and boundary stable equilibria were shown using two-parameter bifurcation diagrams and corresponding diagrams of the (p, N) -plane. The latter diagrams also highlight the high possibility of extinction for most parameter combinations. Other one-humped fitness functions may lead to different conclusions than those obtained in this study. The techniques outlined in this chapter could be used for such investigations.

Chapter 7

Spruce Budworm Model

7.1 Introduction

In this chapter I concentrate on a discrete model of a defoliating insect system. The insect is the spruce budworm and its preferred host trees are balsam fir and white spruce. The model that I have chosen to study was developed by Clark and Ludwig [22]. In it the budworm, the branch surface area of the trees and their foliage are all state variables.

In the next section I give some background to the budworm-forest system as well as to a few of the models which have been formulated to describe it. The model by Clark and Ludwig [22] is fairly complicated and includes a number of processes such as dispersal, predation, food limitation, and parasitism. Section 7.3 gives a description of the equations. Discrete models of this complexity have not been analysed in detail before.

Section 7.4 contains the model analysis. DSTOOL is the main package used. Because the system is discrete and because of its complexity, continuation packages such as AUTO are of limited value. This is discussed in more detail in section 7.4.1. For the analysis I chose to focus on one aspect of the model rather than attempt an exhaustive parameter study. The process I chose is dispersal as it is thought to have a significant effect on the budworm dynamics (Clark [19]). Two parameters that affect small larval dispersal and female adult dispersal, respectively, are allowed to vary. Regions of this two-dimensional parameter space which correspond to budworm extinction, multiple stable states and

periodic outbreak behaviour are identified. While Clark and Ludwig [22] found parameter values which give rise to some of this behaviour, a few additional possibilities are found in this study. An important result is that insect outbreaks are possible for a large number of realistic parameter combinations.

It would be interesting to know which of the many component processes in the model is responsible for the observed behaviour and which ones have a lesser effect. Knowing how each process affects the system behaviour can greatly help in understanding and managing the budworm-forest system. Using a variety of techniques I show that the main process responsible for outbreak cycles is small larval dispersal. This agrees with the findings of Clark [19]. After studying the effects of small larval dispersal on the behaviour of the model in more detail, I use bifurcation analyses once again to compare the effects of predation and small larval dispersal. The main influence of predation is at fairly low budworm densities which means that it affects the time period between outbreaks.

7.2 Background

The eastern spruce budworm, *Choristoneura fumiferana* Clem. (Lepidoptera: Tortricidae) is found throughout the Canadian Maritimes and northern New England as well as westward and northward through middle Canada up to the boreal forest (McNamee [89]). In some regions budworm densities remain low as a result of predators, inadequate resources and weather (Clark [19]). However, these controls break down periodically, particularly in the eastern regions, resulting in budworm outbreaks of epidemic proportions. Damage to the preferred host trees, balsam fir (*Abies balsamea*) and white spruce (*Picea glauca*), is extensive and can approach 100% in dense, mature stands [19]. These

outbreaks are documented as far back as the 1700's with some of the worst ones occurring in the Canadian province of New Brunswick. Intensive insecticide spraying began in this area in 1952 in an attempt to protect the foliage and, thus, limit tree mortality [19]. Contrary to expectations, this led to high endemic populations of budworm which began to kill significant portions of the forest (Baskerville [13]).

The budworm itself is a univoltine insect which means that there is one budworm generation per year. Its life cycle can be divided into egg, larval, pupal and adult stages. The large larvae have the most effect on the dynamics of the budworm-forest system (Jones [65]). This stage causes the most defoliation and large larval feeding levels influence both fecundity and adult dispersal. The large larvae are also subject to bird predation and parasitism and are the target for insecticide spraying. As mentioned earlier, dispersal also affects the dynamics. The small larvae spin silk threads and are transported aerially by wind. If the adults disperse, they may fly from 10 up to 100 kilometres [89].

The system has received a substantial amount of research attention, both empirical and theoretical, in the past few decades (for example, [19, 32, 42, 65, 74, 89, 91, 105, 106]). In the 1970's Jones [65] developed a process-oriented simulation model which takes into account the annual dynamics of the insect and the forest in which it resides. This model has been used as a research tool by forest managers and scientists in New Brunswick (Clark and Holling [21]). However, a full understanding of the behaviour exhibited by the model has been hindered by the large number of component processes involved and the complexity of the equations.

At the other end of the scale, Ludwig *et al.* [74] developed a simplified model consisting of a system of three ordinary differential equations which they studied qualitatively. Although they obtained some interesting results and demonstrated the potential of the model to exhibit outbreak behaviour, Clark and Ludwig [22] note that many processes are ignored or aggregated when simplifying the situation to such an extent.

Another approach is to combine the two approaches and apply qualitative methods to a fairly complicated model. With this aim in mind, Clark and Ludwig [22] developed a condensed version of Jones's model by aggregating new and old foliage into a single variable and ignoring age structure in trees. The result is a discrete system describing the annual dynamics of three basic state variables: budworm density, foliage density and branch surface area density. Their model is more manageable than the one in [65] but still includes important biological components. This model is described in the next section.

7.3 Model equations

7.3.1 Foliage

The foliage variable, F , is the density of green needles found in a unit of branch surface area. It is an average value representing conditions on the whole site and is measured in 'foliage units' where one foliage unit (fu) is the quantity of new foliage produced per unit of branch surface area in the absence of budworm-induced defoliation. In addition to being consumed by budworm larvae, the foliage provides oviposition sites for adult moths [19]. Although balsam fir retains its foliage for about eight years, it is sufficient to consider only two classes ('new' or present year foliage and 'old' foliage which includes all remaining foliage) since this is the only distinction made by the budworm. If budworm density is low, the ratio of new to old foliage is 1:2.8 [65]. For simplicity it is assumed that this ratio is fixed. Total foliage density can then be scaled to have a maximum of $K_F = 3.8$ fu.

If F_b is the initial foliage density then, following Jones, the effect of larval consumption on new foliage can be described by:

$$\text{Remaining new foliage} = e^{-A} \frac{F_b}{K_F} \quad (7.1)$$

where

$$A = d_0 L_b \frac{K_F}{F_b}.$$

Here L_b represents the initial budworm larval density and d_0 is the maximum foliage consumption rate for an individual larva during the feeding season. Equation (7.1) is a standard competition function (see appendix D for an explanation) and it is used to represent the competition between budworm that results from high population densities [65].

If the budworm's food requirements are not met by new foliage alone then old foliage is consumed. Analogues of the above equations are:

$$\text{Remaining old foliage} = e^{-B} \frac{K_F - 1}{K_F} F_b, \quad (7.2)$$

where

$$B = c_1(A - 1 + e^{-A}).$$

($c_1 = 0.357$ is a constant.)

The total amount of foliage, F_1 , remaining after consumption by budworm is obtained by combining equations (7.1) and (7.2) to give:

$$F_1 = \frac{1}{K_F} [e^{-A} + (K_F - 1)e^{-B}] F_b. \quad (7.3)$$

Density-dependent growth of foliage also needs to be taken into account. If we let r_F represent the average growth rate of foliage at low densities and remember that F_e (the foliage density after one year) cannot exceed K_F , then we obtain

$$F_e = \frac{r_F F_1}{1 + \frac{(r_F - 1)}{K_F} F_1}, \quad (7.4)$$

where the denominator introduces density-dependence. This completes the foliage dynamics.

7.3.2 Branch surface area

Another feature of trees that is important to budworm is the surface area of branches. This serves as the budworm habitat. In this model the branch surface area density, S , is an average value for the whole site and is measured in units of ten square feet (tsf) per acre. The original model of Jones used 75 age classes. Since outbreaks tend to synchronise tree development, there is some justification for the simplification to a single age class.

Severe defoliation by budworm may kill branches. This is modelled by setting

$$S_1 = [1 - d_S(1 - \frac{F_1}{F_b})^2]S_b, \quad (7.5)$$

where S_b is the initial branch surface area density and d_S is an average death rate. S_1 represents the living branch surface area which remains after defoliation. Because of the quadratic term $(1 - \frac{F_1}{F_b})^2$, the difference between S_b and S_1 is only significant if there is substantial defoliation, that is, if F_1 is very different from F_b .

Subsequent density-dependent growth of surface area is taken into account by setting

$$S_e = \frac{r_S S_1}{1 + \frac{(r_S - 1)}{K_S} S_1}, \quad (7.6)$$

where r_S is the average growth rate and K_S is the maximum branch surface area density.

7.3.3 Budworm

The preceding equations are only slightly more complicated than the ones in Ludwig *et al.* [74]. However, those for the budworm dynamics are much more complex. Most of the following equations are based on Jones's model [65]. Following his approach, an initial large larval density of L_b larvae per unit of branch surface area (per tsf) is assumed. Parasitism of these larvae is considered first.

Parasitoids are not treated as a dynamic variable in the model since under normal conditions the parasitoids' numerical response is too slow to raise parasitism rates significantly before the outbreak collapse has begun [19]. According to Jones, the rate of parasitism is a decreasing function of larval density, with a maximum of 40% at low budworm densities that decreases exponentially. The number (density) of larvae surviving parasitism is given by

$$L_1 = (1 - q_{\max}e^{-C})L_b, \quad (7.7)$$

where $C = 0.003L_b$ and $q_{\max} = 0.4$.

Large larval survival is also influenced by the amount of food consumed. Following Jones it is assumed that survival is proportional to the average amount of food consumed:

$$L_2 = k_L \left(\frac{F_b - F_1}{d_0 L_b} \right) L_1, \quad (7.8)$$

where $k_L = 0.425$ is a proportionality constant.

Predation by birds is limited to the large larvae. As in Ludwig *et al.* [74] this process is modelled by a Holling type III functional response. Thus,

$$L_3 = e^{-D} L_2, \quad (7.9)$$

where

$$D = \frac{p_{\max} L_2}{S_b (p_{\text{sat}} F_b^2 + L_2^2)},$$

and p_{\max} is the maximum predation rate and p_{sat} is a half-saturation rate. The expression for D requires some explanation. If it is assumed that the number of predators (birds) per acre is fixed, then the number per branch is proportional to p_{\max}/S_b . The predators search foliage and they switch to alternate prey if the ratio of larvae to foliage, L_2/F_b , is too small. If p_{\max}/S_b is small, then predator consumption is

$$\begin{aligned}
L_2 - L_3 &= (1 - e^{-D})L_2 \\
&\approx DL_2 \\
&= \frac{p_{\max}L_2^2}{S_b(p_{\text{sat}}F_b^2 + L_2^2)}
\end{aligned} \tag{7.10}$$

which indicates that p_{sat} is the half-saturation value of the ratio L_2^2/F_b^2 . Clark and Ludwig [22] chose the more complicated exponential form (7.9) over (7.10) in order to take into account competition among predators.

The survival of pupae is correlated with the survival of large larvae [65] and is given by

$$L_4 = (A_p + B_p \frac{L_3}{L_b})L_3 \tag{7.11}$$

where $A_p = 0.473$ and $B_p = 0.828$ are regression constants obtained by Jones [65]. This expression gives the density of adult moths.

According to Jones, female fecundity depends on their weight. He calculates this weight, W , as

$$W = A_{F1} \frac{(1 - e^{-A})}{A} + A_{F2}(K_F - 1) \frac{(1 - e^{-B})}{A} + B_F \tag{7.12}$$

where $A_{F1} = 34.1$, $A_{F2} = 24.9$ and $B_F = -3.4$. This formula expresses the differing nutritional values of new and old foliage. Fecundity is proportional to the cube root of W [65] which results in the following equation for egg density:

$$L_5 = (E_1 W^{1/3} - E_2)A_{sr}L_4 \tag{7.13}$$

where $E_1 = 165.64$ and $E_2 = 328.52$ are regression constants obtained by Jones [65] and A_{sr} is an adult sex ratio which gives the average proportion of females. There is an additional constraint that fecundity be at least 40 eggs per female. If nutrition were so poor as to produce fewer than this, the pupae would not have survived [65].

Dispersal is another process which is thought to have an important effect on local budworm dynamics. It is convenient to think of eggs dispersing rather than adults, as a female moth will deposit some of her eggs on the site under consideration and will remove some to other locations [65]. Following Clark [19], it is assumed that dispersal always leads to death. Thus, in this model, adult dispersal serves to increase egg mortality. Unlike normal mortality, however, this removal of eggs from the population depends on female adult density in the following way:

$$L_6 = \left(1 - \frac{A_{disp} E^m}{1 + E^m}\right) L_5 \quad (7.14)$$

where

$$E = \frac{A_{sr} L_4}{A_{thr}}$$

is the ratio of female adult density to a threshold density, A_{thr} . If the parameter m is large then E^m will be large if $E > 1$ and small if $E < 1$. This means that a fraction A_{disp} of adult females (and hence eggs) disperse if $E > 1$ and no dispersal occurs if $E < 1$. The steepness of the transition between no dispersal and dispersal is controlled by the size of m .

Foliage density and branch surface area are both important factors in determining the survival of small larvae. The reason is that small larvae disperse twice (using silken threads to give them buoyancy in the wind) and the success of their dispersal depends upon landing on suitable foliage. It is assumed that the scaled probability of successful dispersal is given by

$$G = H(2 - H) \quad (7.15)$$

where

$$H = \frac{F_1}{K_F} n.$$

The parameter n is analogous to m in equation (7.14). If n is small, H will only vary slightly as F_1 decreases below its maximum, K_F . But if n is large, changes in F_1 will

greatly affect H . Thus n determines the extent to which foliage density affects the success of small larval dispersal. A graph of G versus H is given in figure 7.1. Notice that G is

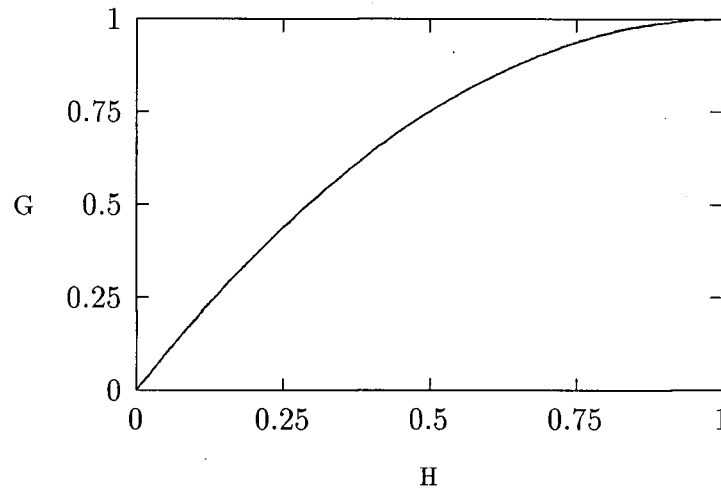


Figure 7.1: Graph of G versus H (equation (7.15)).

close to 1 unless H differs substantially from 1. The effect of both dispersals is included by taking the above factors into account twice. This gives

$$L_e = d_{SL} \frac{S_b}{K_S} G^2 L_6 \quad (7.16)$$

where d_{SL} is an average survival rate for small larvae and S_b/K_S expresses the dependence of dispersal success on branch surface area density. The lifecycle is now complete and L_e represents the new large larval density.

This completes the description of the three-dimensional model developed by Clark and Ludwig [22]. A summary of the equations can be found in appendix D. Table 7.1 gives the standard parameter values. As with all models there are a number of simplifying assumptions. It may already have been noted that adult dispersal is not accurately represented in the model since the model only deals with a single region and has no spatial component. Thus the validity and accuracy of the model predictions need

to be evaluated, but this is outside the scope of the present study.

Parameter	Description	Value
Foliage		
K_F	maximum foliage density	3.8
d_0	maximum foliage consumption rate/larva	0.0074
r_F	foliage growth rate	1.5
Branch surface area		
d_s	branch surface area death rate	0.75
r_s	branch surface area growth rate	1.15
K_s	maximum branch surface area density	24 000
Budworm		
q_{max}	maximum parasitism rate	0.4
p_{max}	maximum predation rate	23 000
p_{sat}	half-saturation value (predation)	0.085
A_{sr}	adult sex ratio (females/total)	0.46
A_{disp}	fraction of females dispersing	0.5
m	steepness of dispersal transition	4.0
A_{thr}	female threshold density (dispersal)	5.0
n	effect of foliage density on larval dispersal	1.0
d_{SL}	small larval survival rate	0.28

Table 7.1: Table of standard parameter values.

7.4 Model analysis

7.4.1 Preliminaries

Traditional methods of qualitative analysis, such as isocline analyses, are not possible in this case as the equations are complex and there are too many component processes. For models of this nature, numerical solution of the equations for a given set of parameter values has been the principal tool for investigating the dynamics. However, numerous solutions for various parameter combinations are required for a meaningful study. This is time-consuming and often misleading as the solutions depend on the initial conditions and on complex joint distributions of parameters [19]. Since many ecological models of

practical interest are similar in complexity to the one under discussion, it is desirable that methods be found for understanding the behaviour of these models. Without an understanding of the range of behaviour that a model can exhibit, it may be difficult to explain results obtained from computer simulations or time series analyses of the model [82].

Although AUTO can perform continuations of equilibrium points for simple systems of difference equations, the complexity of this system causes the numerical algorithms to encounter problems. First of all, for discrete systems AUTO can only detect a period-doubling from an equilibrium point to a 2 point (period-2) cycle (refer to section A.3.5) but this model exhibits 9 point through to 70 point (and multiples thereof) cycles. An analysis using AUTO would clearly be limited as none of these higher period cycles would be detected. Also, as certain parameters are varied the periods of the cycles change. In this model changes occur over small parameter ranges. Since each change in period corresponds to a bifurcation, the stepsize would have to be made very small if these were to be detected using a numerical continuation method. However, very small stepsizes lead to increased computer round-off error and decreased accuracy.

Despite these limitations of continuation software in the context of complex discrete models, it is still possible to obtain the desired qualitative information. However, bifurcation diagrams have to be obtained 'manually' rather than through automated continuation programs. This can be done using DSTOOL as will be described shortly. The types of numerical routines involved in using DSTOOL are generally more robust than those for AUTO when it comes to these complicated discrete models since they involve solving the system for a fixed set of parameter values. No further discretisation or approximation is required as in the case of differential equations.

As in the previous chapters the first step is to decide which parameters to investigate. Those whose values are uncertain or which are thought to have a significant influence on

the dynamics are obvious choices. I chose to study the effects of *dispersal* on the budworm dynamics. An important parameter affecting female adult dispersal is A_{thr} , the threshold value below which no dispersal occurs. The effects of small larval dispersal are controlled by n , which determines the extent to which foliage density affects the success of small larval dispersal, or d_{SL} , which is the average survival rate for small larvae (see equation (7.16)). If we set $n = 1$ then the effects of small larval dispersal can be determined by varying d_{SL} which is more biologically meaningful. (A large value for d_{SL} means that the average survival rate is high and also that foliage condition has a significant effect on survival after dispersal.)

In what follows I look first at d_{SL} and then at A_{thr} . This ordering is arbitrary. The aim is to analyse the effects of varying the values of these parameters and to divide the (d_{SL}, A_{thr}) -parameter space into regions of different qualitative behaviour. Following this I study the effects of different processes on model behaviour to determine which one(s) is(are) responsible for the outbreak cycles. Finally, I study the two processes predation and small larval dispersal in more detail.

Because there are three state variables in the model, a decision had to be made as to the two-dimensional space into which the dynamics should be projected. Since branch surface area varies at a much slower rate than the budworm and foliage dynamics, I decided to look at the budworm versus foliage plane. It should be noted that in all the DSTOOL calculations, branch surface area, S , is still allowed to vary—the results are just projected into the (Foliage, Budworm)-plane. This differs from Clark and Ludwig's study where S was constant in their analysis and means that the following analysis applies to the full three-dimensional model whereas that in [22] is restricted to a simpler two-dimensional system of equations.

7.4.2 The effects of small larval dispersal

My first objective was to determine the effects of varying the parameter d_{SL} on model behaviour. Since d_{SL} is a survival rate it must lie between 0 and 1. To begin I set $d_{SL} = 0.05$ in the SETTINGS-SELECTED window and fixed all the other parameters at their respective values given in table 7.1. Using DSTOOL I found and recorded the equilibrium points corresponding to this parameter set as well as their local stabilities. This is done using icons in the FIXED POINT window. I also used DSTOOL to calculate the corresponding dynamics in the (Foliage,Budworm)-plane. This is done using the mouse to click on different initial points, or entering initial points manually in the SETTINGS-SELECTED window and using FORWARDS and CONTINUE in the ORBITS window to calculate trajectories. The resulting diagrams show whether cyclical behaviour occurs and the amplitudes of the cycles as well as the approximate domains of attraction (see section A.2.5) in the two-dimensional plane.

After recording the results I increased d_{SL} to 0.10 and repeated the above procedure. I continued in this way (incrementing d_{SL} by 0.05 each time) until I reached $d_{SL} = 1.0$. In regions where qualitative changes occurred (such as an equilibrium point changing stability or a change from stable to unstable oscillatory behaviour) I decreased this increment to 0.01. Greater accuracy would have been easy to obtain but it is time-consuming and I did not think it necessary for a qualitative study.

The results of the above parameter study are summarised in the one-parameter bifurcation diagram in figure 7.2. (Similar diagrams for F and S can also be drawn.) This diagram was obtained by plotting the budworm densities of the equilibrium points for each value of d_{SL} and then connecting these points—solid lines for stable equilibria and dotted lines for unstable equilibria. Maxima and minima of the cycles that were found were then plotted—solid dots for stable cycles and open circles for unstable cycles.

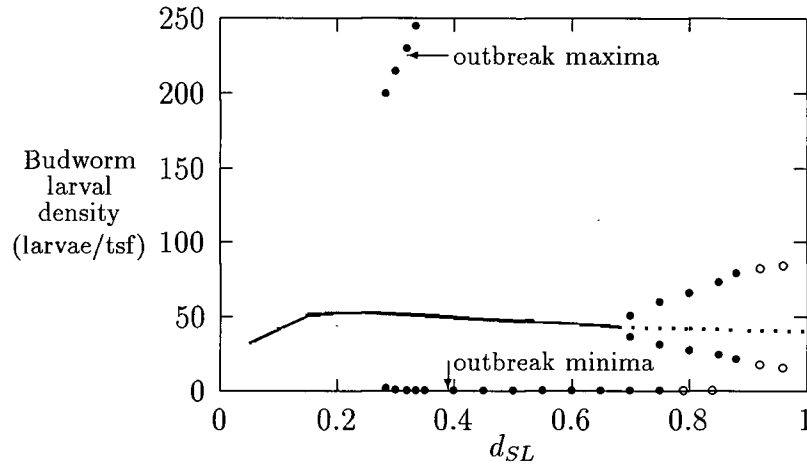


Figure 7.2: One-parameter bifurcation diagram of budworm larval density versus d_{SL} .

We can see from figure 7.2 that for low values of d_{SL} there is a single stable equilibrium value. A diagram of the (Foliage, Budworm)-plane for the particular value $d_{SL} = 0.2$ is shown in figure 7.3(a). All orbits spiral in to the equilibrium point (denoted by the triangle). As d_{SL} increases a bifurcation occurs, and for $d_{SL} \geq 0.28$ there is the possibility of outbreak cycles. Figure 7.3(b) shows the (Foliage, Budworm)-plane for $d_{SL} = 0.35$. In this case, depending on the initial values of the state variables, either stable equilibrium or outbreak behaviour can occur. This is further exemplified in figure 7.4 by the plots of the temporal variation of budworm, foliage and branch surface area for $d_{SL} = 0.35$. As can be seen from these plots, the maximum of the outbreak cycle varies but the period remains fixed at 15 years. (Strictly speaking the period may be some larger multiple of 15 but from a biological viewpoint, we are most interested in the fact that peaks (outbreaks) occur every 15 years, even if the cycle maximum varies slightly in consecutive outbreaks. Cycles of very long period or totally aperiodic motion will both appear to be almost periodic (or chaotic) in a practical biological setting [84].) Since both the equilibrium and the outbreak cycle are stable phenomena, there must be some kind of boundary

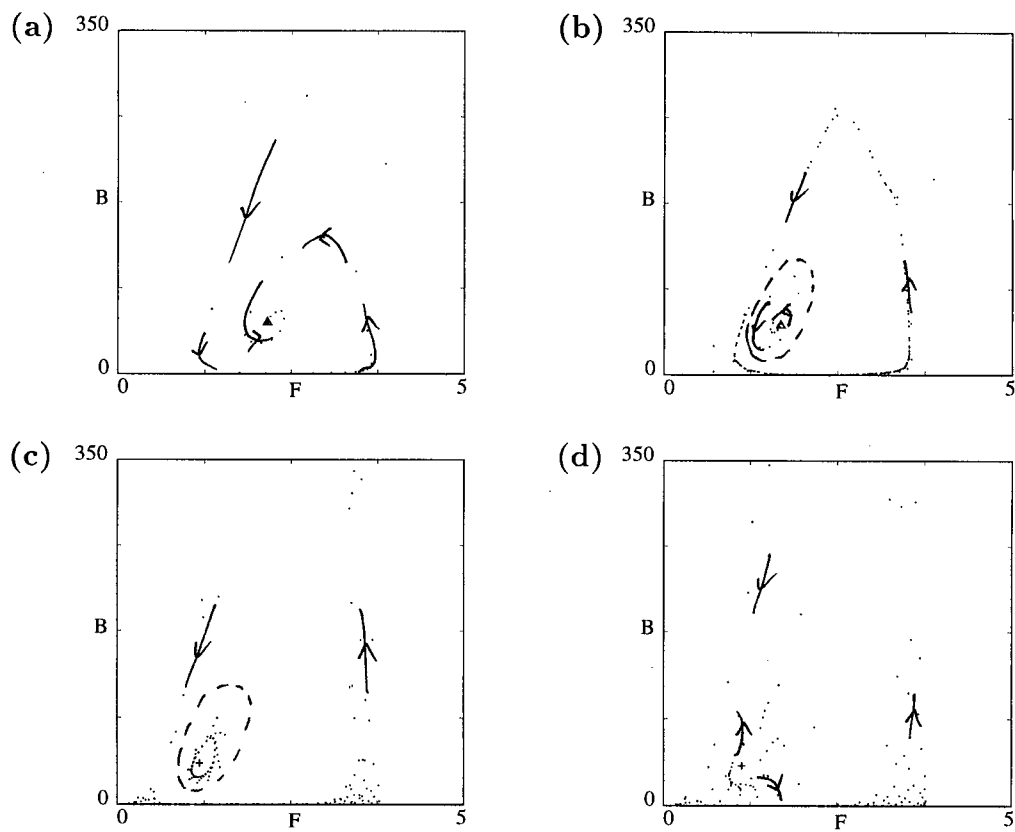


Figure 7.3: Diagrams of budworm larval density versus foliage for (a) $d_{SL} = 0.2$, (b) $d_{SL} = 0.35$, (c) $d_{SL} = 0.8$ and (d) $d_{SL} = 0.9$. The dots indicate densities in consecutive years.

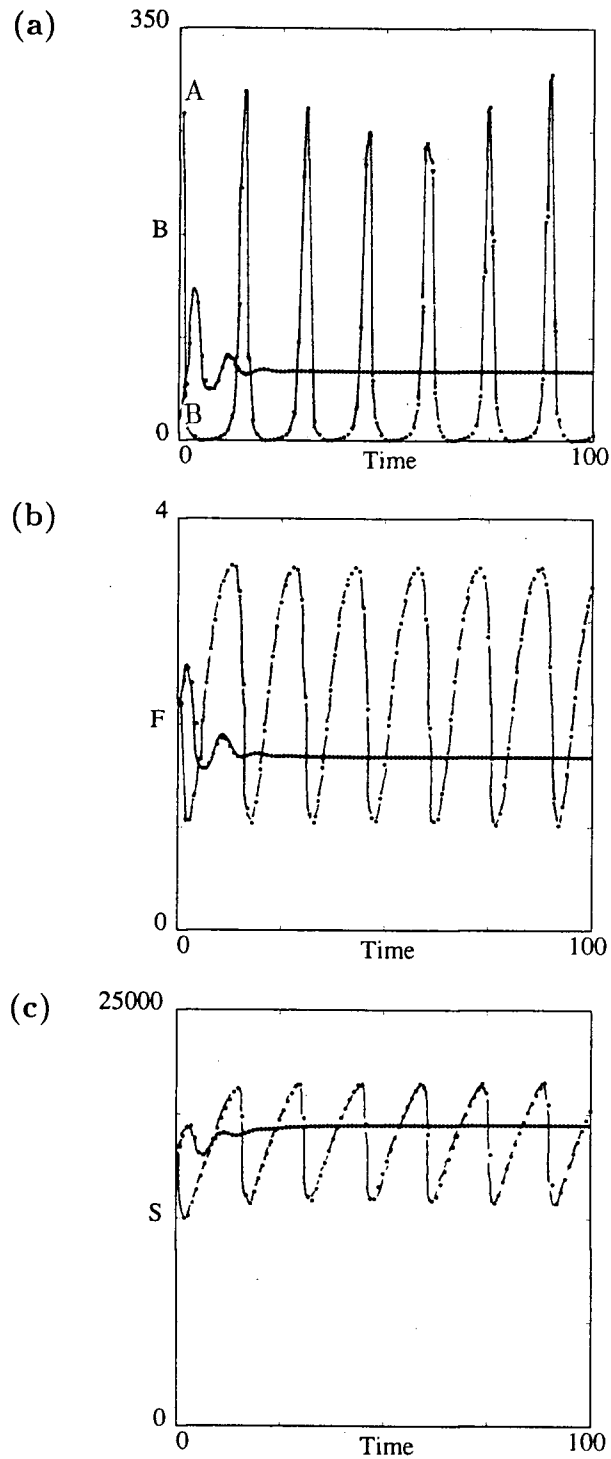


Figure 7.4: Time plots of (a) budworm larval density, (b) foliage density and (c) branch surface area density versus time for $d_{SL} = 0.35$. In each case two trajectories are shown for a time period of 100 years. As can be seen, initial values of the three state variables affect the resulting behaviour of the system. The two starting points, A and B, are the same in all three graphs.

delimiting their domains of attraction (see section A.2.5). This is not easy to locate in three dimensions and may not be a smooth surface. The dashed line in figure 7.3(b) gives a rough approximation to a two-dimensional projection of part of this boundary (the boundary also varies with S) and is only included to indicate that the domain of attraction for the outbreak cycle is much larger than that for the equilibrium point.

For $0.28 \leq d_{SL} \leq 0.68$ the behaviour remains the same qualitatively. Near $d_{SL} = 0.68$ the stable equilibrium undergoes a bifurcation resulting in an unstable equilibrium (denoted by a plus sign in figure 7.3(c)) surrounded by stable cycles of small amplitude. These cycles have periods of 7 or 8 years. Figure 7.3(c) gives the (Foliage, Budworm)-plane for $d_{SL} = 0.8$. Note that the outbreak cycle now has a much larger amplitude than in figure 7.3(b) and that the points corresponding to these outbreaks appear to fill a defined region rather than being confined to a curve as in figure 7.3(b). Time series corresponding to these outbreaks are similar to those in figure 7.4 but the amplitudes of the cycles vary more and there is more variation in the magnitudes of consecutive points in the cycles. However, the period is fixed for a given value of d_{SL} .

Returning to figure 7.2 again we can see that the two cycles become unstable as d_{SL} is increased further, as indicated by the open circles. The (Foliage, Budworm)-plane for $d_{SL} = 0.9$ is shown in figure 7.3(d). For any initial values the system still oscillates but the amplitudes of these oscillations get larger and larger until the budworm finally becomes extinct.

Having classified the dynamical behaviour of the system for different values of d_{SL} , I will now vary A_{thr} , the threshold value for female adult dispersal.

7.4.3 The effects of adult dispersal

To begin I chose three values of d_{SL} (0.2, 0.45 and 0.7) which correspond to regions of different qualitative behaviour in figure 7.2. For each of these values of d_{SL} I varied A_{thr}

in the same manner as described in the previous section in order to obtain one-parameter bifurcation diagrams. In this case A_{thr} is not restricted to lie between 0 and 1 since A_{thr} is the threshold density of female moths above which dispersal occurs. Female adult outbreak densities are around 30 females/tsf [19]. However, dispersal is not limited to outbreaks so we would like to investigate values of A_{thr} between 0 and, say, 20. I used an increment of 0.5 for this study, decreasing this to 0.1 in regions of qualitative change. The resulting bifurcation diagram for $d_{SL} = 0.45$ is shown in figure 7.5. In this case

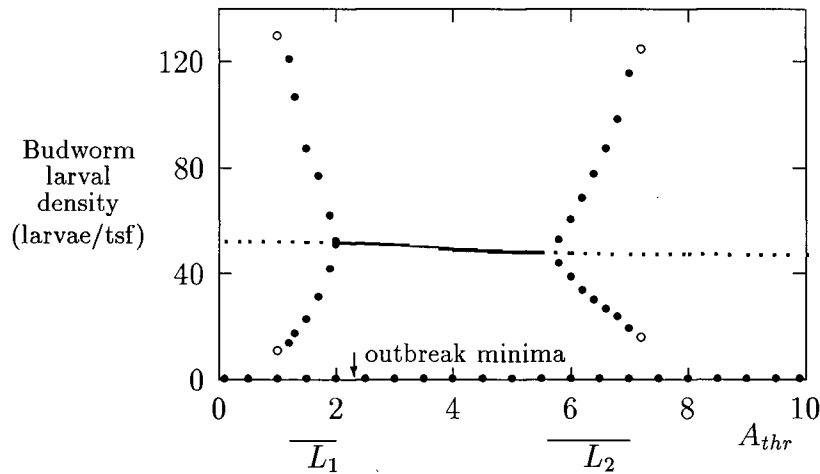


Figure 7.5: One-parameter bifurcation diagram of budworm larval density versus A_{thr} for $d_{SL} = 0.45$.

there are two Hopf bifurcations resulting in two regions, L_1 and L_2 , where periodic orbits of small amplitude (when compared with the outbreak cycles) occur. These orbits have periods of 9 or 10 years. For this value of d_{SL} , outbreak cycles are possible for all A_{thr} values. For clarity of the smaller amplitude orbits, only the minima of the outbreaks are shown in figure 7.5 (these are just above zero). The maxima vary between 355 larvae/tsf at $A_{thr} = 0.01$ and 480 larvae/tsf at $A_{thr} = 14$. For larger A_{thr} values the behaviour corresponds to that at $A_{thr} = 14$ but with greater outbreak amplitudes. The diagrams for the other values of d_{SL} are qualitatively similar—only the values of A_{thr} at which the

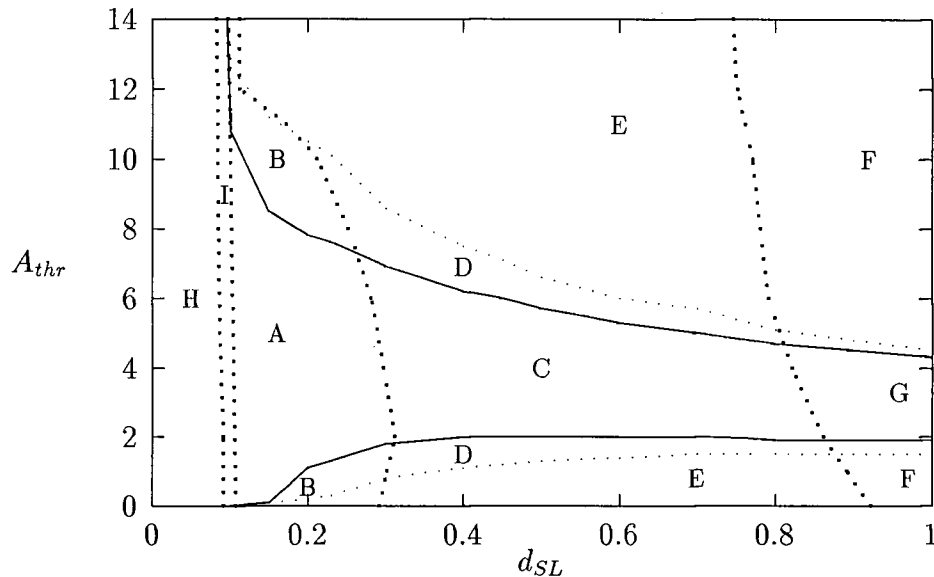


Figure 7.6: Two-parameter bifurcation diagram of A_{thr} versus d_{SL} .

bifurcations occur and the amplitudes of the cycles are different. For $d_{SL} = 0.2$ outbreaks only occur for $A_{thr} > 10.5$.

Having obtained an idea of the qualitative behaviour which corresponds to varying A_{thr} , we can begin constructing a two-parameter bifurcation diagram in the (d_{SL}, A_{thr}) -parameter space. The features we can expect to locate as a result of the above studies are two curves denoting where the Hopf bifurcations occur and a curve dividing the parameter space into regions where outbreak behaviour is or is not possible. Other curves of interest include those indicating the extent of *stable* cycling behaviour.

The values of A_{thr} at which each of the above phenomena occur can be found through incrementing d_{SL} by 0.1 (or 0.05 in regions where significant changes occur). This results in the two-parameter bifurcation diagram shown in figure 7.6. The solid lines indicate where Hopf bifurcations occur and the small dotted lines indicate the outer limits for

stable cycling behaviour corresponding to these bifurcations. The thick dotted line separating regions A and B from C and D indicates the boundary for outbreak cycles, that is, to the left of this curve no periodic outbreak behaviour occurs. The other thick dotted lines indicate the boundaries of the regions F, G and H where budworm extinction occurs and region I where two equilibrium states are possible.

This single diagram summarises nine qualitatively different types of behaviour that can be obtained by varying d_{SL} and A_{thr} . The nine regions are marked A–I. Diagrams of the (Foliage, Budworm)-plane corresponding to each region are shown in figure 7.7. Strictly speaking dots should be used for the trajectories instead of continuous lines since the model is discrete. However, it is easier to denote the direction of flow and the qualitative behaviour when lines are used.

In region A there is one spiral sink (indicated by the triangle) corresponding to positive budworm densities, and an unstable saddle point (indicated by a plus sign) at $(F, S, L) = (K_F, K_S, 0)$ (L represents budworm larval density). All trajectories with positive initial values spiral in towards the sink (see section A.2.21). In region B this sink has become an unstable saddle (see section A.2.20). (In (Foliage, Budworm)-space the behaviour near this saddle resembles that near an unstable spiral (see section A.2.23).) Trajectories starting near this point spiral out towards a stable periodic orbit. Trajectories from other initial points still spiral inwards but in this case they approach the periodic orbit instead of the equilibrium point.

Region C is similar to region A in that the equilibrium points are again a spiral sink and a saddle. However, in this region outbreaks are also possible. Since both the sink and the outbreak cycle are attracting, there must be a basin boundary dividing their domains of attraction. A rough approximation to part of this boundary is denoted by the dashed line. Again, the position of the boundary will vary with S . It appears that in most cases the domain of attraction for the outbreak cycle is much larger than that for

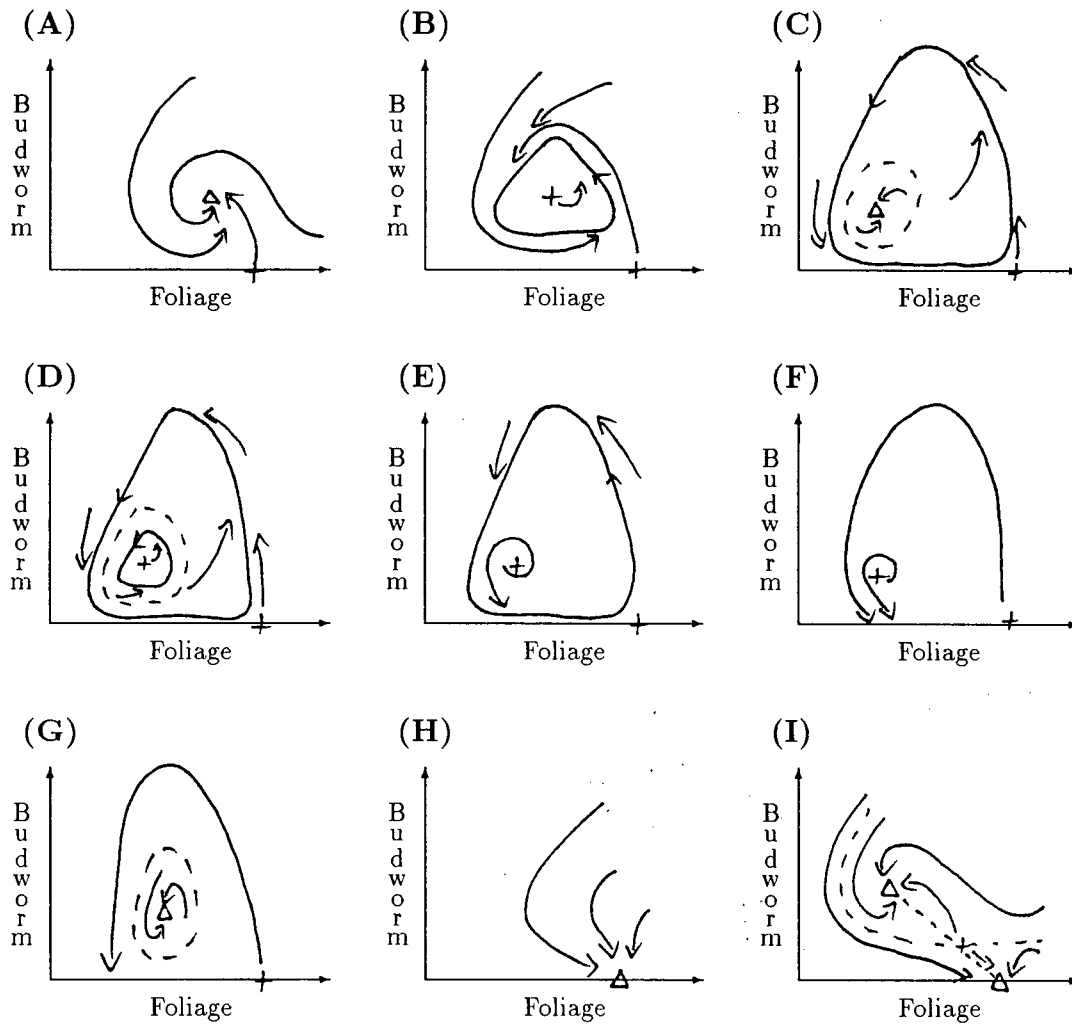


Figure 7.7: Diagrams of budworm larval density versus foliage for the regions marked A–I in figure 7.6. Triangles denote sinks (usually spiral sinks in this model) and plus signs denote unstable saddles (equilibrium points having at least one stable and one unstable eigenvalue—the third eigenvalue may be either stable or unstable).

the sink.

Region D is similar to region C for most of the state space. The only difference is that the spiral sink has been replaced by a stable periodic orbit. As A_{thr} is varied (and we move from region D to E), the periodic orbit becomes unstable and we are left with all the trajectories approaching the outbreak cycle. As we move into region F even the outbreak cycle becomes unstable. The system may oscillate a few times exhibiting cycles of very large amplitude (in terms of budworm density) but then the budworm population crashes and becomes extinct. Region G also has unstable outbreaks but there is a small region where trajectories spiral in towards a stable equilibrium.

The remaining two regions are H and I. These correspond to low d_{SL} values. In region H the point $(F, S, L) = (K_F, K_S, 0)$ is a spiral sink. All trajectories approach this point and thus the budworm becomes extinct without any outbreak occurring since small larval survival is too low for the budworm population to survive even in the most favourable conditions. In region I there are two spiral sinks—one corresponding to no budworm and the other to a positive budworm density. The initial values of F , S and L (budworm larval density) determine which sink is approached.

7.4.4 Biological interpretation

The first point to note is that, from an experimental viewpoint, it may be difficult to distinguish between the equilibrium behaviour associated with regions A and C and the cycling behaviour of regions B and D, respectively, due to random variation and measurement errors. This is true even in the simplest cases. Near a spiral sink the values of the state variables oscillate with the amplitude of oscillation getting smaller as the sink is approached. When a periodic orbit is present the behaviour is similar but the oscillations approach the stable cycle. Because of statistical variation in nature and measurement errors, it is almost impossible to determine whether the system is

approaching a sink or a periodic orbit of small amplitude. Therefore the locations of the solid lines (representing Hopf bifurcations) are not as important as the positions of the small dotted lines. Beyond the latter (in regions E,F and G) no 'desirable' stable behaviour is possible—only periodic outbreaks are found in these regions. In regions F and G, the amplitudes of these outbreaks are so large that the budworm population crashes to zero after a few cycles and becomes extinct.

The actual position of the boundary line of these latter two regions is fairly arbitrary as even before the thick dotted curve is reached the outbreak cycle leads to very small budworm densities for certain parts of the cycle. Such small densities may be equivalent to extinction due to statistical variation. Essentially we have to decide how low budworm densities can drop before extinction occurs.

The other region of extinction is region H. This region corresponds to very low (average and dispersal) survival rates for small larvae. In this region survival is too low to allow the budworm population to be self-sustaining, even if conditions are favourable. In contrast regions F and G correspond to high survival rates. These have the effect of destabilising the system and causing wild oscillations. This destabilisation as a survival rate is increased is a phenomenon characteristic of many ecological models [84].

Region I corresponds to two stable equilibria—one at very low budworm densities and the other at higher population densities. Although the possibility of multiple stable states is of interest to ecologists, this region exists for such a small range of d_{SL} values that it is probably not of practical importance as a small perturbation would move the system into regions A or H. However, C and D are regions of multiple stable states with significant area. From the above discussion figure 7.6 can be simplified to include only the most important phenomena. A simplified diagram is given in figure 7.8.

The above results show that outbreak behaviour is possible for a large number of parameter combinations. In the region of two stable states an alternative, more desirable

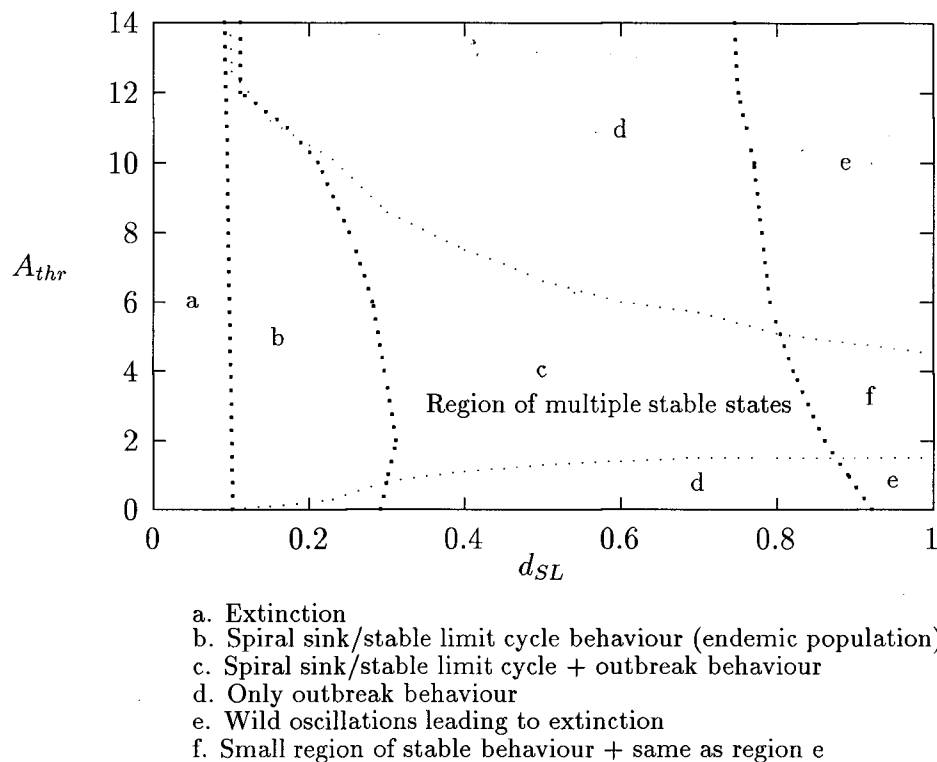


Figure 7.8: Simplified two-parameter bifurcation diagram of A_{thr} versus d_{SL} .

stable state is possible but for the rest of the outbreak region no alternative is possible.

Although figures 7.6 and 7.8 provide a concise summary of results, the one-parameter diagrams (figures 7.2 and 7.5) are also useful. They show the budworm densities corresponding to the equilibria and cycling behaviour as well as the amplitudes of the cycles. The corresponding one-parameter bifurcation diagrams for foliage and branch surface area density show that the equilibrium values for these quantities decrease as d_{SL} and/or A_{thr} are increased. Thus they show the severity of the defoliation corresponding to different dispersal rates.

Although the state space diagrams in the preceding analysis were only for the (Foliage, Budworm)-plane, they could also have been projected into the (Surface Area, Budworm)-

or (Foliage, Surface Area)-plane, since the branch surface area, S , varies in all the situations studied. The dynamics are similar in all the planes—just the shapes of the cycles and the positions of the equilibrium points are different.

7.4.5 What causes outbreak cycles?

Approach

In the preceding sections parameter values corresponding to low (0–2 larvae/tsf) and medium (30–50 larvae/tsf) equilibrium budworm densities as well as values giving rise to outbreaks were obtained. All three types of behaviour (namely, very low budworm densities, endemic equilibria and outbreaks) have been observed in the field [90]. However, the model under discussion is a complex one with many component processes. We would like to know just which processes are responsible for the observed behaviour and which ones are of lesser importance. In particular we would like to know which processes cause the outbreak cycles. One way to investigate the effects of the different processes in the current model is to start with a basic model and add individual processes one at a time (such as parasitism or the effect of larval weight on fecundity) to see what effect this has on model behaviour.

Clark and Ludwig [22] included a number of switches in their model so that the different processes can be turned on and off. In order to remove parasitism, equation (7.7) can be replaced by

$$L_1 = L_b. \quad (7.17)$$

The effect of food on large larval survival (equation (7.8)) can be replaced by a constant survival rate, namely

$$L_2 = k_L L_1. \quad (7.18)$$

As for parasitism, predation (equation (7.9)) can be removed by setting

$$L_3 = L_2. \quad (7.19)$$

Instead of correlating pupal survival with that of large larvae, equation (7.11) can be replaced by

$$L_4 = B_p L_3. \quad (7.20)$$

The effect of pupal weight (and hence feeding history) on female fecundity (equation (7.13)) can be removed by using a constant average fecundity. This gives

$$L_5 = B_{fe} L_4 \quad (7.21)$$

where $B_{fe} = 96$ was the chosen average fecundity per female moth [22]. Female adult dispersal is removed by setting $A_{disp} = 0$ in equation (7.14) and small larval dispersal can be precluded by replacing equation (7.16) with

$$L_e = d_{SL} L_6. \quad (7.22)$$

In order to obtain an idea of the effects of these processes on model behaviour, I turned off all the switches initially and then added each process to the model in turn. For each process I varied its associated parameters to see what range of behaviour could be obtained, and more specifically, whether outbreak cycles could occur.

Results

With all the switches off, the budworm density increases exponentially causing foliage density (and hence branch surface area) to decline to zero. The only process that affects this behaviour significantly when added to the model is small larval dispersal. In fact, the inclusion of this process leads to outbreak cycles for certain values of d_{SL} . (In section 7.4.1 it was explained how varying the small larval survival rate, d_{SL} , effectively varies

the success of small larval dispersal. Higher small larval survival rates also mean that the larvae have a greater chance of dispersing successfully, that is, of surviving dispersal, because of the formulation of equation (7.16). Thus, the two processes are referred to interchangeably.) Even with very high predation rates, predation alone cannot produce cyclical behaviour.

The other processes in the model, namely parasitism, predation, large larval and pupal survival, fecundity and adult dispersal, do not alter the qualitative behaviour significantly when operating alone but do affect the rates at which the budworm population grows and at which foliage and branch surface area vary. In other words, their effects are quantitative rather than qualitative. To demonstrate this more conclusively, I obtained a diagram similar to figure 7.6 using a simplified model containing only a few processes. Small larval dispersal was included in this simplified model as the dynamics depend on it. In order to obtain a diagram similar to figure 7.6, adult dispersal also needs to be included so that A_{thr} can be varied. The switches for all the other processes mentioned above were turned off, that is, equations (7.17)...(7.21) replaced the corresponding equations in the original model. (For brevity this simplified model will be referred to as the dispersal model.) The two-parameter bifurcation diagram in (d_{SL}, A_{thr}) -parameter space shown in figure 7.9 was generated in the same way that figure 7.6 was obtained.

Discussion

If we compare figures 7.6 and 7.9 we can see that all the main phenomena are still present, which supports the claim that dispersal is responsible for the qualitative behaviour of the model. The only feature that is missing from figure 7.9 is the region where the outbreaks lead to extinction (regions F and G in figure 7.6). However, by generating diagrams of the (Foliage, Budworm)-plane or time plots for the simplified model (as is done in the process of obtaining figure 7.9), it is easily seen that the outbreaks for this model have

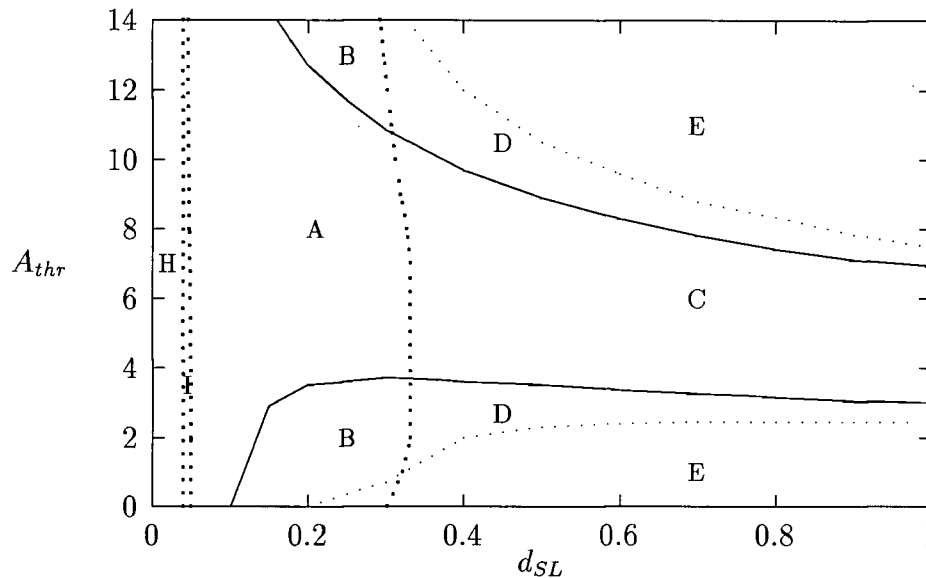


Figure 7.9: Two-parameter bifurcation diagram of A_{thr} versus d_{SL} for the simplified model which only includes dispersal. Regions are marked according to figure 7.6.

very large amplitudes. Even when $d_{SL} = 0.4$ budworm densities vary between 10^{-9} and 820 larvae/tsf within an outbreak cycle. This outbreak amplitude increases as d_{SL} increases with maxima around 2200 larvae/tsf and extremely small minima around 10^{-50} larvae/tsf for $d_{SL} = 0.9$. These values are clearly unrealistic and equivalent to extinction from a biological viewpoint.

If we compare the above observations with the results from the original model, then we can make another important deduction. The processes which have been left out of this simpler dispersal model are important for biological realism. As stated above, their effects are quantitative rather than qualitative. They have a moderating effect on the system dynamics and prevent densities becoming too high or too low for reasonable parameter values. Each process may have a relatively small influence but together they exert considerable control over the system.

The observation that small larval dispersal is responsible for the outbreaks contrasts with McNamee's [89] explanation that cycling is the result of movement between budworm equilibria at low and high budworm densities. However, the result agrees with the findings of Clark [20] who did a detailed study of the effects of dispersal on budworm dynamics. Royama's results [105] also indicate that larval survival, which is linked to dispersal, is the determining factor in the occurrence of outbreaks. In their study of the larch budmoth, Baltensweiler and Fischlin [12] suggest that the cycles in their system appear to stem from regional migration rather than long range migration of adults.

Why does small larval dispersal regulate the outbreak cycles? Clark [20] suggests the following argument. The survival of dispersing larvae depends on the quality and quantity of the foliage on which they land (see equations (7.15) and (7.16)). If foliage density is high then more larvae survive. For an outbreak to occur the forest must be in good condition with high branch surface area and foliage densities. The budworm population then grows rapidly and escapes from the control of parasitoids and predators [90, 119]. However, high budworm densities lead to forest defoliation which induces rapid branch mortality. This lowers the success of small larval dispersers [20] resulting in an epidemic collapse. Fischlin and Baltensweiler [37] come to similar conclusions in their study of the larch/larch budmoth system. They also note that their model is sensitive to the recovery rate of the trees after defoliation but that not much field data is available on this.

McNamee *et al.* [90] recognise the importance of forest biomass on outbreak behaviour but maintain that the outbreaks are movements between high and low equilibrium budworm densities. Their analysis is based on isorecruitment curves in which certain variables are held fixed. However, the analysis of this chapter leads to different conclusions. The state space and bifurcation analyses show that the equilibria and the outbreak cycles are different phenomena and that small larval dispersal is responsible for the cycles. All

the processes were allowed to vary simultaneously in this analysis and the results agree with Clark's extensive analysis of dispersal [20]. Clark notes that the epidemic-collapse behaviour is the hardest to explain because of the strong dynamic feedbacks between the forest and budworm. He also states that direct application of equilibrium manifolds, the method used by McNamee *et al.* [90], is not particularly informative (cf. chapter 4).

7.4.6 The effects of the other processes

I stated above that the effects of the processes other than small larval dispersal are quantitative rather than qualitative. However, a better understanding of these effects would be helpful. It would be informative to know the relative effects of each process on the dynamics of the system and the budworm densities over which their effects are greatest.

Method

A technique suggested by Clark and Ludwig [22] involves beginning with all the processes turned off (as described earlier) and then turning them on one at a time and determining budworm recruitment values over one year for a wide range of initial budworm larval densities. The density range over which each process has the greatest influence can then be determined. This can be done a number of times with the processes being turned on in different orders so that the results can be checked. An example is shown in figure 7.10.

Discussion

From figure 7.10 we can draw a number of conclusions. First of all, the effect of food on large larval survival is only noticeable at high (65 larvae/tsf) budworm densities and even

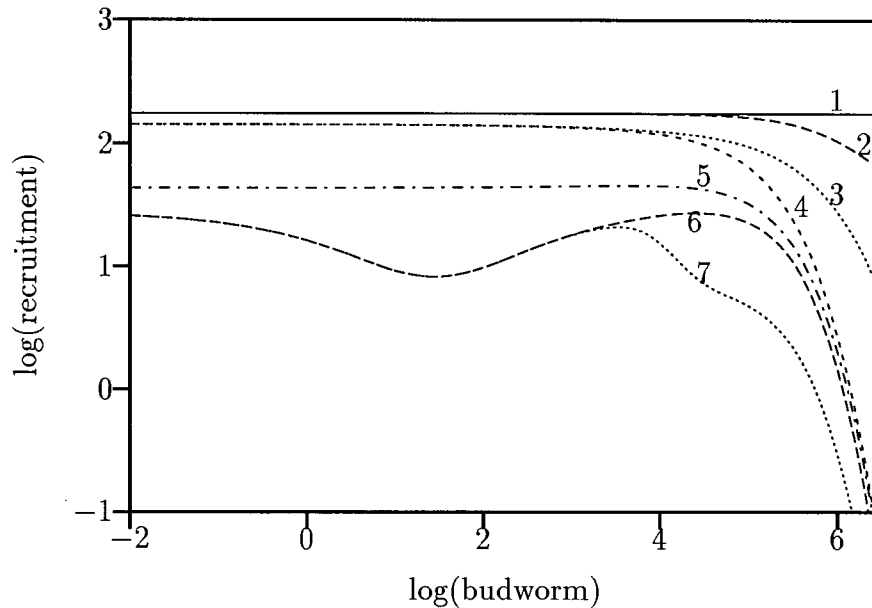


Figure 7.10: Isoclines of recruitment versus budworm density when 1) all processes are switched off, 2) the dependence of large larval survival on food is added, 3) the effect of feeding history on fecundity is also added, 4) small larval dispersal is added, 5) parasitism is added, 6) predation is added, and 7) adult dispersal is added giving rise to the full model.

then the effect is not very pronounced. Feeding history has a small effect on fecundity at all budworm densities and has the most effect at high densities. Parasitism substantially reduces recruitment for densities below about 45 larvae/tsf ($\log(\text{budworm}) < 3.8$) but has less influence at higher densities (the parasitism curve approaches the preceding curve as budworm density increases). The effect of predation is clearly noticeable for fairly low budworm densities between 0.4 and 20 larvae/tsf ($-1 < \log(\text{budworm}) < 3$). However, control by predation declines as budworm densities increase. Adult dispersal exerts most control for budworm densities between 20 and 90 larvae/tsf ($3 < \log(\text{budworm}) < 4.5$) while the influence of small larval dispersal is clearly noticeable for densities greater than 90 larvae/tsf ($\log(\text{budworm}) > 4.5$). These results reiterate that small larval dispersal

is the most important process at high larval densities and hence is the process which is most responsible for outbreak collapses.

In summary, the processes having the greatest effects on budworm dynamics at high larval densities are small larval dispersal and adult dispersal. At low to medium densities we have predation and parasitism. The latter two processes are responsible for controlling budworm densities between outbreaks. It is only when the budworm escapes their control that outbreaks occur. The extent of their influence will therefore affect the length of time between outbreaks.

7.4.7 The effects of predation

Comparing predation and dispersal

In order to further substantiate some of the above claims, a bifurcation analysis can be employed once again. The effect of predation is very pronounced at lower budworm densities (as can be seen from figure 7.10). I thus decided to add predation to the simpler model used earlier, which only included small larval and adult dispersal, to see what effect this would have. This new model will be referred to as the predation model for simplicity (although it also includes dispersal).

The two parameters affecting predation are p_{max} , the maximum predation rate, and p_{sat} , a half-saturation value. Increasing p_{max} or decreasing p_{sat} both lead to increased predation (see equation (7.9)). With these two parameters at their nominal values given in table 7.1, the new two-parameter bifurcation diagram is shown in figure 7.11. Some observations can be made by comparing this diagram with figures 7.6 and 7.9.

First of all, predation does not affect the position of the lower Hopf bifurcation curve (see figures 7.9 and 7.11). However, the upper Hopf bifurcation curve is lowered by predation. Thus predation decreases the size of the region (A,B,C,D and G) where a

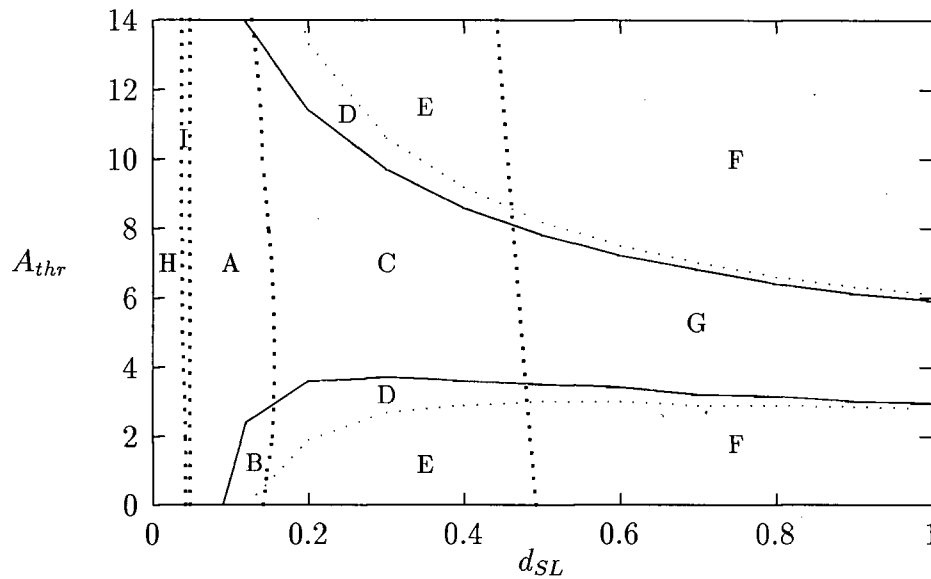


Figure 7.11: Two-parameter bifurcation diagram of A_{thr} versus d_{SL} for the predation model which includes dispersal as well as predation. Regions are marked according to figure 7.6.

stable endemic state is possible.

The other noticeable effect of predation is on the parameter values for which outbreak behaviour occurs. Outbreaks occur for lower d_{SL} values in figure 7.11 than in figure 7.9. Thus predation seems to have a destabilising effect from this point of view. The maxima of the outbreaks are similar to those for the dispersal model at each value of d_{SL} but the budworm population crashes to zero for values of d_{SL} greater than about 0.48 instead of continuing to oscillate (with ever-increasing amplitude as d_{SL} increases) as occurred in the dispersal model. This is due to the appearance of a sink corresponding to zero budworm density in the predation model. However, this technicality is not of biological consequence since the outbreaks in the dispersal model attained such large amplitudes that they became unrealistic and equivalent to extinction.

From figures 7.9 and 7.11 it appears that the main effect of predation is to destabilise

the system as outbreaks occur for lower d_{SL} values and the region of multiple stable states is smaller (due to the shift in the upper Hopf bifurcation curve). However, the qualitative dynamics have not been significantly altered.

Comparing figures 7.6 and 7.11 we can deduce the effects of adding the remaining processes (other than dispersal and predation) which are included in the full model. In figure 7.6, the region of endemic stable states (A,B,C,D and G) has been shifted to lower dispersal thresholds (that is, lower A_{thr} values) by adding these processes since both Hopf bifurcation curves are lower in figure 7.6 than in figure 7.11. In other words, in the full model endemic equilibria occur for higher rates of female adult dispersal than in the predation model since lower dispersal thresholds imply that there is more dispersal (see equation (7.14)).

The region of extinction for low d_{SL} values (region H) is larger in figure 7.6 but the amplitudes of the outbreak cycles are greatly reduced so that the region of extinction for high d_{SL} values (regions F and G) is much smaller. For example, outbreak minima and maxima for $d_{SL} = 0.3$ and $A_{thr} = 5$ are respectively 10^{-21} and 680 larvae/tsf for the predation model as opposed to 1 and 216 larvae/tsf for the full model. For $A_{thr} \leq 12$, the onset of outbreaks occurs for higher d_{SL} values in the full model than in the predation model. This emphasises the above observation that the additional processes in the original model have a stabilising effect on the system provided that adult dispersal is sufficiently high, that is, A_{thr} is sufficiently low (below 12 larvae/tsf in this case).

The role of predation

In order to study the effects of predation in more detail, one-parameter bifurcation diagrams can be generated by varying p_{max} or p_{sat} . I used the original model which includes all the processes since its output is more biologically meaningful. The method used to obtain figures 7.2 and 7.5 was used again and the resulting one-parameter bifurcation

diagram for p_{max} , corresponding to $d_{SL} = 0.4$ and $A_{thr} = 5$, is shown in figure 7.12. To simplify the scale p_{max} is given in multiples of 23 000 which is the nominal value for p_{max} given in table 7.1.

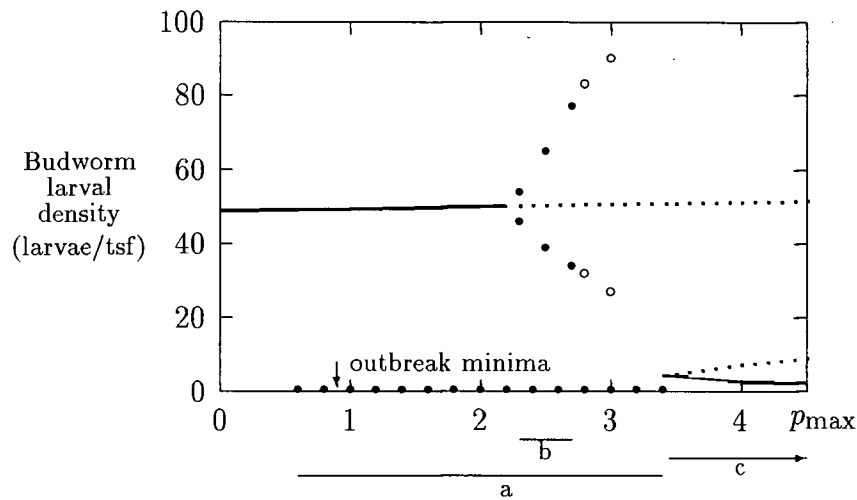


Figure 7.12: One-parameter bifurcation diagram for p_{max} with $d_{SL} = 0.4$ and $A_{thr} = 5$.

For p_{max} less than half its nominal value there is a single equilibrium state, corresponding to endemic budworm densities (see figure 7.12). No outbreaks occur in this range although the system oscillates as it approaches the equilibrium. Outbreaks are possible in the range of p_{max} values denoted by a . Maxima for these cycles are around 270 larvae/tsf for $p_{max} = 0.6 \times 23\,000$ and increase as p_{max} increases. At $p_{max} = 2.7 \times 23\,000$ a maximum of 360 larvae/tsf is attained. These values are much more realistic than the maximum of 820 larvae/tsf produced by the dispersal model for the same values of d_{SL} and A_{thr} .

Around $p_{max} = 2.3 \times 23\,000$ the endemic equilibrium bifurcates to produce a nine year periodic orbit of small amplitude¹. This periodic orbit is attracting for the range

¹To be mathematically correct I should say that a number of bifurcations occur leading to orbits of higher and higher period. However, these bifurcations occur over such a small range of parameter values that it is difficult to detect them using the present techniques. Also, because they occur over

of parameter values denoted by b . In region a , initial values for the budworm and forest variable determine whether the outbreak cycle or an endemic equilibrium state (stable equilibrium point or small amplitude periodic orbit) is attained. For $p_{max} > 3.3 \times 23\,000$ (region c) there is a single equilibrium corresponding to low budworm densities. This suggests that if predation were to control the budworm population and keep it at low levels, the amount of predation would have to be much higher than has been observed in the field. (Recall that the nominal or standard value for p_{max} is $1.0 \times 23\,000$.) The recruitment curves generated earlier (figure 7.10) using the standard parameter values in table 7.1 show that predation has its most significant effect at budworm densities around 5 to 7 larvae/tsf. However, during outbreaks larval densities increase to much higher values very rapidly. This supports the above observation that predation does not have a significant influence on outbreak behaviour, except when predation is so high that budworm densities cannot escape from the low numbers where predation is prevalent.

A diagram similar to figure 7.12 can be obtained by decreasing p_{sat} . From the diagrams of the (Foliage, Budworm)-plane and the time plots generated in doing these parameter studies, an important observation can be made—varying the predation parameters has a significant influence on the periods of the outbreaks. For example, when $p_{max} = 0.6 \times 23\,000$ the outbreak cycle has a period of 13 years. This increases to 50 years for $p_{max} = 3.4 \times 23\,000$. These increased periods do not have much effect on the time span of the actual outbreak which is usually around 7 or 8 years. Instead they increase the number of years for which budworm densities remain below 1 larva/tsf. Figure 7.13 illustrates the above comments. These results again support the conclusion that predation only affects the behaviour at low budworm densities. Once the budworm have escaped the control exerted by predation, an outbreak occurs and the attributes of this

such a small range, they are not of practical importance in themselves. We are more interested in the qualitative change from an equilibrium to cycles.

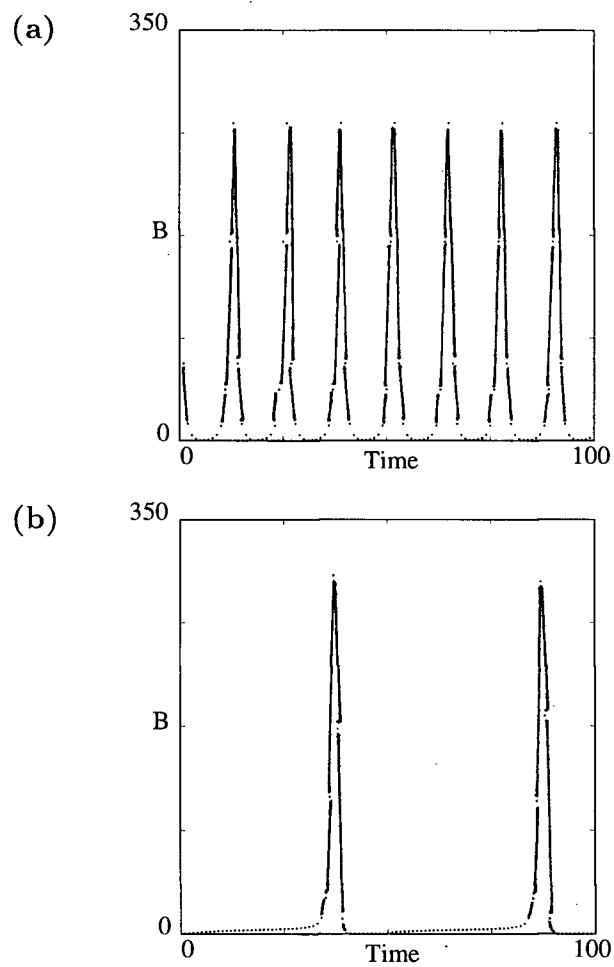


Figure 7.13: Time plots of budworm larval density for (a) $p_{max} = 0.6 \times 23\ 000$ and (b) $p_{max} = 3.4 \times 23\ 000$. Outbreaks last 7 or 8 years in both cases but the time between outbreaks is longer in (b). Both figures are plots of the behaviour after the initial transients have died away.

outbreak (such as its time span) are independent of the rate of predation. However, for higher rates of predation it takes much longer for the budworm to escape this control, hence the longer time periods between outbreaks.

As a final test of the effects of predation relative to small larval dispersal, I constructed a two-parameter bifurcation diagram of p_{max} versus d_{SL} using the full model (which includes all processes). The results are shown in figure 7.14. Clearly, the higher d_{SL} (and

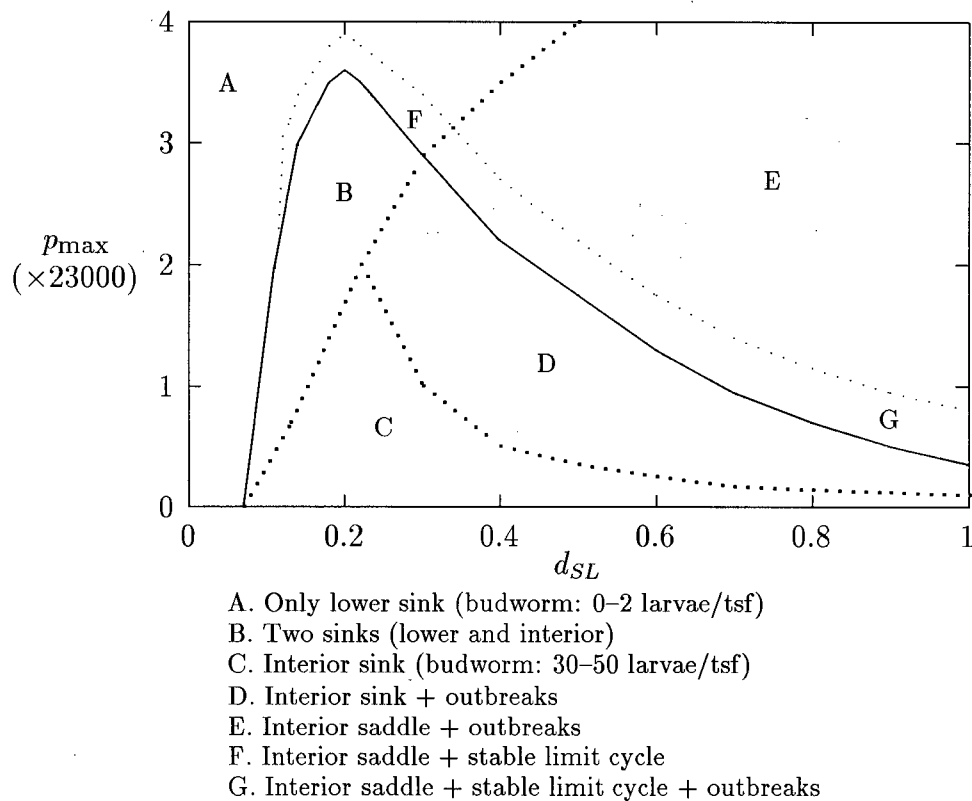


Figure 7.14: Two-parameter bifurcation diagram of p_{max} versus d_{SL} .

hence the greater small larval dispersal success) the greater the chance of outbreaks. Only for low d_{SL} and high p_{max} values does predation exert sufficient control over the budworm population to prevent outbreaks occurring. Note that the nominal value for p_{max} is $1 \times 23\,000$ and at this value the lower budworm equilibrium only exists for

$d_{SL} < 0.12$.

This section emphasises once again the overwhelming importance of small larval dispersal success, and hence the importance of forest condition, on the budworm dynamics.

7.5 Conclusion

This chapter has focussed on analysing the budworm-forest model developed by Jones [65] and Clark and Ludwig [22] using the techniques of dynamical systems theory. Procedures for obtaining one- and two-parameter bifurcation diagrams using diagrams in the (Foliage, Budworm)-plane and time plots from DSTOOL were explained. In the first part of the analysis a classification of the (d_{SL}, A_{thr}) -parameter space was obtained. While Clark and Ludwig [22] found parameter combinations corresponding to behaviour in a number of these regions, namely A, B, C, D and H, this study found some additional possibilities for model behaviour and is much more comprehensive as the resulting bifurcation diagrams summarise the behaviour for all possible combinations of d_{SL} and A_{thr} . The diagrams also show how the system behaviour changes as the two parameters, d_{SL} and A_{thr} , are varied.

Following this the various processes in the model were investigated in more detail using a variety of techniques. It was found that small larval dispersal, and hence forest condition, has the most effect on outbreak cycles in the model and that predation has an added destabilising effect. The main influence of predation is at fairly low budworm densities which means that it affects the time period between outbreaks but not the length or amplitude of the outbreak. Again the use of bifurcation diagrams, state space diagrams and time plots was crucial in the analysis.

Chapter 8

Conclusion

8.1 Main results

A variety of models, both continuous and discrete, theoretical and practical, have been analysed in the preceding chapters. The same basic techniques have been used in each example.

Conclusions which are specific to a particular model have already been noted at the end of each chapter. There are also a number of general results that I wish to highlight. First, the dynamical systems techniques can lead to greater insight into the behaviour of a model and the interactions between various processes in a system than is possible with traditional techniques. For the sheep-hyrax-lynx model in chapter 3 bifurcation diagrams were found to give more information than a traditional sensitivity analysis, and for the ratio-dependent model in chapter 4 the techniques proved more accurate and informative than an isocline analysis. In both these cases the additional information resulted in improvements in the formulations of the models. Thus dynamical systems techniques can be helpful in constructing more plausible models. The techniques can also identify which parameters or processes are crucial for determining the behaviour of the model. This is illustrated in chapters 3 and 7.

The available computer packages allowed us to obtain the results fairly easily without the prerequisite of an extensive mathematical knowledge of dynamical systems theory and without intensive mathematical manipulations. This was highlighted in chapters 2

and 5 where the numerical results were compared with previously obtained theoretical results. In chapter 2 the numerical results were in fact more accurate than Bazykin's approximate analytic results [14]. The computer packages also allow more complicated models to be studied than is possible by hand. All the models illustrate this point. As a result, previously unobtainable insights can be discovered.

In addition, bifurcation diagrams provide a concise way of summarising results and two-parameter diagrams give an idea of the relative frequency of occurrence of the various phenomena.

Although the dynamical systems techniques can be applied in a variety of situations, they are obviously not suitable for all types of ecological models.

8.2 Limitations

Systems of difference equations or ordinary differential equations can be studied but not systems of partial differential equations. Also, the models must not be time or space dependent. These limitations are serious, however it is generally the case that models which are fundamentally different in structure require different methods of solution. For certain types of partial differential equations and time-dependent models it is possible to overcome these limitations by transforming the equations so that they fall into the required categories, but the mathematics required to do this is not trivial.

Although the computer packages allow the dynamical systems techniques to be applied to large models, it is usually more difficult to interpret the results when many state variables and interactions are involved. There is also a greater risk of encountering software restrictions with these large models and the dynamics can become extremely complex because of the higher dimension of the system. Hence, the ease with which the computer packages can be used should not be taken as an argument for building

complicated models. Simple models are still most likely to give us insight into system behaviour because of our own limits in understanding.

As anyone who has used a computer will know, computers and software hardly ever work as smoothly as one might wish. Some of the problems that I encountered have been discussed in previous chapters and others are recorded in appendix B. It is usually a good idea to check the results using an alternative technique or software package.

Although a variety of models have been studied in this thesis, there are many other possibilities for the application of dynamical systems techniques.

8.3 Future possibilities

I did not study any examples of models which include seasonal variation but it is possible to do so (see, for example, [48, 102]). However, the dynamics and bifurcation structure are considerably more complex. Including such an example in this thesis would have confused rather than clarified my intent and would perhaps have discouraged rather than encouraged readers who were considering trying the techniques.

There are probably numerous ways in which dynamical systems theory can be of use in ecological research. These will come to the fore as more people make use of the available computer packages. However, my aims will be fulfilled if a few ecologists start to use the techniques that I have described to analyse their own models. It is always difficult to learn new techniques when one understands and is comfortable with the old ones, but I hope I have demonstrated that the effort is well worth it.

Bibliography

- [1] **P.A. Abrams (1994)**. The fallacies of "ratio-dependent" predation, *Ecology*, **75(6)**: 1842–1850
- [2] **F.R. Adler and W.F. Morris (1994)**. A general test for interaction modification, *Ecology*, **75(6)**: 1552–1559
- [3] **H.R. Akçakaya, R. Arditi and L.R. Ginzburg (1995)**. Ratio-dependent predation: an abstraction that works, *Ecology*, **76(3)**: 995–1004
- [4] **E.L. Allgower and K. Georg (1992)**. Continuation and path following, *Acta Numerica*: 1–64
- [5] **P. Antonelli, X. Lin and R.H. Bradbury (1991)**. A higher-order predator-prey interaction with application to observed starfish waves and cycles, *Ecological Modelling*, **58**: 323–332
- [6] **R. Arditi and H. Saïah (1992)**. Empirical evidence of the role of heterogeneity in ratio-dependent consumption, *Ecology*, **73(5)**: 1544–1551
- [7] **V.I. Arnold (1983)**. *Geometrical Methods in the Theory of Ordinary Differential Equations*, New York : Springer-Verlag
- [8] **M.A. Asmussen (1979)**. Regular and chaotic cycling in models of ecological genetics, *Theoretical Population Biology*, **16**: 172–190
- [9] **M.A. Asmussen and M.W. Feldman (1977)**. Density dependent selection I: A stable feasible equilibrium may not be attainable, *Journal of Theoretical Biology*, **64**: 603–618
- [10] **A. Back, J. Guckenheimer, M. Myers, F. Wicklin and P. Worfolk (1992)**. dstool: Computer assisted exploration of dynamical systems, *Notices of the American Mathematical Society*, **39**: 303–309
- [11] **G.L. Baker and J.P. Gollub (1990)**. *Chaotic Dynamics: An Introduction*, Cambridge : Cambridge University Press
- [12] **W. Baltensweiler and A. Fischlin (1979)**. The role of migration for the population dynamics of the larch bud moth, *Zeiraphera diniana* Gn. (Lepidoptera: Tortricidae), *Bulletin de la Société Entomologique Suisse*, **52**: 259–271

- [13] **G.L. Baskerville (ed.) (1976)**. Report of the task force for evaluation of budworm control alternatives, Department of Natural Resources, Fredericton, New Brunswick, Canada
- [14] **A.D. Bazykin (1974)**. Volterra's system and the Michaelis-Menten equation, in *Problems in Mathematical Genetics*, ed. V.A. Ratner, Novosibirsk : U.S.S.R. Academy of Science, pp. 103–142
- [15] **J.R. Beddington, C.A. Free and J.H. Lawton (1975)**. Dynamic complexity in predator-prey models framed in difference equations, *Nature*, **255**: 58–60
- [16] **P. Bergé, Y. Pomeau and C. Vidal (1984)**. *Order Within Chaos: Towards a Deterministic Approach to Turbulence*, translated from the French by L. Tuckerman, New York : John Wiley and Sons
- [17] **A.A. Berryman (1992)**. The origins and evolution of predator-prey theory, *Ecology*, **73**(5): 1530–1535
- [18] **M. Brylinski (1972)**. Steady-state sensitivity analysis of energy flow in a marine ecosystem, in *Systems Analysis and Simulation in Ecology II*, ed. B.C. Patten, New York: Academic Press
- [19] **W.C. Clark (1979)**. Spatial structure relationships in a forest-insect system: simulation models and analysis, *Mitteilungen der Schweizerischen Entomologischen Gesellschaft*, **52**: 235–257
- [20] **W.C. Clark (1979)**. *Spatial Structure and Population Dynamics in an Insect Epidemic Ecosystem*, PhD thesis, University of British Columbia, Canada
- [21] **W.C. Clark and C.S. Holling (1979)**. Process models, equilibrium structures, and population dynamics: On the formulation and testing of realistic models in ecology, *Fortschritte der Zoologie*, **25**(2–3): 29–52
- [22] **W.C. Clark and D. Ludwig (unpublished manuscript)**. Component processes and qualitative behaviour of the budworm-forest interaction
- [23] **J.B. Collings (1995)**. Bifurcation and stability of a temperature-dependent mite predator-prey interaction model incorporating a prey refuge, *Bulletin of Mathematical Biology*, **57**(1): 63–76
- [24] **J.B. Collings and D.J. Wollkind (1990)**. A global analysis of a temperature-dependent model system for a mite predator-prey interaction, *SIAM Journal of Applied Mathematics*, **50**(5): 1348–1372

- [25] **J.B. Collings, D.J. Wollkind and M.E. Moody (1990)**. Outbreaks and oscillations in a temperature-dependent model for a mite predator-prey interaction, *Theoretical Population Biology*, **38**: 159–191
- [26] **W. Derrick and L. Metzgar (1991)**. Dynamics of Lotka-Volterra systems with exploitation, *Journal of Theoretical Biology*, **153**(4): 455–468
- [27] **P. Deuffhard, B. Fiedler and P. Kunkel (1987)**. Efficient numerical pathfollowing beyond critical points, *SIAM Journal of Numerical Analysis*, **24**: 912–927
- [28] **E.J. Doedel (1981)**. AUTO: A program for the automatic bifurcation analysis of autonomous systems, *Congressus Numerantium*, **30**: 265–284
- [29] **E.J. Doedel (1984)**. The computer-aided bifurcation analysis of predator-prey models, *Journal of Mathematical Biology*, **20**: 1–14
- [30] **E.J. Doedel and J.P. Kernevez (1986)**. *AUTO: Software for Continuation and Bifurcation Problems in Ordinary Differential Equations*, Pasadena: CIT Press
- [31] **E.J. Doedel, X. Wang and T. Fairgrieve (1994)**. *AUTO94: Software for continuation and bifurcation problems in ordinary differential equations*, Pasadena: CIT Press
- [32] **P.B. Dowden, H.A. Jaynes and V.M. Carolin (1953)**. The role of birds in a spruce budworm outbreak in Maine, *Journal of Economic Entomology*, **46**: 307–312
- [33] **S.R. Dunbar (1986)**. Travelling waves in diffusive predator-prey equations. Periodic orbits and point-to-periodic heteroclinic orbits, *SIAM Journal of Applied Mathematics*, **46**(6): 1057–1078
- [34] **L. Edelstein-Keshet (1988)**. *Mathematical Models in Biology*, New York: Random House
- [35] **G.B. Ermentrout (1995)**. *XPPAUT-1.63*
- [36] **V. Fairen and M.G. Velarde (1979)**. Time-periodic oscillations in a model for respiratory process of a bacterial culture, *Journal of Mathematical Biology*, **8**: 147–157
- [37] **A. Fischlin and W. Baltensweiler (1979)**. Systems analysis of the larch bud moth system. Part I: the larch-larch bud moth relationship, *Bulletin de la Société Entomologique Suisse*, **52**: 273–289

- [38] **R. Fitzhugh (1961)**. Impulses and physiological states in theoretical models of nerve membrane, *Biophysical Journal*, **1**: 445-466
- [39] **J.W. Forrester (1961)**. *Industrial Dynamics*, Cambridge, Massachusetts: MIT Press
- [40] **P.M. Frank (1978)**. *Introduction to System Sensitivity Theory*, New York: Academic Press
- [41] **H.I. Freedman and R.M. Mathsen (1993)**. Persistence in predator-prey systems with ratio-dependent predator influence, *Bulletin of Mathematical Biology*, **55(4)**: 817-827
- [42] **J.L. George and R.T. Mitchell (1948)**. Calculations on the extent of spruce budworm control by insectivorous birds, *Journal of Forestry*, **46**: 454-455
- [43] **C.F. Gerald and P.O. Wheatley (1989)**. *Applied Numerical Analysis*, Reading, Massachusetts: Addison-Wesley Publishing Company
- [44] **M.E. Gilpin (1974)**. A model of the predator-prey relationship, *Theoretical Population Biology*, **5**: 333-344
- [45] **L.R. Ginzburg and H.R. Akçakaya (1992)**. Consequences of ratio-dependent predation for steady-state properties of ecosystems, *Ecology*, **73(5)**: 1536-1543
- [46] **S.K. Gleeson (1994)**. Density dependence is better than ratio dependence, *Ecology*, **75(6)**: 1834-1835
- [47] **A. Goldbeter (1980)**. Models for oscillations and excitability in biochemical systems, in *Mathematical Models in Molecular and Cellular Biology*, ed. L.A. Segel, Cambridge : Cambridge University Press, pp. 248-291
- [48] **A. Gragnani and S. Rinaldi (1995)**. A universal bifurcation diagram for seasonally perturbed predator-prey models, *Bulletin of Mathematical Biology*, **57(5)**: 701-712
- [49] **J. Guckenheimer and P. Holmes (1983)**. *Nonlinear Oscillations, Dynamical Systems, and Bifurcation of Vector Fields*, New York : Springer
- [50] **J. Guckenheimer, G. Oster and A. Ipaktchi (1977)**. The dynamics of density dependent population models, *Journal of Mathematical Biology*, **4**: 101-147
- [51] **A.P. Gutierrez (1992)**. Physiological basis of ratio-dependent predator-prey theory: the metabolic pool model as a paradigm, *Ecology*, **73(5)**: 1552-1563

- [52] **A.P. Gutierrez, N.J. Mills, S.J. Schreiber and C.K. Ellis (1994)**. A physiologically based tritrophic perspective on bottom up-top down regulation of populations, *Ecology*, **75**: 2227–2242
- [53] **J. Hadamard (1952)**. *Lectures on Cauchy's Problem in Linear Partial Differential Equations*, New York: Dover Publications
- [54] **J.K. Hale and H. Koçak (1989)**. *Differential and Difference Equations Through Computer Experiments*, New York: Springer-Verlag
- [55] **I. Hanski (1991)**. The functional response of predators: worries about scale, *Trends in Ecology and Evolution*, **6(5)**: 141–142
- [56] **H.W. Hethcote (1976)**. Qualitative analyses of communicable disease models, *Mathematical Biosciences*, **28**: 335–356
- [57] **M.W. Hirsch and S. Smale (1974)**. *Differential Equations, Dynamical Systems, and Linear Algebra*, Orlando, Florida : Academic Press
- [58] **A.L. Hodgkin and A.F. Huxley (1952)**. A quantitative description of membrane current and its application to conduction and excitation in nerve, *Journal of Physiology*, **117**: 500–544
- [59] **C.S. Holling (1959)**. The components of predation as revealed by a study of small mammal predation on the European pine sawfly, *Canadian Entomologist*, **91**: 293–320
- [60] **C.S. Holling (1965)**. The functional response of predators to prey density and its role in mimicry and population regulation, *Memoirs of the Entomological Society of Canada*, **45**: 1–60
- [61] **C.S. Holling (1973)**. Resilience and stability of ecological systems, *Annual Review of Ecology and Systematics*, **4**: 1–23
- [62] **C.S. Holling, D.D. Jones and W.C. Clark (1976)**. Ecological policy design: a case study of forest pest management, in *Pest Management: Proceedings of an International Conference, October 25–29, 1976*, ed. G.A. Norton and C.S. Holling, Pergamon Press, International Institute for Applied Systems Analysis proceedings series 4
- [63] **P.F. Hultquist (1988)**. *Numerical Methods for Engineers and Computer Scientists*, Menlo Park, California: Benjamin Cummings
- [64] **J.N.R. Jeffers (1978)**. *An Introduction to Systems Analysis: With Ecological Applications*, Baltimore, Maryland: University Park Press

- [65] **D.D. Jones (1976)**. The budworm site model, in *Pest Management: Proceedings of an International Conference, October 25–29, 1976*, ed. G.A. Norton and C.S. Holling, Pergamon Press, International Institute for Applied Systems Analysis proceedings series 4
- [66] **C. Kaas-Petersen (1989)**. *PATH—User's Guide*, University of Leeds, England
- [67] **H.B. Keller (1977)**. Numerical solution of bifurcation and nonlinear eigenvalue problems, in *Applications of Bifurcation Theory*, ed. P.H. Rabinowitz, New York : Academic Press, pp. 359–384
- [68] **A. Khibnik, Y. Kuznetsov, V. Levitin and E. Nikolaev (1993)**. Continuation techniques and interactive software for bifurcation analysis of ordinary differential equations and iterated maps, *Physica D*, **62**: 360–371
- [69] **N.E. Kowal (1971)**. A rationale for modeling dynamic ecological systems, in *Systems Analysis and Simulation in Ecology I*, ed. B.C. Patten, New York: Academic Press
- [70] **S.H. Levine (1975)**. Discrete time modeling of ecosystems with applications in environmental enrichment, *Mathematical Biosciences*, **24**: 307–317
- [71] **T.Y. Li and J.A. Yorke (1975)**. Period three implies chaos, *American Mathematical Monthly*, **82**: 985–992
- [72] **J.A. Logan and F.P. Hain (eds) (1991)**. *Chaos and Insect Ecology*, papers presented at the symposium *Does chaos exist in ecological systems?*, Montréal, August 1990, Virginia Experiment Station Information Series 91-3, Virginia Polytechnic Institute and State University : Blacksburg
- [73] **A.J. Lotka (1925)**. *Elements of Physical Biology*, Baltimore: Williams and Wilkins
- [74] **D. Ludwig, D.D. Jones and C.S. Holling (1978)**. Qualitative analysis of insect outbreak systems: the spruce budworm and forest, *Journal of Animal Ecology*, **47**: 315–332
- [75] **P. Lundberg and J.M. Fryxell (1995)**. Expected population density versus productivity in ratio-dependent and prey-dependent models, *The American Naturalist*, **146**(1): 153–161
- [76] **R. MacArthur (1970)**. Graphical analysis of ecological systems, in *Lectures on Mathematics in the Life Sciences 2*, Providence: American Mathematical Society
- [77] **N. MacDonald (1978)**. *Time Lags in Biological Models*, Berlin: Springer-Verlag

- [78] **N. MacDonald (1989)**. *Biological Delay Systems*, Cambridge: Cambridge University Press
- [79] **R.M. May (1972)**. Limit cycles in predator-prey communities, *Science*, **177**: 900-902
- [80] **R.M. May (1973)**. *Stability and Complexity in Model Ecosystems*, Princeton: Princeton University Press
- [81] **R.M. May (1973b)**. Time delay versus stability in population models with two and three trophic levels, *Ecology*, **54**: 315-325
- [82] **R.M. May (1975)**. Biological populations obeying difference equations: stable points, stable cycles, and chaos, *Journal of Theoretical Biology*, **51**: 511-524
- [83] **R.M. May (1976)**. Simple mathematical models with very complicated dynamics, *Nature*, **261**: 459-467
- [84] **R.M. May and G. Oster (1976)**. Bifurcations and dynamic complexity in simple ecological models, *American Naturalist*, **110**: 573-599
- [85] **J. Maynard Smith (1974)**. *Models in Ecology*, Cambridge: Cambridge University Press
- [86] **H.I. McCallum (1992)**. Effects of immigration on chaotic population dynamics, *Journal of Theoretical Biology*, **154**: 277-284
- [87] **K. McCann and P. Yodzis (1994)**. Biological conditions for chaos in a three-species food chain, *Ecology*, **75**(2): 561
- [88] **M.A. McCarthy, L.R. Ginzburg and H.R. Akçakaya (1995)**. Predator interference across trophic chains, *Ecology*, **76**(4): 1310-1319
- [89] **P.J. McNamee (1987)**. *The Equilibrium Structure and Behaviour of Defoliating Insect Systems*, PhD thesis, University of British Columbia, Canada
- [90] **P.J. McNamee, J.M. McLeod and C.S. Holling (1981)**. The structure and behaviour of defoliating insect/forest systems, *Researches on Population Ecology*, **23**: 280-298
- [91] **R.F. Morris (ed.) (1963)**. The dynamics of epidemic spruce budworm populations, *Memoirs of the Entomological Society of Canada*, **31**: 1-332
- [92] **J.D. Murray (1981)**. A pre-pattern formation mechanism for animal coat markings, *Journal of Theoretical Biology*, **88**: 161-199

- [93] **G. Namkoong, J. Bishir and J.H. Roberds (1993)**. Evolutionary effects of density dependent selection in plants, *Genetical Research*, **62**: 57–62
- [94] **A.J. Nicholson and V.A. Bailey (1935)**. The balance of animal populations: Part I, *Proceedings of the Zoological Society of London*, **3**: 551–598
- [95] **I. Noy-Meir (1975)**. Stability of grazing ecosystems: an application of predator-prey graphs, *Journal of Ecology*, **63**: 459–481
- [96] **H.E. Nusse and J.A. Yorke (1994)**. *Dynamics: Numerical Explorations*, Applied Mathematical Sciences, **101**, New York: Springer-Verlag
- [97] **G. Oster and J. Guckenheimer (1976)**. Bifurcation phenomena in population models, in *The Hopf Bifurcation and its Applications*, ed. J.E. Marsden and M. McCracken, New York: Springer-Verlag, pp. 327–353
- [98] **G. Oster and Y. Takahashi (1974)**. Models for age specific interactions in a periodic environment, *Ecological Monographs*, **44**: 483–501
- [99] **B.C. Patten (1971)**. A primer for ecological modeling and simulation with analog and digital computers in *Systems Analysis and Simulation in Ecology I*, ed. B.C. Patten, New York: Academic Press
- [100] **W.C. Rheinboldt and J.V. Burkardt (1983)**. A locally-parametrized continuation process, *ACM Transactions on Mathematical Software*, **9**: 215–235
- [101] **W.C. Rheinboldt and J.V. Burkardt (1983)**. Algorithm 596: A program for a locally parametrized continuation process, *ACM Transactions on Mathematical Software*, **9**: 236–241
- [102] **S. Rinaldi, S. Muratori and Y. Kuznetsov (1993)**. Multiple attractors, catastrophes and chaos in seasonally perturbed predator-prey communities, *Bulletin of Mathematical Biology*, **55**(1): 15–35
- [103] **M.L. Rosenzweig and R.H. MacArthur (1963)**. Graphic representation and stability conditions of predator-prey interactions, *The American Naturalist*, **97**: 209–223
- [104] **J. Roughgarden (1979)**. *Theory of Population Genetics and Evolutionary Ecology: An Introduction*, New York: MacMillan
- [105] **T. Royama (1984)**. Population dynamics of the spruce budworm *Choristoneura Fumiferana*, *Ecological Monographs*, **54**(4): 429–462

- [106] **C.J. Sanders, R.W. Stark, E.J. Mullins and J. Murphy (eds) (1985).** *Recent Advances in Spruce Budworms Research*, Proceedings of CANUSA Spruce Budworms Research Symposium, 16–20 September 1984, Bangor, Maine, Canadian Forestry Service, Ottawa, Ontario
- [107] **O. Sarnelle (1994).** Inferring process from pattern: trophic level abundances and imbedded interactions, *Ecology*, **75(6)**: 1835–1841
- [108] **L.A. Segel (1984).** *Modelling Dynamic Phenomena in Molecular and Cellular Biology*, Cambridge : Cambridge University Press
- [109] **J.F. Selgrade and G. Namkoong (1991).** Population interactions with growth rates dependent on weighted densities, in *Differential Equations Models in Biology, Epidemiology and Ecology*, ed. S. Busenberg and M. Martelli, New York: Springer-Verlag, pp. 247–256
- [110] **J.F. Selgrade and G. Namkoong (1992).** Dynamical behaviour for population genetics models of differential and difference equations with nonmonotone fitnesses, *Journal of Mathematical Biology*, **30**: 815–826
- [111] **R. Seydel (1988).** *From Equilibrium to Chaos: Practical Bifurcation and Stability Analysis*, New York : Elsevier
- [112] **R. Seydel (1991).** *BIFPACK: A Program Package for Continuation, Bifurcation and Stability Analysis, Version 2.3+*, University of Ulm, Germany
- [113] **A.M. Starfield and A.L. Bleloch (1986).** *Building Models for Conservation and Wildlife Management*, New York : Macmillan
- [114] **L. Stone (1993).** Period-doubling reversals and chaos in simple ecological models, *Nature*, **365**: 617–620
- [115] **J. Swart (1987).** Sensitivity of a hyrax-lynx mathematical model to parameter uncertainty, *South African Journal of Science*, **83**: 545–547
- [116] **J. Swart and J.W. Hearne (1989).** A mathematical model to analyze predation and competition problems in a sheep-farming region, *System Dynamics Review*, **5**: 35–50
- [117] **M. Taylor and Y. Kevrekidis (unpublished course notes).** *Interactive AUTO: A Graphical Interface for AUTO86*, Princeton University
- [118] **R. Tomovic (1963).** *Sensitivity Analysis of Dynamic Systems*, translated by D. Tornquist, London, England: McGraw-Hill

- [119] **P.M. Turchinsky (1981)**. *Man in competition with the spruce budworm: an application of differential equations*, Boston: Birkhäuser
- [120] **V. Volterra (1931)**. Variations and fluctuations of the number of individuals in animal species living together, in *Animal Ecology*, ed. R.N. Chapman, New York: McGraw-Hill, pp. 409–448
- [121] **B.H. Walker, D. Ludwig, C.S. Holling and R.M. Peterman (1981)**. Stability of semi-arid savanna grazing systems, *Journal of Ecology*, **69**: 473–498
- [122] **Waterloo Maple Software (1990–1992)**. *The Maple Roots Report*, Waterloo Maple Software, Waterloo, Canada
- [123] **K.E.F. Watt (1966)**. The nature of systems analysis, in *Systems Analysis in Ecology*, ed. K.E.F. Watt, New York: Academic Press
- [124] **S. Wiggins (1990)**. *Introduction to Applied Nonlinear Dynamical Systems and Chaos*, New York : Springer-Verlag
- [125] **T. Williams and C. Kelley (unpublished)**. *GNUPLOT: An Interactive Plotting Program* (user manual)
- [126] **S. Wolfram (1991)**. *MATHEMATICA: A System for Doing Mathematics by Computer*, Redwood City, California: Addison-Wesley
- [127] **D.J. Wollkind, J.B. Collings and J.A. Logan (1988)**. Metastability in a temperature-dependent model system for predator-prey mite outbreak interactions on fruit trees, *Bulletin of Mathematical Biology*, **50(4)**: 379–409
- [128] **P. Yodzis (1989)**. *Introduction to Theoretical Ecology*, New York: Harper and Row

Appendix A

Dynamical systems theory

A.1 Introduction

This appendix explains the dynamical systems terminology used in my thesis. Section A.2 is a glossary of the basic concepts such as equilibrium point, domain of attraction and bifurcation point. Extensive use is made of diagrams in order to introduce the concepts as simply and intuitively as possible. Section A.3 describes some of the more formal mathematical details associated with these concepts. However, the mathematics is kept to a minimum since the appendix is intended for biologists. Further details can be found in any introductory text on dynamical systems theory. A few examples which I found particularly readable include [57, 111, 128].

A.2 Basic concepts

This section is ordered alphabetically. All the examples given are for continuous systems of equations. Discrete systems are discussed in section A.3.5. Within each subsection in this glossary, italics is used to highlight terms which are explained in a separate subsection.

A.2.1 Bifurcation diagram

A one-parameter bifurcation diagram summarises the *qualitative behaviour* corresponding to different values of a *parameter*. A *state variable* (or combination of state variables) is

plotted on the y-axis and the parameter on the x-axis. The positions and local stabilities of *equilibrium points* as well as *limit cycles* are indicated using different line types. Solid curves are used to represent *locally stable* equilibria and dotted curves are used for *locally unstable* equilibria. Maxima and minima of limit cycles are indicated using circles—solid ones for stable cycles and open circles for unstable cycles. See, for example, the figures in sections A.2.10, A.2.13, A.2.16, A.2.18, A.2.25.

It is important to note that bifurcation diagrams summarise the behaviour associated with a range of parameter values. They do not represent the dynamics corresponding to a continually varying parameter [124]. In order to read a bifurcation diagram, fix the parameter at a particular value and mentally draw a vertical line at that value. Each crossing of this line with a curve in the diagram corresponds to an equilibrium point or a periodic orbit (limit cycle). The *local stability* properties of a particular phenomenon are given by the type of curve, that is, solid, dotted, or open or closed circles. For example, the *phase portraits* in figure A.17(b)(i) and (ii) were obtained by mentally drawing vertical lines at the parameter values $\mu = \mu_1$ and $\mu = \mu_2$ respectively in figure A.17(a).

A two-parameter bifurcation diagram shows how the positions of *bifurcation points* change as two *parameters* are varied. For example, if a bifurcation point is encountered in a one-parameter bifurcation diagram, a second parameter may be varied to see how it affects the position of the bifurcation point. An example involving *limit points* is shown in figure A.19. λ and μ are parameters and x_1 is a state variable. Part (a) of this figure shows a two-parameter bifurcation diagram and part (b) shows one-parameter bifurcation diagrams corresponding to different fixed values of the parameter λ .

A.2.2 Bifurcation point

A bifurcation point is a point in parameter space at which the *qualitative behaviour* of the system changes. A *stable equilibrium* may become *unstable* at this point or there may

be a change from a stable equilibrium to oscillatory behaviour. Examples can be found in sections A.2.10, A.2.13, A.2.16, A.2.18, A.2.25.

A.2.3 Chaos

Chaos is difficult to define but intuitively it refers to the (apparently) irregular and unpredictable behaviour which many nonlinear mathematical models (systems of equations) exhibit [11]. If a system is chaotic then initial values which are very close together may lead to vastly different behaviour as time progresses. However, this behaviour is still bounded by a region in space. Chapters 5 and 6 contain examples of chaotic behaviour.

A.2.4 Continuation branch

A solution or continuation *branch* is a curve of *equilibrium points* (or *limit cycles* or *bifurcation points*) that indicates how the position and properties of the equilibrium point (or limit cycle or bifurcation point) change as a *parameter* (or parameters) is altered. Together a number of these branches make up a *bifurcation diagram*.

A.2.5 Domain of attraction

Suppose the system in which we are interested has a stable *equilibrium point* (see section A.2.14). Then the collection of all initial *state variable* values from which the system tends towards this equilibrium as time progresses is the domain (or basin) of attraction of the equilibrium point. The equilibrium point is called an ‘attractor’. Any stable phenomenon, such as a stable *limit cycle*, also has a domain of attraction and is referred to as an attractor.

For example, in figure A.1 a population density of 10 is locally stable. For initial population values which lie between 5 and 20 the population tends towards a density of 10 as time progresses. For initial values below 5 the population tends to extinction and for initial values greater than 20 it increases steadily. The range of values between 5 and 20 is the domain of attraction for the equilibrium point at 10. Part (a) of figure A.1 shows time plots corresponding to various initial points and part (b) is a one-dimensional phase portrait of the situation.

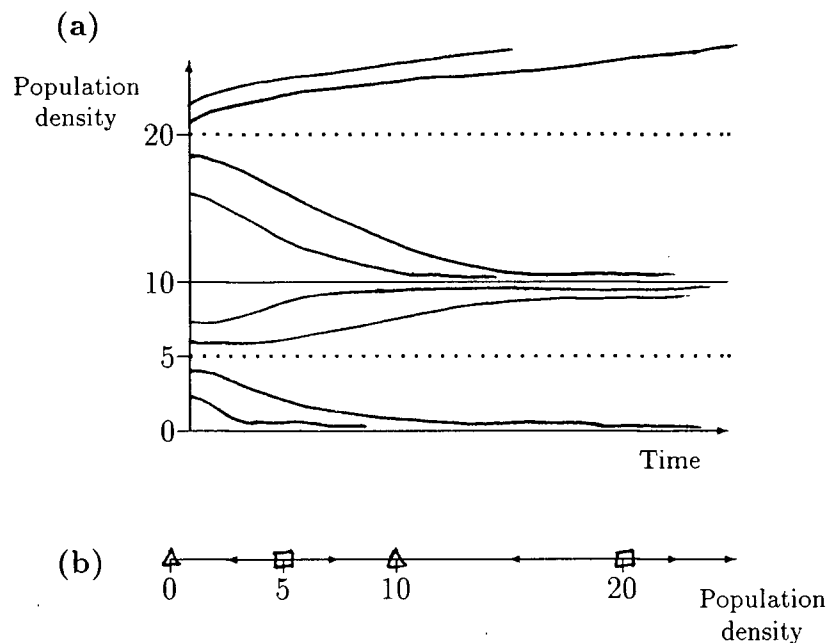


Figure A.1: (a) Time plots showing the domain of attraction of an equilibrium point. A population density of 10 is stable and the range of initial population values between 5 and 20 constitutes its domain of attraction. The values 5 and 20 are unstable equilibrium points. (b) A one-dimensional phase portrait of the situation in (a). The arrows indicate the direction of change corresponding to initial points in each range of values.

Suppose our system consists of two competing populations. We can represent their dynamics using a *phase portrait* such as in figure A.2. In this case the points A and C are stable equilibria. The domain of attraction of A is the shaded region and the remaining

region is the domain of attraction of C. The curve separating these regions is called a separatrix. Curves with arrows indicate how the population densities vary over time beginning at various initial points.

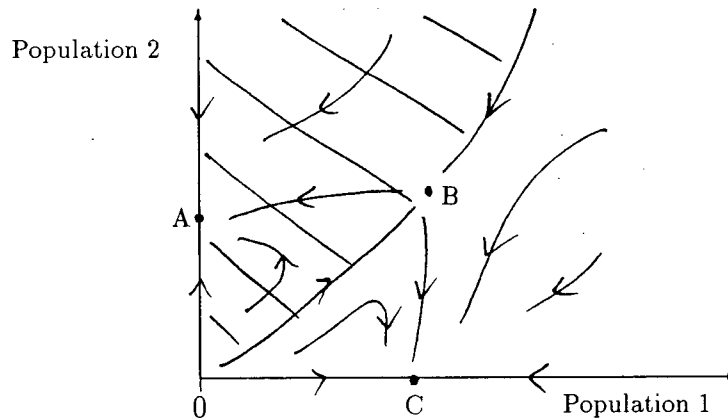


Figure A.2: Phase portrait showing the domains of attraction of two equilibrium points in two dimensions. A and C are stable equilibria. The arrows indicate how the population densities vary over time beginning at various initial points.

A.2.6 Equilibrium point

If the values of the *state variables* representing an ecological system do not change as time progresses then we say that the system is at an equilibrium point. Other commonly used terminology is singular point or fixed point. See also section A.2.14.

A.2.7 Hard loss of stability

In the case of a *Hopf bifurcation* this occurs when there is a sudden change from stable equilibrium behaviour to stable *limit cycles* of large amplitude. An example is shown in figure A.3. When the *parameter* μ is increased beyond the Hopf bifurcation at μ^* , the system suddenly jumps to limit cycles of large amplitude instead of starting off with

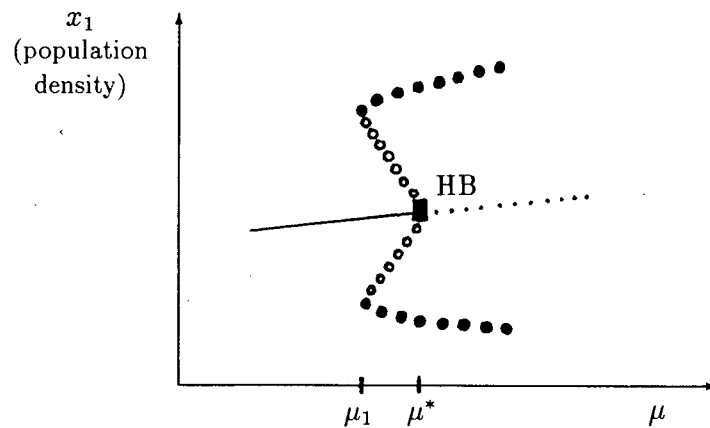


Figure A.3: Hard loss of stability (adapted from [111], p.74). This phenomenon gives rise to sudden changes between stable equilibrium behaviour and limit cycles of large amplitude.

small limit cycles which grow in size as μ increases. The latter phenomenon is shown in figure A.6(a) and is called *soft loss of stability*. Also, as μ is decreased, there is a jump from large amplitude cycles to a zero amplitude equilibrium point but this takes place at μ_1 which is less than μ^* . For $\mu_1 < \mu < \mu^*$ there are two stable attractors—an *equilibrium point* and a *limit cycle*. This is a kind of *hysteresis* phenomenon. Examples of hard loss of stability arise in the analysis of the ratio-dependent model in chapter 4.

Equilibrium states can also undergo a hard loss of stability (for example, in the vicinity of a *pitchfork bifurcation*). However, such phenomena are not encountered in the main body of the thesis.

A.2.8 Heteroclinic orbit

Consider a system having both predator and prey populations and suppose there are two *equilibrium points* one of which is unstable (a *saddle* or a *source*) and where the other is either a saddle or a *sink*. If an unstable manifold (see page 241 for an explanation of this term) of the unstable equilibrium point intersects a stable manifold of the other

equilibrium point then the system is said to have a heteroclinic orbit. An example is shown in figure A.4. For any initial point on this orbit the system will tend towards the

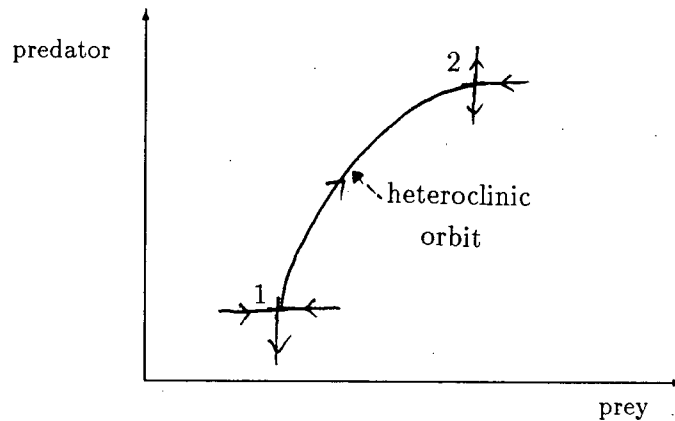


Figure A.4: Example of a heteroclinic orbit. An unstable manifold of saddle point 1 intersects a stable manifold of saddle point 2.

equilibrium point 2. The *parameter* value at which the heteroclinic orbit occurs is called a *heteroclinic bifurcation point*.

For a more detailed explanation of this phenomenon see section A.3.3.

A.2.9 Homoclinic orbit

This is similar to a *heteroclinic orbit* except that in this case the unstable and stable manifolds of the *same* equilibrium point (which must be a *saddle*) intersect. An example is shown in figure A.5. Further details are given in section A.3.3 and an example arises in chapter 2. The unique parameter value giving rise to the homoclinic orbit is a *homoclinic bifurcation point*.

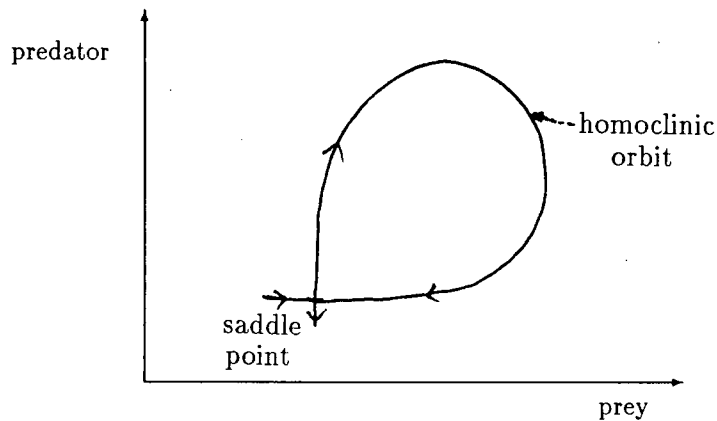


Figure A.5: Example of a homoclinic orbit. An unstable and a stable manifold of the saddle point intersect.

A.2.10 Hopf bifurcation

A Hopf bifurcation¹ (HB) is a *bifurcation point* at which an *equilibrium point* alters *stability* and a *limit cycle* (period orbit) is initiated. An example is given in figure A.6. Part (a) of the figure is a *bifurcation diagram*. The large dots denote the maxima and minima of the limit cycles. The *phase portrait* in figure A.6(b)(i) shows the dynamics in the (x_1, x_2) -phase space for $\mu = \mu_1$. A is a stable equilibrium point or *sink*. After the Hopf bifurcation is encountered at $\mu = \mu^*$, A becomes a *source* and a stable limit cycle is initiated. The corresponding dynamics at $\mu = \mu_2$ are shown in figure A.6(b)(ii). Notice that the amplitude of the limit cycle increases as μ increases (see figure A.6(a)). This is called *soft loss of stability*.

In figure A.6 a stable limit cycle surrounds an unstable equilibrium point. It is also possible for an unstable limit cycle to encircle a locally stable equilibrium point (see figure A.7). Unstable periodic orbits are indicated by open circles instead of solid ones.

¹Although the name Hopf bifurcation is usually used, Arnold [7] points out that this is inaccurate. Both Poincaré and Andronov studied this bifurcation prior to Hopf. Wiggins [124] refers to the Poincaré-Andronov-Hopf bifurcation.

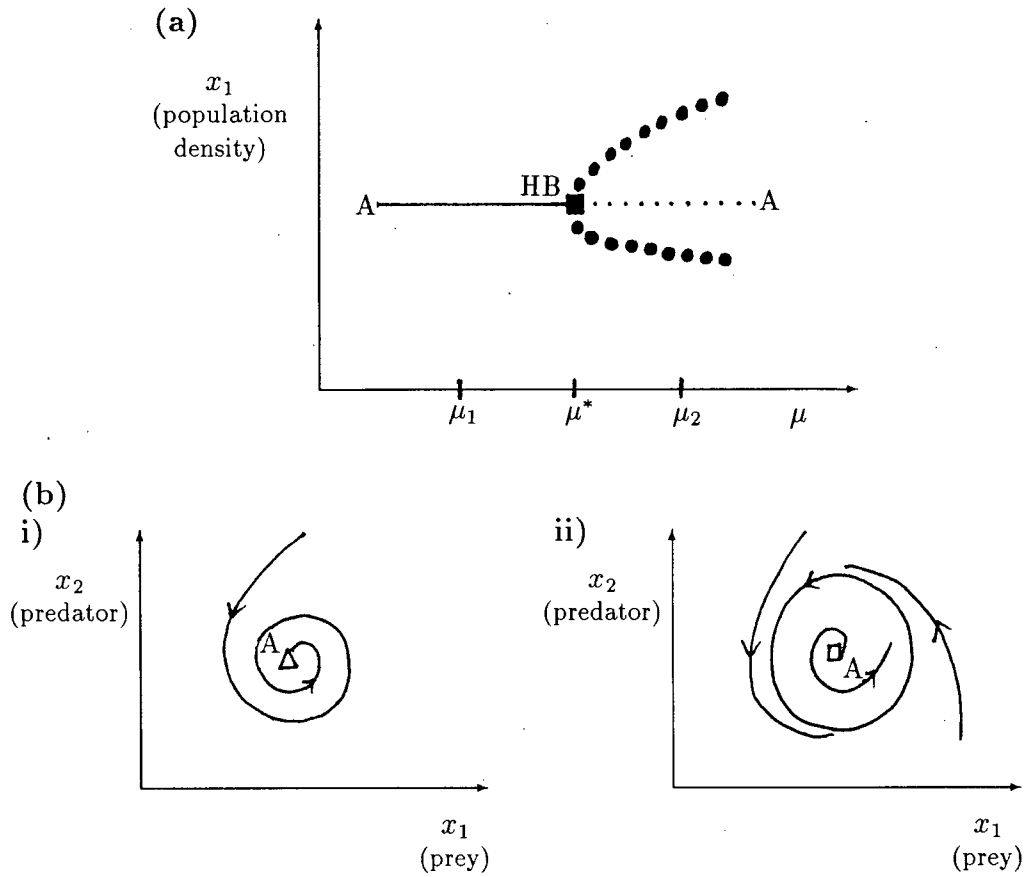


Figure A.6: (a) A bifurcation diagram of a Hopf bifurcation (HB), (b)(i) a phase portrait corresponding to $\mu = \mu_1$ at which there is a stable equilibrium point and (b)(ii) a phase portrait corresponding to $\mu = \mu_2$ at which there is an unstable equilibrium point surrounded by a stable limit cycle.

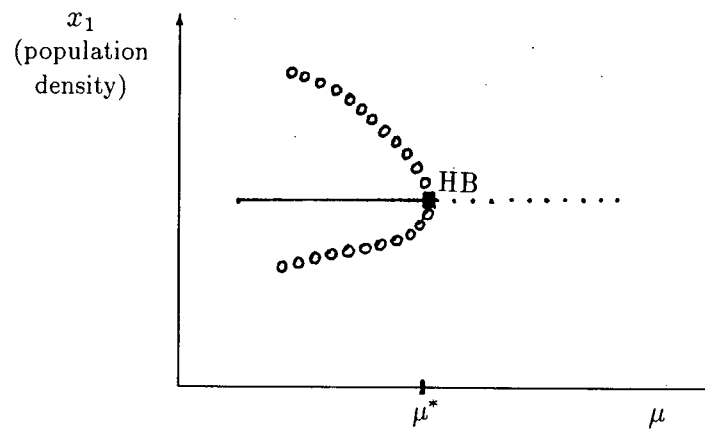


Figure A.7: Bifurcation diagram of a Hopf bifurcation where unstable periodic orbits surround a stable equilibrium point.

The first examples of Hopf bifurcations occur in chapter 2. See also sections A.2.7, A.2.22.

A.2.11 Hysteresis

A hysteresis phenomenon occurs when two *limit points* are connected as shown in figure A.8. This results in multiple equilibria corresponding to a single parameter value. For $\mu < \mu^*_1$ and $\mu > \mu^*_2$ there is a single *equilibrium point*, which is stable in this example. For parameter values $\mu^*_1 < \mu < \mu^*_2$ there are three equilibrium points—two stable and one unstable. The unstable equilibrium point divides the *domains of attraction* of the stable equilibria. For initial population densities above the dotted line in the range $\mu^*_1 < \mu < \mu^*_2$ the population tends towards C. For initial values below the dotted line the population is attracted towards A.

The way in which the behaviour of the system changes differs depending on whether μ is increased or decreased. Suppose we are at *equilibrium point C* at $\mu = \mu_1$. If μ is increased then solution trajectories will continue to tend towards C for all μ such that

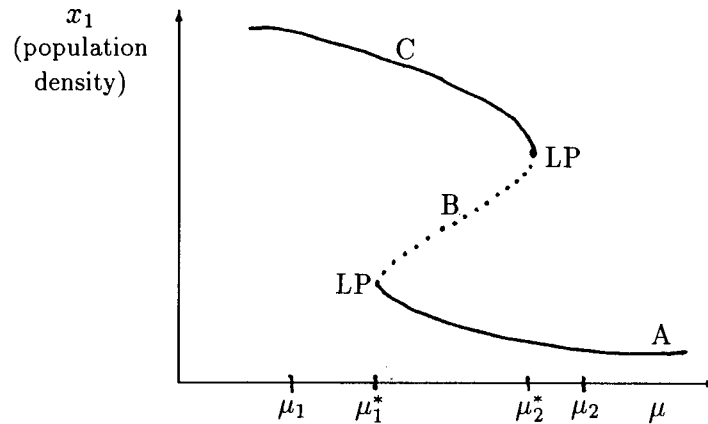


Figure A.8: Bifurcation diagram of hysteresis.

$\mu < \mu_2^*$ since our initial point is above the boundary B of the *domain of attraction* of C. However, as μ increases beyond μ_2^* a catastrophe or sudden change occurs and the system tends towards A instead. What is more, if μ is now decreased we do not return to the equilibrium at C. The system continues to tend towards A as we are below the dividing point B. This occurs until μ_1^* is passed. Then the system jumps up towards C again. The situation that has been described is known as hysteresis. Occurrences of this phenomenon arise in chapter 4.

In nature there are many unpredictable influences on a system which means that there will be fluctuations around any equilibrium. Notice that the domain of attraction of C is smaller the closer μ is to μ_2^* . This makes the system much more susceptible to crashing towards A as μ_2^* is approached [128].

A.2.12 Limit cycle

Limit cycle behaviour occurs when a *state variable* (such as a population density) oscillates in a regular repetitive manner. Temporal behaviour for a single population is shown in figure A.9(a) and a *phase portrait* for two interdependent cycling populations

is shown in part (b). These diagrams show the eventual or limiting behaviour once the initial transients have died away. A limit cycle is also called a periodic orbit and is often associated with a *Hopf bifurcation*. Limit cycles may be *locally stable* or unstable (see section A.3.4 for more details).

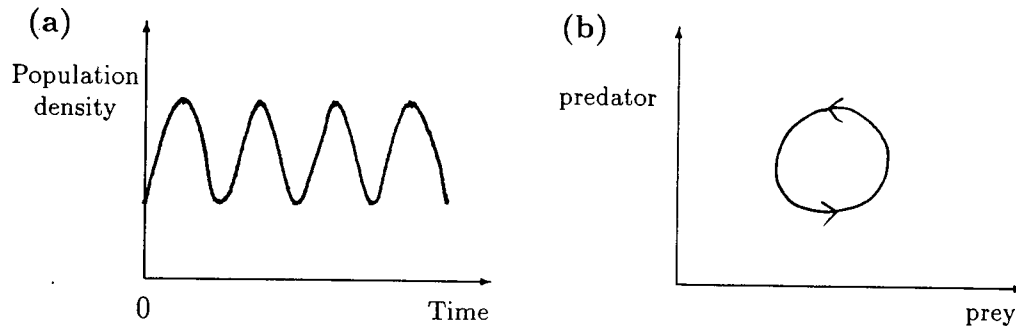


Figure A.9: (a) Time plot and (b) phase portrait of stable limit cycle behaviour.

A.2.13 Limit point

A limit point or saddle-node bifurcation occurs when there are two *equilibrium points* on one side of the *bifurcation point* but none on the other side. Figure A.10(a) shows an example of a *bifurcation diagram* of a limit point (LP). For $\mu < \mu^*$ there are no equilibrium points at which both populations are nonzero. μ^* is thus the limiting value of μ for which equilibrium points exist, hence the name *limit point*. A possible *phase portrait* in two dimensions for $\mu > \mu^*$ is shown in figure A.10(b) for the particular value $\mu = \mu_1$. A is a *locally stable* equilibrium point and B is a *saddle point*. The initial values of x_1 and x_2 determine the subsequent behaviour of the system. If the initial point is in the *domain of attraction* of A (to the right of point B in figure A.10(b)), then the system will approach A. If the initial point lies on the other side of B, however, it will be repelled away from B in the opposite direction to A. Notice how the size of the domain

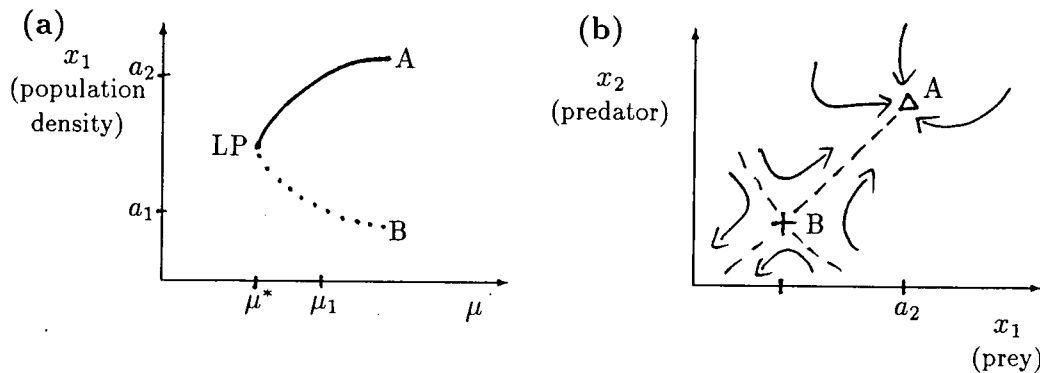


Figure A.10: (a) Bifurcation diagram showing a limit point (LP) and (b) a phase portrait corresponding to $\mu = \mu_1$. For $\mu < \mu^*$ there are no equilibrium points at which both populations are nonzero.

of attraction of A, in terms of the state variable x_1 , decreases as μ decreases towards μ^* (see figure A.10(a)).

The first example of this type of bifurcation in the main body of the thesis occurs in chapter 2.

A.2.14 Local stability

Suppose the system in which we are interested is disturbed slightly from its *equilibrium point*. For example, a week of warmer weather may cause an insect's growth rate to increase slightly. If after the disturbance is removed the system returns to its original equilibrium, then the equilibrium point is said to be *locally stable* and is called an 'attractor'. Otherwise it is said to be *unstable* and is a 'repeller'. Locally stable equilibrium points are called *sinks* and locally unstable ones are called *saddle points* or *sources*.

A.2.15 Parameter

A parameter is a quantity such as a fecundity rate or predation rate which is used in describing the dynamics of a *state variable*. Whereas a state variable evolves with time,

a parameter is kept constant as time progresses. In this thesis parameter values are varied across ranges of values to see how their values affect the *qualitative behaviour* of the state variables. For example, increasing the fecundity rate of a population which is at equilibrium may cause the population to start cycling.

A.2.16 Period-doubling bifurcation

A period-doubling bifurcation occurs when a *limit cycle* undergoes a bifurcation and there is an exchange of stability to cycles having double the period. The situation is depicted graphically in figure A.11. Part (a) shows a *bifurcation diagram* with period-doubling bifurcations at λ_1 and λ_2 , and part (b) shows the behaviour over time for different values of the *parameter* λ . Chapter 4 contains the first examples of this phenomenon in the main body of the thesis.

A.2.17 Phase portrait

Suppose our system has two *state variables*, say a prey (x_1) and a predator (x_2). We can represent the behaviour of *both* populations in a single diagram called a phase portrait. An example is shown on the square base of the diagram in figure A.12. In this example both x_1 and x_2 exhibit oscillations of decreasing amplitude as they approach the stable *equilibrium point*. This translates into an inward spiral in the (x_1, x_2) -phase space.

In this thesis *sinks* are represented by triangles, *saddles* by plus signs, and *sources* by squares. In most cases solid lines are used to denote solution trajectories and dashed lines denote boundaries of *domains of attraction*.

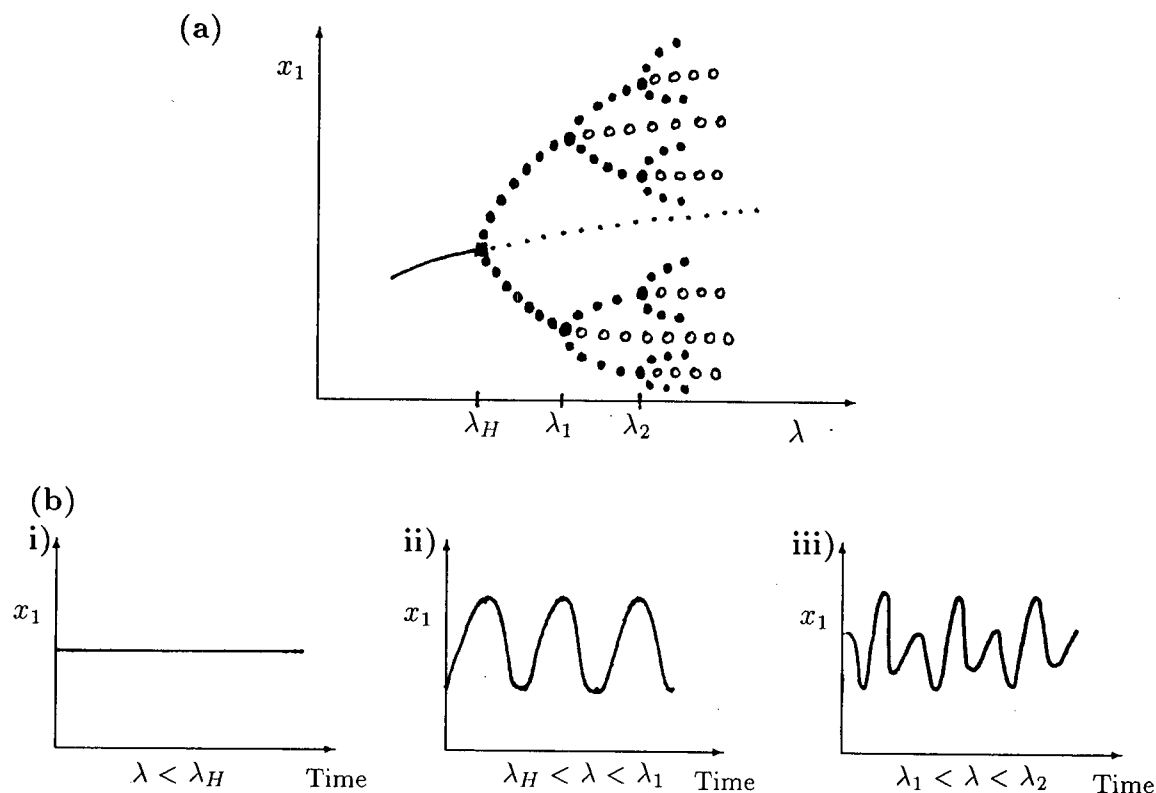


Figure A.11: (a) Period-doubling bifurcations at λ_1 and λ_2 (adapted from [111], p.259). (b) Behaviour over time for the state variable x_1 for (i) $\lambda < \lambda_H$ (stable equilibrium), (ii) $\lambda_H < \lambda < \lambda_1$ (limit cycle) and (iii) $\lambda_1 < \lambda < \lambda_2$ (period-2 cycle—each cycle consists of a big hump and a small hump).

A.2.18 Pitchfork bifurcation

A pitchfork bifurcation occurs when there is a unique *equilibrium point* for *parameter* values on one side of the *bifurcation point* but there are three equilibrium points on the other side. An example is shown in figure A.13. Part (a) shows a *bifurcation diagram* and part (b) gives *phase portraits* for parameter values on either side of the bifurcation point. In the example shown in figure A.13, A is a stable equilibrium point for $\mu < \mu^*$. For $\mu > \mu^*$ A is a *source* and the other two equilibrium points, B and C, are *locally stable*. These stability properties vary from situation to situation but the symmetry is

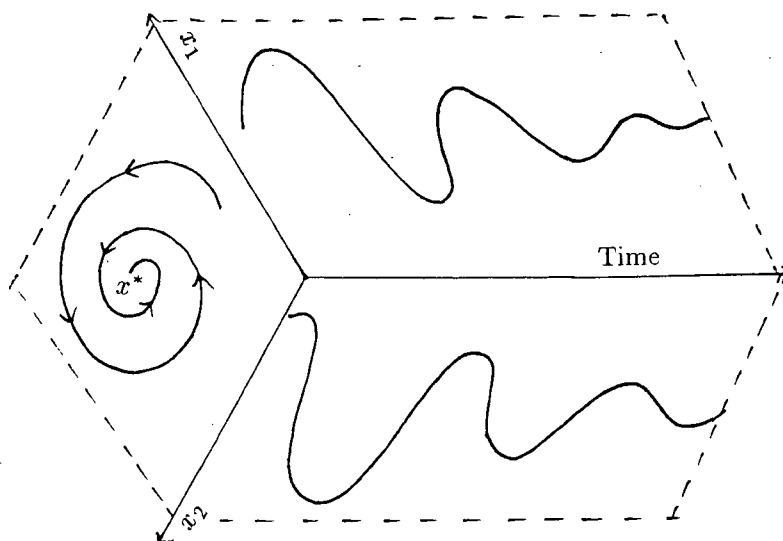


Figure A.12: Derivation of a phase plane showing the time-dependent behaviour of two variables, x_1 and x_2 (adapted from [61], p.3). Damped oscillations over time give rise to an inward spiral in the phase plane.

always maintained, that is, B and C always have the same stability assignment and this assignment is the same as that for A on the opposite side of the bifurcation point, μ^* . For $\mu > \mu^*$ A is a kind of threshold point as it separates the *domains of attraction* of B and C. The initial values of x_1 and x_2 determine whether the system tends towards B or C (see figure A.13(b)(ii)).

No examples of this type of bifurcation occur in this thesis but the above description is included for completeness.

A.2.19 Qualitative behaviour

When we refer to the qualitative behaviour or dynamics of a system we are interested in the long-term general behaviour of the system rather than exact (quantitative) population densities for each instant in time. For example, different types of qualitative

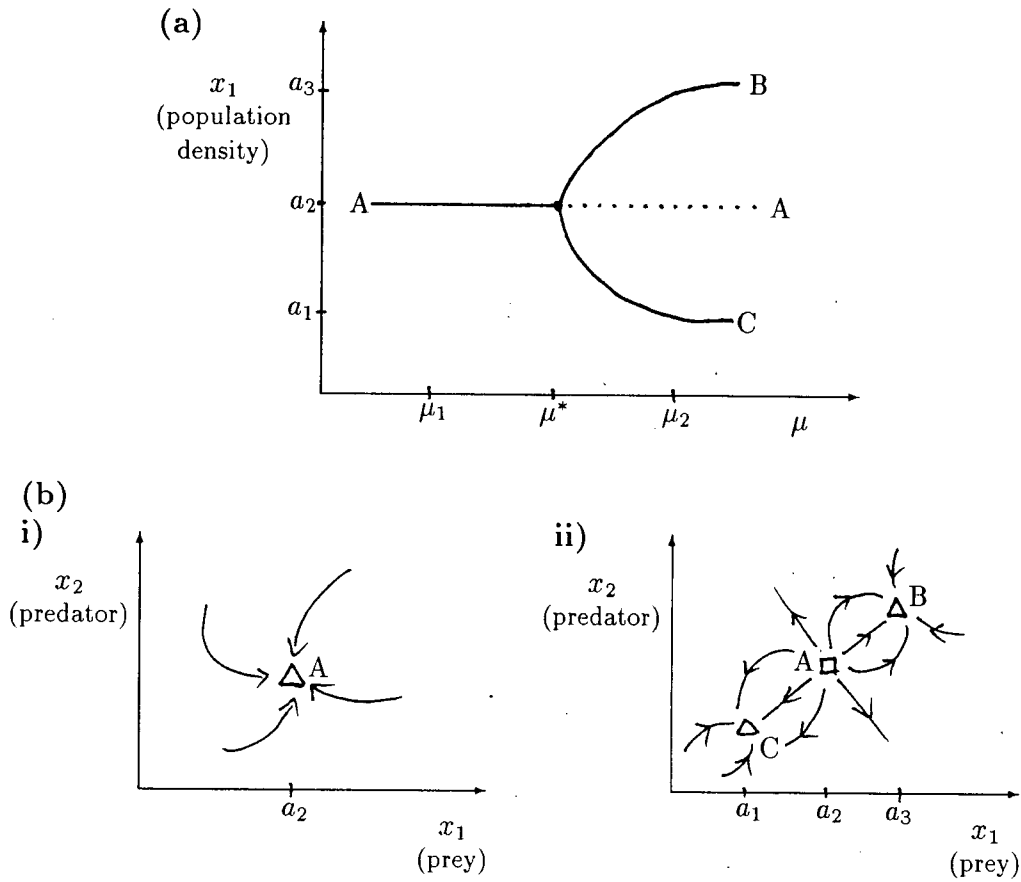


Figure A.13: (a) Bifurcation diagram of a pitchfork bifurcation, (b)(i) a phase portrait corresponding to $\mu = \mu_1$ and (b)(ii) a phase portrait corresponding to $\mu = \mu_2$. In (b)(ii) the unstable manifolds from A divide up the domains of attraction for B and C.

behaviour include a population declining to extinction, a population tending towards a stable *equilibrium point*, or a population undergoing *limit cycle* oscillations. Thus, qualitative behaviour is determined by the presence and nature of attractors (see section A.2.5).

A.2.20 Saddle point

A saddle point is an *equilibrium point* which attracts in certain directions and repels in others. In figure A.14 the equilibrium point has an unstable manifold (see page 241) and a stable manifold as indicated by the dashed lines. Initial points lying on these manifolds are repelled from or attracted towards the equilibrium point respectively. Other initial points may first be attracted and then repelled as shown by the solid lines.

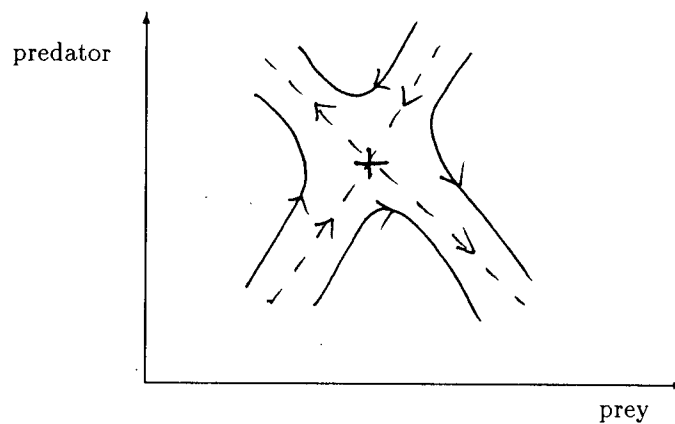


Figure A.14: Example of a saddle point (plus sign) and the associated dynamics. Stable and unstable manifolds are indicated by the dashed lines and solution trajectories from different initial points by the solid lines.

A.2.21 Sink

A sink is a *locally stable equilibrium point*. A sink may be either a stable node or a spiral attractor. *Phase portraits* and time plots corresponding to these two possibilities are shown in figures A.15(a) and A.15(b) respectively. The time plots begin at the point marked with a * in the phase portraits.

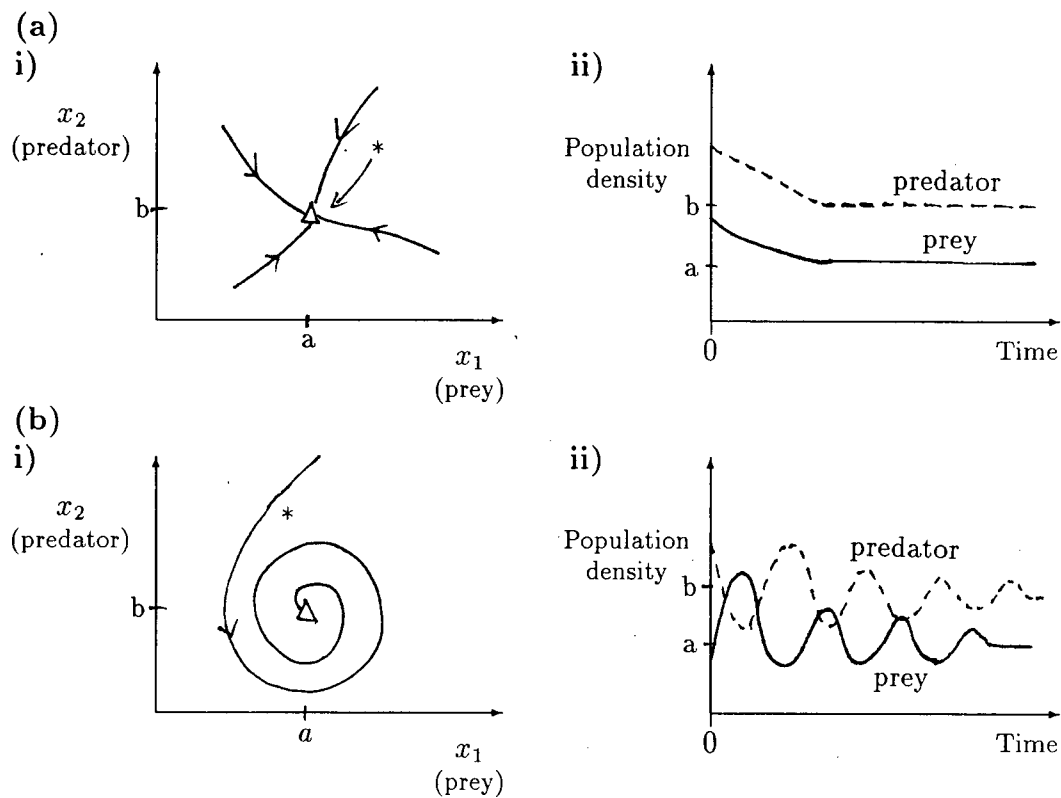


Figure A.15: (a)(i) Phase portrait of a stable node and (a)(ii) time plots starting at point $*$ in (a)(i). (b)(i) Phase portrait of a spiral attractor and (b)(ii) time plots starting at point $*$ in (b)(i).

A.2.22 Soft loss of stability

For a *Hopf bifurcation* this occurs when there is a continuous change from stable *equilibrium* behaviour to *limit cycles* of small amplitude. The amplitude of these cycles increases gradually for *parameter* values further from the Hopf bifurcation. Figure A.6(a) gives an example of soft loss of stability. See also section A.2.7. The first example of this phenomenon in the main body of the thesis occurs in chapter 2.

A.2.23 Source

A source is an *equilibrium point* which is *locally unstable*. Any disturbance to the system will cause the *state variables* to move away from this point. An unstable node and a spiral repeller are shown in figures A.16(a) and A.16(b) respectively. Both are examples of sources.

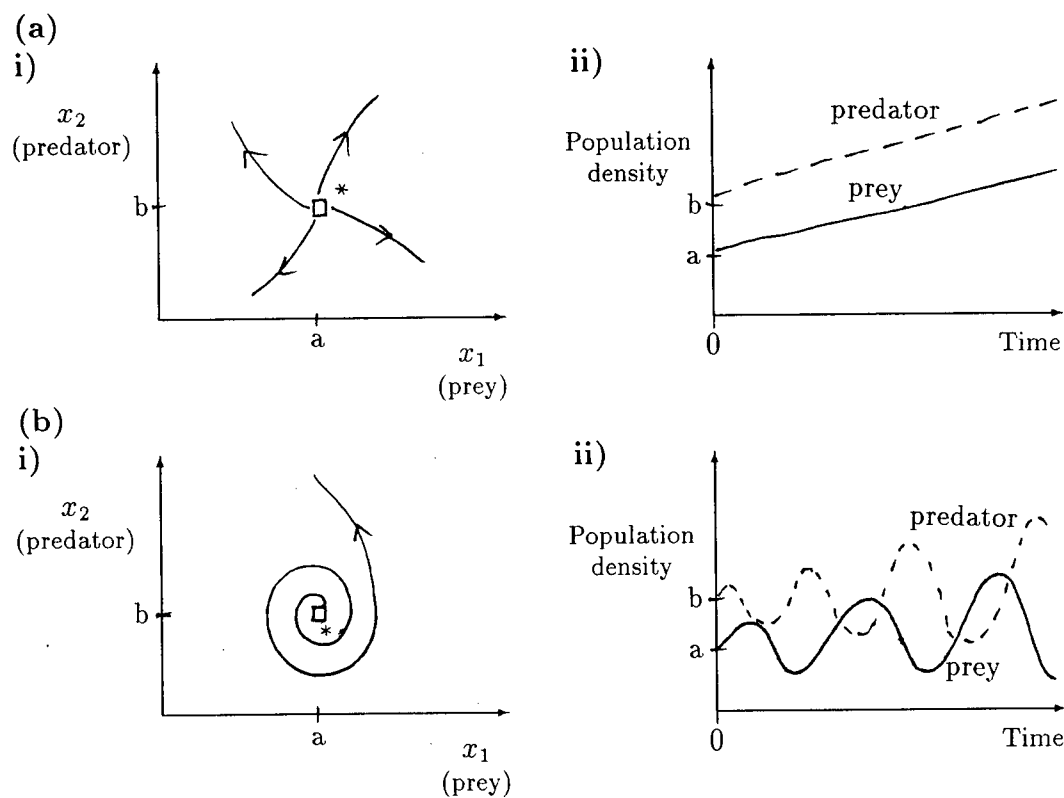


Figure A.16: (a)(i) Phase portrait of an unstable node and (a)(ii) time plots starting at point $*$ in (a)(i). (b)(i) Phase portrait of a spiral repeller and (b)(ii) time plots starting at point $*$ in b(i).

A.2.24 State variable

Suppose we are interested in a system consisting of plants, herbivores and predators. Then the 'state' of the system can be described by the relative biomasses or densities of

these populations. The variables that are used in a mathematical model of the system to represent these biomasses or densities are called state variables.

A.2.25 Transcritical bifurcation

At a transcritical *bifurcation point* two *equilibrium points* coincide and exchange stabilities. An example is shown in figure A.17. There are two equilibrium points, A and B,

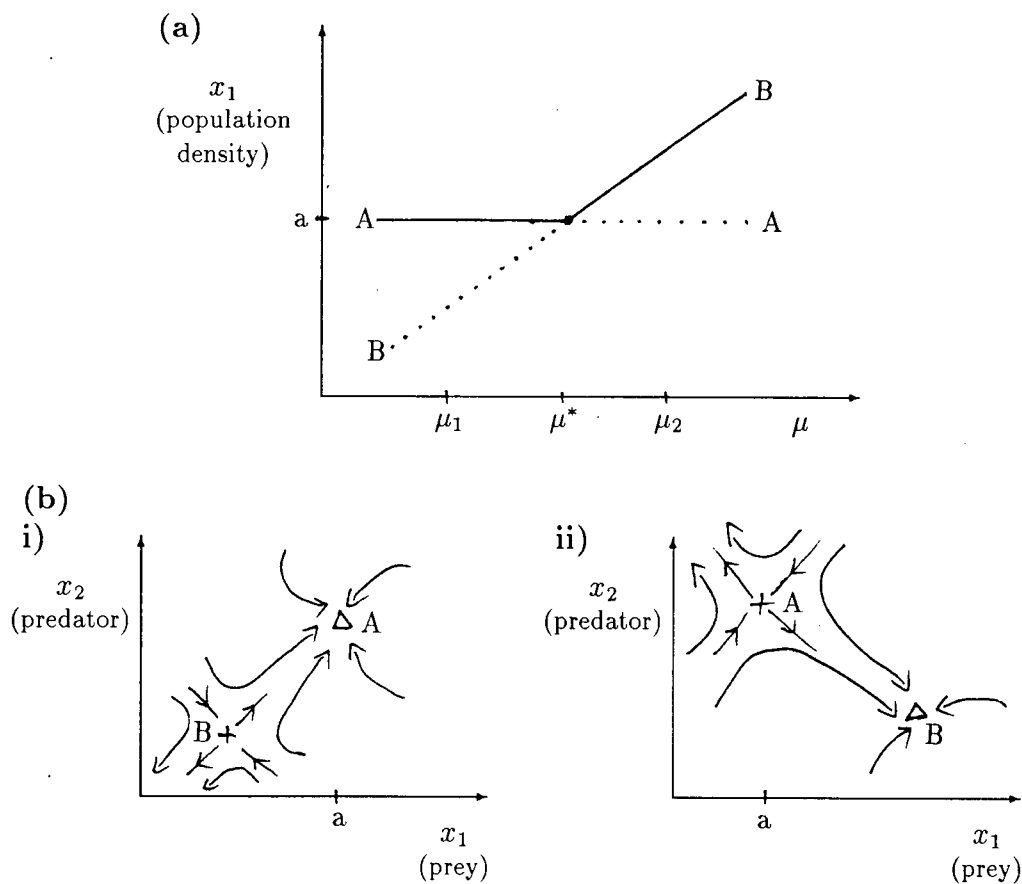


Figure A.17: (a) A bifurcation diagram of a transcritical bifurcation, (b)(i) a phase portrait corresponding to $\mu = \mu_1$ and (b)(ii) a phase portrait corresponding to $\mu = \mu_2$. The stabilities of the two equilibrium points interchange for parameter values on either side of the bifurcation point.

at each value of the *parameter* μ . A is stable for $\mu < \mu^*$ and a *saddle point* for $\mu > \mu^*$.

The situation is reversed for B. Figures A.17(b)(i) and A.17(b)(ii) show possible *phase portraits* in two dimensions for $\mu = \mu_1$ and $\mu = \mu_2$ respectively. Note that the *bifurcation diagram* in figure A.17(a) only indicates the positions of the equilibrium points in terms of one of the *state variables*, x_1 . Chapter 2 contains an example of this type of bifurcation.

A.3 Some mathematical details

A.3.1 Introduction

This section gives a brief introduction to some of the mathematical details of dynamical systems theory. Texts such as [49, 57, 111, 124, 128] give more complete expositions.

For most of the section I will assume that the model under study consists of a system of m ordinary differential equations of the form:

$$\dot{\mathbf{x}} = \mathbf{f}(\mathbf{x}) \quad (\text{A.1})$$

where \mathbf{x} is a vector of m state variables and the dot denotes differentiation with respect to time, that is, $\dot{\mathbf{x}} = \frac{d\mathbf{x}}{dt}$. For example, if we were studying a predator-prey model then we would have $m = 2$ and equation (A.1) in expanded form would be

$$\begin{aligned} \dot{x}_1 &= f_1(x_1, x_2) \\ \dot{x}_2 &= f_2(x_1, x_2) \end{aligned}$$

where f_1 and f_2 are the components of \mathbf{f} representing the dynamics of x_1 (prey density, say) and x_2 (predator density), respectively.

The results for systems of difference equations (discrete models) of the form:

$$\mathbf{x} \mapsto \mathbf{f}(\mathbf{x}) \quad (\text{A.2})$$

or

$$\mathbf{x}_{t+1} = \mathbf{f}(\mathbf{x}_t), \quad t = 0, 1, 2, \dots \quad (\text{A.3})$$

are very similar. Section A.3.5 highlights some of the differences.

A.3.2 Equilibrium points and local stability

An equilibrium point (fixed point) \mathbf{x}^* of the system of equations (A.1) satisfies

$$\mathbf{f}(\mathbf{x}^*) = \mathbf{0}.$$

If system (A.1) were to start at \mathbf{x}^* at time zero, it would remain there for all time. However, in nature it is very unlikely that a system will remain exactly at an equilibrium point since numerous factors perturb systems continually. So we would like to know whether solutions of the system of equations (A.1) starting near \mathbf{x}^* move towards or away from \mathbf{x}^* as time progresses. That is, we would like to determine the local stability behaviour near \mathbf{x}^* .

We can sometimes do this by using a linearised analysis². We begin by perturbing the system slightly from \mathbf{x}^* . That is, we replace \mathbf{x} by $\mathbf{x}^* + \mathbf{u}$ in equation (A.1) where \mathbf{u} is a small perturbation. (We use a *small* perturbation since we are investigating the *local* behaviour near the equilibrium point.) Our new vector of state variables is \mathbf{u} since \mathbf{x}^* is fixed. Expanding \mathbf{f} in a Taylor series about \mathbf{x}^* and neglecting nonlinear terms in \mathbf{u} (since \mathbf{u} is small) we obtain the linearised system

$$\dot{\mathbf{u}} = \mathbf{A}\mathbf{u}$$

where \mathbf{A} is the matrix of first order partial derivatives of \mathbf{f} evaluated at the equilibrium point $\mathbf{x} = \mathbf{x}^*$.

By solving the characteristic equation of \mathbf{A} we obtain m numbers, $\lambda = (\lambda_1, \dots, \lambda_m)$, known as the eigenvalues of \mathbf{A} . Eigenvalues may be real numbers or complex numbers. It is these eigenvalues which determine the local stability properties of \mathbf{x}^* . If all the

²More detailed introductions to linear analysis can be found in [34, 128].

eigenvalues of \mathbf{A} have non-zero real parts³ then \mathbf{x}^* is said to be a *hyperbolic* equilibrium point of (A.1). If any eigenvalue has a zero real part then \mathbf{x}^* is said to be a *nonhyperbolic* equilibrium point. The local stability behaviour near hyperbolic equilibrium points is relatively easy to determine. Nonhyperbolic equilibrium points are more difficult to classify but it is at these points that interesting bifurcations (see section A.2.2) occur. Let us consider hyperbolic equilibrium points first.

Hyperbolic equilibrium points

If the real part of λ is negative (that is, $\Re\lambda < 0$) for *all* eigenvalues λ of \mathbf{A} , then \mathbf{x}^* is an asymptotically stable equilibrium point of (A.1) (that is, trajectories starting near \mathbf{x}^* move towards \mathbf{x}^* as time progresses). If $\Re\lambda > 0$ for *any* eigenvalue λ of \mathbf{A} , then \mathbf{x}^* is said to be unstable. In the special case of a two-dimensional system ($m = 2$ in (A.1)) even more information can be obtained about the behaviour near

$$\mathbf{x}^* = \begin{pmatrix} x_1^* \\ x_2^* \end{pmatrix}.$$

In this case there are two (since $m = 2$) eigenvalues, λ_1 and λ_2 , of \mathbf{A} . They satisfy the equation

$$\lambda_{1,2} = \frac{\text{Tr}\mathbf{A} \pm \sqrt{(\text{Tr}\mathbf{A})^2 - 4\text{Det}\mathbf{A}}}{2}$$

where $\text{Tr}\mathbf{A}$ = trace of \mathbf{A} = the sum of the diagonal elements of \mathbf{A} and $\text{Det}\mathbf{A}$ = determinant of \mathbf{A} . In two-dimensional cases we can represent the behaviour near \mathbf{x}^* using a phase portrait (see section A.2.17). The various possibilities are summarised in figure A.18. Alternatively, the results can be summarised as follows:

³A complex number, λ , has a real part, $\Re\lambda$, and a complex or imaginary part, $\Im\lambda$. For a brief introduction to the relevant theory of complex numbers see the appendix in [128].

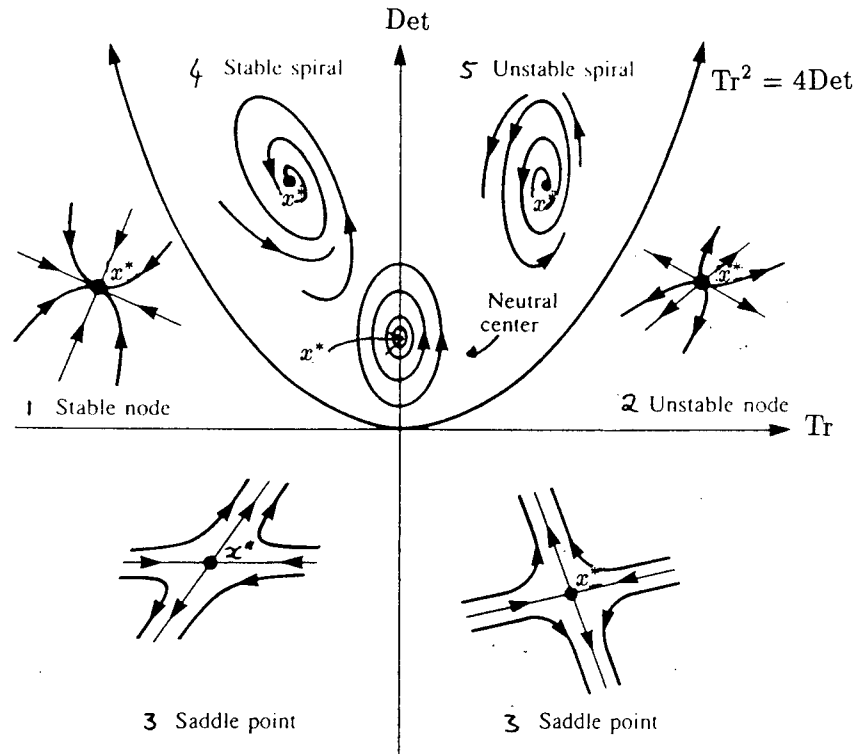


Figure A.18: A summary of the local stability behaviour near an equilibrium point, \mathbf{x}^* , of (A.1) when $m = 2$ (adapted from [34], p.190).

λ_1, λ_2 real

- $\lambda_1 < 0, \lambda_2 < 0 \Rightarrow \mathbf{x}^*$ is a stable node (region 1 in figure (A.18))
- $\lambda_1 > 0, \lambda_2 > 0 \Rightarrow \mathbf{x}^*$ is an unstable node (region 2 in figure (A.18))
- $\lambda_1 > 0, \lambda_2 < 0$ (or vice versa) $\Rightarrow \mathbf{x}^*$ is a saddle point (region 3).

λ_1, λ_2 complex

- $\Re\lambda_1 < 0, \Re\lambda_2 < 0 \Rightarrow$ stable spiral or focus (region 4)
- $\Re\lambda_1 > 0, \Re\lambda_2 > 0 \Rightarrow$ unstable spiral or focus (region 5).

Saddle points and sources are both unstable equilibrium points (see section A.2.14) but a saddle point differs from a source in that solutions may be attracted towards it for a while before being repelled, depending on the initial values of the variables (see region 3 in figure A.18). In the case $m = 2$ a saddle point has one unstable eigenvalue while a source has two. This means that (for $m = 2$) a saddle point has one stable *manifold* and one unstable *manifold* associated with it. These manifolds are curves in phase space such that initial points on these curves are attracted towards the saddle point (for initial points on the stable manifold) or repelled away from the saddle point (for points on the unstable manifold) (see region 3 in figure A.18).

Nonhyperbolic equilibrium points

As mentioned earlier it is the nonhyperbolic equilibrium points that are associated with bifurcations, that is, with changes in the qualitative behaviour of the system of equations. There will be a threshold value at which the change in behaviour occurs—the bifurcation value. This value corresponds to (at least) one eigenvalue (or its real part) passing through zero as it changes sign from negative to positive or vice versa. Examples of bifurcations can be found in sections A.2.10, A.2.13, A.2.16, A.2.18, A.2.25.

For nonhyperbolic equilibrium points the principle of linearised stability used above does not apply and other methods need to be used. Two of these are centre manifold theory and normal form theory. Centre manifold theory reduces or simplifies the system of equations so that only those parts which affect the local dynamics near the bifurcation point remain. Normal form theory uses systematic coordinate changes to transform this reduced system of equations into a ‘normal form’. The behaviour corresponding to a number of normal forms has already been classified by various mathematicians and can be found in most dynamical systems texts. The abovementioned examples have all been

classified using normal form theory. Another method due to Liapunov is described in Wiggins [124].

One-parameter local bifurcations Suppose that the system of equations (A.1) has the form

$$\dot{\mathbf{x}} = \mathbf{f}(\mathbf{x}, \mu) \quad (\text{A.4})$$

where μ is a parameter⁴ and suppose that the equilibrium point \mathbf{x}^* undergoes a bifurcation at $\mu = \mu^*$. (We assume initially that there is only one zero eigenvalue or one pair of complex conjugate eigenvalues with zero real parts—the greater the number of zero eigenvalues associated with a bifurcation point the more degenerate it is and the more complicated the dynamics associated with it.) Such a bifurcation point is called a one-parameter local bifurcation. Examples of bifurcation points having one zero eigenvalue include limit point (see section A.2.13), pitchfork (see section A.2.18), and transcritical (see section A.2.25) bifurcations. A Hopf bifurcation (see section A.2.10) is also a one-parameter bifurcation but it has one pair of complex conjugate eigenvalues whose real parts are zero.

Two-parameter local bifurcations Suppose we allow two parameters in our model to vary, that is,

$$\dot{\mathbf{x}} = \mathbf{f}(\mathbf{x}, \mu, \lambda) \quad (\text{A.5})$$

where μ and λ are parameters. With two parameters more complex behavioural patterns such as hysteresis, which is described in section A.2.11, are possible.

The extent of the region of overlap in figure A.8 (that is, the difference $\mu^*_2 - \mu^*_1$) may vary with a second parameter, λ , as shown in the *two-parameter* bifurcation diagram

⁴Typically a system of equations has more than one parameter but we only need to consider one of these explicitly at the present time. We assume that the values of any other parameters are fixed.

in figure A.19(a). Part (b) of this figure shows *one-parameter* bifurcation diagrams

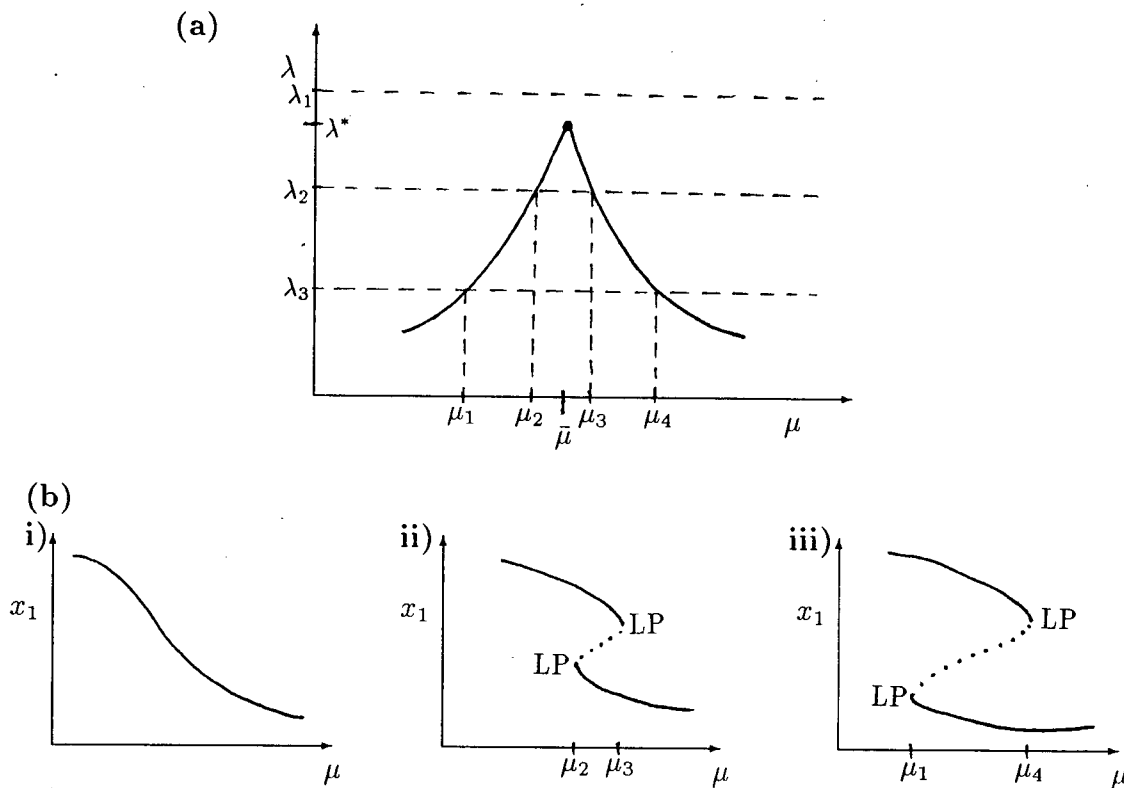


Figure A.19: (a) Two-parameter bifurcation diagram showing a cusp point and the positions of the two limit points associated with the hysteresis as both μ and λ are varied. (b) One-parameter bifurcation diagrams corresponding to different, fixed values of λ in part (a) and with μ as the bifurcation parameter. (i) $\lambda = \lambda_1$, (ii) $\lambda = \lambda_2$ and (iii) $\lambda = \lambda_3$. These one-parameter bifurcation diagrams correspond to the horizontal dashed lines in part (a).

corresponding to different values of λ (that is, corresponding to the horizontal dashed lines in part (a)). At $\lambda = \lambda_1$ the equilibrium point does not undergo any bifurcations in behaviour. For $\lambda = \lambda_2$ the two limit points are close together and for $\lambda = \lambda_3$ they are further apart. The point $(\mu, \lambda) = (\bar{\mu}, \lambda^*)$ is called a *cusp point*. At this point the two limit points coincide. The curves in figure A.19(a) thus show how the positions of the limit points (*bifurcation points*) vary with μ and λ . Compare this with *one-parameter*

bifurcation diagrams which show how the positions of *equilibrium* points vary as a single parameter changes.

A.3.3 Global bifurcations

So far we have been looking at the local dynamics associated with bifurcations of equilibrium points and limit cycles. However, some dynamical properties cannot be deduced from local information [49]. These are called *global* properties. The simplest situation involves homoclinic and heteroclinic orbits.

Suppose we have two equilibrium points and let μ be the bifurcation parameter. Phase portraits of two possible degenerate situations that can arise are shown in figure A.20. In

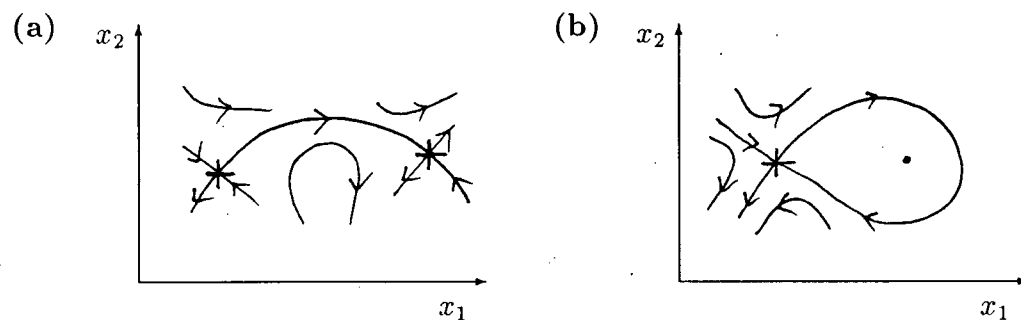


Figure A.20: (a)Phase portrait of a saddle connection or heteroclinic orbit. (b)Phase portrait of a saddle loop or homoclinic orbit.

part (a) of this figure a heteroclinic orbit joins two saddle points. That is, the unstable manifold of one saddle point coincides with the stable manifold of the other saddle point. In (b) the stable and unstable manifolds of the *same* saddle point coincide and encircle the other equilibrium point. The dynamics associated with the second equilibrium point vary depending on the model equations.

The situations in figure A.20 are degenerate. That is, they only exist for a particular value of μ . Almost any small perturbation will disrupt the coincidence of the stable and

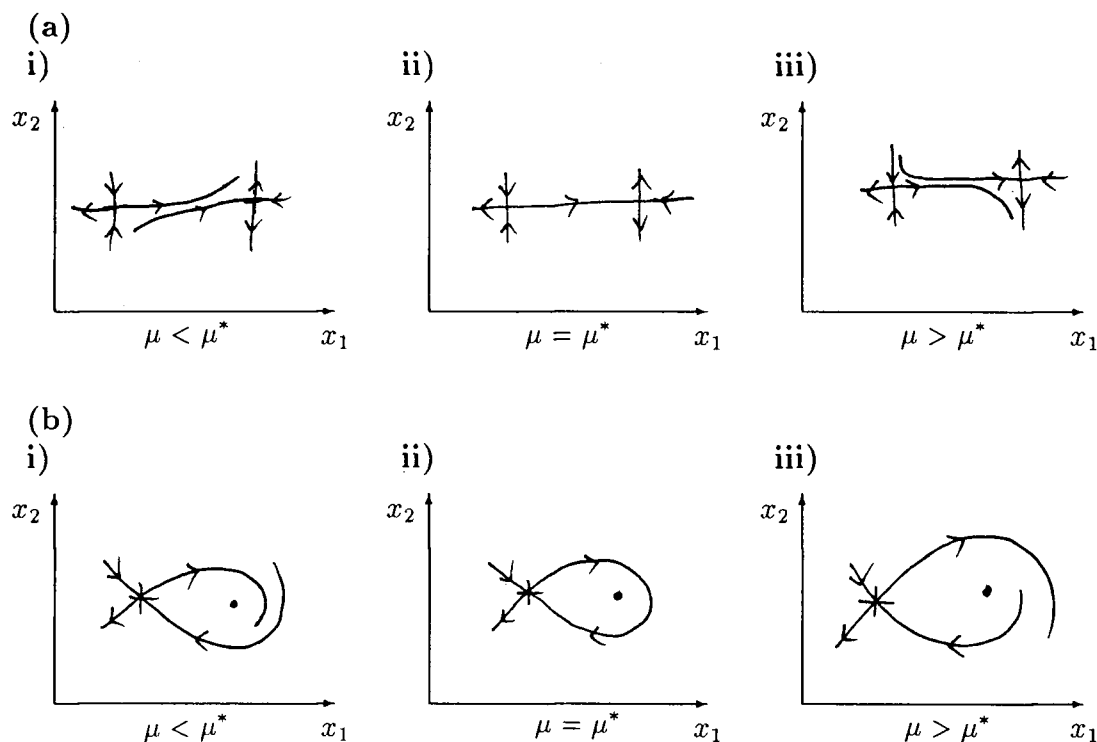


Figure A.21: (a)Phase portraits for parameter values near a saddle connection or heteroclinic orbit. (b)Phase portraits for parameter values near a saddle loop or homoclinic orbit. (i) $\mu < \mu^*$, (ii) $\mu = \mu^*$ and (iii) $\mu > \mu^*$. (μ^* is the point at which the heteroclinic or homoclinic orbit occurs.)

unstable manifolds. In figure A.21 we see what happens to the stable and unstable manifolds when μ is perturbed from the bifurcation point, μ^* . The reader may be wondering what happens near the second equilibrium point in part (b) of this figure. Some examples of possible phase portraits are shown in figure A.22.

An important point to note is that the time period required to get from one saddle point to the other along a heteroclinic orbit, or to return to the same saddle point along a homoclinic orbit, is infinite. This has important consequences for practical studies as can be seen in chapter 2 (section 2.4).

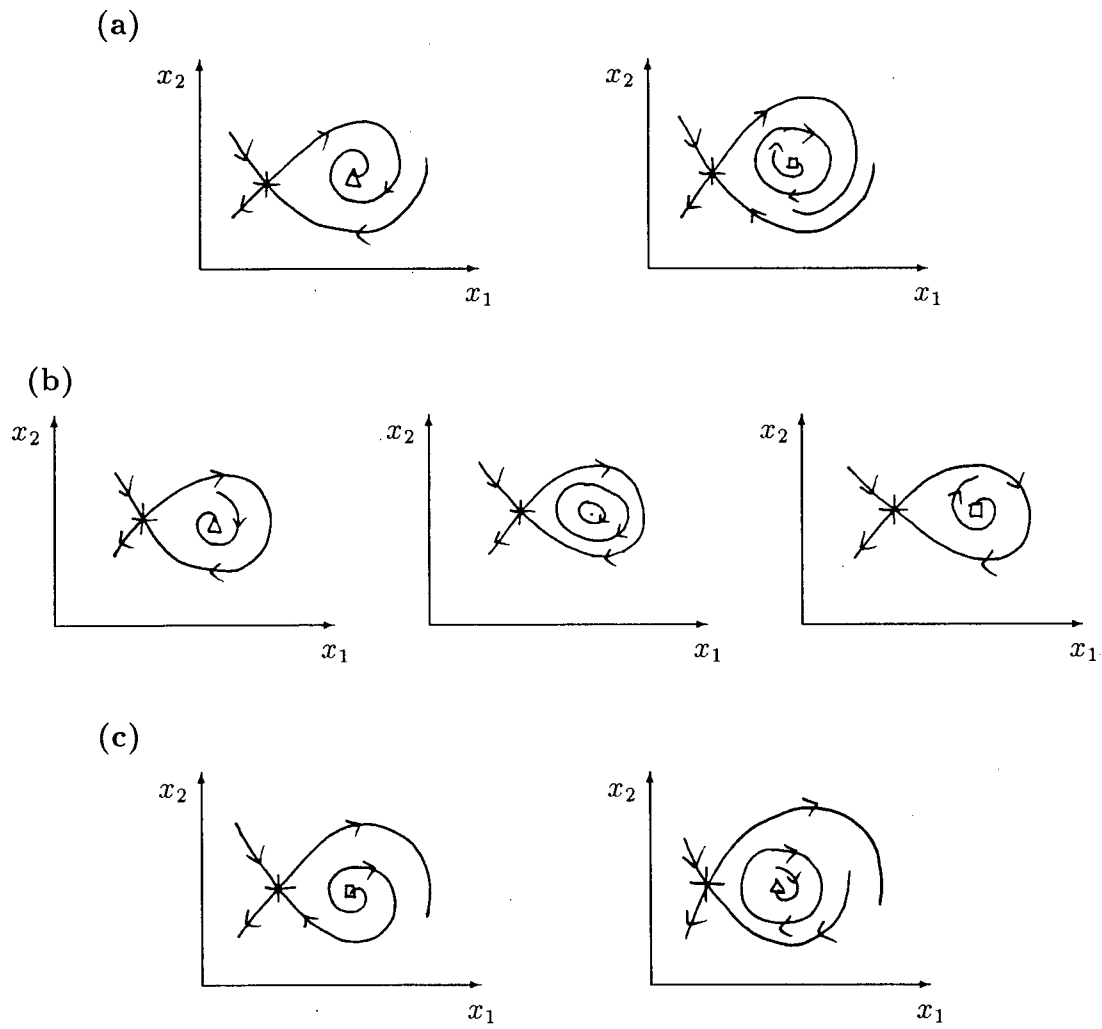


Figure A.22: Phase portraits near a saddle loop or homoclinic orbit showing possible behaviour near the second equilibrium point.

A.3.4 Periodic orbits

Local stability

So far we have discussed equilibrium points and the stability behaviour associated with them. The concept of a Hopf bifurcation introduced the idea of periodic orbits or limit cycles. Cycles have been studied in many biological settings (for example, the spruce budworm [74], nerve action potentials [58], glycolysis [47], cellular slime mold [108], predator-prey interactions [14]). An important aspect is whether the periodic orbits exhibited by a system of equations are locally stable or unstable. For this purpose I introduce the concept of Poincaré maps. However, only the main results are presented here. More detailed discussions can be found in [49] and [124].

In general⁵, a Poincaré section S is an $(m - 1)$ -dimensional hypersurface chosen so that all trajectories of (A.1) a) intersect the hypersurface transversally, and b) cross the hypersurface in the same direction. In particular, the limit cycle passes through the hypersurface transversally at a particular point, \mathbf{q}^* . Figure A.23 shows a periodic orbit in three dimensions and a two-dimensional Poincaré section, S . The periodic orbit intersects S at the point \mathbf{q}^* .

If T is the period of the limit cycle and $\varphi(t; \mathbf{z})$ is a solution of (A.1) starting at \mathbf{z} (that is, satisfying the initial condition $\mathbf{x}(0) = \mathbf{z}$), then

$$\mathbf{q}^* = \varphi(T; \mathbf{q}^*).$$

Let \mathbf{q} be a point on S and let $T_\varphi(\mathbf{q})$ be the time taken for a trajectory $\mathbf{x}(t; \mathbf{q})$ to first return to S . Then the Poincaré map or first return map $\mathbf{P}(\mathbf{q})$ is defined by

$$\mathbf{P}(\mathbf{q}) = \varphi(T_\varphi(\mathbf{q}); \mathbf{q}).$$

This is illustrated in figure A.23. Note that $\mathbf{P}(\mathbf{q}^*) = \mathbf{q}^*$ and $T_\varphi(\mathbf{q}^*) = T$.

⁵The following is summarised from [111].

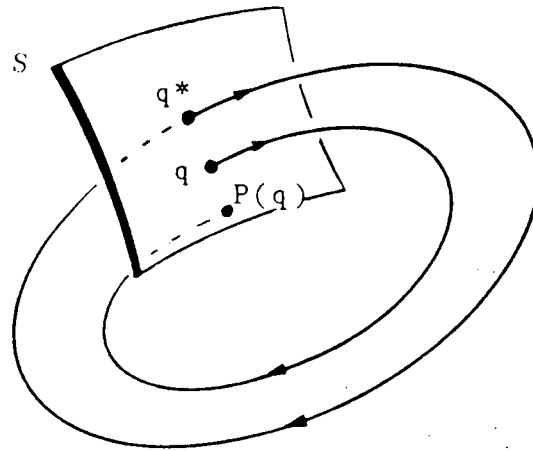


Figure A.23: Schematic representation of a Poincaré section and a limit cycle in three dimensions (from [111], p.244). \mathbf{q}^* is a point on S that lies on the limit cycle. \mathbf{q} is another point on S and $\mathbf{P}(\mathbf{q})$ is its point of first return to S .

In order to determine the stability of the periodic orbit, we need only investigate the behaviour of \mathbf{P} near its equilibrium point \mathbf{q}^* . That is, we need to determine whether this equilibrium point is attracting or repelling. As in section A.3.2 we linearise \mathbf{P} about the equilibrium point \mathbf{q}^* . In this case $\mathbf{A} = \frac{\partial \mathbf{P}(\mathbf{q}^*)}{\partial \mathbf{q}}$. Stability is again related to the eigenvalues of \mathbf{A} but the conditions are slightly different as we are dealing with a map (discrete system) here and not a continuous system such as (A.1). We have the following result (see [111]): a) If the moduli of all the eigenvalues are smaller than 1, then \mathbf{q}^* is stable; b) If the modulus of at least one eigenvalue is larger than 1, then \mathbf{q}^* is unstable.

It turns out that the eigenvalues of $\mathbf{A} = \frac{\partial \mathbf{P}(\mathbf{q}^*)}{\partial \mathbf{q}}$ can be found from the eigenvalues of the matrix

$$\mathbf{M} = \frac{\partial \varphi(T; \mathbf{q}^*)}{\partial \mathbf{z}}.$$

The matrix \mathbf{M} always has an eigenvalue equal to 1. It can be shown that the remaining $(m - 1)$ eigenvalues are the eigenvalues of $\mathbf{A} = \frac{\partial \mathbf{P}(\mathbf{q}^*)}{\partial \mathbf{q}}$. The eigenvalues of \mathbf{M} are called *Floquet multipliers*. Analogous to the discussion on equilibrium points of (A.1), the

stability of a periodic orbit can be determined by calculating the Floquet multipliers. These are easier to find than the eigenvalues of \mathbf{A} . In general, in the vicinity of a Hopf bifurcation, unstable periodic orbits encircle stable equilibrium points and stable periodic orbits encircle unstable equilibrium points however there are some other possibilities. A few cases are shown in figure A.24. Both the minima and maxima of the periodic orbits

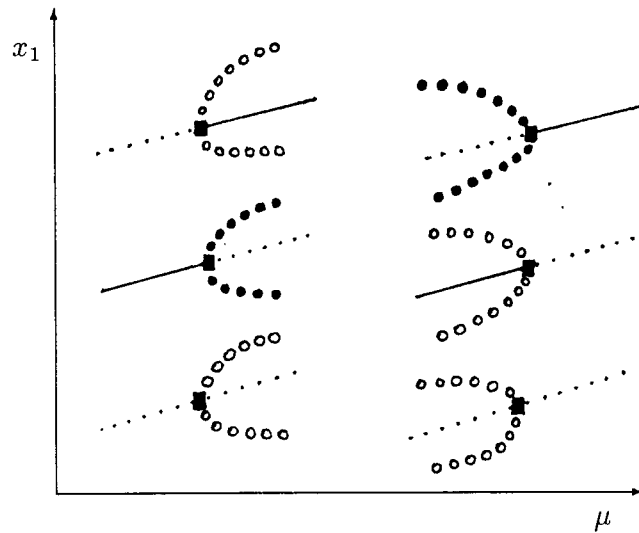


Figure A.24: Examples of Hopf bifurcations having soft loss of stability (adapted from [111], p.72).

are shown.

Figure A.24 gives examples of *soft* loss of stability or *soft* generation of limit cycles (see section A.2.22). Section A.2.7 gives an example of *hard* loss of stability or *hard* generation of limit cycles.

Bifurcations of periodic orbits

The above discussion has focussed on local stability near a Hopf bifurcation. It is also possible for the periodic orbits themselves to undergo stability changes. These occur when the Poincaré map undergoes bifurcations. If the Poincaré map undergoes a simple

bifurcation, then there may be an exchange of stability of the periodic orbit from stable to unstable or vice versa. If the Poincaré map \mathbf{P} has an eigenvalue of -1 at the bifurcation point μ^* then the second iterate of the map, $\mathbf{P}^2 = \mathbf{P}(\mathbf{P})$, undergoes a bifurcation. We call this a period-doubling or flip bifurcation. At this point there is an exchange of stability of the periodic orbits to orbits having double the period. The situation is depicted in figure A.11.

Period-doubling occurs in many situations such as chemical reactions, nerve models, the Navier-Stokes equations and ecological models involving three trophic levels. (Period-doubling does not occur in fewer than three dimensions for continuous systems, that is, $m \geq 3$ is required.) In some cases a sequence of period-doublings may occur and this may lead to chaotic behaviour (see section A.2.3).

Another way in which a periodic orbit may exchange stability is through bifurcation into a torus (Hopf bifurcation of the corresponding Poincaré map). This occurs when a complex pair of Floquet multipliers moves into or out of the unit circle. Again $m \geq 3$ is required. Details of this can be found in [111, 124]. From a practical point of view it is probably more informative to return to generating numerical solutions of a model over time when these complicated phenomena are encountered in a bifurcation analysis so that the behaviour of the system near these points can be seen explicitly. I will not present the mathematical details of these bifurcations here.

Chaos

A brief description of chaos was given in section A.2.3. Further mathematical details can be found in [11, 16, 124, 128]. Currently there is wide debate as to the practical application of chaos. In ecological systems it is very difficult (probably impossible) to distinguish between stochastic noise and chaotic behaviour (see the preface in [72]). In Stone [114] it is shown that the addition of a single small term to a logistic type model

removes the chaotic behaviour. However, in [82, 84] it is demonstrated that chaos is prevalent in many discrete ecological models and that higher order systems display chaotic behaviour more readily than one-dimensional systems. A good overview of the current debate is given in the collection of papers in [72].

A.3.5 Maps (systems of difference equations)

The discussion so far has been restricted to models consisting of systems of ordinary differential equations. A very similar theory can be developed for maps given by (A.2) or (A.3). I will briefly mention some of the differences that occur. More detailed discussions can be found in [124, 128].

Referring to equations (A.2) and (A.3), an equilibrium point occurs when

$$\mathbf{f}(\mathbf{x}) = \mathbf{x}$$

or

$$\mathbf{x}_{t+1} = \mathbf{x}_t.$$

A linear stability analysis can again be done for hyperbolic equilibrium points. For maps a hyperbolic equilibrium point is one for which none of the eigenvalues of the matrix of partial derivatives has unit modulus (that is, no eigenvalues have a magnitude of 1). Again it is the nonhyperbolic equilibrium points which result in interesting bifurcations.

If the linearised matrix has a single eigenvalue equal to 1 then a limit point, transcritical or pitchfork bifurcation may occur. The bifurcation diagrams are the same as for continuous models. However, it must be remembered that the 'phase portraits' or diagrams in state space consist of discrete points rather than continuous curves. Examples corresponding to a spiral sink are shown in figure A.25. Consecutive points are labelled in the discrete case.

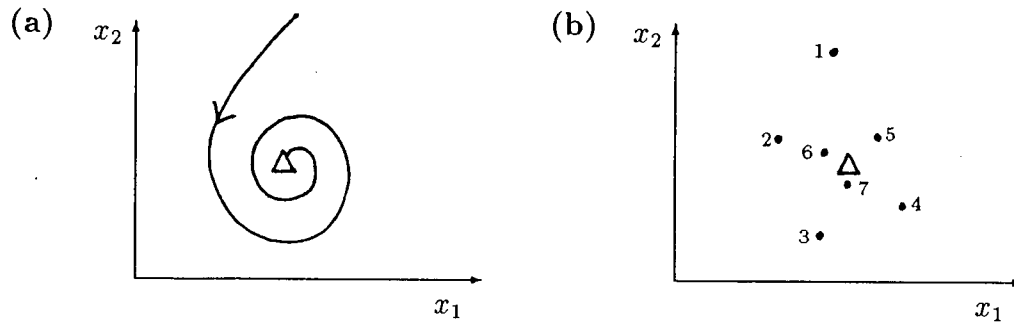


Figure A.25: State space diagrams of a spiral sink for (a) a continuous model and (b) a discrete model.

For maps the special case of a single eigenvalue equal to -1 introduces another type of bifurcation called a *period-doubling bifurcation*. Figure A.26(a) shows a stable equilibrium point undergoing a period-doubling bifurcation to become a stable period-2 orbit as μ is increased. This period-2 orbit undergoes a further period-doubling to produce a stable period-4 orbit. Figure A.26(b) gives examples of diagrams in state space corresponding to these situations. Notice that this situation is analogous to the period-doublings of periodic orbits for continuous models. This is not surprising since that theory is based on Poincaré maps which are discrete.

It is important to note that periodic orbits for discrete systems are different from those for continuous systems. In particular they have integral periods. Consider the second iterate, \mathbf{f}^2 , of the map (A.3):

$$\mathbf{f}^2(\mathbf{x}_t) = \mathbf{f}(\mathbf{f}(\mathbf{x}_t)) = \mathbf{f}(\mathbf{x}_{t+1}) = \mathbf{x}_{t+2}.$$

In general, the k^{th} iterate of the map is given by

$$\mathbf{f}^k(\mathbf{x}_t) = \mathbf{x}_{t+k}.$$

Suppose there exists a value of \mathbf{x} , $\hat{\mathbf{x}}$, such that

$$\mathbf{f}^k(\hat{\mathbf{x}}) = \hat{\mathbf{x}}$$

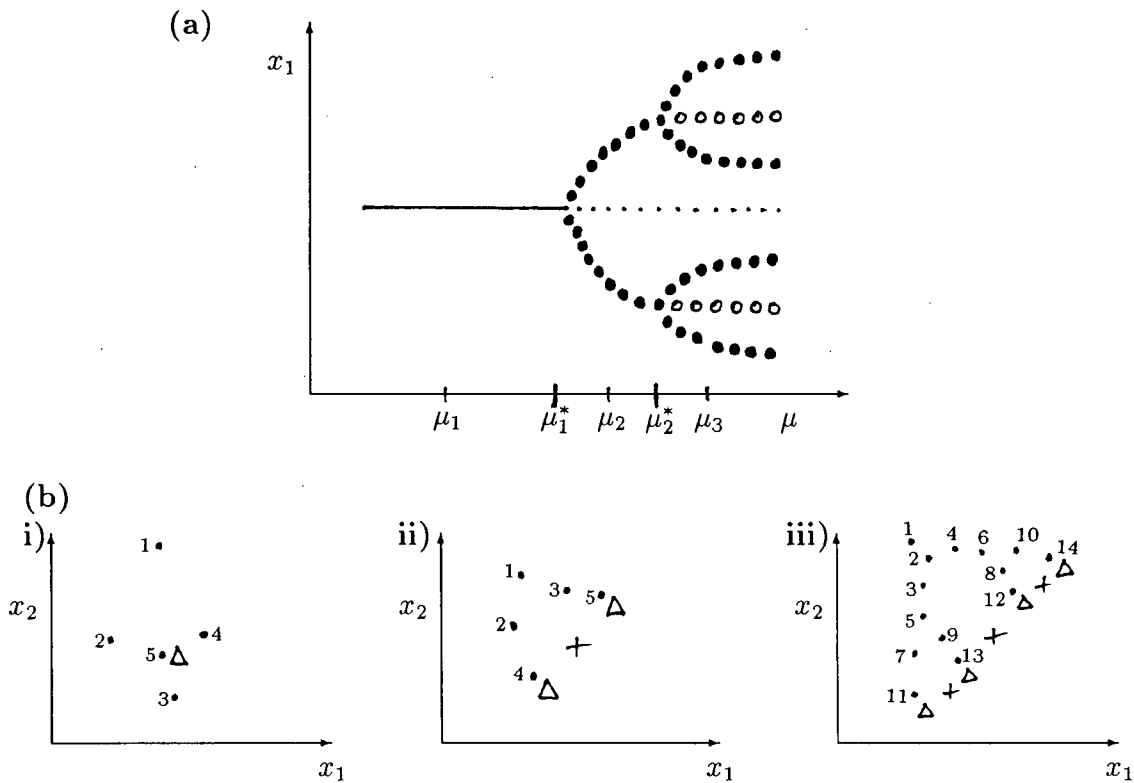


Figure A.26: (a) One-parameter bifurcation diagram showing period-doubling bifurcations at $\mu = \mu_1^*$ and $\mu = \mu_2^*$ for a discrete system. (b) State space diagrams showing the dynamics at (i) $\mu = \mu_1$ (stable equilibrium), (ii) $\mu = \mu_2$ (stable period-2 orbit) and (iii) $\mu = \mu_3$ (stable period-4 orbit).

but

$$f^j(\hat{x}) \neq \hat{x} \text{ for } j=1,2,\dots,k-1.$$

Then \hat{x} is called an equilibrium or fixed point of period k . This means that the system has a cycle or periodic orbit whose period is equal to k time units. Suppose $k = 2$ and we have a one-dimensional system. Then

$$f^2(\hat{x}) = f(f(\hat{x})) = \hat{x}$$

but

$$f(\hat{x}) \neq \hat{x}.$$

Hence, if we start at \hat{x} then after the first time unit we are at $f(\hat{x})$ but after the second time unit we have returned to \hat{x} . This is shown in figure A.27. A state space diagram

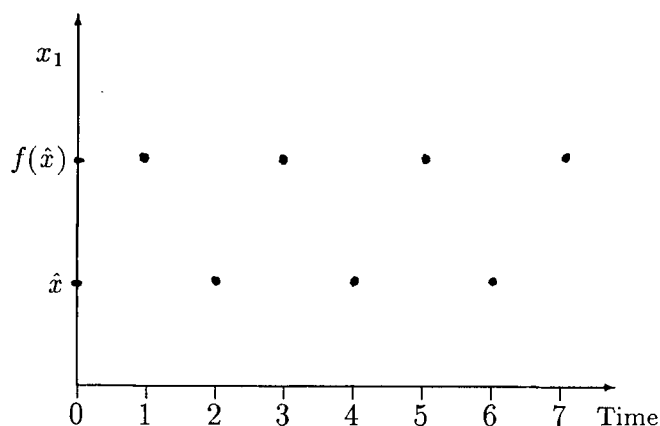


Figure A.27: Time plot of a period-2 orbit for a discrete system.

for such a situation in two dimensions (that is, for two state variables) is shown in figure A.26(b)(ii). In this example both x_1 and x_2 will have time plots resembling figure A.27.

An analogue of the Hopf bifurcation also exists for maps. It is sometimes referred to as the *Naimark-Sacker bifurcation* [124] but is also simply called the *Hopf bifurcation for maps*. This bifurcation corresponds to a pair of eigenvalues of modulus 1. Instead of a periodic orbit, however, an invariant circle is initiated at this bifurcation point. While geometrically similar to a periodic orbit, the dynamics are different. A state space diagram of an invariant circle is shown in figure A.28 together with a time plot. The stability of this circle is intuitively similar to a periodic orbit but the methods of analysis are quite different [124].

There are two possibilities for an invariant circle. Either point 10 coincides with point 1 in figure A.28(a), point 11 coincides with point 2 and so on, or subsequent points are distinct from all the earlier ones but still lie on the circle. If the map is allowed to iterate for a long time in the latter case, then what is eventually observed in state space will

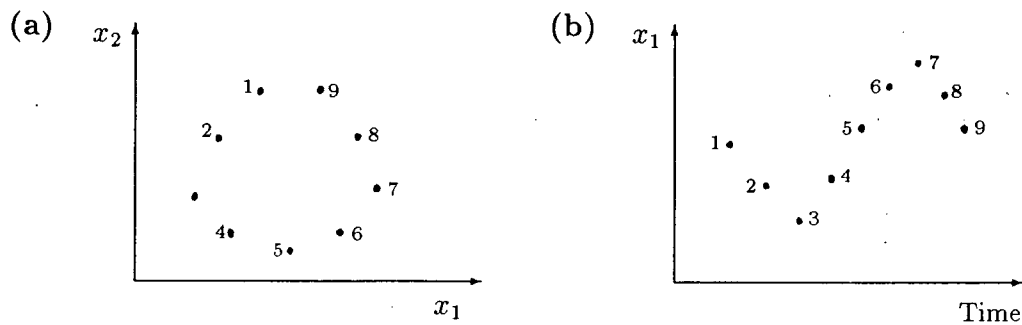


Figure A.28: (a) State space diagram showing an invariant circle. (b) Time plot of the situation in (a) in terms of x_1 .

appear to be a continuous circle.

In general, the behaviour associated with discrete models is more complicated than that for continuous models because of the built-in time delays in the feedback relationships [128]. Even one-dimensional maps can exhibit chaotic behaviour. May [82] shows how the behaviour of the discrete analogue of the logistic equation changes from stable equilibrium behaviour, to periodic behaviour, and finally to chaos as the growth rate is increased. The reader is referred to the literature that has been cited for further details on the dynamics of discrete models.

A.3.6 Stability of bifurcations under perturbations

The question of robustness or structural stability of a model is an important one. In order to determine how robust a model is, we need to see whether or not perturbing the model alters its qualitative structure. It turns out (see [124]) that limit point bifurcations, Hopf bifurcations and hysteresis phenomena are stable under small perturbations but transcritical and pitchfork bifurcations are not unless constraints or symmetries are preserved by perturbations. That is, small perturbations of the model do not affect whether or not the former three bifurcations occur (they only affect properties such as

the parameter value at which the bifurcations occur and the positions of the equilibrium points and periodic orbits) but can affect the occurrence of the latter two. Figure A.29 illustrates the destruction of transcritical and pitchfork bifurcations graphically. It turns out that all bifurcations of one parameter families of equations which have an equilibrium point with a single zero eigenvalue (or single eigenvalue of modulus 1 for maps) can be perturbed to limit point bifurcations [49].

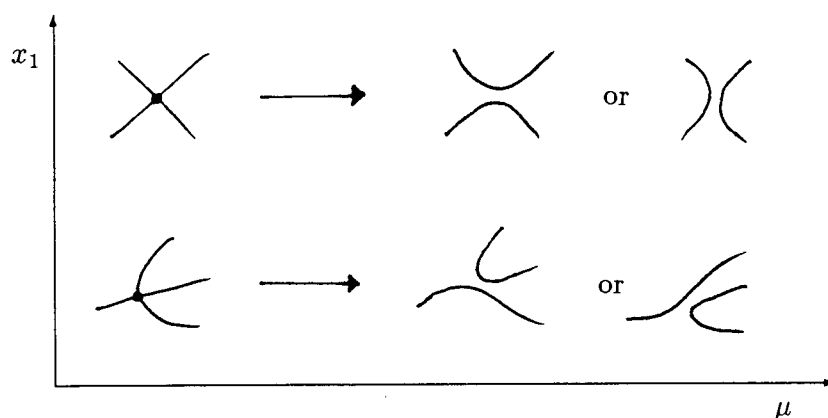


Figure A.29: Possible results of perturbing transcritical and pitchfork bifurcations (adapted from [111], p.83).

However, we cannot make such rapid conclusions when the model contains more than one free parameter. In these circumstances the idea of *codimension* of a bifurcation becomes important. However, for $m \geq 3$ the analysis is very complicated. An introduction to this theory can be found in [124]. The only point I would like to make here is that, because the models in this dissertation have more than three parameters, none of the bifurcations that have been described in this appendix can be dismissed as being unimportant.

A.3.7 Multiple degeneracy

All the cases discussed so far have assumed simple zero eigenvalues or a single complex conjugate pair of eigenvalues with zero real part (or the analogous situations for maps). Higher order singularities, or multiple degeneracies do, of course, occur but the behavioural dynamics associated with them can be difficult to interpret and there is still much research being done in this area. Thus, at this stage, it is probably best to either solve the system of equations numerically or to generate phase portraits for parameter combinations in a region surrounding these complex points rather than struggling with the details of the bifurcation structure. For those interested some of these higher order degeneracies are investigated in [124].

A.4 Conclusion

The introduction to dynamical systems theory given in this appendix has been mainly intuitive and not mathematically rigorous. Although the concepts are fairly simple, the mathematics involved in studying a particular system of equations can be quite formidable. Appendix B describes how computers can be useful in this regard.

Appendix B

Numerical details

B.1 Introduction

This appendix describes some of the computer software that is available for analysing systems of equations. Packages such as AUTO86 [28], AUTO94 [31], Interactive AUTO [117], XPPAUT [35] and some others that will be mentioned later, enable particular solutions to be ‘continued’ as a parameter is varied in order to produce a bifurcation diagram. In other words, these continuation programs trace out the location of equilibrium points and periodic orbits as a parameter is varied. Bifurcation points that are encountered along the way are also detected and classified. In this way a whole range of different modes of model behaviour can be obtained with much greater ease than if the mathematics had to be done by hand. The process can be repeated for different parameters in order to obtain a more comprehensive picture of the qualitative behaviour associated with different regions in the parameter space.

Section B.2 introduces some of the techniques used by continuation programs for continuing equilibrium points and determining the stability of the solution branches (see section A.2.4). Methods for detecting bifurcations along these branches are also described with particular reference to AUTO¹. The section is intended as a brief overview. More

¹I will use the abbreviation AUTO to refer to AUTO86, AUTO94 and Interactive AUTO as the latter is in essence just a graphical interface for AUTO86 and AUTO94 is an updated version of AUTO86 together with a graphical interface. Even when using XPPAUT I will refer to AUTO when talking about bifurcation diagrams since XPPAUT generates these diagrams through a graphical interface with AUTO86. In cases where I need to distinguish between the packages, I will use their full names.

detailed discussions as well as a comprehensive list of references can be found in Allgower and Georg [4] and Seydel [111].

Following this theoretical introduction section B.3 describes the capabilities and limitations of the packages that I used and section B.4 describes how to obtain time plots, phase portraits and bifurcation diagrams. Finally, section B.5 gives a few pointers and warnings regarding the use of some of the packages. These are based on my experiences gained through analysing the models in the main body of the thesis.

B.2 Theory

B.2.1 Continuation methods

As has already been mentioned, continuation or path-following methods generate a chain of solutions (equilibrium points, periodic orbits or bifurcation points) as a parameter is varied. A typical path-following method is the predictor-corrector method. This involves the repetition of two different steps. The predictor step approximates the next point on the curve, often by using the direction of the tangent to the curve (Euler predictor) [4]. A number of iterative steps (called corrector steps) then aim to improve this approximation and bring it back to the actual curve [4]. Typically Newton or gradient type methods are used in this step [4].

Some form of parameterisation of the curve is required for these steps. The obvious choice is the control parameter (that is, the parameter being varied) as it has physical significance. However, this leads to difficulties at limit points (see section A.2.13) [111]. An alternative is to choose another variable which involves adding another equation to the system. This extended system can then be solved using the predictor-corrector methods mentioned above [111]. Popular choices for this alternative parameter are arclength or a pseudo-arclength parameter proposed by Keller [67]. AUTO uses the latter choice and

details are given in [30, 67].

The accuracy of the predictor-corrector method depends on the choice of steplength. In general, shorter steplengths lead to greater accuracy (provided that they are not so small that computer round-off errors become large) but they are more costly in terms of time. In some cases the objective is just to follow the curve as rapidly and safely as possible until a critical point (such as a bifurcation point) is reached [4] and then a smaller steplength is needed for greater accuracy. Thus, for an efficient algorithm, the steplength needs to be adaptive and not fixed [4, 111]. Ideally a continuation method should also allow the user to have some control over the choice of steplength. AUTO fulfills both criteria. Stepsizes are changed automatically in the program depending on the speed of convergence of Newton's method (that is, depending on the number of iterations required to fulfill the stopping criteria). Maximum and minimum stepsizes and convergence criteria are given by the user.

There are many different ways in which choices of predictor, corrector, parameterization and step control can be combined to produce a continuation method. Because of this no numerical comparison of different path-following methods has so far been done and, hence, no particular method can be recommended exclusively [111]. Simple Euler predictors together with Newton-type correctors have been found to be satisfactory in many circumstances [4]. Because of the stability of Newton correctors, more stable higher order predictors based on polynomial interpolation (instead of on the direction of the tangent to the curve as with an Euler predictor) are often advantageous [4].

No continuation method can guarantee that all possible solutions will be found in a given example [111]. Isolated branches (branches which are not attached to other branches via bifurcation points) are very difficult to detect. It is suggested in the AUTO86 manual [30] and by Seydel [111] that time integration of the governing system of equations using random initial data may be worthwhile for generating a starting point on an as yet

undetected solution branch. DSTOOL [10] can also be useful for locating equilibrium points which lie on these isolated branches.

B.2.2 Detection of bifurcations

As a continuation method traces out a path, it needs to be able to detect bifurcation points. Techniques for doing this can be divided into direct and indirect methods [111]. Direct methods involve enlarging the original system of equations by including additional equations which characterise the bifurcation point. Indirect methods on the other hand utilise data obtained during a continuation together with a test function. The latter are generally recommended in practical computations (and are used in AUTO) as direct methods involve solving much larger systems of equations and have higher storage requirements. Indirect methods do have more difficulty achieving high accuracy but when discretisation errors are present and when bifurcation points are unstable to perturbations, this greater accuracy is not needed [111]. If higher accuracy is required then a direct method can be applied once an indirect method has obtained an approximate result.

An indirect method detects bifurcation points using ‘test functions’ which are evaluated during branch tracing [111]. A bifurcation point is indicated by a zero of the test function, τ . (In practice, an algorithm checks for a change of sign of τ .) For simple bifurcation points a natural choice for τ is the maximum of all real parts α_i of the eigenvalues of the Jacobian matrix \mathbf{A} (see section A.3.2). However, this choice may not be smooth and it does not signal bifurcations in which only unstable branches coalesce [111]. This problem can be overcome by choosing $\tau = \alpha_k$ with $|\alpha_k| = \min\{|\alpha_1|, \dots, |\alpha_m|\}$. This choice also detects Hopf bifurcations. In general, the accuracy of τ depends on the accuracy with which \mathbf{A} is evaluated.

There are many possibilities for the choice of test function. However, not much

attention has been paid to which drawbacks are significant or which test function is best for which purpose [111]. Some authors have studied classes of test functions for various types of singular points (see [4] for references).

Once a bifurcation or branch point has been detected, a method needs to be found for switching branches. All that is needed is a single point on the new branch as then the continuation method can be used to trace out the rest of the branch. Predictors and correctors can again be used for switching branches. Seydel [111] and Allgower and Georg [4] describe a few different approaches and give further references. AUTO uses a method suggested by Keller [67]. Doedel [30] notes that this method performs well in most applications although difficulties can occur if the angle of intersection of the branches is very small.

At a Hopf bifurcation point periodic orbits are introduced. Once a solution point on the branch of periodic solutions has been located, a continuation procedure can be used to trace out the branch. After imposing an integral condition in order to fix the phase of the orbit, the continuation procedure becomes a special case of the path-following techniques that have already been discussed. Details of the method as well as further references can be found in the AUTO86 manual [30].

B.2.3 Stability

Stationary branches

The stability of stationary branches (that is, of continuations of equilibrium points) is determined from the real parts of the eigenvalues of the Jacobian matrix \mathbf{A} . The calculation of eigenvalues (for example, via QR factorisation or LU decomposition methods [4, 111]) can be very time-consuming especially when accurate approximations are required, such as near bifurcation points, and when the system of equations is large. However, the

fact that the eigenvalues play an important role in the detection of bifurcations, as well as in determining stability, provides justification for using more accurate techniques. AUTO uses the IMSL subroutine EIGRF for computing the eigenvalues of a general real matrix [30]. Interactive AUTO [117] assigns different colours to continuation branches depending on the number of unstable eigenvalues while XPPAUT [35] uses thick lines to indicate stable branches and thin lines to indicate branches having one or more unstable eigenvalues.

Periodic branches

It is the values of the Floquet multipliers (see page 248) that determine the stability of periodic orbits. These multipliers are eigenvalues of a particular matrix and, thus, an eigenvalue solver is again required. Since Floquet multipliers can be very large or very small in value, there may be a loss of accuracy when evaluating them numerically. This is especially true for unstable orbits [111] and near orbits of infinite period [30]. In the AUTO86 manual [30] it is noted that orbits normally retain their accuracy even when the computation of Floquet multipliers (and hence stability determination) breaks down. In XPPAUT and AUTO94 the routine for calculating Floquet multipliers has been improved and is more accurate than that in AUTO86, and hence in Interactive AUTO. Floquet multipliers are also used for detecting higher order periodic bifurcations such as period-doubling bifurcations or bifurcations to tori.

B.3 Available computer packages

In this section I list the capabilities of a number of computer packages and also list some advantages and disadvantages related to choosing one package over another.

B.3.1 AUTO86

Since Interactive AUTO, XPPAUT and AUTO94 are all based on AUTO86 [28], their basic capabilities are very similar. Although I have not used AUTO86 directly (it runs as a batch process), I will describe its capabilities and limitations since most of them apply to the abovementioned packages. I highlight the differences between the packages in subsequent sections.

Capabilities

(These are taken directly from the AUTO86 manual [30].)

AUTO can do a limited bifurcation analysis of algebraic systems of the form

$$\mathbf{f}(\mathbf{x}, \lambda) = \mathbf{0}, \quad \mathbf{x}, \lambda \in \mathcal{R}^m \quad (\text{B.6})$$

where λ denotes one or more free parameters, and of systems of ordinary differential equations of the form

$$\dot{\mathbf{x}} = \mathbf{f}(\mathbf{x}, \lambda), \quad \mathbf{x}, \lambda \in \mathcal{R}^m. \quad (\text{B.7})$$

It can also do certain continuation and evolution computations for the diffusive system

$$\mathbf{x}_t = \mathbf{D}\mathbf{x}_{uu} + \mathbf{f}(\mathbf{x}, \lambda), \quad \mathbf{x}, \lambda \in \mathcal{R}^m. \quad (\text{B.8})$$

where $\mathbf{x} = \mathbf{x}(\mathbf{u}, t)$ and \mathbf{D} denotes a diagonal matrix of diffusion constants. For the algebraic system (B.6) AUTO can:

- trace out branches of solutions.
- locate bifurcation points and compute bifurcation branches.
- locate limit points (saddle-node bifurcations) and continue these in two parameters.

- do all of the above for fixed points of the discrete dynamical system

$$\mathbf{x}_{t+1} = \mathbf{f}(\mathbf{x}_t, \lambda). \quad (\text{B.9})$$

- optimisation: find extrema of an objective function along the solution branches and successively continue such extrema in more parameters.

For the ordinary differential equations (B.7) AUTO can:

- compute branches of stable or unstable periodic solutions and Floquet multipliers. Starting data for the computation of periodic orbits are generated automatically at Hopf bifurcation points.
- locate limit points, transcritical and pitchfork bifurcations, period-doubling bifurcations and bifurcations to tori along branches of periodic solutions. Branch switching is possible at transcritical, pitchfork and period-doubling bifurcations.
- continue Hopf bifurcation points, limit points and orbits of fixed period in two parameters.
- compute curves of solutions to (B.7) on the interval $[0,1]$ subject to general nonlinear boundary or integral conditions.
- locate limit points and bifurcation points for such boundary value problems. Branch switching is possible at bifurcation points. Curves of limit points can be computed in two parameters.

For the parabolic system (B.8) AUTO can:

- detect bifurcations to wave train solutions of given wave speed from spatially homogeneous solutions. These are detected as Hopf bifurcations along fixed point branches of a related system of ordinary differential equations.

- trace out the branches of wave solutions to (B.8) and detect bifurcations. The wave speed c is fixed but the wave length L will normally vary.
- trace out branches of waves of fixed wave length L in two parameters. If L is large, then one gets a branch of approximate solitary wave solutions.
- do time evolution calculations for (B.8) with periodic boundary conditions on $[0, L]$.

In this thesis systems of the form (B.7) and (B.9) are analysed.

The discretisation used in AUTO to approximate ordinary differential equations and for calculating periodic solutions is orthogonal collocation with $2, \dots, 7$ Gauss collocation points per mesh interval. The mesh automatically adapts to the solution so that a measure of the local discretisation error is equi-distributed. Also, the adaptive mesh guards to some extent against computing spurious solutions. When spurious solutions do occur they are often easy to recognise by the jagged appearance of the solution branch.

Some general limitations of AUTO86 are listed below.

Limitations

The following difficulties are noted in the manual [30]:

- degenerate (multiple) bifurcations cannot be detected in general. Also, bifurcations that are close together may not be noticed when the pseudo-arclength step size is not sufficiently small.
- Hopf bifurcation points may go unnoticed if no clear crossing of the imaginary axis takes place. This may happen when other real or complex eigenvalues are near the imaginary axis and when the pseudo-arclength step is large compared to the rate of change of the critical eigenvalue pair. An often occurring case is a Hopf bifurcation close to a limit point (saddle-node bifurcation).

- similarly, Hopf bifurcations may go undetected if switching from real to complex conjugate, followed by crossing of the imaginary axis, occurs rapidly with respect to the pseudo-arclength step size.
- secondary periodic bifurcations may not be detected for very similar reasons.
- for periodic orbits the numerical output should be checked to make sure that points labelled as bifurcation points, limit points, period-doubling bifurcations or bifurcations to tori have been classified correctly.

Some of the above problems may be solved by decreasing the minimum step size, $dsmin$, to allow AUTO to take smaller steps. This is particularly helpful when two continuation branches or two bifurcation points are very close together. In the former situation AUTO needs to take small steps to ensure that it does not switch branches during the calculation. Decreasing $dsmax$ may also help as this prevents AUTO from taking large steps and missing important bifurcations.

As noted above AUTO may have some difficulty with identifying bifurcations on periodic orbits. Problems arise when Floquet multipliers are close to the unit circle. Also, unstable orbits can be difficult to locate, especially when they are close to a stable orbit or equilibrium. Accuracy may be increased by decreasing $dsmin$ or increasing $ntst$, the number of mesh points used in the discretisation of the periodic orbits.

Some other limitations of AUTO which have resulted from doing bifurcation analyses on a few models are as follows:

- transcritical and pitchfork bifurcations cannot be continued in two parameters because the determinant of the Jacobian matrix \mathbf{A} is zero at these bifurcation points. Other continuation and bifurcation packages will have the same limitation. A possible solution is to do a number of one-parameter continuations with different (fixed)

values of the second parameter and then to plot the bifurcation points obtained from each continuation in two-parameter space. An approximate curve can be drawn through these points. This is done in chapter 2.

- error messages from AUTO can be misleading (as with most computer packages!). In many cases the problem is solved by checking the driving program for typing errors and variable or parameter names which begin with letters between h and o as such quantities are assumed to be integers by default.

B.3.2 Interactive AUTO

Capabilities

In addition to the capabilities listed for AUTO86, Interactive AUTO [117] allows the user to change the program constants interactively and to observe the development of a bifurcation diagram while a calculation is in progress. The corresponding eigenvalues are shown simultaneously in a separate graphics window.

The advantages and disadvantages listed below relate mainly to the suitability of this package for analysing ecological models and are included for comparison with the other packages. Since the packages were not set up specifically for the models that are analysed in this thesis, these comments are not necessarily criticisms.

Advantages

- This package has good on-screen graphics. Different colours are used to indicate the number of unstable eigenvalues corresponding to a particular branch. The locations of the eigenvalues relative to the real and imaginary axes and the unit circle are also shown. Bifurcation diagrams can be viewed in three dimensions if desired and the mouse can be used to shift diagrams and to zoom in and out.

Disadvantages

- Bifurcation diagrams cannot be printed out or saved as postscript files for later printing.
- Each time the model equations are altered the driving routine needs to be recompiled.
- The package only runs on Personal Iris and Iris 4D workstations (instead of on all systems supporting X-windows as for the other packages).
- Interactive control of the graphics output is limited. Once a one-parameter bifurcation diagram has been generated it is not possible to view it with a different variable on the y-axis. The scales of the axes are also not visible.

B.3.3 XPPAUT

This package (as well as the tutorial) can be obtained via anonymous ftp from

ftp.math.pitt.edu

and is in the directory *pub/bardware*.

Capabilities

The AUTO interface allows most of the capabilities of AUTO86 to be enjoyed. However, the aim of making AUTO easier to use has led to some restrictions which will be mentioned below.

This package also solves systems of equations numerically (there is a choice of algorithms) and generates time plots and phase portraits (in two and three dimensions).

Hardcopies of these diagrams can be obtained. With reference to phase portraits it is possible to obtain nullclines, arrows indicating the direction of flow, as well as the positions and stabilities of equilibrium points (singular points).

Other capabilities include curve-fitting of data, spreadsheet type data manipulation and generation of histograms.

Advantages

- Time plots, phase portraits and bifurcation diagrams can all be generated using the same computer package.
- The AUTO interface is easy to use—the number of constants that need to be altered has been reduced.
- Hardcopies of bifurcation diagrams can be obtained through saving them as postscript files. The data can also be saved so that it can be read into other graphics packages.
- The package has good on-screen graphics. The development of a bifurcation diagram can be seen while a calculation is in progress. The eigenvalues are shown simultaneously relative to the real and imaginary axes and the unit circle. It is possible to zoom in on specific regions of a diagram and the most recent one- and two-parameter bifurcation diagrams viewed are kept in memory. Once a one-parameter bifurcation diagram has been generated the variable on the y-axis can be altered. It is also possible to plot the period or the frequency of a periodic orbit as a function of the bifurcation parameter. Minima as well as maxima of periodic orbits can be plotted simultaneously.
- AUTO86's Floquet multiplier routine has been improved.
- It is possible to start continuations from a numerically calculated periodic orbit.

- Three-dimensional phase portraits are possible.
- The driving program is easy to write for most systems and is compiled automatically when the XPPAUT command is given.
- When calculating time plots and phase portraits, data information for auxiliary variables (variables which are subcomponents or composite functions of the state variables) can also be observed.
- The package runs on any X-windows system as well as on LINUX.
- There is a comprehensive tutorial on the World Wide Web to help the user become acquainted with the package. The address is:

<ftp://mthbard.math.pitt.edu/pub/bardware/xpptut/start.html>.

Disadvantages

- When generating phase portraits only one equilibrium point is located at a time and the initial point often has to be quite close by.
- The AUTO interface is not set up for discrete equations and error tolerances for AUTO cannot be altered. Also, the automatic detection of limit points cannot be turned off in this version of AUTO. This may cause difficulties when calculating periodic orbits as at a limit point of a periodic orbit two Floquet multipliers equal 1 and this affects the convergence properties of the continuation algorithm. Decreasing *dsmin* and *dsmax* may help.
- There is limited control of the appearance of printouts. The stability nature of a particular branch in a bifurcation diagram is often obscured when consecutive continuation points are very close together. Dashed lines for unstable branches then

appear as solid lines and, instead of individual dots, periodic branches become thick lines. In some cases this can be overcome by increasing the maximum step size, *dsmax*. Also, the data for a diagram can be saved separately and then read into another graphics package. When two-parameter bifurcation diagrams are printed out, data from the previously generated one-parameter diagram is superimposed.

B.3.4 AUTO94

Capabilities

This package is an updated version of and graphical interface for AUTO86. The graphical interface allows program constants to be altered interactively and bifurcation diagrams can be viewed.

Advantages

- There is a help menu which describes the functions of the program constants.
- Demonstration examples show how the various capabilities of the package can be used.
- Model equations can be changed interactively.
- The package runs on any X-windows system.
- It is possible to start a continuation from a numerically calculated periodic orbit.
- The routine for calculating Floquet multipliers has been improved.

Disadvantages

- Printouts of bifurcation diagrams cannot be obtained.

- The on-screen graphics are more cumbersome to use than those of Interactive AUTO and XPPAUT. Changes to a bifurcation diagram can only be viewed at the end of a calculation using a separate command instead of while the program is running. The way in which bifurcation points are labelled also makes the diagrams difficult to read. The disadvantages were the main reason why I did not make use of AUTO94.

B.3.5 DSTOOL

This package can be obtained via anonymous ftp from

macomb.tn.cornell.edu

and is in the *pub/dstool* directory.

Capabilities

This package generates time plots and two-dimensional phase portraits for both discrete and continuous systems of equations. It calculates equilibrium points and their stabilities as well as stable and unstable manifolds for saddle points. There is provision for extensions to the package—three-dimensional graphics as well as continuation and bifurcation routines may be incorporated in the near future.

Advantages

- A mouse can be used for specifying starting points for time plots and phase portraits. This is very convenient and speeds up the generation of these diagrams considerably.
- The package is good at locating periodic points for discrete models.

- Printouts of diagrams can be obtained.
- For ordinary differential equation models trajectories can be calculated forwards or backwards.
- The package runs on any X-windows system as well as on LINUX.

Disadvantages

- Three subroutines need to be modified each time a new model is entered.
- The package sometimes crashes when calculating equilibrium points for difficult parameter values.

B.3.6 Other packages

Some other packages are available for analysing dynamical systems. Part of the following list can be found in [4].

1. ALCON [27]. This is a continuation method for algebraic equations $\mathbf{f}(\mathbf{x}, \lambda) = \mathbf{0}$. Limit points and simple bifurcations can be computed on demand.
2. BIFPACK [112]. This is an interactive program for continuation of large systems of nonlinear equations. Bifurcation points are also detected.
3. DYNAMICS [96]. This package iterates maps, solves differential equations, and plots trajectories. It runs on both IBM PC's and UNIX workstations which support X-windows.
4. LOCBIF [68]. This is an interactive program designed for multiparameter bifurcation analysis of equilibrium points, limit cycles and fixed points of maps. At

present it is set up for IBM PC's but a UNIX version is in process and is being incorporated into DSTOOL.

5. PATH [66]. This software package for dynamical systems can apparently handle much larger systems of ordinary differential equations than AUTO.
6. PHASER [54]. This package generates phase portraits for continuous and discrete dynamical systems. It runs on IBM PC's.
7. PITCON [100, 101]. This is a Fortran subprogram for continuation of equilibrium points and for detecting limit points.

As has already been mentioned, no comprehensive comparison of different techniques has been done because of the enormity of the task. None of the abovementioned packages analyses a model at the touch of a button and complementary analytical techniques, as well as other numerical techniques, are still needed in order to obtain a complete understanding of any model. Parameter studies are as much an art as a science [111]. In the next section I explain how to generate time plots, phase portraits and bifurcation diagrams using some of the packages I have mentioned.

B.4 Using the packages

Although this section gives some guidelines for using the various packages, it is important that anyone wishing to use these packages reads the relevant user manuals to find out the exact commands for performing various tasks. Many of the manuals have introductory examples for the reader to work through and these are invaluable for getting acquainted with the capabilities of the package. There is a comprehensive tutorial for using XPPAUT on the World Wide Web. The address is:

<ftp://mthbard.math.pitt.edu/pub/bardware/xpptut/start.html>.

Time plots

These can be obtained using either DSTOOL or XPPAUT. The user simply chooses *time* as the variable to be plotted on the x-axis and one of the state variables for the y-axis. After entering initial values for the state variables and the time period over which to simulate the model, the 'run' or 'go' command can be chosen. The process may be repeated after changing one or more initial values or parameter values. These steps can all be done interactively.

Both packages have a number of choices for the numerical algorithm that is used to calculate solutions. Minimum and maximum or fixed stepsizes can be chosen as well as error tolerances. In most cases the default choices are quite adequate.

If the mouse is used to choose an initial point, then only the initial time and the value of the state variable on the y-axis will be altered automatically. Values for the other state variables will remain unchanged unless new values are typed in.

When analysing a discrete system using DSTOOL, changing the time increment to 1 in the 'orbit' window and using the 'continue' icon allows the user to determine the period of a cycle. The amplitude of the cycle can be deduced by looking at the state variable values in the 'settings' window that correspond to the maximum and minimum of the cycle.

Phase portraits

These can again be generated using either DSTOOL or XPPAUT. Although three-dimensional portraits are possible in XPPAUT, I will only discuss two-dimensional portraits as I find them much easier to interpret and, hence, find them more useful in most situations. (Note that the dimension of the system can be greater than two but the results are projected into a two-dimensional plane.)

In order to generate a phase portrait one of the state variables needs to be chosen for plotting on the x-axis and another for the y-axis. For systems of dimension greater than two the solution trajectories will be projected into this plane. Initial values can be typed in manually or the mouse may be used. Only the values of the state variables shown on the axes will be altered when using the mouse. The user can again choose between the various numerical methods for calculating solution trajectories.

In addition to solution trajectories the positions of equilibrium points can be shown in phase diagrams. When asked to find equilibrium points (also called fixed points or singular points) both DSTOOL and XPPAUT automatically calculate the eigenvalues and hence the stability of these points. XPPAUT tends to locate one singular point at a time and often the initial point has to be fairly close to the fixed point if the search is to be successful. DSTOOL uses a Monte Carlo technique to generate a specified number (the default is 10) starting points and then searches for fixed points beginning at these starting values. This method is fairly efficient and choosing the 'find' option in the 'fixed point' window a few times generally locates all the relevant points. If desired, the user can choose the initial point from which to begin a calculation instead of using the Monte Carlo technique. For discrete models DSTOOL also finds periodic points.

For continuous systems both packages also calculate one-dimensional stable and unstable manifolds associated with saddle points in the plane. These help delimit domains of attraction. XPPAUT can calculate nullclines (curves showing where each differential equation is equal to zero) and display these in the phase portrait. Equilibrium points are located at intersections of nullclines corresponding to different state variables.

One-parameter bifurcation diagrams

For systems of ordinary differential equations one-parameter bifurcation diagrams can be generated using Interactive AUTO, AUTO94 and XPPAUT. For discrete systems either

of the former two packages can be used. The first step is to choose the bifurcation parameter to be plotted on the x-axis. One of the state variables can be chosen for the y-axis. This choice must be specified in the driving program for Interactive AUTO but can be done interactively in the other two packages.

In addition to choosing the scales for the axes there are a number of other program constants which need to be set. These govern, for example: the length and type of continuation; the output to the screen; the detection of limit points; error tolerances, steplengths and mesh intervals for the various numerical routines; and a number of other aspects of the computation. The various possibilities are listed in the AUTO86 manual [30] as well as in the HELP menu in AUTO94. The example or demonstration programs also give an idea of appropriate values. In XPPAUT some of these constants have been preset to simplify the use of AUTO. This is very convenient in most situations but can be restrictive in others.

In order to begin generating a bifurcation diagram a fixed point (equilibrium point), corresponding to a particular parameter set, is required. Such a point can be determined analytically (where possible) or numerically using XPPAUT or DSTOOL. A continuation can then be started from this point. At transcritical, pitchfork and period-doubling bifurcations AUTO automatically calculates the various intersecting branches. At Hopf bifurcation points the user must specifically initiate the calculation of periodic orbits by choosing the relevant restart label. In Interactive AUTO and AUTO94 one of the program constants also needs to be altered. In order to extend any continuation branch across a wider range of parameter values, the endpoint of the branch can be chosen as the restart value.

For discrete systems period-doubling bifurcations are labelled as Hopf bifurcations by AUTO but the period-2 branches emanating from this bifurcation cannot be calculated directly. The second iterate of the model must be used for this purpose. Since a (period-1)

equilibrium point of the original model is also an equilibrium point of the second iterate of the model, both the period-1 and the period-2 equilibrium point branches will be traced out using this latter model. However, for higher order period-doublings higher order iterates of the model are required and the process is more tedious.

In such cases as well as for complicated discrete models whose second iterate is difficult to calculate, DSTOOL can be used to generate an approximate bifurcation diagram. Equilibrium points can be calculated at regular intervals across a range of parameter values and their coordinates recorded. These points can then be plotted using some other graphics package, such as GNUPLOT [125], to obtain an approximate bifurcation diagram. This approach is used in chapter 7.

Two-parameter bifurcation diagrams

Once a limit point or Hopf bifurcation point has been detected in a one-parameter continuation, it can be continued in a second parameter. This is done by choosing the appropriate restart value corresponding to the bifurcation point, a second parameter for the y-axis, and either altering the relevant program constant in Interactive AUTO and AUTO94 or choosing the two-parameter option in XPPAUT.

Limit cycles of fixed period can also be continued in two parameters. This is useful for approximating homoclinic or heteroclinic bifurcation curves since homoclinic and heteroclinic orbits have infinite period. Designating a USZR function to locate an orbit of high period, say period=100 or 1000, when constructing a one-parameter bifurcation diagram allows a two-parameter continuation of this orbit to be done². The resulting two-parameter curve gives the required approximation to the curve of homoclinic or heteroclinic bifurcation points. This technique is used in section 2.4. When continuing

²A point satisfying the USZR function will be given a label which can be used as a restart value for the two-parameter continuation.

these curves in two parameters, detection of limit points should be turned off as it may lead to spurious bifurcation points. This is done automatically in XPPAUT. Any bifurcation points should also be checked against the numerical output to see whether an eigenvalue or Floquet multiplier has, in fact, changed sign.

B.5 Pointers and warnings

As with all computer packages, the ones that I have discussed do not work exactly as one might wish in a given situation. Each model is unique and requires a slightly different approach whereas a computer package is built for more general use. In this section I list some problems and suggestions arising from my experiences with the packages. Many of these will only make sense once the examples in the main chapters of the thesis have been studied, but I have included them here so that most of the computer technicalities are confined to one place for ease of reference.

- When calculating fixed points using DSTOOL, the package sometimes hangs and will not respond to input. I have not been able to locate the cause of this but quitting DSTOOL and restarting the package, although frustrating, does solve the problem.
- When starting a fixed point continuation in AUTO, the error tolerances cannot be set lower than the accuracy of the state variables that have been given as the starting point. If the starting points are only known to low accuracy, then a short continuation can be done on low accuracy (high error tolerance). The continuation can then be restarted at higher accuracy using the values calculated by AUTO. (Accuracy is increased by decreasing $dsmax$, the maximum step length, decreasing the error tolerances, or increasing $ntst$, the number of discretisation points.)

- AUTO will generate bifurcation diagrams faster if the accuracy is lower. In many cases the results are still sufficiently accurate, however some bifurcation points may need to be checked with greater accuracy calculations. It is a good idea to check the eigenvalues and Floquet multipliers in the numerical output files created by AUTO to see whether a bifurcation point has been correctly labelled. Also, if there is a sudden jump in a continuation, or a curve becomes very jagged, then the continuation should be repeated using greater accuracy.
- The choice of step size depends on the extent of the parameter range over which changes in behaviour occur. In most cases $ds = 0.02$ and $dsm_{ax} = 0.05$ are good choices. However, I used $ds = 0.0001$ and dsm_{ax} between 0.001 and 0.01 for the population genetics models as the bifurcations take place within fairly small parameter ranges. Scaling the equations and parameters (as is done in chapters 3 and 4) circumvents this problem.
- Bifurcation diagrams can become very complicated even when studying simple models. However, not all continuation branches are always of interest. For example, some may correspond to negative or zero values of the state variables. Also, when studying a particular aspect of a model, some branches may be superfluous. It is important to look at the numerical output which is printed to the screen during a continuation so that one can keep track of which branches are relevant and which are not.
- It is a good idea to generate a number of starting points at a variety of parameter values to ensure that a complete bifurcation diagram is obtained and that isolated branches have not been overlooked. DSTOOL is convenient for this purpose.

- Results can often be checked using more than one package. For example, a bifurcation diagram generated by AUTO can be checked by choosing a number of parameter combinations corresponding to different qualitative regions and generating phase portraits for these combinations (using XPPAUT or DSTOOL) to check the dynamics. This is most convenient in XPPAUT where the bifurcation diagrams and phase portraits can be generated within the same package. Time plots and phase portraits can be checked by choosing different numerical methods to calculate solutions. Both DSTOOL and XPPAUT offer a variety of methods. By looking at the eigenvalues corresponding to an equilibrium point one can check that the stability of the point has been correctly labelled.
- It is easy to get side-tracked into studying the bifurcation structure of a model and into studying complicated behavioural changes instead of concentrating on phenomena which are of biological interest. In general, sharp boundaries and the exact values at which bifurcations occur are not important as biological parameters are hardly ever known with certainty. The general behaviour and the types of changes that can occur are of greater practical interest. For example, limit cycles of small amplitude will be indistinguishable from equilibrium points due to the natural variation of field data. Also, a system will easily be perturbed from a stable node with a small domain of attraction and, hence, such a phenomenon may be of minor interest. It is also important to look at time plots corresponding to fixed parameter combinations to see how quickly a system approaches the limiting behaviour indicated in a bifurcation diagram. If a system takes a long time to attain its equilibrium configuration then the transient dynamics may be more important than the final equilibrium values.

- It is sometimes enlightening to generate bifurcation diagrams for a larger range of parameter values than is of direct interest as there may be hysteresis phenomena or bifurcation points outside the range of interest which affect the behaviour inside this range.

Other suggestions which are best described with reference to a particular model are included in the relevant chapters. Clearly, the more one utilises the techniques and packages that have been introduced, the more familiar one becomes with them, and the more creative one can be in their use. The above comments will be most useful to those researchers actively involved in analysing their own models.

Appendix C

Mathematical details for the sheep-hyrax-lynx model

C.1 Modelling delays in system dynamics models

A system does not always respond immediately to a change in one of its components. Often there is a time lag between the initial change and the response of the system. For example, a change in hyrax population density will only affect the size of the hyrax population the following season. It takes time for an increase in population density to affect the reproductive success of the hyrax and the survival of their offspring.

In order to represent this in the model, averaged or smoothed versions of certain quantities are used in calculating growth rates. Three quantities are averaged in this model—hyrax density (H_D), prey abundance (A_P), and the grazing multiplier (G_M). For example, when sheep have been grazing more than their usual amount their condition is expected to improve resulting in a decline in juvenile mortality and a rise in fecundity (Swart and Hearne [116]). However, this will only occur after a prolonged increase in the average amount of pasture consumed. Hence, sheep fecundity and juvenile mortality are functions of the grazing multiplier average, \bar{G}_M , instead of G_M . A first order distributed delay (see MacDonald [77] or May [81]) is used to calculate \bar{G}_M . That is,

$$\frac{d\bar{G}_M}{dt} = \frac{G_M - \bar{G}_M}{t_{del}}$$

where t_{del} is the average delay time. Examples of this type of delay equation can be found in Forrester [39] and a detailed explanation of the mathematics underlying the above differential equation can be found in MacDonald [77]. The above ordinary differential

equation is added to the original system of model equations thus increasing the dimension of the system to be solved. Fortunately this increase in dimension does not pose a problem when solving the system numerically.

Further discussions on delays in biological systems and their effects on system behaviour can be found in [78, 81]. For the sheep-hyrax-lynx model the delays were not found to affect stability even for large average delay times.

C.2 Rescaling model equations

Suppose the differential equation for the state variable v_i is given by

$$\frac{dv_i}{dt} = f_i(v_1, \dots, v_i, \dots, v_m).$$

Let $v_i = s_i \bar{v}_i$, then

$$\bar{v}_i = \frac{v_i}{s_i}$$

and

$$\begin{aligned} \frac{d\bar{v}_i}{dt} &= \frac{1}{s_i} \frac{dv_i}{dt} \\ &= \frac{1}{s_i} f_i(s_1 \bar{v}_1, \dots, s_i \bar{v}_i, \dots, s_m \bar{v}_m). \end{aligned}$$

Dropping the bars for convenience we get

$$\frac{dv_i}{dt} = \frac{1}{s_i} f_i(s_1 v_1, \dots, s_i v_i, \dots, s_m v_m)$$

as required. The state variables have been replaced by $s_i v_i$ and the differential equation for v_i is divided through by s_i as stated in section 3.4.

Appendix D

Mathematical details for the budworm-forest model

D.1 Derivation of new foliage equation in spruce budworm model

We expect the amount of new foliage consumed by an individual larva to depend on the availability of new foliage per larva, that is, to depend on $\frac{F_b/K_F}{L_b}$ (F_b/K_F represents the amount of foliage that is *new* foliage). The larvae prefer new foliage to old and thus, in most circumstances, will eat all the new foliage before moving on to old foliage. Assuming that larval densities do not get so low that there is an overabundance of new foliage, we have

$$\text{new foliage consumption/larva} = \frac{F_b/K_F}{L_b}.$$

However, when larval densities are high, competition among budworm for new foliage becomes significant and larvae eat old foliage more readily than before. We can model this competition (see Starfield and Bleloch [113]) by including the factor

$$\left(1 - \frac{d_0 L_b}{F_b/K_F}\right)$$

where d_0 is the maximum foliage consumption rate per larva. This factor is close to 1 when there is abundant new foliage per larva (that is, when $\frac{F_b/K_F}{L_b}$ is large) and close to 0 when there is an overabundance of larvae resulting in intraspecific competition. The new equation is

$$\text{new foliage consumption/larva} = \frac{F_b}{K_F L_b} \left(1 - \frac{d_0 K_F L_b}{F_b}\right).$$

This factor is rather severe and could lead to negative values for very large larval densities. Instead we can use a negative exponential function [113] which approaches zero when there is very little new foliage available per larva. This gives

$$\text{new foliage consumption/larva} = \frac{F_b}{K_F L_b} \left(1 - e^{-\frac{d_0 K_F L_b}{F_b}} \right).$$

The total amount of new foliage consumed is then

$$\text{new foliage consumption} = \left[\frac{F_b}{K_F L_b} \left(1 - e^{-\frac{d_0 K_F L_b}{F_b}} \right) \right] L_b$$

and this gives

$$\begin{aligned} \text{remaining new foliage} &= \frac{F_b}{K_F} - \frac{F_b}{K_F} (1 - e^{-A}) \\ &= e^{-A} \frac{F_b}{K_F} \end{aligned}$$

where

$$A = \frac{d_0 K_F L_b}{F_b}.$$

D.2 Summary of model equations

The subscript b denotes the initial or base value for the state variable and subscript e denotes the new value after one year.

Foliage (F)

$$F_e = \frac{r_F F_1}{1 + \frac{(r_F - 1)}{K_F} F_1},$$

where

$$F_1 = \frac{1}{K_F} [e^{-A} + (K_F - 1)e^{-B}] F_b,$$

$$\begin{aligned}
 A &= d_0 L_b \frac{K_F}{F_b}, \\
 B &= c_1 (A - 1 + e^{-A}), \\
 c_1 &= 0.357.
 \end{aligned}$$

Branch surface area (S)

$$S_e = \frac{r_S S_1}{1 + \frac{(r_S - 1) S_1}{K_S}},$$

where

$$S_1 = [1 - d_S (1 - \frac{F_1}{F_b})^2] S_b.$$

Budworm (L)

$$L_e = d_{SL} \frac{S_b}{K_S} G^2 L_6$$

where

$$\begin{aligned}
 G &= H(2 - H), \\
 H &= \frac{F_1}{K_F} n, \\
 L_6 &= (1 - \frac{A_{disp} E^m}{1 + E^m}) L_5, \\
 E &= \frac{A_{sr} L_4}{A_{thr}}, \\
 L_5 &= (E_1 W^{1/3} - E_2) A_{sr} L_4, \\
 E_1 &= 165.64 \text{ and } E_2 = 328.52, \\
 W &= A_{F1} \frac{(1 - e^{-A})}{A} + A_{F2} (K_F - 1) \frac{(1 - e^{-B})}{A} + B_F, \\
 A_{F1} &= 34.1, \quad A_{F2} = 24.9 \text{ and } B_F = -3.4,
 \end{aligned}$$

$$\begin{aligned}
L_4 &= (A_p + B_p \frac{L_3}{L_b}) L_3, \\
A_p &= 0.473 \text{ and } B_p = 0.828, \\
L_3 &= e^{-D} L_2, \\
D &= \frac{p_{\max} L_2}{S_b (p_{\text{sat}} F_b^2 + L_2^2)}, \\
L_2 &= k_L \left(\frac{F_b - F_1}{d_0 L_b} \right) L_1, \\
k_L &= 0.425, \\
L_1 &= (1 - q_{\max} e^{-C}) L_b, \\
C &= 0.003 L_b.
\end{aligned}$$

Reference values for the parameters are given in table 7.1.

Listings

Examples of the calling programs for the various models are listed here. The entire calling program does not need to be rewritten each time. Once one file has been created, only those lines which define the model equations and set the parameter values and program constants need to be altered.

Bazykin model with prey competition—XPPAUT

```
# Model equations.  
dx/dt=a*x-b*x*y/(1+alp*x)-eps*x*x  
dy/dt=-c*y+d*x*y/(1+alp*x)  
# Initial values.  
x(0)=0.2  
y(0)=0.2  
# Parameters and nominal values.  
param a=0.6,b=0.3,c=0.4,d=0.2,alp=0.3,eps=0.001  
done
```

System dynamics model—XPPAUT

```

# Sheep, hyrax, lynx and pasture model with pasture limiting function.
#
# Differential equations for the state variables.
dpas/dt=(temp*ppn*area*plm(pai)-tssu*gn*gm(pai))/pmax
dhj/dt=(hfmax*hf*hfn*hdhm(hda)-hjmax*hj*hjdn*hjdm(hda)-ahjdm(pai)
-hjmax*hj*hjmn-hp*hjmax*hj/(hjmax*hj+hfmax*hf+hmmax*hm))/hjmax
dhf/dt=(0.5*hjmax*hj*hjmn-hfmax*hf*hfdn-hfdm(pai)-hfmax*hf*hcn
-hp*hfmax*hf/(hjmax*hj+hfmax*hf+hmmax*hm))/hfmax
dhm/dt=(0.5*hjmax*hj*hjmn-hmmax*hm*hmdn-hmdm(pai)-hmmax*hm*hcn
-hp*hmmax*hm/(hjmax*hj+hfmax*hf+hmmax*hm))/hmmax
dlj/dt=(lfmax*lf*lfm(paa)-ljmax*lj*ljdn*ljdm(paa)-ljmax*lj*ljmn)/ljmax
dlf/dt=(0.5*lj*ljmax*ljmn-lfmax*lf*lfdn-lfmax*lf*lcn)/lfmax
dlm/dt=(0.5*ljmax*lj*ljmn-lmmax*lm*lmdn-lmmax*lm*lcn)/lmmax
dsj/dt=(sfmax*sf*sfn*sdfm(gma)-sjmax*sj*sjdn*sjdm(gma)-sjmax*sj*sjmn-
max(0,1-lpm(pa))*lut*sjpn-sjmax*sj*sjcn*sjcm)/sjmax
dsf/dt=(0.5*sjmax*sj*sjmn-sfmax*sf*sfdn-sfmax*sf*sfcn)/sfmax
dsm/dt=(0.5*sjmax*sj*sjmn-smmax*sm*smdn-smmax*sm*smcn*smcm)/smmax
dhda/dt=(hd-hda)/del1
dpaa/dt=(pa-paa)/del2
dgamma/dt=(gm(pai)-gma)/del3
dtr/dt=(-tr+(mutwool-culling-cssu*ssu+ssu*ssuval)/trmax)/tau
#
# State variables and initial values.
pas(0)=0.66,hj(0)=0.7,hf(0)=0.525,hm(0)=0.525
lj(0)=0.4,lf(0)=0.6,lm(0)=0.6,sj(0)=0.80670,sf(0)=0.75567,sm(0)=0.50379
hda(0)=1.0,paa(0)=1.0,gma(0)=1.0,tr(0)=3.9069
#
# Fixed variables—these are quantities which are used repeatedly
# in the model equations. Making them fixed variables simplifies
# the appearance of the calculations considerably.
hut=hjmax*hjr*hj+hfmax*hf+hmmax*hm
lut=ljr*ljmax*lj+lmmax*lm+lfmax*lf
ssu=sjr*sjmax*sj+sfmax*sf+smmax*sm
hd=hut/hun
pa=(hut/lut)/(hun/lun)

```

```

pai=pmax*pas/pav
tssu=ssu+max(0,(hut-hun)/hs)
hp=lut*lpn*lpm(pa)
sjcm=(2.01-argf(1.01,0.01,1.2,gma))/2
smcm=2.01-argf(1.01,0.01,1.2,gma)
#
# Fixed variables needed to define revenue (mutton and wool sales and cost
# of culling).
mutwool=sjmv*sjmax*sj*sjcn*sjcm+sfmv*sfmax*sf*sfcn+smmv*smmmax
      *sm*smcn*smcm+sjwv*sjmax*sj+sfwv*sfmax*sf+smwv*smmmax*sm
culling=ccl*(lfmax*lf*lcn+lmmax*lm*lcn)+cch*(hfmax*hf*hcn+hmmax*hm*hcn)
#
# Auxiliary variables—these are quantities other than the state
# variables whose values we would like to appear in XPPAUT's
# data window. Here we have revenue and total revenue.
# Total revenue is the quantity referred to in the analysis as revenue.
aux rev=mutwool-culling-cssu*ssu
aux totrev=mutwool-culling-cssu*ssu+ssu*ssuval
#
# In order to view the values of the fixed variables in the data window
# we need to have the following statements:
fhut=hut
flut=lut
fssu=ssu
fhd=hd
fpa=pa
fpai=pai
ftssu=tssu
fhp=hp
fsjcm=sjcm
fsmcm=smcm
#
# Parameters and nominal values.
param hjr=0.5,ljr=0.5,sjr=0.67,hun=700000,lun=700,pav=6.6e7
param hs=18,ppn=332,area=200000,gn=365,sub=0.000005,temp=1.0
param hfn=1.5,hjdn=0.5,hfdn=0.1,hmdn=0.1,hjmn=1.0,lpn=84.11,hcn=0.0
param lfn=0.7,ljdn=0.5,lfdn=0.13,lmdn=0.13,ljmn=1.0,lcn=0.0

```

```

param sfn=0.75,sjdn=0.1,sfdn=0.02,smdn=0.02,sjmn=0.5
param sjpn=90.0,sjcn=0.09,sfcn=0.28,smcn=0.28
param sjmv=55.0,sfmv=79.0,smmv=75.0,sjwv=5.0,sfwv=7.0,smwv=9.0
param ccl=30.0,cch=1.0,cssu=2.0,ssuval=200.0,pmax=1.0e8
param hjmax=500000,hfmax=500000,hmmax=500000,ljmax=500,lfmax=500
param lmmax=500,sjmax=100000,sfmax=100000,smmmax=100000
param del1=0.9,del2=0.6,del3=0.9,tau=0.05,trmax=1.0e7
#
# User functions—these are the multiplier functions.
argE(A,B)=(A/B)-1
argC(A,B)=ln(argE(A,B)/(A-1))
argr(A,B,slope)=slope*A/((A-1)*argC(A,B))
argf(A,B,slope,x)=A/(1+argE(A,B)*exp(-argC(A,B)
    *exp(argr(A,B,slope)*ln(max(x,sub))))))
plm(x)=3.25*(x+0.001)*exp(-1.2*(x+0.001))
gm(x)=argf(1.5,0.1,0.8,x)
hdfm(x)=2.5-argf(2.4,0.1,1.3,x+0.4)
hjdkm(x)=argf(1.8,0.1,1.0,x)
lpm(x)=argf(1.6,0.8,0.5,x)
lfm(x)=argf(1.5,0.01,0.7,x)
ljdm(x)=2.0-argf(1.9,0.05,1.1,x+0.2)
sdfm(x)=argf(2.8,0.4,1.3,x)
sjdm(x)=12.0-argf(11.5,0.1,2.7,x+1.6)
ahjdkm(x)=max(0,exp(-3*x)*(hut-hun)*hj*hjmax/(hjmax*hj+hfmax*hf+hmmax*hm))
hfdm(x)=max(0,exp(-3*x)*(hut-hun)*hfmax*hf/(hjmax*hj+hfmax*hf+hmmax*hm))
hmdm(x)=max(0,exp(-3*x)*(hut-hun)*hmmax*hm/(hjmax*hj+hfmax*hf+hmmax*hm))
#
done

```

Ratio-dependent model—XPPAUT

```
# Model equations.
dM1/dt=gam1*(1-exp(-omega1/M1)-M1^b1)*M1-
(1-exp(-omega2*M1/M2))*phi2*M2/omega2
dM2/dt=gam2*(1-exp(-omega2*M1/M2)-M2^b2)*M2-
(1-exp(-omega3*M2/M3))*phi3*M3/omega3
dM3/dt=gam3*(1-exp(-omega3*M2/M3)-M3^b3)*M3
# Initial values.
M1(0)=0.8
M2(0)=0.2
M3(0)=0.2
# Nondimensionalised parameters and values.
param omega1=14.0,omega2=20.0,omega3=16.67
param gam1=0.65,gam2=0.4,gam3=0.4
param phi2=0.07,phi3=0.06
param b1=0.02,b2=0.02,b3=0.0
done
```

Population genetics model I—Interactive AUTO.

```
c Note: lines beginning with c are comments.
c
c Population genetics model with exponential fitness functions.
c
  PROGRAM AUTO
c
  IMPLICIT DOUBLE PRECISION (A-H,O-Z)
c
c NOTE: parameters liw and lw are VERY IMPORTANT. They set aside
c space for AUTO in the work arrays IW and W. In Interactive AUTO
c they must be "hardwired" into the code. If you begin to have problems
c with large continuations (e.g. periodic solutions using a big NTST), try
c setting liw and lw larger and recompiling the executable. c
  PARAMETER(liw = 10000)
  PARAMETER(lw = 250000)
  dimension IW(liw),W(lw)
  dimension ipar(50),rpar(50),icp(20)
  character*10 params(20)
  character*50 name
c
  call dfinit
c
c NDIM (number of state variables)
  ipar( 1)=2
c IPS (+1 for ode's, -1 for maps)
  ipar( 2)=-1
c IRS
  ipar( 3)=0
c ILP
  ipar( 4)=0
c NTST
  ipar( 5)=15
c NCOL
  ipar( 6)=4
c IAD
```

```

    ipar( 7)=3
c ISP
    ipar( 8)=1
c ISW
    ipar( 9)=1
c IPLT
    ipar(10)=0
c NBC
    ipar(11)=0
c NINT
    ipar(12)=0
c IADS
    ipar(13)=1
c NMX
    ipar(14)=100
c NUZR
    ipar(15)=0
c NPR
    ipar(16)=50
c MXBF
    ipar(17)=5
c IID
    ipar(18)=2
c ITMX
    ipar(19)=8
c ITNW
    ipar(20)=5
c NWTN
    ipar(21)=3
c JAC
    ipar(22)=0
c
c ICP(i)
    icp(1) = 1
    icp(2) = 2
    DO 1 I=1,2
    ipar(30+i)=icp(i)

```

```

1 CONTINUE
c
c DS
  rpar(1)=0.0001d0
c DSMIN
  rpar(2)=0.000002d0
c DSMAX
  rpar(3)=0.01d0
c RL0
  rpar(4)=0.0
c RL1
  rpar(5)=4.0
c A0
  rpar(6)=-10.0
c A1
  rpar(7)= 250.0
c EPSS
  rpar(8) = 1.d-6
c EPSL(i), i=1,20
  rpar(9) = 1.d-6
c EPSU
  rpar(10) = 1.d-6
c nparams=number of parameters that you want to vary
  nparams = 6
c declaration of parameter names
  params(1) = 'a11'
  params(2) = 'a12'
  params(3) = 'a22'
  params(4) = 'b11'
  params(5) = 'b12'
  params(6) = 'b22'
c
  name = ' Genetics model '
c
  call autool(ipar,rpar,iw,liw,w,lw,params,nparams,name)
  stop
  end

```

```

c
  SUBROUTINE VECFLD(ndim,u,icp,par,ijac,f,t)
c
c This subroutine evaluates the right hand side of the first order system
c
c input parameters :
c  ndim - dimension of u and f.
c  u - vector containing u.
c  par - array of parameters in the differential equations.
c  icp - par(icp(1)) is the initial 'free' parameter.
c  par(icp(2)) is a secondary 'free' parameter,
c  for subsequent 2-parameter continuations.
c  ijac - =1 if the jacobians dfdu and dfdp are to be returned,
c  =0 if only f(u,par) is to be returned in this call.
c  t - current time.
c
c value to be returned :
c  f - f(u,par) the right hand side of the ode.
c
  implicit double precision (a-h,o-z)
c
  dimension u(ndim),par(30)
  dimension f(ndim)
c Parameters
  a11 = par(1)
  a12 = par(2)
  a22 = par(3)
  b11 = par(4)
  b12 = par(5)
  b22 = par(6)
c State variables
  P = u(1)
  eN = u(2)
c Fitness functions
  w11 = exp(a11-b11*eN)
  w12 = exp(a12-b12*eN)
  w22 = exp(a22-b22*eN)

```

```

c Mean fitnesses
  w1marg = P*w11+(1-P)*w12
  w2marg = P*w12+(1-P)*w22
  fitmean = P*w1marg+(1-P)*w2marg
c
c DIFFERENCE EQUATIONS
c
  f(1)= P*w1marg/fitmean
  f(2)= fitmean*eN
c
  return
  end
c
  SUBROUTINE PARDER(ndim,u,icp,par,ijac,dfdu,t)
c
c this subroutine evaluates the derivatives
c of the first order system and with respect to (u(1),u(2)).
c Not included for this model hence ijac=0 in the first subroutine.
c
  return
  end
c
  SUBROUTINE DFDPAR(ndim,u,icp,par,ijac,dfdp,t)
c
c this subroutine evaluates the derivatives
c of the first order system and with respect to free parameters.
c Not included for this model.
c
  return
  end
c
  SUBROUTINE STPNT(ndim,u,par)
c
c in this subroutine the steady state starting point must be defined.
c (used when not restarting from a previously computed solution).
c the problem parameters (par) may be initialized here or else in init.
c

```

```

c  ndim - dimension of the system of equations.
c  u - vector of dimension ndim.
c  upon return u should contain a steady state solution
c  corresponding to the values assigned to par.
c  par - array of parameters in the differential equations.
c
c  implicit double precision (a-h,o-z)
c
c  dimension u(ndim),par(30)
c
c initialize the problem parameters.
  par(1)=2.1d0
  par(2)=1.9d0
  par(3)=1.1d0
  par(4)=1.0d0
  par(5)=0.904d0
  par(6)=0.524d0
  par(14) = DBLE( 1 )
c initialize the steady state.
  u(1)=0.5d0
  u(2)=2.1008d0
c
c  return
c  end
c
c  SUBROUTINE SPROJ (ndim, u, isw, icp, par, vaxis, pt)
c
c this subroutine can be used to define a special projection
c in the bifurcation window. This subroutine is called
c when the 'SP' is toggled ON (issue the command successively
c to turn the toggle from ON to OFF, and vice versa).
c
c input values:
c  ndim - dimension of u.
c  u - vector containing coordinates of current solution.
c  isw - the number of parameters being used in the current
c  continuation.

```

```

c  icp - par(icp(1)) is the initial 'free' parameter.
c  par(icp(2)) is a secondary 'free' parameter,
c  for subsequent 2-parameter continuations.
c  par - array of parameters in the differential equations.
c  vaxis - controlled by program constant IPLT (see
c  AUTO86 User Manual). this is the second number
c  per line written in unit 7 (file fort.7).
c
c return values:
c  pt - array whose 1st, 2nd and 3rd elements are plotted on
c  the x, y and z axes, respectively.
c
c  implicit double precision (a-h,o-z)
c
c  dimension icp(20)
c  dimension u(ndim), par(30), pt(3)
c
c  if (isw.eq.1) then
c    pt(1) = par( 1)
c    pt(2) = u(2)
c    pt(3) = vaxis
c  else if (isw.eq.2) then
c    pt(1) = par( 1 )
c    pt(2) = par( 2 )
c    pt(3) = vaxis
c  endif
c
c  return
c  end
c
c  SUBROUTINE SPJAXS (ndim, isw, icp, axes )
c
c  this subroutine defines the names of the axes used in
c  the projection defined in the subroutine sproj.
c
c  input value:
c  ndim - dimension of u.

```

```

c  IABS(isw) - the number of parameters being used in the current
c  continuation.
c  icp - par(icp(1)) is the initial 'free' parameter.
c  par(icp(2)) is a secondary 'free' parameter,
c  for subsequent 2-parameter continuations.
c return value:
c  axes - character string array with the x, y, and
c  z axes names, respectively.
c
c  integer*4 ndim, isw, icp(20)
c  character*10 axes(3)
c
c  if (isw.eq.1) then
c    axes(1) = 'icp(1)'
c    axes(2) = 'N'
c    axes(3) = ''
c  else if (isw.eq.2) then
c    axes(1) = 'icp(1)'
c    axes(2) = 'icp(2)'
c    axes(3) = ''
c  endif
c
c  return
c  end
c
c*** graphics initializations for interactive AUTO
c
c  SUBROUTINE GPHDFT( ldebug, lintog, labtog, ldsplt,
c  @ leigen, lftog, lsavpt,
c  @ lgraph, lvideo, lsproj, nproj,
c  @ ndmplt, delay, sclbif, scldis,
c  @ sclev, filext )
c
c  logical ldebug, lintog, labtog, ldsplt, leigen, lftog
c  logical lsavpt, lgraph, lvideo, lsproj
c  integer*4 nproj, ndmplt
c  real*8 delay

```

```

    real*8 sclbif(6), scldis(6), sclev(6)
    character*10 filext(2)
c
c*** toggles
c ldebug: T => debugging output
c lintog: T => plotting of lines between points
c labtog: T => plots two-character identifier at bifurcation points
c ldsplt: T => open optional UNIX Graph window
c leigen: T => open eigenvalue plotting window
c lftog: T => illuminates points temporarily as they are plotted
c lgraph: T => use graphics (F => can then run jobs in the background)
c lvideo: T => reposition windows in botton 1/4 of screen for videotaping
c lsproj: T => plot special projection defined in subroutine sproj
c in the bifurcation window
c lsavpt: T => eigenvalues saved in fort.11 ('svaut *' moves this to m.*)
c DO NOT ALTER the following lines.
    ldebug = .false.
    lintog = .false.
    labtog = .true.
    ldsplt = .false.
    leigen = .true.
    lftog = .false.
    lcomfl = .false.
    loutfl = .false.
    lgraph = .true.
    lvideo = .false.
    lsproj = .false.
    lsavpt = .false.
c
c*** default window scales
c ... Bifurcation window scales
c eg. when isw = 1 => default plot axes x,y,z = par(icp(1)), u(1), u(2);
c when isw = 2 => default plot axes x,y,z = par(icp(1)), par(icp(2)), u(1)
c The following lines can also be changed interactively.
    sclbif(1) = 0.5d0
    sclbif(2) = 0.56d0
    sclbif(3) = 0.0d0

```

```

    sclbif(4) = 1.0d0
    sclbif(5) = 0.0d0
    sclbif(6) = 10.0d0
c ... Eigenvalue window scales
    sclev(1) = -2.0d0
    sclev(2) = 2.0d0
    sclev(3) = -2.0d0
    sclev(4) = 2.0d0
c
c*** set files names
c
    comfil = 'input '
    outfil = 'output '
c
c*** file strings for saving, deleting, etc.
c
    filext(1) = 'gen '
    filext(2) = 'gen2 '
c
c*** other stuff
c nproj = number of projections to be plotted (up to nine)
c ndmplt = dimension of the bifurcation window plot
c delay = factor for duration of flash display
c
    nproj = 2
    ndmplt = 3
    delay = 0.0d00
c
    return
end

```

Population genetics model I—DSTOOL.

```
# include <model_headers.h>
/* Note: The symbols /* and */ denote the beginning and end of comments
respectively. */
/* _____
Required function used to define the vector field or map.
The values of the vector field mapping at point x with parameter
values p are returned in the pre-allocated array f. For vector fields,
the last components of both f and x are time components. All arrays are
indexed starting from 0.
_____ */
int genetics_def(f,x,p)
double *f,*x,*p;
{
double a11,a12,a22,b11,b12,b22,P,N;
double w11,w12,w22,margw1,margw2,meanfit;

/* Parameters whose values can be changed interactively. */
a11 = p[0];
a12 = p[1];
a22 = p[2];
b11 = p[3];
b12 = p[4];
b22 = p[5];
/*
STATE VARIABLES
*/
P = x[0]; /* Frequency of allele A1 */
N = x[1]; /* Population density */
/*
FITNESS FUNCTIONS
* /
w11 = exp(a11-b11*N);
w12 = exp(a12-b12*N);
w22 = exp(a22-b22*N);
*/
```

MARGINAL FITNESS FUNCTIONS

```
* /  
margw1 = P*w11+(1-P)*w12;  
margw2 = P*w12+(1-P)*w22;  
meanfit = P*margw1+(1-P)*margw2;  
/*
```

DIFFERENCE EQUATIONS

```
* /  
f[0] = P*margw1/meanfit;  
f[1] = meanfit*N;  
} /* End of model equations. */
```

```
/* _____  
Optional function used to define the Jacobian m at point x with  
parameters p. The matrix m is pre-allocated (by the routine dmatrix);  
At exit, m[i][j] is to be the partial derivative of the i'th component  
of f with respect to the j'th component of x.
```

```
_____ */
```

```
/*  
int user_jac(m,x,p)  
double **m, *x, *p;  
{  
}  
*/
```

```
/* _____  
Optional function used to define the inverse or approximate inverse y at  
the point x with parameter values p. The array y is pre-allocated.
```

```
_____ */
```

```
/*  
int user_inv(y,x,p)  
double *y,*x,*p;  
{  
}  
*/
```

```
/* _____  
Optional function used to define aux functions f of the variables x  
and parameters p. The array f is pre-allocated. Time is available as the
```

last component of x.

_____ */

```
/*  
int user_aux_func(f,x,p)  
double *f,*x,*p;  
{  
}
```

```
*/
```

_____ */

Required procedure to define default data for the dynamical system.

NOTE: You may change the entries for each variable but PLEASE DO NOT change the list of items. If a variable is unused, NULL or zero the entry, as appropriate.

_____ */

```
int genetics_init()  
{
```

```
/* _____ define the dynamical system in this segment _____ */  
int n_varb=2; /* dim of phase space */
```

```
static char *variable_names[]={”P”,”N”}; /* list of phase varb names */  
static double variables[]={0.,0.}; /* default varb initial values */
```

```
static double variable_min[]={0.,0.}; /* default varb min for display */  
static double variable_max[]={1.,5.}; /* default varb max for display */
```

```
static char *indep_varb_name=”time”; /* name of indep variable */
```

```
double indep_varb_min=0.; /* default indep varb min for display */
```

```
double indep_varb_max=100.; /* default indep varb max for display */
```

```
int n_param=6; /* dim of parameter space */
```

```
static char *parameter_names[]={”a11”,”a12”,”a22”,”b11”,”b12”,”b22”}; /*  
list of param names */
```

```
static double parameters[]={2.1,1.9,1.1,1.0,0.904,0.56}; /* initial parameter  
values */
```

```
static double parameter_min[]={0.,0.,0.,0.,0.,0.}; /* default param min for  
display */
```

```
static double parameter_max[]={2.,2.,2.,3.,3.,3.}; /* default param max for  
display */
```

```

int n_funct=0; /* number of user-defined functions */
static char *funct_names[]={""}; /* list of funct names; {""} if none */
static double funct_min[]={0.}; /* default funct min for display */
static double funct_max[]={0.}; /* default funct max for display */

int manifold_type=EUCLIDEAN; /* PERIODIC (a periodic varb) or EU-
CLIDEAN */
static int periodic_varb[]={FALSE, FALSE}; /* if PERIODIC, which varbs
are periodic? */
static double period_start[]={0.,0.}; /* if PERIODIC, begin fundamental do-
main */
static double period_end[]={1.,1.}; /* if PERIODIC, end of fundamental do-
main */

int mapping_toggle=TRUE; /* this is a map? TRUE or FALSE */
int inverse_toggle=FALSE; /* if so, is inverse FALSE, APPROX_INV, */
/* or EXPLICIT_INV? FALSE for vec field */

/* In this section, input NULL or the name of the function which contains...
*/
int (*def_name)()=genetics_def; /* the eqns of motion */
int (*jac_name)()=NULL; /* the jacobian (deriv w.r.t. space) */
int (*aux_func_name)()=NULL; /* the auxiliary functions */
int (*inv_name)()=NULL; /* the inverse or approx inverse */
int (*dfdt_name)()=NULL; /* the deriv w.r.t time */
int (*dfdparam_name)()=NULL; /* the derivs w.r.t. parameters */
/* ----- end of dynamical system definition ----- */
#include <ds_define.c>
}

```

Spruce budworm model—DSTOOL.

```
# include <model_headers.h>
/* Note: The symbols /* and */ denote the beginning and end of comments
respectively. */
/* _____
Required function used to define the vector field or map.
The values of the vector field mapping at point x with parameter
values p are returned in the pre-allocated array f. For vector fields,
the last components of both f and x are time components. All arrays are
indexed starting from 0.
_____ */
int budworm_def(f,x,p)
double *f,*x,*p;
{
int npara,nfood,npred,nsurv,nhist,mdisp,ndisp;
double slsurv,sdie,predmax,defsat,dsearch;
double fgrow,fmax,smax,sgrow,predsats,sharp;
double exfrac,exthr,A,B,folnew,folold,foltot,C,S1,BL1;
double BL2,D,BL3,BL4,BL5,BL6,W,E1,H,G,BL7,BL8,FO,S,BL,temp1;

/* Parameters whose values can be changed interactively. */
slsurv = p[0];
sdie = p[1];
predmax = p[2];
defsat = p[3];
exfrac = p[4];
exthr = p[5];
predsat = p[6];
/*
STATE VARIABLES
*/
FO = x[0]; /* Foliage */
S = x[1]; /* Branch surface area */
BL = x[2]; /* Budworm density */
/*
FLAGS
```

```

* /
npara = 1;
nfood = 1;
npred = 1;
nsurv = 1;
nhist = 1;
mdisp = 1;
ndisp = 1;
/*
CONSTANTS
* /
fgrow = 1.5;
fmax = 3.8;
smax = 2.4E4;
sgrow = 1.15;
sharp = 4;
dsearch = 1.0;
/*
PRELIMINARY EQUATIONS

Foliage dynamics
* /
A = defsat*BL*fmax/FO;
folnew = exp(-A)*FO/fmax;
B = 0.357*(A-1+exp(-A));
folold = exp(-B)*FO*(fmax-1)/fmax;
foltot = folnew+folold;
/*
Surface area dynamics
* /
S1 = (1-sdie*(1-foltot/FO)*(1-foltot/FO))*S;
/*
Budworm dynamics
* /
/* The if-then statements in this section are for the switches. */
C = 0.003*BL;
if (npara == 1)

```

```

    BL1 = (1-0.4*exp(-C))*BL;
else
    BL1 = BL;
if (nfood == 1)
    BL2 = (0.425*(FO-foltot)/(defsat*BL))*BL1;
else
    BL2 = 0.425*BL1;
if (npred == 1)
    {temp1 = predsat*FO*FO+BL2*BL2;
    D = (predmax*2.3E4)*BL2/(S*temp1);
    }
else
    D = 0;
BL3 = exp(-D)*BL2;
if (nsurv == 1)
    BL4 = (0.473+0.826*BL3/BL)*BL3;
else
    BL4 = 0.825*BL3;
if (nhist == 1)
    {temp1 = 24.9*(fmax-1)*(1-exp(-B))/A;
    W = 34.1*(1-exp(-A))/A+temp1-3.4;
    if (W > 0)
        {BL5 = (166.0*exp((log(W))/3)-329.0)*0.46*BL4;
        }
    else
        BL5 = 96.0*BL4;
    }
else
    BL5 = 96*BL4;
if (BL5 <= 20.0*BL4)
    BL5 = 20.0*BL4;
if (mdisp == 1)
    { E1 = 0.46*BL4/exthr;
    if (E1 > 0)
        {temp1 = exp(sharp*log(E1));
        BL6 = (1-(exfrac*temp1)/(1+temp1))*BL5;
        }
    }

```

```

    else
        BL6 = BL5;
    }
else
    BL6 = BL5;
if (ndisp == 1)
    { H = (foltot/fmax)*dsearch;
      G = H*(2-H);
      BL7 = slsurv*S*G*G*BL6/smax;
    }
else
    BL7 = slsurv*BL6;
BL8 = (S1/S)*BL7;
/*
DIFFERENCE EQUATIONS
* /
f[0]= fgrow*foltot/(1+(fgrow-1)*foltot/fmax);
f[1]= sgrow*S1/(1+(sgrow-1)*S1/smax);
f[2]= BL7;
} /* End of model equations. */

/* -----
Optional function used to define the Jacobian m at point x with
parameters p. The matrix m is pre-allocated (by the routine dmatrix);
At exit, m[i][j] is to be the partial derivative of the i'th component
of f with respect to the j'th component of x.
----- */
/*
int user_jac(m,x,p)
double **m, *x, *p;
{
}
* /
/* -----
Optional function used to define the inverse or approximate inverse y at
the point x with parameter values p. The array y is pre-allocated.
----- */

```

```

/*
int user_inv(y,x,p)
double *y,*x,*p;
{
}
*/
/* _____
Optional function used to define aux functions f of the variables x
and parameters p. The array f is pre-allocated. Time is available as the
last component of x.
_____ */
int budworm_aux(f,x,p)
double *f,*x,*p;
{
if (x[2] > 0)
f[0] = log(x[2]);
else
f[0] = 0;
}
/* _____
Required procedure to define default data for the dynamical system.
NOTE: You may change the entries for each variable but PLEASE DO
NOT change the list of items. If a variable is unused, NULL or zero the
entry, as appropriate.
_____ */
int budworm_init()
{
/* _____ define the dynamical system in this segment _____ */
int n_varb=3; /* dim of phase space */
static char *variable_names[]={"F","S","B"}; /* list of phase varb names */
static double variables[]={0.,1.68E4,0.}; /* default varb initial values */
static double variable_min[]={0.,0.,0.}; /* default varb min for display */
static double variable_max[]={5.,40000.,350.}; /* default varb max for display */

static char *indep_varb_name="time"; /* name of indep variable */
double indep_varb_min=0.; /* default indep varb min for display */

```

```

double indep_varb_max=1000.; /* default indep varb max for display */

int n_param=7; /* dim of parameter space */
static char *parameter_names[]={"slsurv","sdie","predmax","defsat",
"exfrac","extr","predsat"}; /* list of param names */
static double parameters[]={0.28,0.75,1.0,0.0074,0.5,5.0,0.085}; /* initial pa-
parameter values */
static double parameter_min[]={0.,0.,0.,0.,0.,0.,0.}; /* default param min for
display */
static double parameter_max[]={1.,1.,3.,1.,1.,20.,1.}; /* default param max
for display */

int n_funct=1; /* number of user-defined functions */
static char *funct_names[]={"lnB"}; /* list of funct names; {""} if none */
static double funct_min[]={-2.0}; /* default funct min for display */
static double funct_max[]={3.0}; /* default funct max for display */

int manifold_type=EUCLIDEAN; /* PERIODIC (a periodic varb) or EU-
CLIDEAN */
static int periodic_varb[]={FALSE, FALSE, FALSE}; /* if PERIODIC, which
varbs are periodic? */
static double period_start[]={0.,0.,0.}; /* if PERIODIC, begin fundamental
domain */
static double period_end[]={1.,1.,1.}; /* if PERIODIC, end of fundamental
domain */

int mapping_toggle=TRUE; /* this is a map? TRUE or FALSE */
int inverse_toggle=FALSE; /* if so, is inverse FALSE, APPROX_INV, */
/* or EXPLICIT_INV? FALSE for vec field */

/* In this section, input NULL or the name of the function which contains...
*/
int (*def_name)()=budworm_def; /* the eqns of motion */
int (*jac_name)()=NULL; /* the jacobian (deriv w.r.t. space) */
int (*aux_func_name)()=budworm_aux; /* the auxiliary functions */
int (*inv_name)()=NULL; /* the inverse or approx inverse */
int (*dfdt_name)()=NULL; /* the deriv w.r.t time */

```

```
int (*dfdparam_name)()=NULL; /* the derivs w.r.t. parameters */
/* ----- end of dynamical system definition ----- */
# include <ds_define.c>
}
```